# Seismoacoustic Study of the Shallow Gas Transport and Reservoirs in the Vicinity of Seabed Fluid Seepage of the Black Sea

## Dissertation

Zur Erlangung des
Doktorgrades der Naturwissenschaften
(Dr. rer. Nat.)

Im Fachbereich der Geowissenschaften
der Universität Bremen

Vorgelegt von
**Junhui Xing**

**N a m e** : .......Junhui Xing.............................................. Datum ......27.10.2013.........

Anschrift : .........Leobener Str. 4, App, 11-01. 28359, Bremen..............

# **E r k l ä r u n g**

Hiermit versichere ich, dass ich

1. die Arbeit ohne unerlaubte fremde Hilfe angefertigt habe,

2. keine anderen als die von mir angegebenen Quellen und Hilfsmittel benutzt habe und

3. die den benutzten Werken wörtlich oder inhaltlich entnommenen Stellen als solche kenntlich gemacht habe.

_____, den ...................................

------------------------------------------------------------------
(Unterschrift)

**Table of contents**

# Abstract

In recent years, gas release through seabed fluid seepage has received increasing attention from geoscientists. On the one hand it contributes greater amounts of gas and fluids, dominated by methane (a powerful greenhouse gas) to the biosphere, the hydrosphere and the atmosphere. It can also cause marine geohazards such as slope failures, or can be used to predict the presence of oil and gas fields or gas hydrates fields. The Black Sea is the world's largest anoxic intercontinental basin with a maximum water depth of 2200 m, which created by a back-arc extension due to the subduction of the Thetyan Ocean during the Late Cretaceous period. The collision between the Arabian and Eurasian plates has led to compressive deformation at the margins of the Black Sea since the Eocene. Combined with thick sediment coverage, a considerable amount of gas related to seabed fluid seepage was generated by over-pressured fluids and upward fluid migration. Two study areas: the central Black Sea and the Kerch Peninsula margin were selected to further investigate the shallow expressions of such gas transport and release. Mainly high-resolution multichannel seismic datasets were used to study the near-surface seismostratigraphy, complemented by bathymetric and sediment echosounder (Parasound) data. The datasets of the central Black Sea were collected during the Meteor Cruise M52/1 in 2002. The datasets of the Kerch Peninsula margin were acquired during the Meteor Cruise M72/3b in 2007.

In the central Black Sea, six large mud volcanoes: MSU, Yuzhmorgeologiya, Malyshev, Kornev, Goncharov and Vassoevitch with great morphological variability and clear near-surface sediment structures were imaged by high-resolution seismic data. Gas discharge is commonly associated with mud volcanism. As gas emissions at mud volcanoes are dominated by methane, mud volcanoes represent an important natural source of methane contribution to the environment. Four types of pathways for gas and fluid migration and three types of gas reservoirs were recognized, according to the analysis of acoustic anomalies and studied near-surface sediment structures of these mud volcanoes. The formation history of the gas reservoirs was studied in detail, which reveals that the free gas reservoirs were probably sealed by gas hydrates or fine-grained sediments. Two to three major eruption episodes of these mud volcanoes were observed. These eruptive episodes appeared be related to distinct sea level falls during the Pleistocene, which seem to be one of the main trigger factors of the mud volcano eruptions in the central Black Sea.

The Parasound sediment echosounder data collected in the Kerch Peninsula margin during cruise M72/3b presented many gas flares located on the continental slope in water depths shallower than ~700 m, which is the upper boundary of the gas hydrate stability zone (GHSZ). Gas flares of more than ~400 m height above the sea floor were observed at a water depth of ~900 m within the GHSZ, which was named as the Kerch seep area. Strong evidence was found in seismoacoustic water column and subsurface data for free gas, distributed in numerous bright spots within, beneath and above the GHSZ. The presence of gas hydrates in conjunction with the deformation history of the sedimentary units appears as the main factor of gas distribution, migration and seepage. Therefore, six seismic units in terms of their approximate geological ages, seismic facies character and distribution, depocenter locations, provenance, and tectonic movement of the Crimean

Mountains and Black Sea basin were described and interpreted to gain some insight into the deformation history of the sedimentary units. Based on the sedimentary processes of the study area and seismic anomalous features, two geological models for the gas hydrate occurrence and gas trap-leakage processes for the Kerch seep area and for the upper slope are presented.

In summary, although the two different study areas selected in the Black Sea have different tectonic settings, both of them were influenced by the compressional tectonic events, high sedimentation rates and tectonic subsidence. The mud volcanoes are morphology positive and gas seeps appear without apparent morphological features. They are caused by overpressured and upward migrating gas/fluids from the Maikopian formation. The near-surface geological processes including gas hydrate formation also have a significant influence on the occurrence and distribution of the mud volcanoes and gas seeps.

## Outline of the Dissertation

The dissertation is comprised of five chapters. Chapter 1 is an introduction to the background knowledge of the dissertation about: the importance and different seabed features of the seabed fluid seepage related to the hydrocarbons; an overview of gas hydrates; the objectives of this study; the geological setting of the two study areas selected in the Black Sea; the method and datasets used in this PhD research work. After Chapter 1, three manuscripts (Chapters 2, 3 and 4) summarize the outcomes of the study. Chapter 2 discusses the gas migration and gas reservoirs related to mud volcanoes in the central Black Sea, and the possible trigger factors of mud volcanoes eruptions. Chapter 3 focuses on the research of the sedimentary processes and tectonic movements of the Kerch Peninsula margin. In Chapter 4, the distribution and formation of the gas seeps area was studied, together with the role of gas hydrates, sedimentary processes and tectonic movements, especially the anomalous situation - Kerch seep area. The conclusion of the dissertation and an outlook are presented in Chapter 5.

### Chapter 2. Shallow Gas Transport and Reservoirs in the Vicinity of Deeply Rooted Mud Volcanoes in the Central Black Sea

In Chapter 2, a set of 2D high-resolution seismic profiles is presented across six large mud volcanoes. Acoustic anomalies and near-surface sediment structures of deeply rooted mud volcanoes were studied based on the seismic dataset. Three types of the gas/gas hydrate reservoirs and four types of pathways for gas/fluid migration are recognized. A clear "Bottom Simulating Reflection" (BSR) was identified in only one of the seismic profiles. The formation history of the gas reservoirs was inferred, which were sealed by gas hydrates or fine-grained sediments. Six mud volcanoes reveal two to three major and concurrent eruption episodes. All these eruptive episodes are probably related to distinct sea level falls, which seem to be one of the main trigger factors of the mud volcano eruptions in the central Black Sea. A structural model for the MSU mud volcano was presented with respect to mechanisms of gas migration and the origin of the gas.

### Chapter 3. Sedimentary Evolution of the Kerch Peninsula margin, Black Sea

Chapter 3 presents a set of 2D high resolution seismic lines was acquired near the Kerch Peninsula during R/V Meteor Cruise M72/3 in March/April 2007 to the Eastern Black Sea. The research target is to understand the sedimentary evolution of the study area. Seven seismic facies types were identified and six seismic units could be mapped. Based on seismic line interpretation, isopach and seismic facies distribution maps, a chronostratigraphic framework could be established for the study area. Syndepositional tectonic movements and sea level influenced the sediment deposits. Possible slope fan deposits developed during the late Miocene and early Pliocene. The Messinian erosional truncation surface can be observed in our seismic dataset. Along with a major transgressional phase occurred during the Pliocene, the Paleo-Don River flowed into the Black Sea leading to fan deposition during the late Pliocene as a result of intensified tectonic movements. The seismic facies variation of the seismic units is related to the sea-level curve, which reflects grain size variations and the shift of the river mouth. During the Quaternary, the Crimean Mountain and the Paleo-Don and Kuban rivers provided high terrigenous input to the study area. Hemipelagic fine-grained sediments interbedded

with coarse grained sediments developed in the study area, along with slumps or channels and river fan deposits.

## Chapter 4. Distribution of shallow gas in the subsurface, gas flares and the role of gas hydrate near the Kerch Peninsula, Black Sea

For this case study, a set of 2D high-resolution seismic profiles and Parasound data were used to study the distribution of gas flares and shallow gas reservoirs in the subsurface. Strong evidence was found in seismoacoustic water column and subsurface data for free gas, distributed in numerous bright spots within, beneath and above the GHSZ. The presence of gas hydrates in conjunction with the deformation history of the sedimentary units appears as the main factor of gas distribution, migration and seepage. A BSR cannot be clearly identified in the study area. Instead, other seismic features like the boundary of zones, where high amplitude reflectors (HATZ) or bright spots terminate (BSTZ), may indicate the location of BGHSZ. Both types of terminations zones closely coincide with the calculated BGHSZ. Two geological models were developed for the gas hydrate occurrence and gas trap-leakage processes for the Kerch seep area and for the upper slope.

# Chapter 1. Introduction

## 1.1 Gas and fluids in marine sediments

In present-day oceans, shallow gas commonly accumulates in marine sediments, which has been reported in over 100 locations worldwide (Fleischer et al., 2001). Methane is almost always the dominant component of the natural gas mixtures. It can originate from biogenic or thermogenic processes (e.g. Floodgate and Judd, 1992). Biogenic methane is produced from organic matter by methanogenic bacteria, which generally occur in shallow marine sediments (Claypool and Kaplan, 1974; Sloan, 1990). However, biogenic methane can also be generated in considerable depths (examples from as deep as 3350 m sub-bottom are quoted by Rice and Claypool, 1981). Methane and higher hydrocarbons are generated thermogenically from organic matter by catagenesis and metagenesis at temperatures between 50 °C and 200 °C at greater depth (Fig. 1), which is normally greater than 1000 m (Floodgate and Judd, 1992). Due to the different nature of the original organic material and the different depth of burial, various hydrocarbon compounds may be formed (Judd, 2003). Methane is the most abundant and mobile gas, and it can migrate to the surface to form shallow gas accumulations.
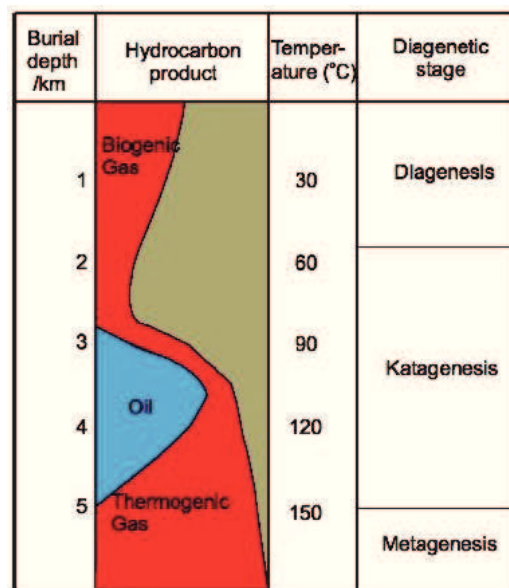


**Figure 1** Generalized relationship between temperatures, hydrocarbon generation, diagenesis (after Shu, 2012)

Fluid flow is common in marine sedimentary basins, which are sediment-filled depressions and preserve sufficient permeability to permit fluid flow. Many basins contain important mineral and energy resources, which have been generated by fluid flow or the interaction between fluid and rocks (Bitzer, 2001). About the origin of the fluid flow, internally derived fluids such as formation waters and hydrocarbons, and externally derived fluids such as meteoric and metamorphic fluids are distinguished (Lawrence and Cornford, 1995). Another main source of internal fluids is clay dehydration which may lead to the overpressure in the sedimentary basins. Overpressure in the sedimentary

basins can be generated by many dynamic mechanisms, including disequilibrium compaction (Bethke 1986; Shi and Wang 1986), tectonic collision (Ge and Garven 1992), aquathermal expansion (Sharp 1983), clay dehydration (Burst 1969), gravity flow (Toth 1962; Lee and Bethke 1994; Wolf et al. 2005), gas capillary seals (Revil et al. 1998; Lee and Deming 2002) and hydrocarbon generation (Luo and Vasseur 1996; Lee and Williams 2000). Overpressure can create and widen faults and fractures, which serve as the main migration pathway for upward-moving fluids. For fluids to migrate upwards, driving forces are needed to overcome gravity. These include pressure gradient, buoyancy and diffusion. Among these forces, buoyancy plays a dominant role in fluid migration in sediments. It can drive the fluids and hydrocarbons not only through available pathways (e.g. faults, cracks) or porous paths, but may also make their own way through rather impermeable sediment intervals (Nunn, 1996; Ding, 2008).
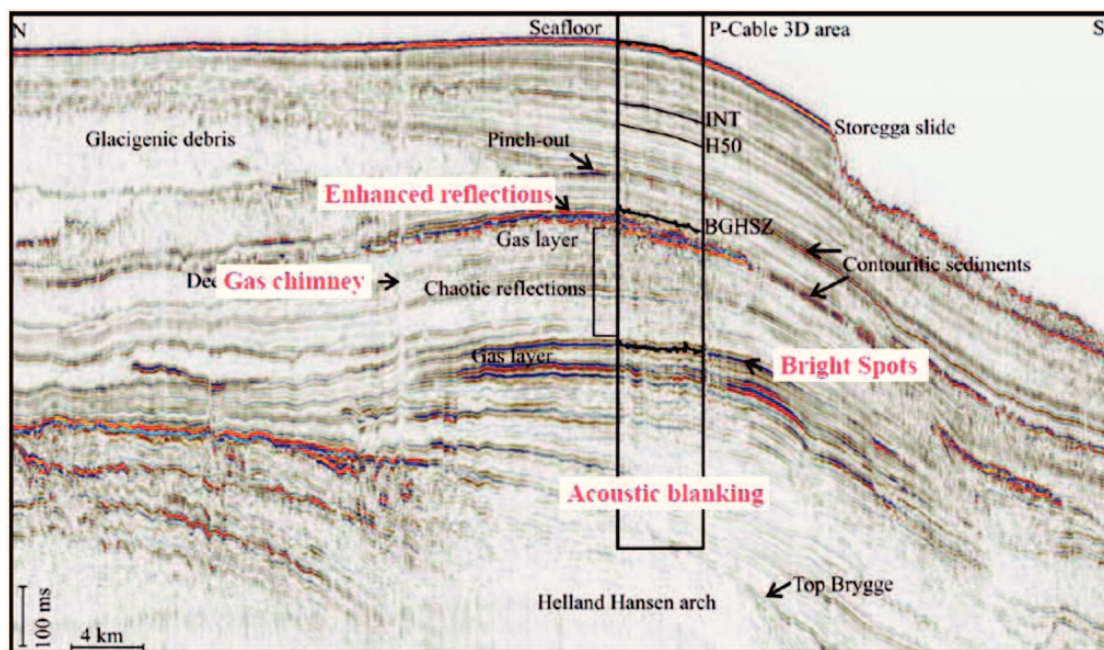


**Figure 2** Examples of seismic evidence (e.g. Bright Spots, enhanced reflections, gas chimney and acoustic blanking) are shown in the 2D seismic section in Nyegga (after Plaza-Faverola et al., 2012).

Methane can dissolve in the fluid or be in a gaseous phase, migrating either in a diffusive or focused way through sediments (Ginsburg and Soloviev, 1997). Before reaching the sea floor, most of the methane is trapped or consumed, such as dissolved in interstitial water, stored as gas accumulations, condensed to gas hydrates or consumed by the anaerobic oxidation of methane (AOM). Although it has global significance, the mechanism of AOM is still uncertain (Boetius et al., 2000).

Although it is difficult to detect the gas directly, variations in seismic attributes may indicate the change of physical properties of marine sediments caused by the gas migration and accumulation (Minshull and White, 1989). According to Judd and Hovland (2007), the main types of seismic evidence of gassy sediments include: (1) Acoustic turbidity, acoustic energy is attenuated by gas bubbles in marine sediments; (2) Enhanced

reflections, interpreted as minor accumulations of gas within thin and relatively porous sediment layers; (3) Pull-down, the effect presented on coherent reflections located below units of gas-charged sediments; (4) Gas chimneys, vertical zones shown on 2D and 3D seismic datasets and caused by the previous or on-going gas migration; (5) Bright Spots, which are characterized by high-amplitude and negative-phase reflections and regarded as key characteristics of gas accumulations; (6) Flat spots, coherent reflection occurring at the gas-water interface in a hydrocarbon reservoir; (7) Acoustic blanking and columnar disturbances, which indicate the presence of free gas. Some examples of seismic evidence are shown in Figure 2. Furthermore, focused fluid flow can also be indicated by the narrow vertical acoustic blanking zones (chimneys), faults and fractures, which are the potential conduits for fluid flow migration (Gay et al., 2003; Wagner-Friedrichs, 2007).
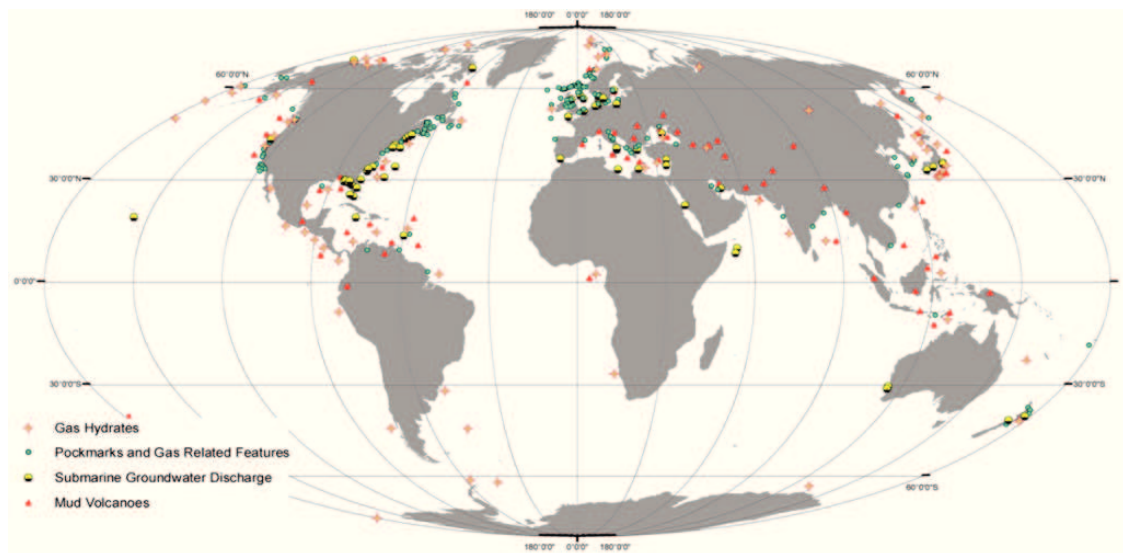


**Figure 3** Global distribution of gas hydrates, pockmarks, mud volcanoes and other gas/fluid related structures (gas seeps) (from http://www.awi.de)

Gas and fluid flow within marine sediments can be significant in shaping the morphology of marine seafloor. Gas and fluid flow related structures are widely distributed throughout the world's oceans (Fig. 3). Different types of seabed fluid seepage result from the extrusion of gas- and fluid-rich sediments, such as mud volcanoes and pockmarks (Judd and Hovland, 2007; Kopf, 2002). Therefore, gas- and fluid-charged sediments are considered a major hazard by the oil and gas industry. Scientific research has also revealed a close correspondence to climate and environmental issues and geological hazards with gas- and fluid-charged sediments.

## 1.2 Seabed fluid seepage

Seabed fluid seepage can be formed by a wide range of fluids (gases and liquids), which originate from sediments and pass through the seabed to the seawater and to the atmosphere (Judd and Hovland 2007). It includes not only cold seeps, but also volcanic

and hydrothermal fluid vents from ocean spreading centers, island arcs, and intra-plate volcanism, and groundwater flows in some coastal areas (Judd, 2003). In this dissertation, the direct link to seabed fluid seepage is through cold seeps, from which methane escapes. Seeps can occur in all geological contexts, e.g. active and passive continental margins and the deep oceans, where fluids and hydrocarbons are from sub-ducting sediments, or migrate from deep gas/oil reservoirs; such as the Gulf of Mexico (e.g. Sager et al., 2003, Ding et al., 2008; Ding et al., 2010), the Cascadia Continental Margin (e.g. Collier and Lilley, 2005), the Black Sea (e.g. Dimitrov, 2002a; Klaucke et al., 2006; Wagner-Friedrichs et al., 2008; Römer et al., 2012), the Sea of Okhotsk (e.g. Obzhirov et al., 2004), the West African Basins (e.g. Gay et al., 2003; Pilcher and Argent, 2007), the continental shelf of the U.K., including Torry Bay, Firth of Forth, Scotland (e.g. Judd et al., 1997, 2002b), the Costa Rican coast (e.g. Mau et al., 2006) and the Barbados accretionary complex (e.g. Henry et al., 1990; Le Pichon et al., 1990). It is clearly widespread (Fig. 3) and contributes greater amounts of gas and fluids, dominated by methane, to the biosphere, the hydrosphere and the atmosphere (Hovland and Judd, 1988; Judd, 2003). However, the exact distribution and number of seep sites remain uncertain due to the limited number of investigations restricted so far to only a small portion of the world's seas and oceans (Judd, 2003). The spectrum of morphologies can vary from pockmarks (King and MacLean, 1970; Hovland and Judd, 1988) to mud volcanoes of various sizes and seeps with little effect on the seafloor sediments (Fig. 4) (Dimitrov, 2002b; Judd and Hovland, 2007).

## 1.2.1 Importance

### 1.2.1.1 Climate and environment

Emission products of seabed fluid seepage include solid, liquid and gaseous materials. The gaseous materials not only contain higher hydrocarbons but also methane. Methane is considered as the most important emission. Because methane is a powerful greenhouse gas, it can play an important role in global climate change. Solomon et al. (2007) pointed that each molecule of methane has 25 times the direct global warming potential of a molecule of $CO_2$ over a period of 100 years. And the atmospheric mixing ratio of methane has increased to more than double during the last century (Rowland, 1985). Methane can originated from both anthropogenic (360-430 $x10^6$T/yr) and natural sources (160-240 $x10^6$T/yr) of either biologic or geologic origin (Prather et al., 1995; Kvenvolden and Rogers, 2005). Although some of the emitted methane from marine seepage dissolves into the ocean during transit from the seabed to the sea surface (Leifer and Judd, 2002), a greater fraction of methane can reach the atmosphere when larger bubbles are generated during eruptive episodes (e.g. blowouts) or during more rapid upwelling flow (Leifer et al., 2004, 2006). Marine seeps are estimated to contribute about 31 to 48% of the annual global methane emission into the atmosphere from geological sources (53± 11×10$^6$ T/yr, Etiope and Ciccioli, 2009; Etiope et al., 2008). According to climatologists' prediction, if the concentration of greenhouse gases in the atmosphere increases, the Earth's temperature will increase considerably during the next decades. For this reason, it can cause changes in local climate, loss of arable land and a potential increase in sea level (Kopf, 2003).

Submarine gas seeps, pockmarks and mud volcanoes on land and the seafloor seem to be the largest geologic methane sources. Among them, mud volcanoes can be the most important source of methane with other hydrocarbon and non-hydrocarbon gases to the atmosphere and the ocean. The global methane flux from mud volcanoes nearly equals the global gas flux (Milkov et al., 2003; Etiope and Milkov, 2004).
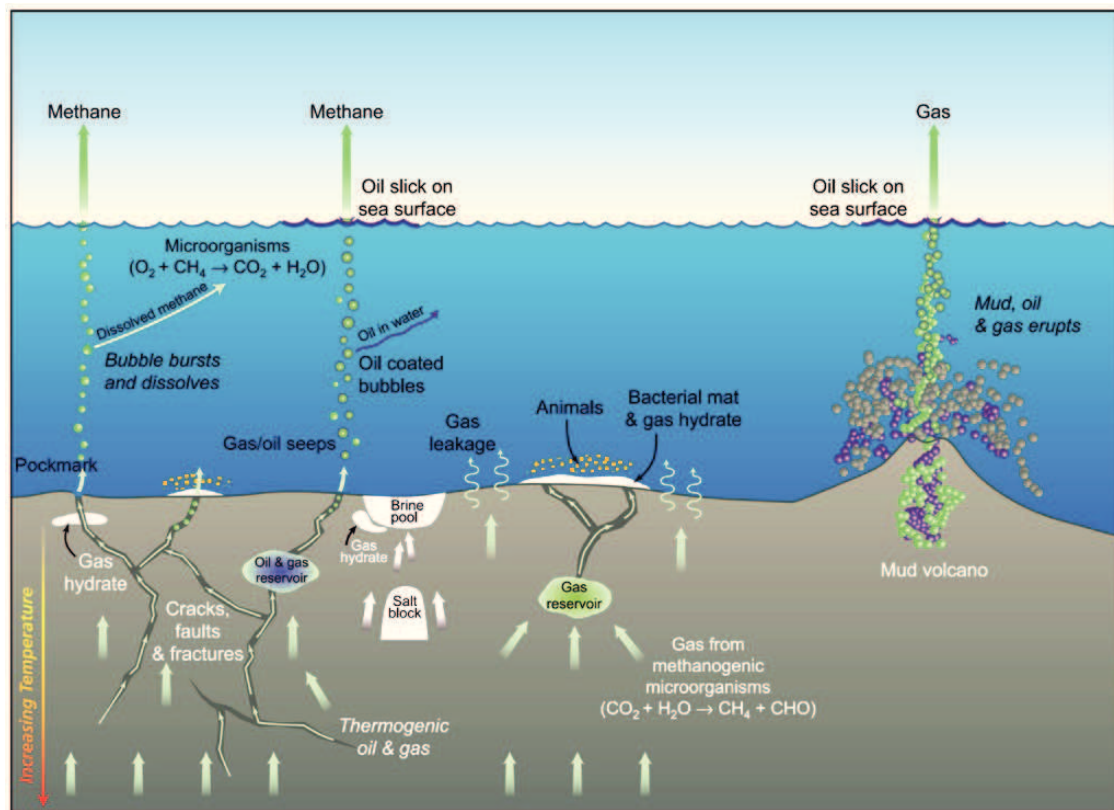


**Figure 4** Summary of methane-related seabed fluid seepage structures, such as gas seeps, mud volcanoes and pockmarks, and the process of methane release from marine sediments to the atmosphere (after Whelan et al., 2005).

The influence of methane from seabed fluid seepage on climate change is not only confined to the modern climate, but also can influence the paleo-climate. According to methane from mud volcanoes alone can generate deep effects on the Earth's climate since the Paleozoic (570 Ma) (Kopf, 2003). A close relationship between global temperature and atmospheric methane concentrations was proved in ice cores from Greenland (over a 40 000 year period; Chappellaz et al., 1993) and Antarctica (over 150 000 years; Jouzel et al., 1993), which suggests a link between methane emissions and the Quaternary glacial-interglacial cycles (Judd et al., 2002a). Moreover, massive methane emission is considered to be responsible for paleo-warming events (Luyendyk et al. 2005; Kennett et al., 2003; Nisbet, 2002), or even mass extinctions (Ryskin, 2003).

### 1.2.1.2 Geological processes

Gases, fluid and gas hydrates within marine sediments can influence the geopressure and physical properties, which are considered the significant factors which shape the morphology of continental margins and the deep-sea basins, and which cause marine geohazards (Fig. 5). Different types of seabed morphologies associated with seabed gas/fluid flow include seeps, pockmarks and mud volcanoes, which will be introduced in details in the following sections. Marine geohazards can be divided into two aspects, one is those associated with natural features and events (slope failures, seismicity, mud volcano eruptions, etc.); the other is those that occur as a result of human's intervention with the natural seabed environment (Judd and Hovland, 2007) (blowouts, such as Gulf of Mexico oil spill 2010 ).
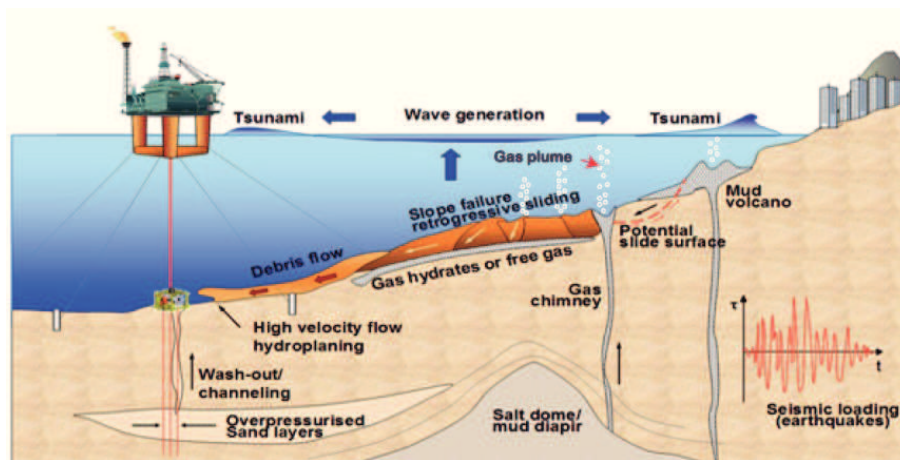


**Figure 5** Schematic diagram shows main marine geohazards, such as slope instability and mass wasting processes, pore pressure phenomena and seismicity. (After http://www.ngi.no/en/Geohazards/Research/ Offshore-Geohazards/).

Submarine slope failure can be triggered by many factors, apart from seismicity, active sedimentation and erosion, salt tectonics (McAdoo et al., 2000), also by gas/fluids and gas hydrates. It is the most serious threat of offshore and coastal areas, because it can give rise to tsunamis. Furthermore, mass amounts of methane may be released into hydrosphere and atmosphere when slope failures occur.

### 1.2.1.3 Benefits

Gas- and oil-related seabed fluid seepage can be used to predict the presence of oil and gas fields or gas hydrate fields (Link, 1952; Kutas et al., 2004), and have guided petroleum exploration for centuries. The methods to investigate the seeps including satellite imaging, acoustic surveying, gravity coring and water column chemical sniffers, etc., which are in low cost to conventional exploration methods, and reduce the risk of exploration (Ding, 2008).

Judd and Hovland (2007) pointed out that fish productivity could be enhanced in seep areas, such as the offshore part of the Eel River Delta, northern California, and North Sea,

which have documented active gas seeps. The biotechnology industry can find new 'resources' in the microbes of chemosynthetic communities of vents and seeps (Querellou, 2003).

### 1.2.2 Related seabed features

### 1.2.2.1 Gas seeps

Gas seeps belong to natural springs where liquid and gaseous hydrocarbons leak out of the seafloor. While freshwater springs are fed by underground water, gas seeps are fed by natural subsurface reservoirs of oil and natural gas.

Gas seeps are generated by focused upward fluid migration (e.g. Judd, 2003), and the composition of gas seep fluids is dominated by methane. Based on the proportion of methane and the different nature of the accompanying fluids, methane seeps could be divided into four groups: (1) those dominated by microbial methane; (2) those dominated by thermogenic methane; (3) seeps associated with gas hydrates from a thermogenic-methane source; and (4) those associated with gas hydrates with a microbial-methane source (Judd and Hovland, 2007). Generally, gas seeps are related to shallow gas/gas hydrate accumulations or deeper hydrocarbon deposits (Kvenvolden, 1993; Buffet, 2000). They are globally distributed (Fig. 3), especially in the marine sediment of modern continental margins (Dimitrov, 2002b; Judd, 2003). However, the exact number and distribution of seep sites have so far not been clarified due to the fact that most of the world's seas and oceans have not been studied sufficiently (Judd, 2003).
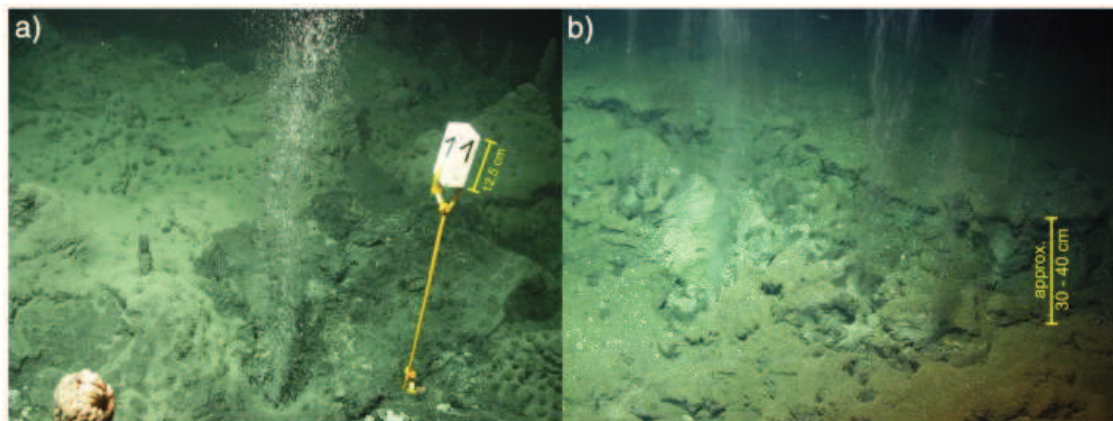


**Figure 6** Gas bubble plumes from the Batumi seep area, Black Sea during ROV observations in spring 2007 (from Pape et al., 2011).

Unique endemic ecosystems of marine organisms could be supported by gas seeps, containing chemoautotrophic clams, tubeworms and bacterial mats, which use the hydrogen sulphide and methane as energy source at the seafloor surface (Hovland et al., 1985; Suess et al., 1985). Aharon (1994), Roberts and Carney (1997), and Olu et al. (1997) suggested that the locations of seeps and the rate, spatial variability and longevity of the flow can be indicated by the cold seep communities.

If methane and other gases are to escape through the seabed into the water column, the flux rate must exceed the microbial utilization rate. At high flux rates, dense bubble plumes (Fig. 6) are generated by large quantities of methane (Michaelis et al., 2002). Gas bubbles rising from the seabed can be detected directly by video observation or as gas flares (Fig. 7) by high-frequency acoustic systems such as echosounders, side scan sonar, and shallow subbottom profiles (Judd and Hovland, 2007). Rising velocities of gas bubbles can also be determined based on visual investigations and hydroacoustic measurements. For example velocities of 19-22 cm/s near the seafloor and 12-14 cm/s at the top of flares are observed at the Dvurechenskiy mud volcano in the Sorokin Trough, Black Sea (Greinert et al., 2006).
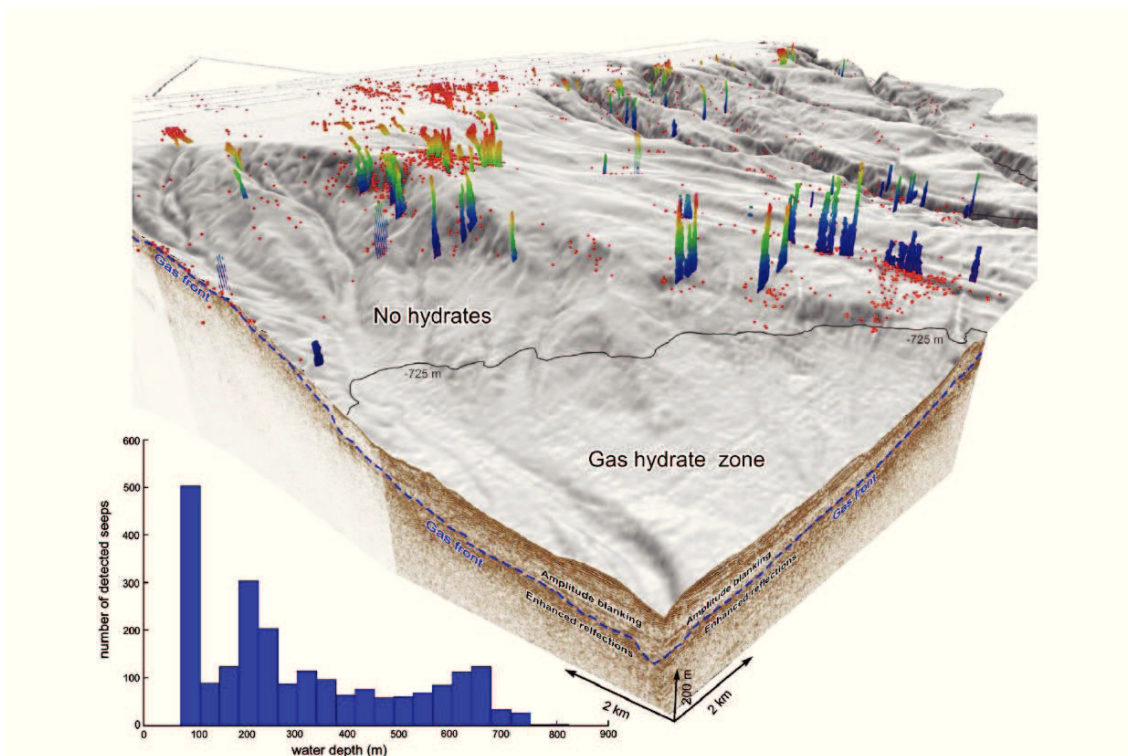


**Figure 7** Numerous methane seeps in the Dnepr paleo-delta, northwestern Black Sea, at water depths of 66 to 825 m (from Naudts et al., 2006).

An abundant presence of methane seeps has been observed at the margins of the Black Sea, such as in the Dnepr paleo-delta, northwestern Black Sea (Fig. 7; Naudts et al., 2006). Gas seeps may occur with or without the formation of pockmarks and mud volcanoes. These morphological features can be easily recognized in bathymetric, side scan sonar and seismic data (e.g. Hovland and Judd, 1988). Gas seeps without apparent morphological features can be detected in backscatter data. High backscatter signatures except those caused by high topographic gradients are thought to correspond to authigenic carbonates, free gas and gas hydrates close to the seafloor or the seep-related chemosynthetic communities, such as tubeworms, mussels and even corals. The high backscatter responses are often characterized by circular or flow-like shape (Anderson and Bryant, 1990; Sager et al., 2003). Shallow gas accumulation or columns of focused

fluid migration related to seeps can be indicated by the acoustic anomalies in seismic data (Judd and Hovland, 2007; Wagner-Friedrichs, 2007).

### 1.2.2.2 Mud volcanoes

One of the most important types of gas seep-related structures is mud volcanoes, which reveal a morphology positive (Fig. 4). Mud volcanoes are present in many parts of the world, on land as well as offshore (Fig. 3), including the shallow waters of continental shelves, the deep waters of the continental slopes and rises, and the deep-sea basins (Milkov, 2000; Dimitrov, 2002b; Kopf, 2002). The number of mud volcanoes reaches about 1000 onshore, 500 on the continental shelves, and 5000 in deep waters; however, the offshore estimates are very speculative (Judd and Hovland, 2007). Onshore mud volcanoes have been well studied for over 200 years (Ansted, 1866), but research on offshore mud volcanoes just began ~40 years ago (Dimitrov, 2003). There are some well-known mud volcano areas, like the Black Sea and the Caspian Sea (Ginsburg and Soloviev, 1994; Ivanov et al., 1996; Limonov et al., 1997), the Norwegian Sea (e.g. Hovland and Judd, 1988), the Gulf of Mexico (Kohl and Roberts, 1994), the Mediterranean Ridge (Ivanov et al., 1996; Woodside et al., 1997), etc.

Mud volcanoes form because of the emission of clay materials and fluids, including sediments, gas, water, brine or oil (Milkov, 2000). The solid component of the emission products of a mud volcano is generally known as mud breccias, which range in diameter from a few millimeters to more than 10 meters. Mud breccias, gas and water emitted at mud volcanoes are mainly sourced in rocks and muddy sediments at greater depth of several km. The emitted gas usually shows a mixed composition including biogenic and thermogenic gas (Dimitrov, 2002b; Kopf, 2002). Mud diapirs can also be termed a "mud volcano" when they reach the seafloor, based on the evidence of extruding sediment and/or fluid, which are the sediment (generally muddy or shaly) structures that have arisen through a sedimentary sequence, piercing or deforming younger sediments (Judd and Hovland, 2007). What are the main driving forces for mud volcanoes and diapirs formation? Dimitrov (2002b) lists the three driving forces: 1. Internal buoyancy forces caused by density inversion of light, gasified, buoyant, plastic clays beneath a denser overburden; 2. High pore-fluid pressure, provided by expanding gases, trapped inside the plastic clays and other internal processes; 3. Structurally or tectonically induced high pore-fluid pressure. Individual factors may vary in the different regions.

Submarine mud volcanoes are essentially similar to those found on land. Their geometry and size varies in connection with the nature (viscosity, density, grain size) of the emission products, the nature and frequency (slow, rapid, or even explosive) of the emissions, and the volumes of the material and fluids produced. For example, the lower the viscosity, the larger and flatter the body; the higher the pore-fluid pressure, the more violent the eruption; the more frequent the activity, the larger the structure (Dimitrov, 2002b; Judd and Hovland, 2007). The area of mud volcanoes may vary from 10 m² up to 100 km², heights change from one to two meters to several hundred meters, and diameters range from only a few meters to several kilometers (Jakubov et al., 1971; Sturz et al., 1992; Dimitrov, 2002b; Kopf, 2002). The general structure of a mud volcano is shown in Figure 8. Generally, emission products of a mud volcano are extruded from the

main conduit called feeder channel. The outcrop of the feeder channel is named a central crater, which can have several different shapes, including classic volcano cone shape, or other forms like sharp cones, domes, flat plateau, shallow depressions, and calderas. Large mud volcanoes may be composites with several craters of different shapes (Dimitrov, 2002b; Judd and Hovland, 2007). Smaller lateral pipes can branch off the feeder channel to the flanks of the mud volcano structure, called griphones (Dimitrov, 2002; Kopf, 2002).
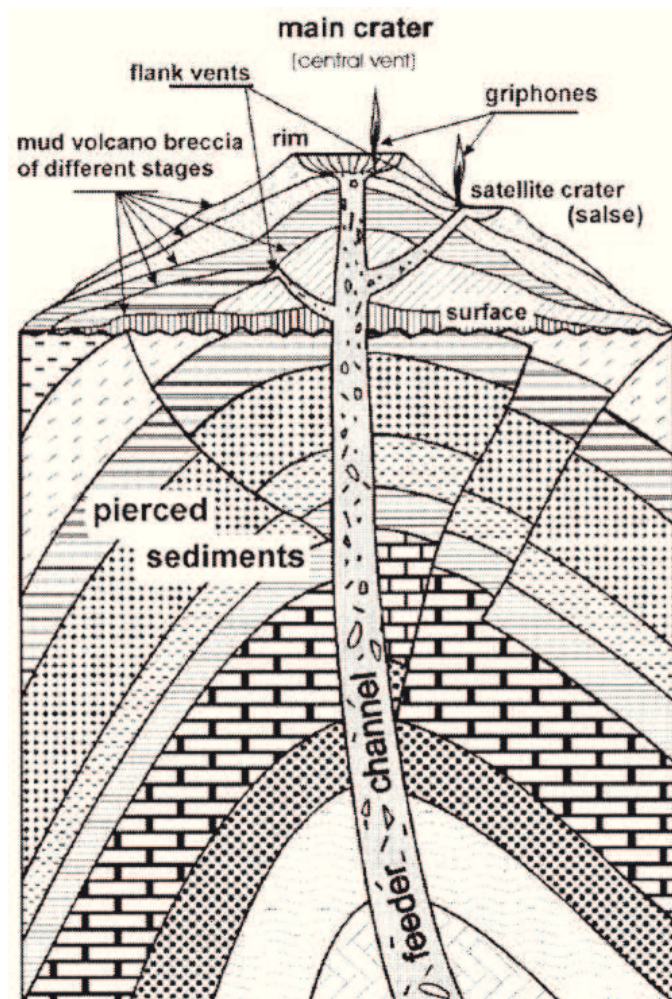


**Figure 8** The general structure and main elements of a conical mud volcano, (from Dimitrov, 2002b)

Milkov (2000) and Judd and Hovland (2007) suggested criteria for recognizing submarine mud volcanoes, as shown below:

- Core samples showing 'mud breccia' containing sediments with a range of different ages, compositions and structures.
- Strong backscatter on side-scan sonar records representing topographic features (craters, cones, mud flows, etc.).

- Evidence of gas seepage and associated features (bacterial mats, cold-seep communities or Methane-derived authigenic carbonate – MDAC).
- High backscatter from ejected rock clasts, and/or from cold-seep communities and MDAC.
- Seismic evidence of feeder channels and/or mud diapirs.
- (For deep-water mud volcanoes) gas hydrates in an otherwise hydrate-free area.

Mud volcanoes can provide an extremely fast-rising stream of gas not only during eruptive phases characterized by mostly short periods (hours to days), but also even during periods of quiescence (years to centuries) (Dimitrov, 2002; Kopf, 2002). In addition, the global methane flux from mud volcanoes nearly equals the global gas flux. Mud volcanoes have also been considered a source of fossil gases in the atmosphere (Milkov et al., 2003; Etiope and Milkov, 2004). Mud volcanoes are a source of methane flux from lithosphere to hydrosphere and atmosphere (greenhouse effect and climatic change). Milkov (2000) summarizes further importance of research on submarine mud volcanoes as follows: 1. They could be the indicators of high petroleum potential in the deep subsurface; 2. Useful data about the sedimentary section in mud volcanic areas can be determined by examination of rock fragments incorporated in mud volcanic sediments (breccias); 3. Drilling operations, ring installations and pipeline routings may be impacted by the activity of submarine mud volcanoes; 4. Gas hydrates associated with deep-water mud volcanoes are a potential energy resource.

### 1.2.2.3 Pockmarks

In contrast to mud volcanoes, pockmarks are negative morphological features (crater-like depressions), which commonly occur worldwide (Fig. 3) where fluid flow is focused and escape is from low-permeability and fine-grain seabed sediments (Hovland and Judd, 1988). Pockmarks were first discovered on the continental shelf offshore Nova Scotia, Canada after the advent of acoustic areal mapping systems (King and MacLean, 1970).

The composition of fluids generating the pockmarks can range from oil, thermogenic and biogenic gas (methane), to pore water (brine) and even fresh water (ground water) (Hovland and Judd, 1988; 2003; Schroot et al., 2005; Gay et al., 2006). Pockmarks can not only occur as single isolated depressions, but also as pockmark fields or as strings of pockmarks (Hovland et al., 2002). The size and shape of pockmarks depend on the capacity, overpressure and fluid composition of the involved fluid reservoir (Hovland and Judd, 1988), the nature of the fluid escape (Bøe et al., 1998), the rheology and grain size of the seabed sediments and the relations of the underlying structures that facilitate fluid flow (Gay et al., 2006). There are many varieties of shapes, the most common pockmarks are circular and elliptical (Fig. 9). Generally, pockmarks range in diameter from 50 to 100 m with depths in the range of 1-3 m. Moreover, in the deepest parts of basins, the sizes of pockmarks are larger than 100 m (Judd and Hovland, 2007). Pockmarks are not only found on the seafloor, but also in the various sediment horizons (Long, 1992), which are called buried or fossil pockmarks. These features can be identified on two-dimensional and three-dimensional seismic profiles.
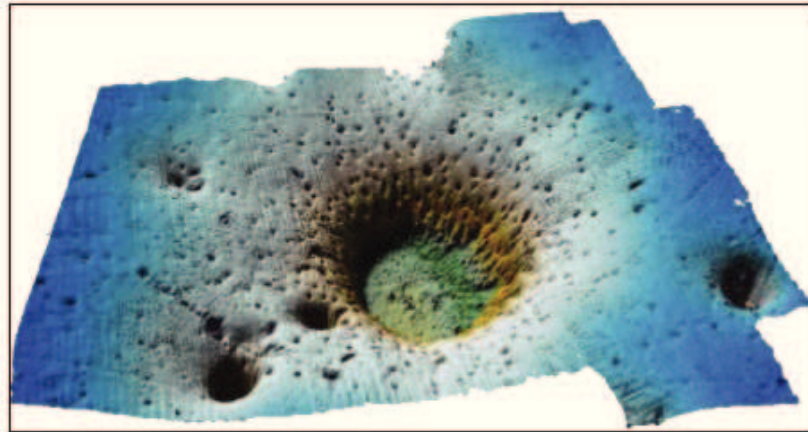
**Figure 9** Bathymetric image of a pockmark from the North Sea (from http://folk.uio.no/karenel/research.html)

Nowadays, pockmarks as an important geological phenomenon have become favored research objects. Pockmarks may be of significance to the energy industry, because they are important indicators of gas-escape events, which usually occur above the hydrocarbon fields. Pockmarks are frequently correlated to carbonate precipitates, unusual biological activity, and underground fluid flows. Hovland et al. (2002) suggests that pockmarks have great significance as natural monitors of the underground fluid pressure domain in earthquake-prone regions. On the other hand, pockmarks are used to indicate the subsurface hydraulic activity that may lead to the slope failure and seabed instability (Hovland et al., 2002; Judd and Hovland, 2007).

**1.2.2.4 Other related features**

While mud volcanoes and pockmarks are the best-known gas seep- and fluid flow-related features, there are still some other, less well-known features. According to Judd and Hovland (2007), they are as follows: seabed doming, collapse depressions, freak sandwaves, shallow mud diapirs and mud volcanoes, Red Sea diapirs, sand intrusions and extrusions, diatremes, and polygonal faults. All these features include the movement of fluids/gas within sediments, and through the seabed mostly. The differences of them result from individual local conditions (Judd and Hovland, 2007).

**1.3 Gas hydrates**

Gas hydrates are also called gas clathrates. Natural gas hydrates are crystalline solids composed of water and gas that form at high pressure and low temperature. The gas molecules (guests) are trapped in water cavities (host) that are composed of hydrogen-bonded water molecules. The gas molecules include methane, ethane, propane, and carbon dioxide (Sloan and Koh, 2008). However, most gas hydrates in nature consist of more than 99% methane from among the hydrocarbons, and are therefore known as methane hydrates (Sloan, 1998; Kvenvolden and Lorenson, 2001).

The three main different crystal structures of gas hydrates are known as Structures I, II and H (Fig. 10) (Sloan, 1998). The Structures I and II were investigated with X-ray diffraction methods by von Stackelberg and Müller (1954). The Structure H was first reported by Ripmeester et al. (1987). The three structures have different types of cavities. Structure I and II have two types of cavities, while Structure H has three types of cavities. Gas hydrates with Structure I are most common in marine sediments and mostly contain methane with a small amount of $CO_2$ and $H_2S$. Significant amounts of propane and higher-carbon gases in gas hydrates can form Structure II or H. While structures I, II and H are the most common clathrate hydrates, a few other clathrate hydrate phases have also been identified (Sloan and Koh, 2008). For example, Dyadin et al. (1997) first reported the existence of a new methane hydrate phase at very high pressures (500 MPa).
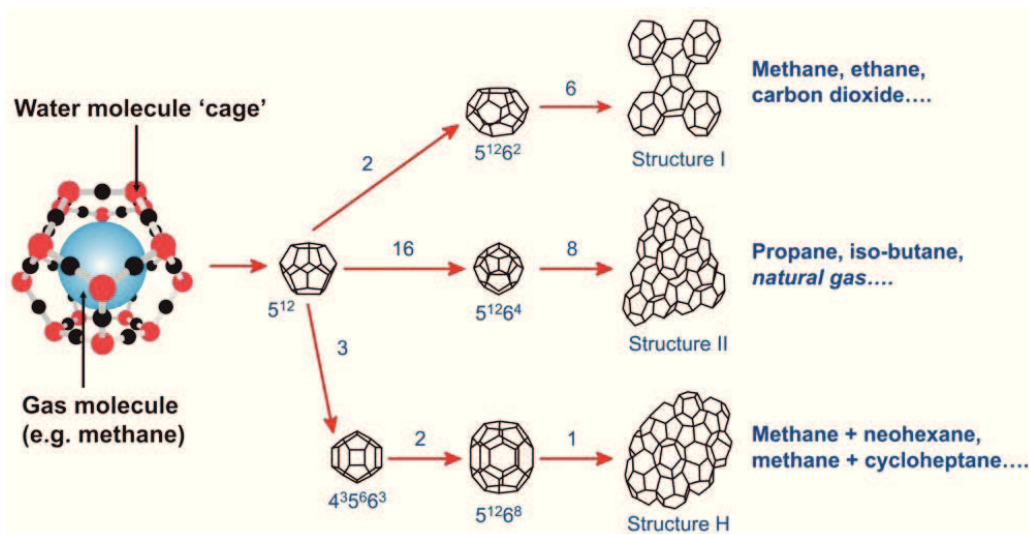


**Figure 10** The three primary unit crystal structures of gas hydrates: Structure I, Structure II and Structure H. Pure methane and ethane form Structure I hydrate, but certain compositions of their mixtures undergo phase transition to form Structure II hydrates. The structure-H has three different types of cavities, three $5^{12}$ cavities which are common to all known hydrate structures, two new 12-faced $4^3 5^6 6^3$ cavities, and one new large $5^{12} 6^8$ cavity. Picture taken from http://www.pet.hw.ac.uk/research/hydrate/hydrates_what.cfm

In the last decades, gas hydrates (methane hydrates) have become of major interest, because they are not only seen as an important future natural energy resource, but also as a potential factor for producing geological hazards and playing a role in the global climate change. Natural gas hydrates are known to exist all over the world (Fig. 3), but need the suitable pressure and temperature conditions. They can occur in permafrost regions (Fig. 11) at depths shallower than ~1 to 2 km, and in the uppermost tens to several hundreds of meters of marine sediments on continental margins with water depths greater than ~300 m (Kvenvolden and Barnard, 1983; Kvenvolden, 1993; Ruppel, 2011). The estimated amount of gas in the hydrate accumulations of the world greatly exceeds the volume of known conventional gas reserves. World estimates for the amount of natural gas in gas hydrate deposits range from 14 trillion to 34,000 trillion cubic meters of permafrost areas and from 3,100 trillion to 7,600,000 trillion cubic meters of oceanic sediments. The estimates of the amount of methane in the world's gas hydrate accumulations are in rough accord at about 20,000 trillion cubic meters (Max, 2000).
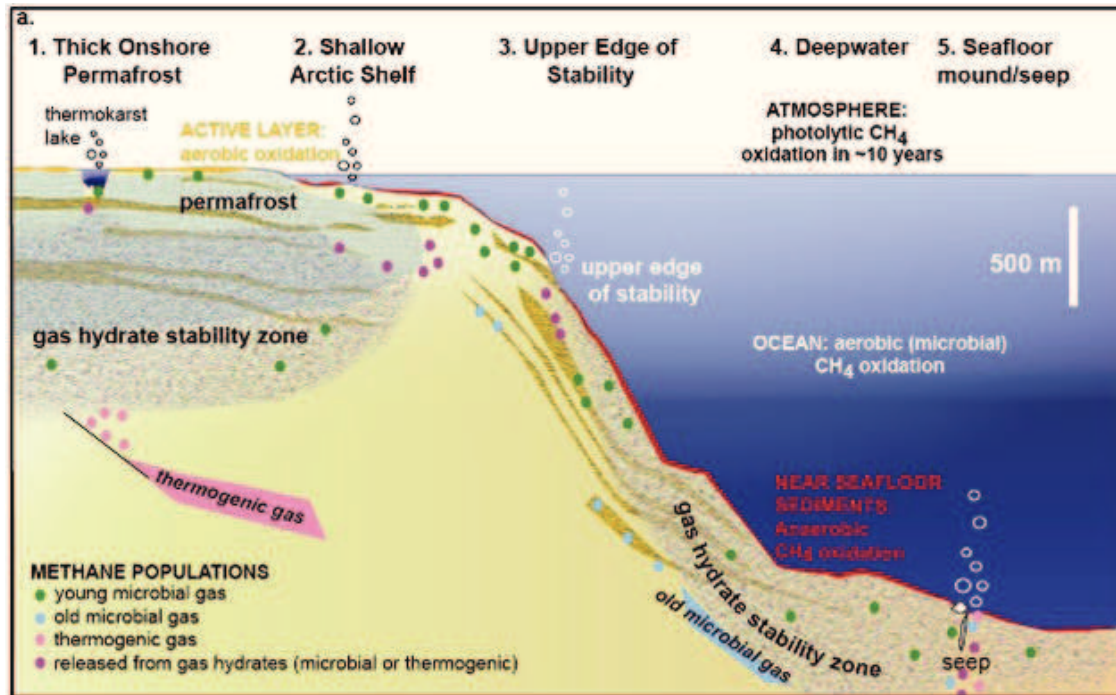
**Figure 11** Gas hydrates occur in five different geographic settings: 1. onshore permafrost; 2. shallow offshore subsea permafrost; 3. upper continental slope; 4. deepwater; 5. an area of gas seeps (from Ruppel, 2011)

Generally, gas hydrates are stable in the subsurface under suitable pressure–temperature conditions in most part of the world. In practice, the thickness of the gas hydrate stability zone (GHSZ) is defined with the seafloor as its upper limit and the depth of the intersection of the geothermal gradient and of the methane hydrate stability in equilibrium with pure or sea water as the lower limit (Fig. 12) (Kvenvolden 1988; Ginsburg and Soloviev 1997). However, favorable stability conditions of pressure–temperature are not the only requirement; sea bottom temperature, gas composition, salinity of water and local geology can also control the stability of gas hydrate (Kvenvolden 1993). In fact, it is difficult to estimate the thickness of the GHSZ accurately when these parameters present variations in situ and can't be precisely predicted (Ginsburg and Soloviev 1997; Thakur and Rajput, 2011). But the theoretical depths of the base of GHSZ beneath the ocean can be estimated by assuming the following conditions: constant hydrostatic pressure gradient, typical hydrothermal gradient, variable geothermal gradient, methane hydrate co-located with water and methane mixed with other gases (Thakur and Rajput, 2011).

Methane, which is the prime constituent of gas hydrates, can be generated in the earth from different physical, chemical and biological processes. The origins of the methane forming methane hydrates in continental margin sediments are summarized as follows: (1) biogenic methane is formed in sediments by the decomposition of the organic matter, which is because of biological processes and chemical reactions, within the GHSZ (Claypool and Kaplan, 1974); (2) upward migration of methane rich fluids (thermogenic)

from deeper sources in the earth (Kvenvolden and McDonald, 1985); (3) recycling of methane during the process of hydrate dissociation accompanying sedimentation (Paull et al., 1994).
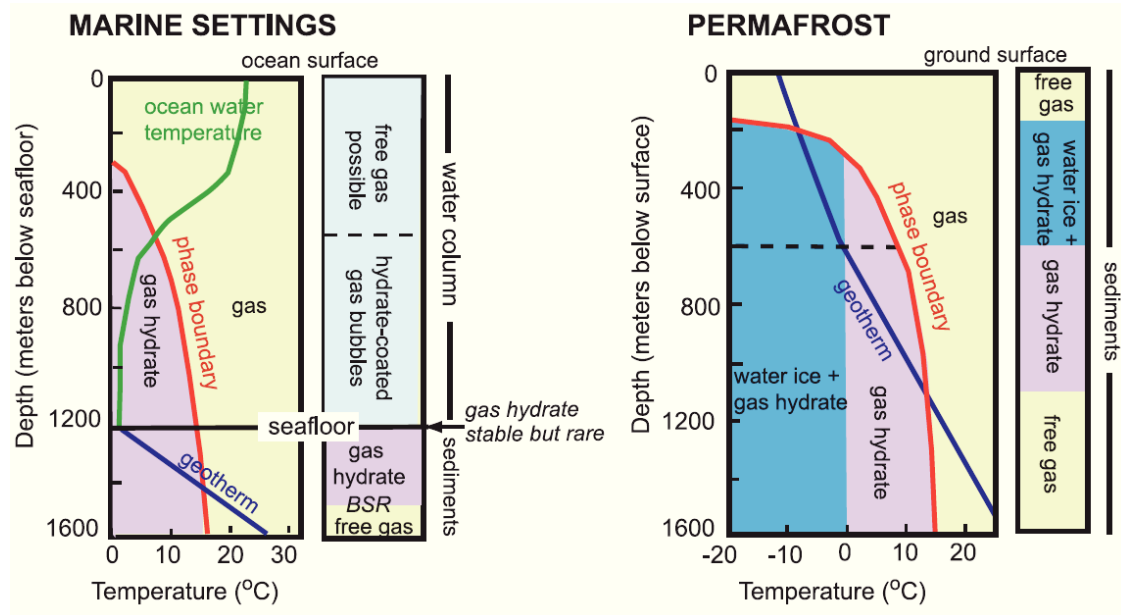


**Figure 12** Pressure–Temperature conditions and methane hydrate stability in (left) marine settings and (right) permafrost settings (from Ruppel, 2007).

Gas hydrate in marine sediments can usually be inferred from the bottom-simulating reflector (BSR) in seismic reflection profiles (e.g. Kvenvolden and Barnard, 1983). Most BSRs are formed due to the high acoustic impedance contrast between gas hydrates and associated free gas underneath (Fig. 13). They can cut across the stratigraphy of sediments, are roughly parallel to the topography of the sea floor, and generate a strong reflector with reversed polarity relative to the seafloor (Dillon and Paull, 1983; Thakur and Rajput, 2011). Gas hydrate can also occur without a BSR, and the existence of a BSR is no guarantee that there are detectable amounts of gas hydrates or free gas in the sediments (Paull, 1997). The controls on the formation of BSR are not well understood (Holbrook et al., 2002). From the depths of BSRs and the bottom water temperature, the geothermal gradient and heat flow can be estimated (Shipley et al., 1979, Yamano et al., 1982).

Gas hydrate formation is controlled by different geological processes like sediment deposition and distribution, diapirism, and fluid migration features. These geological processes can shape a potential gas hydrate reservoir (Thakur and Rajput, 2011). As for sediment deposition, the hydrate accumulation is controlled by the deposition rate and the nature of host sediment as much as by the presence of the necessary "ingredients" and conditions (water, gas, nucleation sites, temperature and pressure). During diapirism, increased heat flow above the diapir and its upward migration can cause the base of the gas hydrate to move up from the diapir, creating a dome at the base of the hydrate-cemented sediment (Dillon et al., 1980; Macleod, 1982). Because gas-charged mud is a potential source of diapir, the dome can be used as a trap for the gas released by

disintegrating gas hydrate above the diapir and gas migrating up-dip from strata surrounding it (Thakur and Rajput, 2011). Upward fluid migration, whether dispersed or focused, is one of the main processes in the formation of gas hydrates. Associated features, such as pockmarks, mud volcanoes, or fault zones, can therefore be considered geological indicators to locate possible gas hydrate zones (Milkov, 2000).
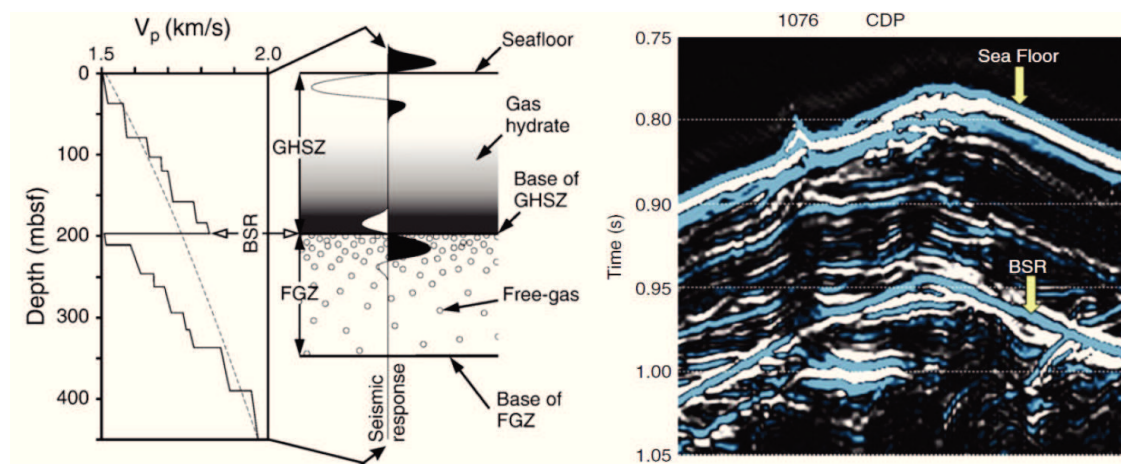


**Figure 13** Illustration of a submarine sedimentary section containing gas hydrates (above) and free gas (below) the bottom-simulating reflector (BSR) (Haacke et al., 2007) (left). A classic example of identified BSR is from Hydrate Ridge Offshore USA (from Thakur and Rajput, 2011) (right).

Various means, including geophysical, geological and geochemical investigations, can be used to identify and assess gas hydrate bearing sediments. Among those, geophysical investigations are the most popular and most important. There are several different geophysical techniques including many kinds of types of seismic survey (e.g. 2D/3D conventional, ocean bottom seismic (OBC), vertical seismic profiling (VSP), cross-well seismic and multi-component), well logging, and controlled-source electromagnetic surveys, which are used for gas hydrate exploration. Seismic indicators are the main characteristics for the identification of gas hydrate and associated free gas. Beside the BSR, seismic indicators also include Bright Spots, enhanced seismic reflections, seismic chimneys, hydrate mounds and amplitude blanking and so on (Thakur and Rajput, 2011). Based on these anomalous seismic signatures, gas hydrate-free gas system models can be established to illustrate the occurrence of gas hydrates and migration of free gas, etc.

Nowadays, an interest in natural gas hydrates as a potential energy resource has grown significantly as awareness of the volumes of recoverable gas, which becomes more focused (Sloan and Koh, 2008). The amount of gas hydrates has very significant implications for worldwide energy supplies when it becomes technically and economically viable to produce. There are still several unresolved challenges before full-scale hydrate reservoir exploitation: (1) localizing, characterizing, and evaluating resources; (2) technology for safe and economic production; (3) safety and seafloor stability issues related to drilling and production (Geir, 2010). Comprehensive mapping of hydrate has been carried out at many of the world's continental margins in recent years;

numerous countries such as the United States, Japan, India, and South Korea are showing substantial interest in exploiting this resource over the long term.
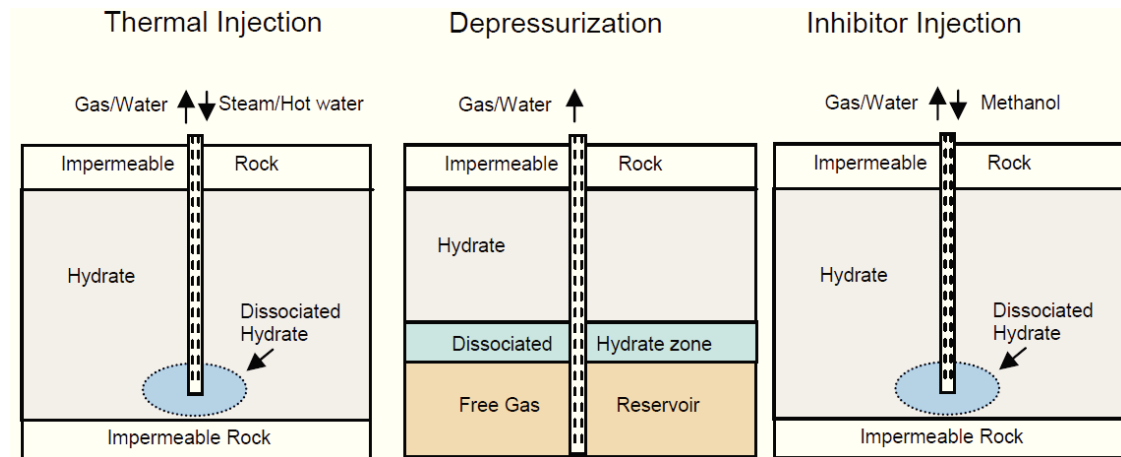


**Figure 14** Gas hydrate production options (from Geir, 2010)

In order to produce natural gas from hydrates, it is necessary to dissociate the hydrate. Based on the dissociation techniques involved, the exploitation methods are divided into three major potential gas production methods, which are illustrated by Geir (2010) (Fig. 14) as follows: (1) the thermal stimulation method involves dissociating hydrates by increasing the in situ temperature above the gas hydrate equilibrium point - as illustrated, hydrate reservoirs are heated by injecting hot water, steam, or hot salt water; (2) the depressurization technique is the method of discharging part of the gas from the gas hydrate reservoir to reduce pressure below the hydrate equilibrium value, making hydrate become unstable and decompose; (3) the chemical injection method utilizes some kind of thermodynamic inhibitor, such as salts and alcohols, which cause a shift in the P-T equilibrium. Beside the traditional methods, some new exploitation methods have also been proposed, such as $CO_2$ replacement, electromagnetic heating, and microwave heating (Geir, 2010; Liu, 2012).

## 1.4 Main objectives of this study

The main scientific goal of the PhD study is to understand the interaction and relationship between gas/gas hydrate reservoirs, gas transport, near-subsurface structures, sedimentary processes, tectonic movements, and the occurrence and evolution of seabed fluid seepage. The Black Sea provides excellent conditions for these investigations, because it is the world's largest anoxic basin and the largest surface reservoir of dissolved methane. A thick sedimentary coverage is combined with compressive deformation at the margins, caused by the collision between Arabia and Eurasia since the Eocene. Methane seeps, mud volcanoes, and gas hydrates are well known in the continental margins and deep sea basin. In order to achieve the goals, two study areas were chosen from the Black Sea: the central Black Sea and the Kerch Peninsula margin, which will be introduced in detail in Chapter 1.5.

The specific objectives of this study have been focused on the following aims and questions:

- To map and seismically characterize mud volcanoes and gas seeps together with the subsurface structures
- To study gas/fluid migration pathways, shallow gas reservoirs and the GHSZ related to the mud volcanoes and gas seeps
- To analyze the sedimentary processes and tectonic movements of the Kerch Peninsula margin
- To study the formation reasons of the Kerch seep area within the GHSZ and the gas seeps on the upper slope above the GHSZ
- To develop geological models for the mud volcanoes and gas seeps

To serve these specific objectives, proper datasets are required, which can reveal near-surface features of the seepage area and further hints into the geological processes behind these features. The main datasets from the two study areas were collected on two cruises on board R/V METEOR to the Black Sea. High-resolution multichannel seismic was chosen as the main dataset, combined with Parasound sediment echosounder and Hydrosweep swath bathymetric datasets. These provide detailed subsurface structural information and seafloor morphological features. Datasets and methods are described in detail in Chapter 1.6.
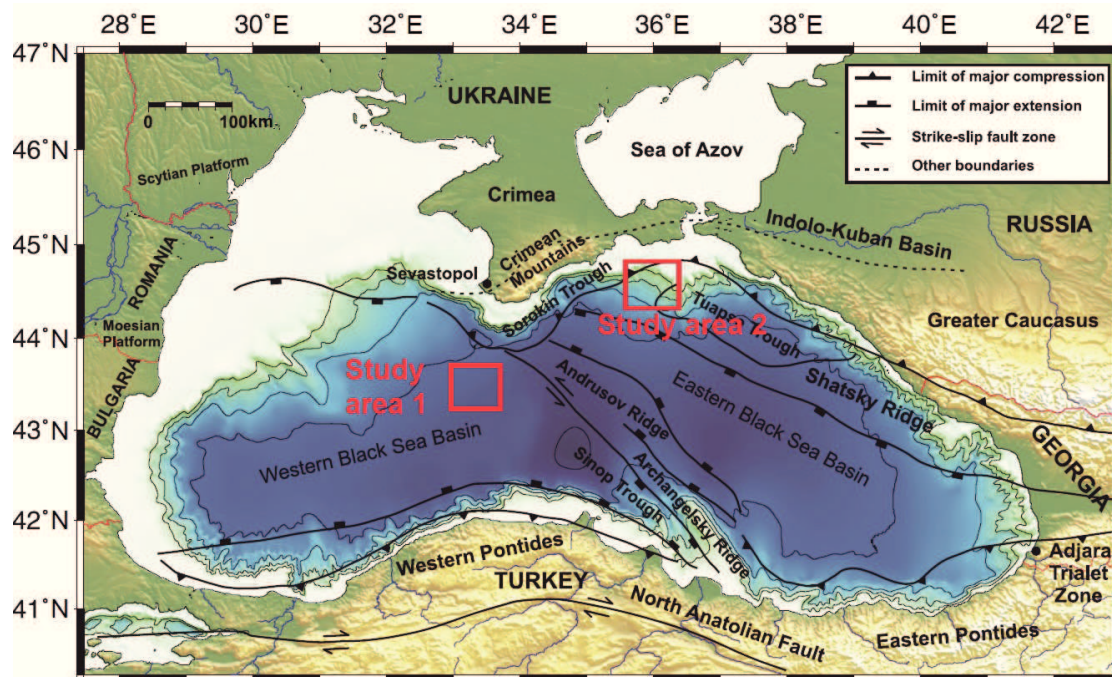
## 1.5 Geological setting of the Black Sea



**Figure 15** General geological structures and tectonic elements of the Black Sea (modified after Wagner, 2007 and Robinson et al., 1996) combined with bathymetric map of the Black Sea (Gebco 1-min grid). Two study areas are marked by red rectangles.

The Black Sea basin is surrounded by Late Cenozoic mountain belts (the Great Caucasus, Pontides, Southern Crimea and Balkanides), and represents the world's largest anoxic intercontinental basin with a maximum water depth of 2200 m (Finetti et al., 1988; Nikishin et al., 2003). It is composed of two deep sub-basins, the Western Black Sea basin and the Eastern Black Sea basin (Fig. 15). The Western Black Sea basin is underlain by oceanic to sub-oceanic crust and contains a sedimentary cover of up to 19 km thickness, and the Eastern Black Sea basin is underlain by a thinned continental crust approximately 10 km in thickness and up to 12 km thickness of sediments. These basins are separated by the Andrusov Ridge (Finetti et al., 1988; Beloussov and Volvovsky, 1989; Robinson, 1997; Nikishin et al., 2003), which is formed by a continental crust overlain by 5-6 km of sediments (Nikishin et al., 2001, 2003).

It is generally agreed that the Black Sea was originated by a back-arc extension due to the subduction of the Thetyan Ocean in the Late Cretaceous, and has undergone compressive deformation due to subsequent collision between the African and Eurasian plates since the Eocene (Fig. 16) (Dercourt et al., 1986; Zonenshain and Le Pichon, 1986; Görür, 1988; Robinson et al., 1995; Spadini et al., 1996; Nikishin et al., 2003). The Western Black Sea Basin is considered to be older than the eastern Black Sea Basin (Banks and Robinson, 1997). It opened by the separation of the Western and Central Pontides continental strip from the Moesian Platform and Odessa Shelf in the Mid-Cretaceous (Robinson et al., 1996). The timing of the opening of the eastern Black Sea

Basin is less certain; it probably started during the middle Paleocene (Banks and Robinson, 1997). A coeval opening of both the western and eastern sub-basins was suggested by different researchers (Zonenshain and Le Pichon, 1986; Nikishin et al., 2003). At the end of the Eocene, two new sedimentary realms on both sides of the alpine orogenic belts were formed: the Mediterranean Sea to the south, and the Paratethys to the north. The Black Sea belongs to the Eastern Paratethys (Gillet et al., 2007). During the late Eocene to middle Miocene, the Paratethys was characterized by a long-term trend of decreasing marine influence. At the Miocene-Pliocene boundary, an important event is the Messinian Salinity Crisis, which caused a dramatic fall in sea level and erosion surfaces on the shelves (Gillet et al., 2007). The Black Sea region did not connect to the Mediterranean Sea, but only connected to the Caspian Sea by the northeast pathway (Paluska and Degens, 1979; Popov et al., 2004). Gillet (2007) confirms that the Black Sea was severely affected by the Messinian Salinity Crisis and suffered a drastic lowering of its water level at the end of the Messinian. During the middle Pliocene to late Pliocene, the development of the present-day paleogeographic features and river systems were initiated by vertical movements (Popov et al., 2004). The climate of the Black Sea has undergone a series of glacial and interglacial events, (transgessive-regressive cycles) accompanied by intensive tectonic movement in the Quaternary, and the shelf was either uplifted above sea level in large areas or covered with sea water. This is recognized as Gurian, Chaudian, Old Euxinian, Euxino-Uzunlarian, Karangatian, Post-Karangatian, New Euxinian regional stages (Gozhik et al., 2008). The early Quaternary section was dominated by a shallow marine environment, which changed rapidly into a deep water environment (Paluska and Degens 1979). The increased sediment supply led to high sedimentation rates and significant subsidence, but the water depth decreased only slightly to the present depth of 2200 m (Robinson et al., 1995). Sedimentation rates for the Pliocene-Quaternary are estimated to be not less than 10 cm/kyr (Limonov et al., 1994). The margins of the Black Sea are recently characterized by compressive deformation (Robinson et al., 1995; Spadini et al., 1996). Stress field observations and GPS data support the idea that the Black Sea region is still in a predominantly compressional environment (Reilinger et al. 1997).

Nowdays the only connection to the global ocean is provided by the narrow and shallow Bosporus Strait (~ 36 m deep) in the Southwest. In the North, the Black Sea is connected by the Kerch Strait to the Sea of Azov. Several major rivers, such as the Danube, Dniester and Don bring a large sedimentary influx to the northern and northwestern margin of the Black Sea, generating wide continental shelves. Only a few small rivers drain into it from the South.

For the western and eastern Black Sea basin, five main seismic sedimentary units have been distinguished: (1) the upper Cretaceous, dominated by carbonates with a thickness of 5-6 km in the west and 3-4 km in the east, (2) the Paleocene-Eocene unit of terrigeneous and carbonate components of 5 km in the West and 3 km in the East, (3) the Oligocene-Lower Miocene clays of the Maikopian Formation with a thickness of 5 km in the West and 4 km in the East, (4) the Middle-Upper Miocene unit composed of terrigenous siliciclastic material with a thickness varying from several hundred meters to 3 km, and (5) the Pliocene-Quarternary consisting mostly of clays with a thickness of 2-3.5 km in the inner parts of basin (Tugolesov et al., 1985; Nikishin et al., 2003). The five

main sequences consist of nearly horizontal and undeformed layers within the basin. The basement beneath is disrupted by several normal faults, supporting the extensional origin of the basins (Tugolesov et al., 1985; Zonenshain et al., 1986).
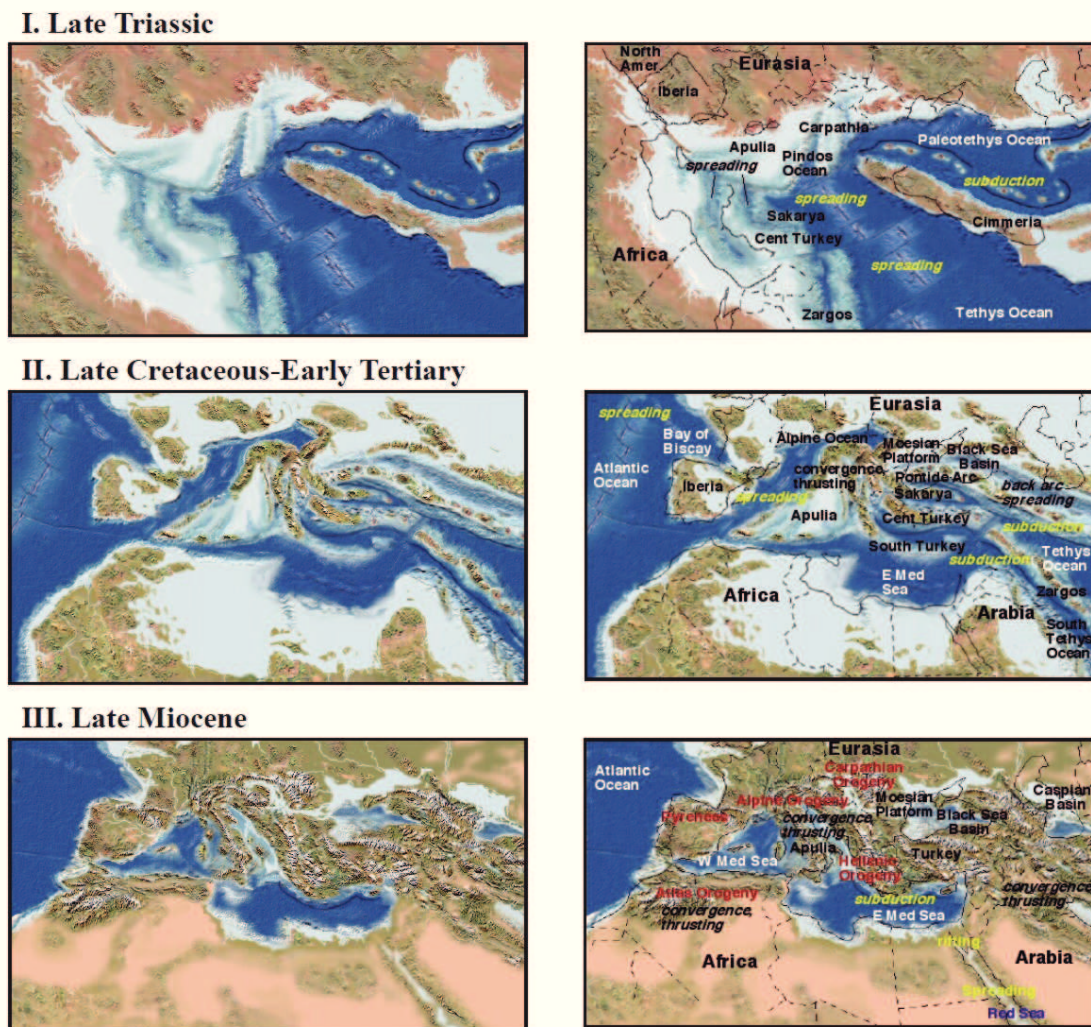


**Figure 16** The three panels I-III present the plate tectonic development history of the Mediterranean and Black Sea regions since the Late Triassic (I) through the Late Cretaceous-Early Tertiary (II) to the Late Miocene (III). Picture reference: http://jan.ucc.nau.edu/~rcb7/paleogeographic_alps.html.

The Black Sea is well known for the presence of gas seeps and seep-related structures (Fig. 17), such as mud volcanoes, which have been reported from various areas, e.g. at the north-western margins (Shnukov et al., 1995; Peckmann et al., 2001; Michaelis et al., 2002; Mazzini et al., 2004; Naudts et al., 2006), in the central and north-eastern parts (Ivanov et al., 1989, 1998; Ginsburg et al., 1990; Limonov et al., 1994; Woodside et al., 1997; Kenyon et al., 2002; Blinova et al., 2003; Bohrmann et al., 2003; Krastel et al., 2003; Aloisi et al., 2004; Mazzini et al., 2004; Greinert et al., 2006), as well as along the south-eastern slopes of the Black Sea (Kruglyakova et al., 1993; Cifci et al., 2002; Ergün et al., 2002; Klaucke et al., 2006). Gas hydrates in the Black Sea were sampled for the

first time in 1974. This recovery was the first direct observation of natural gas hydrates in marine sediments in the world (Yefremova and Zhizhchenko, 1974). The area of the Black Sea that is suitable for gas hydrate formation is about 288,100 km$^2$ theoretically, representing about 68% of the total Black Sea or almost 91% of the deep-water basin (Vassilev and Dimitrov 2002). The typical bottom water temperature is 9°C, which results in stable gas hydrates below a water depth of 700 m (Ginsburg et al., 1990).
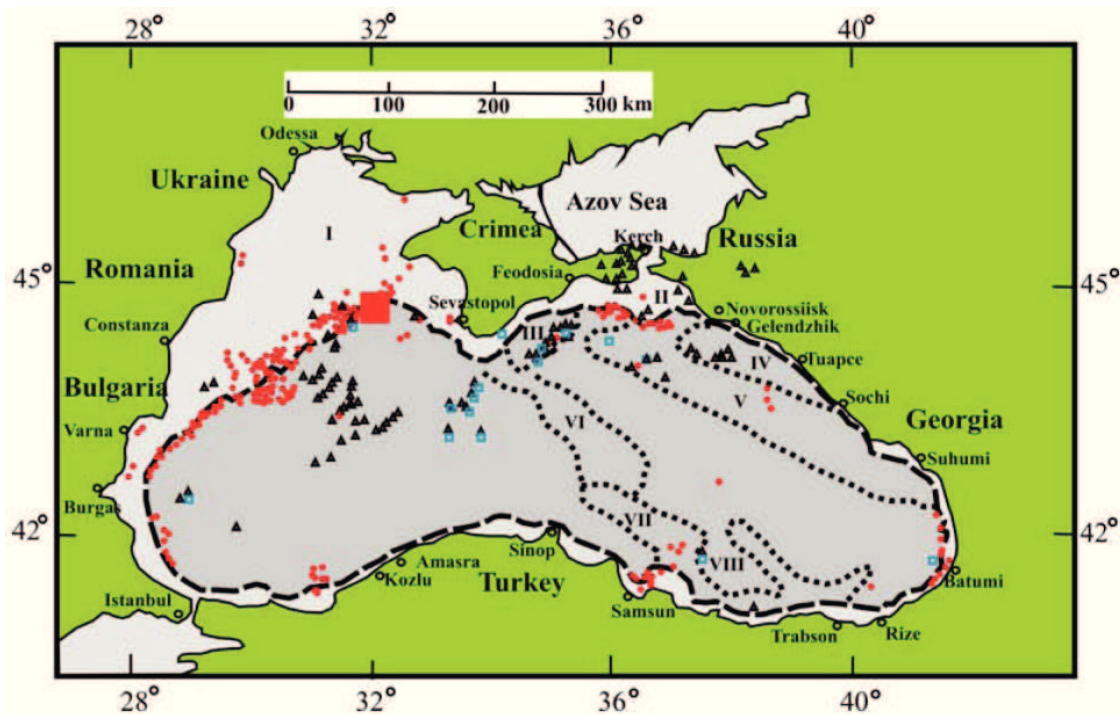


**Figure 17** Location of the mud volcanoes gas seeps and gas hydrates in the Black Sea (C¸ ifc¸i et al. 2002; Kutas et al. 2002; Vassilev and Dimitrov 2002; Egorov et al. 2003; Shnyukov and Ziborov 2004; Klauke et al 2006; Popescu et al. 2007). Triangles in black, mud volcanoes; circles in red, gas seeps; squares in ice blue, gas hydrate; bold dashed lines in black, shelf edge; bold squared lines, boundaries of tectonic units; filled rectangles in red, Dnipro palaeo-delta area; I, NW Shelf; II, Kerch-Taman trough; III, Sorokin trough; IV, Tuapse trough; V, Shatsky ridge; VI, Andrusov ridge; VII, Arkhangelsky ridge; VIII, Giresuan basin (from Starostenko et al., 2010).

## 1.5.1 The central Black Sea

The central Black Sea, one of the study areas of this thesis, is located in the Western Black Sea basin south of the Crimean Peninsula (Fig. 17) and adjacent to the Andrusov Ridge, which separates the Eastern and Western Black Sea basins. The Western Black Sea contains a sedimentary basin-fill on top of the basement of up to 15 km thickness. These sediments include about 6 km of Paleocene-Eocene deposits, more than 5 km of the Maikopian (Oligocene-Lower Miocene) Formation and about 2.5 km of Plio-Quaternary sediments (Tugolesov et al., 1985). The topography within this area is very flat (Gaynanov et al., 1998) with water depths deeper than 2000 m. The six big mud volcanoes in this study area are well expressed on the sea bottom as cone-shaped features of 300-2000 m in diameter and up to 120 m height (Fig. 18). Some of them have

craterlike depressions with rims on the top. The feeder channels of the mud volcanoes vary in diameter from several hundred meters to 3.5 km (Gaynanov et al., 1998). The roots of these mud volcanoes are not exactly known, but their origin is clearly related to the layers of plastic clay of the Maikopian Formation (Ivanov et al., 1996), which are highly enriched with organic matter (Dimitrov, 2002). The sedimentary layers as shown on seismic profiles are almost horizontal. However, in the mud volcano area they are locally influenced by low-amplitude folds, flexures, and normal faults. These features imply a general tensional tectonic regime in the basin and are probably related to the West Crimean Wrench Fault, which is the major regional strike-slip fault in the eastern part of the Western Black Sea basin and was active from the Cretaceous through the Miocene. Seismically imaged normal faults cut Quaternary sediments, suggesting possible reactivation of the West Crimean fault (Limonov et al., 1997; Bocaletti et al., 1988; Finetti et al., 1988; Slack et al., 1998).
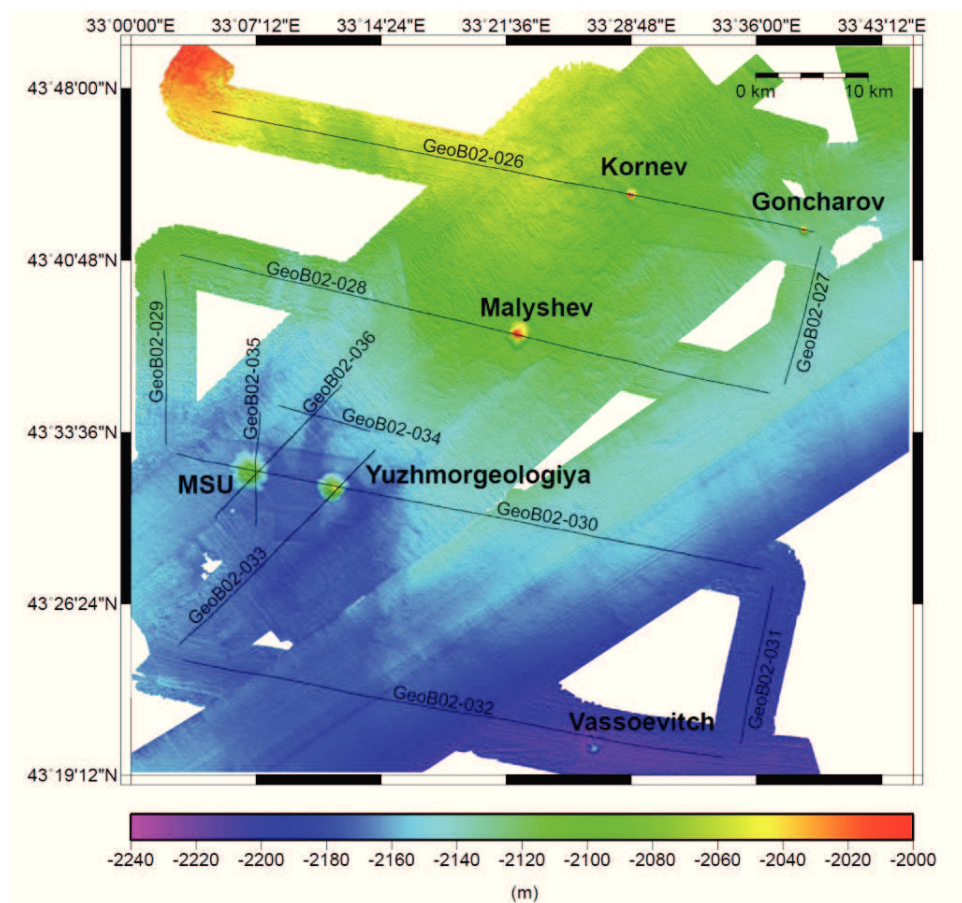


**Figure 18** Bathymetry of the area of investigation in the central Black Sea together with the seismic lines and names of mud volcanoes (bathymetry data from TTR6, M52-1, M72-3, MSM15-2 and M84-2). Six mud volcanoes were mapped.

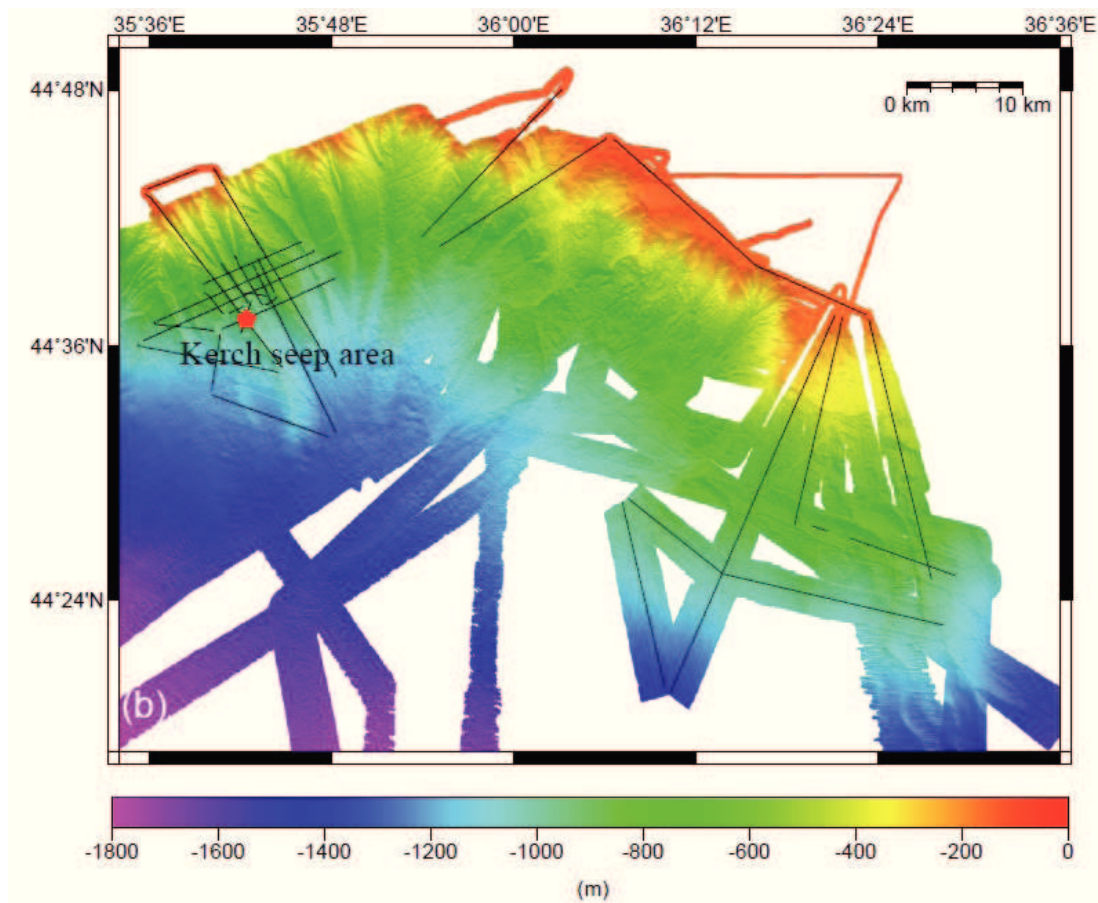## 1.5.2 The Kerch Peninsula margin, Black Sea



**Figure 19** Bathymetry map of the Kerch Peninsula margin, Black Sea. The red pentagon indicates the location of the Kerch seep area. Black lines indicate the location of the seismic profiles.

The Kerch Peninsula margin is located in the Eastern Black Sea Basin, which most likely began to rift in the Early Cretaceous. The Kerch Peninsula is a prominent geographic feature located in the eastern portion of Crimea. It is between two neighboring seas: the Azov Sea and the Black Sea. A large fan south of the Kerch Strait indicates the paleo-delta of the Don and Kuban rivers (Barg, 2007; Starostenko et al., 2010).

This study area is located south of the continental slope of the Kerch Peninsula, and characterized by NNW-SSE striking canyons and ridges. The continental slope is bordered by the Crimean Mountain in the North and Northwest, by the Sorokin Trough in the Southwest, by the Kerch-Taman Trough in the East and by the Tetyaev-Shatsky Ridge in the South (Fig. 19). The water depths in this area range from 100 m to 1400 m. Numerous gas seeps were recorded by the Parasound acoustic system during the R/V METEOR Cruise M72/3b in March/April 2007. The Kerch flares of more than 400 m height above the sea floor were observed in water depths of 900 m, named as the Kerch seep area (Bohrmann et al. 2007). The sedimentary cover of the study area consists of

Jurassic – Paleogene, Upper Eocene – Lower Miocene, Middle Miocene and Upper Miocene- Quaternary sequences, and with a total thickness of up to 15km (Stovba et al., 2009).
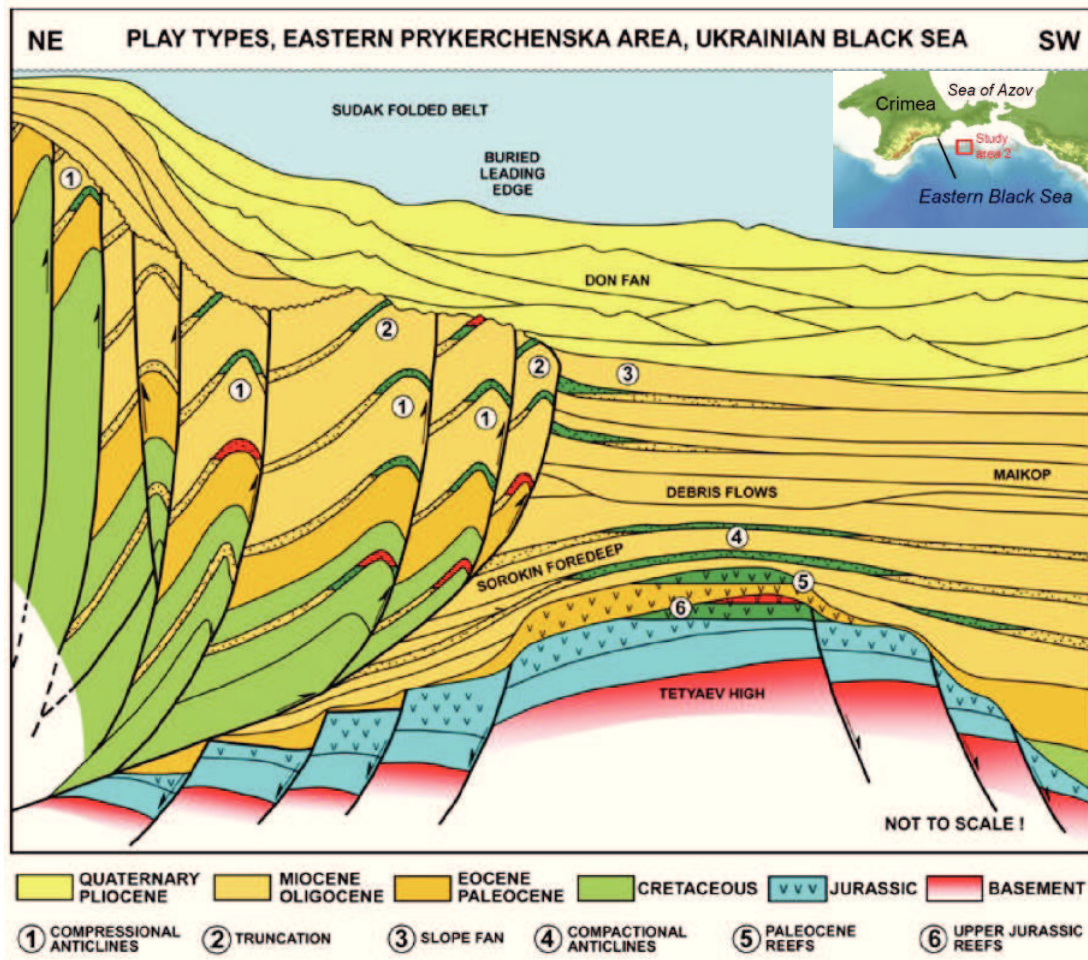


**Figure 20** Deepwater play types in the area south of Crimea and the Kerch peninsula. Image taken in 2008 from the public website of Vanco Energy Company: http://www.vanco-energy.com/. This profile is located in the west of the study area 2.

The entire eastern Ukrainian Black Sea was affected by inversion tectonics and compressional events during the Middle Eocene, Late Eocene, Early Miocene and Middle Miocene. These compression phases took place with the continuing post-rift basin subsidence. The geometry of probable EW – trending structures, such as the Sorokin Trough and the Tetyaev – Shatsky ridge, indicated the southeastern Crimea Black Sea to be influenced by NS – directed compression. There are numerous anticline structures formed by compressional events (Stovba et al., 2009). The anticline structures can serve as structural traps for oil and gas fields (Fig. 20). The sedimentary cover of our study area consists of Jurassic – Paleogene, Upper Eocene – Lower Miocene, Middle Miocene and Upper Miocene – Quaternary sequences, with a total thickness up to 15km (Stovba et al., 2009). The Oligocene-Miocene Maikopian formation, which is most probably the source

of seeps in the Black Sea (Ivanov et al., 1996), is buried beneath younger sediments. The steep upthrust faults (Alexander and Irina, 2005), which may be the main pathway for gas migrating to the upper part sediments, occur on the basinward side of the anticlines.

## 1.6 Materials and methods

### 1.6.1 High-resolution multichannel seismic

The high-resolution multichannel seismic data used in the study were collected during R/V Meteor Cruises M52/1 and M72/3 in 2002 and 2007, respectively (Bohrmann and Schenk, 2002; Bohrmann et al., 2007). The seismic system is specifically designed by the University of Bremen to acquire high-resolution seismic data through optimizing all system components and procedural parameters. Different seismic system setups were used during the M52/1 and M72/3 Cruises. Both of them are outlined in Figures 21 and 22, and described in detail below.

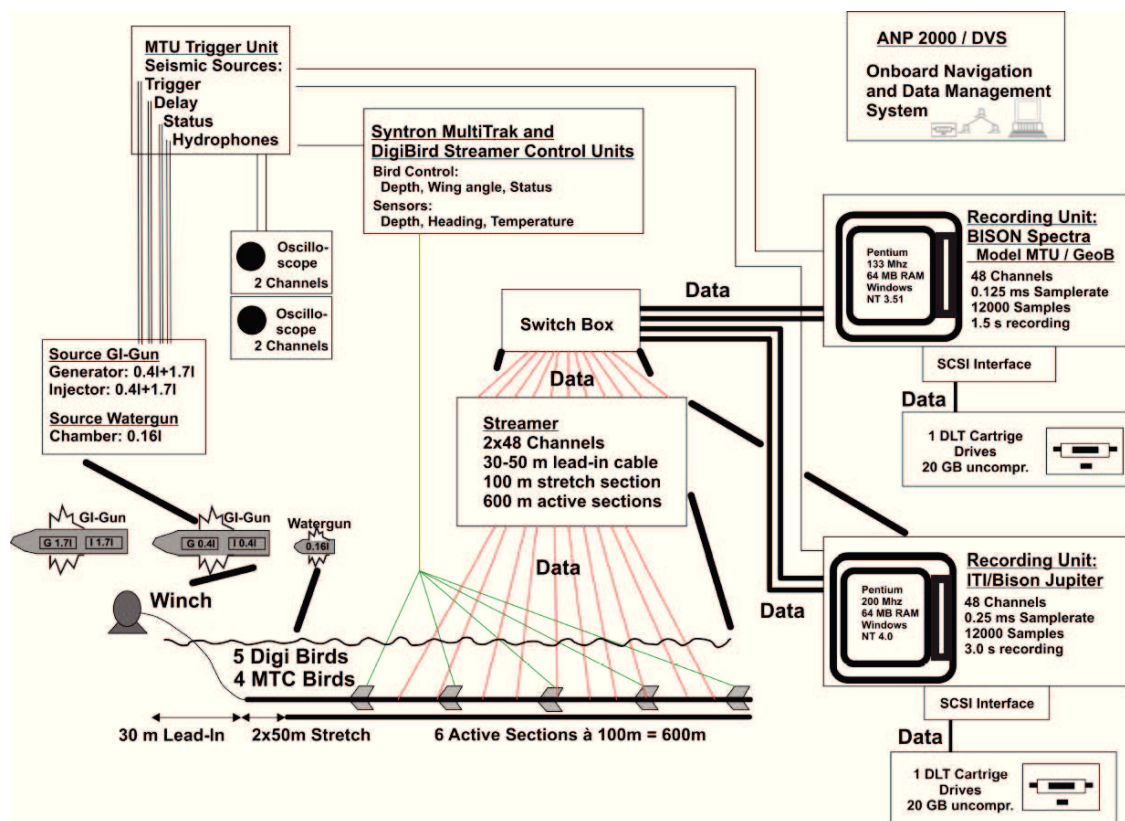### 1.6.1.1 Data acquisition



**Figure 21** Outline of the Bremen high resolution reflection seismic system during R/V Meteor Cruises M52/1

During the M52/1 seismic survey, three seismic sources were used, including two types of GI- (generator-injector) guns with chamber volumes of 2 x 1.7 L and 2 x 0.4 L,

respectively, and one water gun (0.16 L). The guns were operated on a quasi-simultaneous mode at a time interval of 9 s. The presented 2D seismic Lines GeoB02-026 – GeoB02-036 were shot with the larger GI-gun 2 x 1.7 L), towed at 1.4 m water depth, generating main frequencies in the range of 50 to 500 Hz. The return signal was recorded by a multichannel seismic streamer (SYNTRON). This included a 35 m tow-lead, a stretch section of 50 m, and six active sections of 100 m length each. The active sections with 48 channels of 6.25 m length and a group distance of 12.5 m recorded the GI-Gun data. The streamer was kept in a water depth of 3 m (+/- 0.5 m) by four MultiTrak Remote Units (MTC Birds) and five DigiCourse Birds (DigiBirds). Each bird includes a depth and a heading sensor as well as adjustable wings. The birds were controlled by two controllers from the seismic lab. The streamer was connected with a deck cable via a switch box to the recording system. The Jupiter/ITI/Bison seismograph digitized the GI-Gun data at a sampling frequency of 4 kHz over an interval of 3 seconds, which allowed online display of shot gathers and a demultiplexing of the data. Positioning was based on GPS recordings. A recording delay was adjusted depending on the current water depth. Data were stored in SEG-Y format on DLT4000 cartridge tape with 20 GByte of uncompressed capacity.
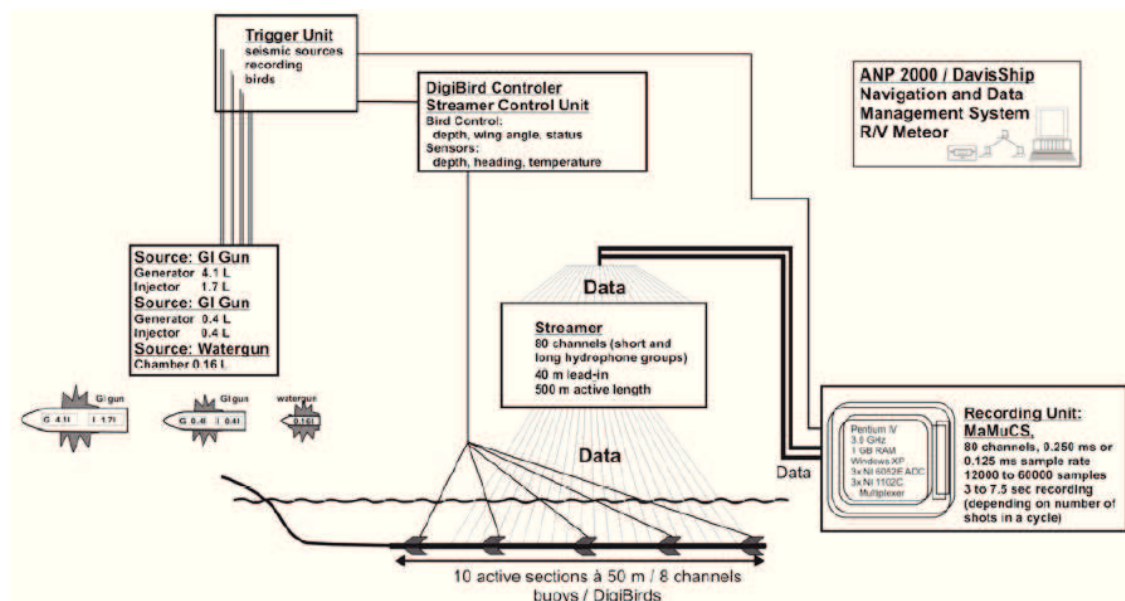


**Figure 22** Outline of the Bremen high resolution reflection seismic system during R/V Meteor Cruises M72/3

During the M72/3 Cruise, three seismic sources were used in various combinations. The aim of the seismic survey was to investigate the shallow and deeper subsurface structures in the vicinity of seep locations. The 2D seismic Lines GeoB07-137 – GeoB07-157, analyzed in this thesis, were shot with a GI gun with extended chamber volume (4.1 L generator and 1.7 L injector) in a frequency range of 30 - 300 Hz. The source was shot at an air pressure of ~150 bar provided by the compressor container. The multichannel seismic streamer (SYNTRON) included a tow-lead, a stretch section of 44 m and ten

active sections of 50 m length each. A long meteor rope of 30 m with a buoy at the end was connected to the tail swivel, resulting in a total tow length of 574 m. The streamer was connected with a 30 m long deck cable to the recording system. Data were received by the 500 m long streamer section with 80 channels at a group distance of 6.25 m. The streamer was kept in a water depth of 3 m (+/- 0.5 m) by the attachment of 5 cable levelers. The data digitization and recording were performed by the MaMuCS system (Marine Multichannel System), a custom designed software which can digitize and store simultaneously a maximum of 96 channels. In addition, during recording, MaMuCS can provide an online data display of shot gathers as well as a brute stack section of the range of channels of the user's choice. It also can receive and record ship navigation differential GPS data, and stores data in SEG-Y format on the internal hard disk drive.

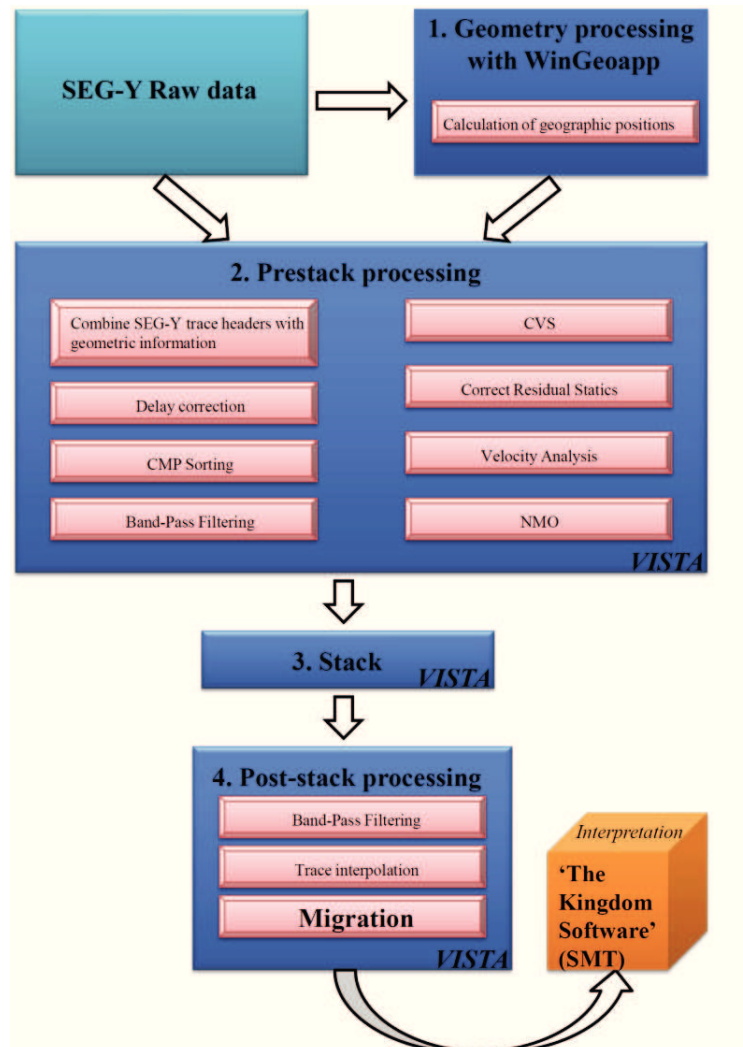## 1.6.1.2 Data processing



**Figure 23** Seismic processing flow applied to the 2D seismic data.

During the seismic data processing, I used a multichannel seismic processing method to process the seismic data from both M52/1 and M72/3. Figure 23 shows the specific processing flow applied to the 2D seismic data. The software for processing was the commercial software package Vista Seismic Processing. Custom software (WinGeoapp, developed by H. Keil, University of Bremen) was used for geometry calculations. Common mid-points (CMPs), which are the reflection midpoints between the sources and the receivers, were calculated for each trace based on the information of the navigation and heading data. For the M52/1 seismic data (Fig. 24), the CMP binning distance was chosen to be 10 m, leading to 15-16 fold coverage. To the M72/3 seismic data, a CMP binning distance of 2 m was finally applied, after also 5 m and 10 m bin distances had been tested. Dead and low-quality channels were removed.
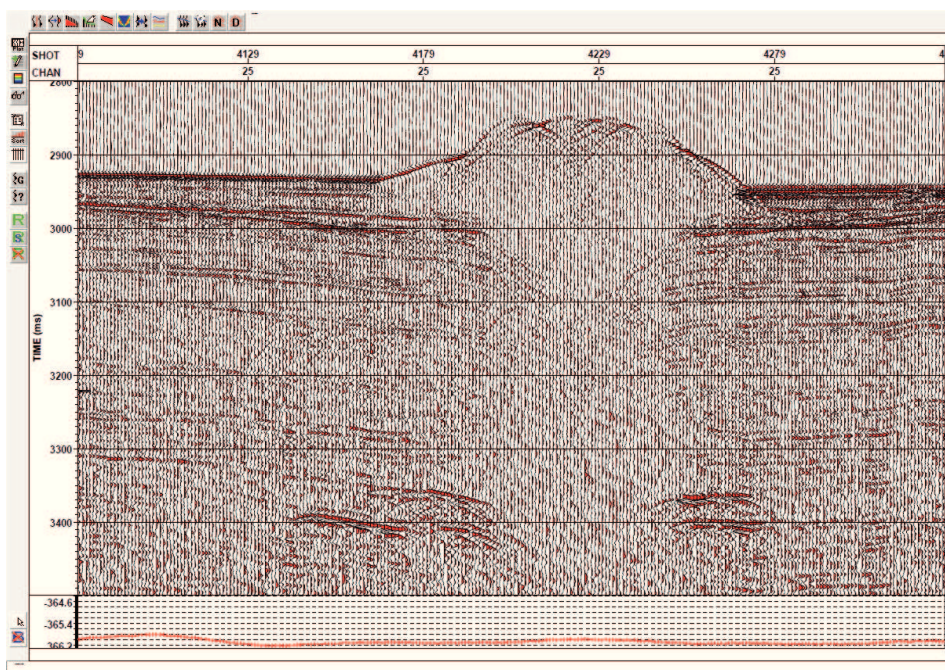


**Figure 24** An example of seismic dataset. A single channel profile of the seismic line GeoB02-030 crossing the MSU mud volcano after delay correction is presented. See the delay correction step the flow in Figure 23.

Velocity was picked for all profiles, and used for the normal move-out (NMO) correction and CMP stacking. The datasets were filtered with a broad band-pass filter, for the M52/1 seismic data and the M72/3 seismic data, 50/100-600/800 Hz and 10/30 - 250/400 Hz were chosen respectively to preserve both the high-resolution and the deeper-penetration signals. Before the stack step, a manual post-processing static correction was always necessary to remove residual static generated by oceanic waves. After the stack step, the signal to noise (S/N) ratio of seismic data can be highly improved (Fig. 25). The stacked seismic profiles were processed with time migration with a finite difference method (Fig. 26). The step of migration could collapse these diffractions and migrate dipping reflectors to their correct positions and angles. After the processing work, both stacked and migrated profiles were exported from the Vista software as SEG-Y data and

imported into the commercial software package 'The Kingdom Software' (SMT) for subsequent interpretation work.
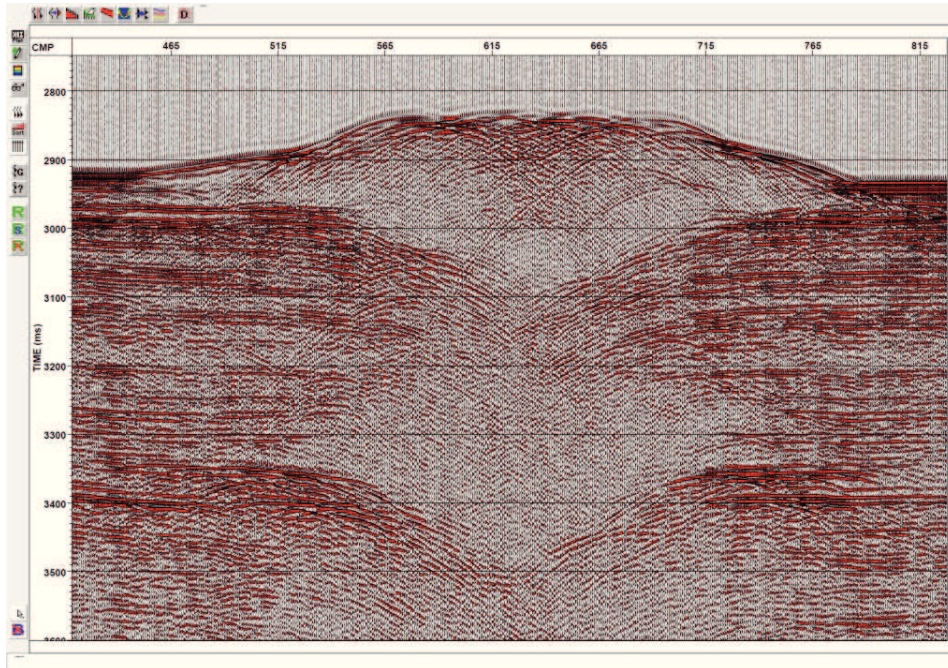


**Figure 25** The stacked profile of the seismic line GeoB02-030 crossing the MSU mud volcano. See the stack step in the flow in Figure 23.
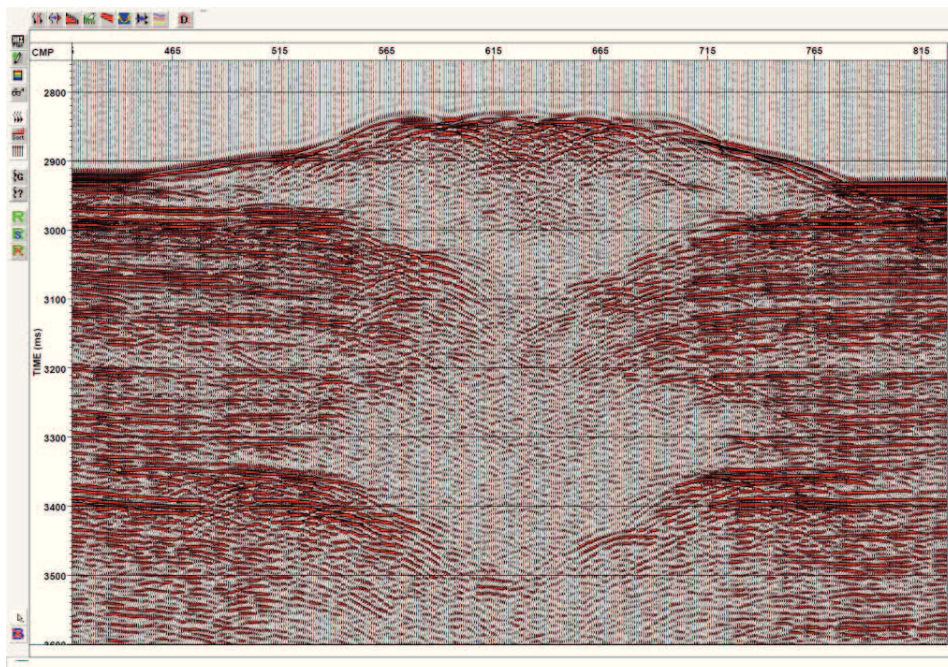


**Figure 26** The migrated profile of the seismic line GeoB02-030 crossing the MSU mud volcano. See the migration step in the flow in Figure 23.

### 1.6.2 The Parasound sediment echosounder

Parasound data of the Kerch Peninsula margin during M72/3 Cruise were used for the analysis of the locations of gas flares and the shallow subbottom structures (Chapter 4). The hull-mounted narrow-beam Parasound sediment echosounder is permanently installed on the R/V Meteor. This sound beam system has an opening angle of 4°, the pinging rate is controlled by the depth of the water column where it is operating. The echosounder profiles were registered at ship speeds of ~5 kns when surveying gas flares areas. The system was operated at a primary high frequency (PHF) of 18 kHz and secondary low frequency (SLF) of 4 kHz. PHF is used to detect the gas flares in the water column, while SLF provides images of subbottom structures. Penetration into the subsurface varies between 0 - 200 m, depending on the type of sediment and attenuation (Grant and Schreiber, 1990). PHF and SLF were emitted simultaneously. The software ATLAS PARASTORE was used to archive the acoustic data into PS3 data files. The custom-made program SeNT (H. Keil, University of Bremen) was used to routinely post-process the PS3 data, aiming to provide the detailed analysis of echo returns from gas flares at 18 kHz. The final images used in Chapter 4 were generated by the program SeNT (developed by H. Keil, University of Bremen).

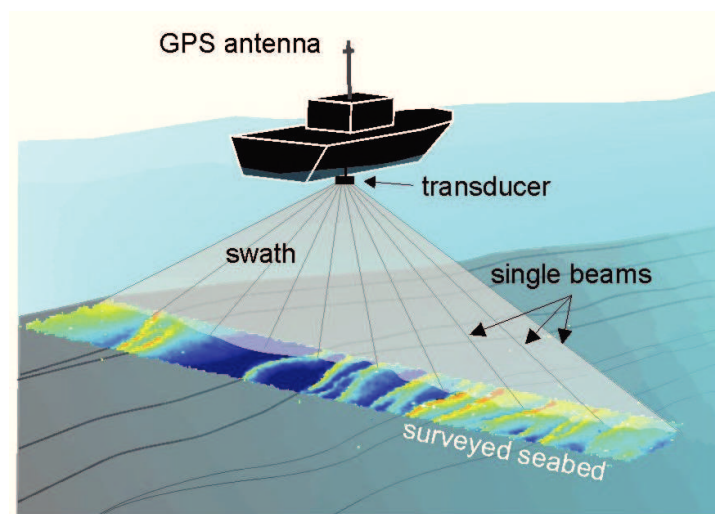### 1.6.3 The swath bathymetry systems



**Figure 27** Multibeam echosounder systems (from www.marum.de/en/Methods_4.html).

During the M52/1 Cruise, bathymetric data were recorded using the HYDROSWEEP multibeam system (Fig. 27). The system maps the seafloor by generating 59 pre-formed beams in a swath of 90° at an operating frequency of 15.5 kHz, obtaining seafloor information of a swath with a width of twice the water depth (Grant and Schreiber, 1990). The resolution depends on the water depth and the slant angle and was about 80 to 200 m in water depths of 2000 to 2500 m. The public domain software package MB-System (Caress and Chayes, 1996) was used to process HYDROSWEEP multibeam data, including the correction of the navigation data and the depth values. Bad outer beams and abnormal depth values were removed. Previously available bathymetry data (e.g. from

the TTR-6 cruise) in the central Black Sea were also incorporated in the newly produced map.

During the M72/3 Cruise, the ship-mounted multibeam system Simrad[TM] EM120 (Kongsberg) was used for the acquisition equipment of bathymetric data, which were used in the second study area-the continental slope near Kerch Peninsula. The EM120 (120 kHz) can cover virtually the entire ocean depth range. The opening angle was usually 140°, changing with varying weather conditions and ship velocity. Many other settings such as yaw correction can be automatically adjusted by the recording software. The processing was carried out by the IFREMER Caraibes software. For the second study area, a 10 m grid spacing was applied for detailed bathymetric displays.

In this thesis, the GMT software (Wessel and Smith, 1991) was used to generate and display the bathymetric grid and seismic line locations of the two study areas.

## References for Chapter 1

Banks, C.J. and A.G. Robinson, 1997, Mesozoic strike-slip back-arc basin of the Western Black Sea region. In: A.G. Robinson (Ed.), Regional and Petroleum Geology of the Black Sea and Surrounding Region: AAPG Memoir 68, Tulsa, OK, p. 53-62.

Barg I, 2007. Age and origin of the Kerch Strait and the Sea of Azov. Doklady Earth Sciences 412:17-18

Bethke, C.M. 1986. Inverse hydrologic analysis of the distribution and origin of the Gulf Coast-type geopressured zones. Journal of Geophysical Research, 91, 6536–6545.

Bitzer, K., A. Trave´, and J.M. Carmona, 2001. Fluid flow processes at basin scale. Acta Geol. Hisp., 36, 1–20.

Bøe, R., Rise, L. and Ottesen, D., 1998. Elongate depressions on the southern slope of the Norwegian Trench (Skagerrak): morphology and evolution. Marine Geology, 146, 191-203.

Boetius. A., Ravenschlag, K, Schuber, C.J., Rickerf, D., Widdel, F., Gieseke, A., Amann, R., Jørgensen, B.B., Witte, U., and Pfannkuche, O., 2000. A marine microbial consortium apparently mediating anaerobic oxidation of methane. Nature 407, 623-626.

Bohrmann G., T. Pape, and cruise participants, 2007. Report and preliminary results of R/V METEOR Cruise M72/3, Istanbul – Trabzon – Istanbul, 17 March – 23 April, 2007.Marine gas hydrates of the Eastern Black Sea. Berichte, Fachbereich Geowissenschaften, Universität Bremen, No. 261, 176 pages. Bremen, 2007.

Bohrmann, G., and Schenck, S., 2002. GEOMAR Cruise Report M52/1, MARGARSCH, RV Meteor, marine gas hydrates of the Black Sea. GEOMAR, Kiel.

Buffet, B.A., 2000. Clathrate hydrates, annual review of earth planetary sciences. Annual Review of Earth Planetary Sciences, 28: 477-507.

Burst, J.F., 1969. Diagenesis of Gulf Coast clayed sediments and its possible relation to petroleum migration. AAPG Bulletin, 53, 73–93.

Caress, D.W., and Chayes, D.N., 1996. Improved Processing of Hydrosweep Multibeam Data on the R/V Maurice Ewing. Marine Geophysical Researches, 18: 631-650.

Chappellaz, J., Blunier, T., Raynaud, D., Barnola, J.M., Schwander, J., and Stauffer, B., 1993. Synchronous changes in atmospheric CH4 and Greenland climate between 40 and 8 kyr BP. Nature 366, 443–445.

Claypool, G.E., and Kaplan, I.R., 1974. The origin and distribution of methane in marine sediments. Natural Gases in Marine Sediments. Plenum Press, New York: 99-139.

Collier, R.W. and M.D. Lilley. 2005. Composition of shelf methane seeps on the Cascadia Continental Margin. Geophysical Research Letters 32(6): L06609.

Dillon, W.P., and Paull, C.K., 1983. Marine gas hydrates II. Geophysical evidences. In: Cox JL 8ed) Natural gas hydrates, properties, occurrence and recovery. Butterworth, Woburn, MA: 73-90.

Dillon, W.P., Grow, J.A., and Paull, C.K., 1980. Unconventional gas hydrate seals may trap gas off southeast US. Oil and Gas Journal 78, 124–130.

Dimitrov, L., 2002a. Contribution to atmospheric methane by natural seepages on the Bulgarian continental shelf. Continental Shelf Research 22(16): 2429-2442.

Dimitrov, L., 2002b. Mud volcanoes—the most important pathway for degassing deeply buried sediments. Earth Science Reviews 59, 49–76.

Dimitrov, L., and Woodside, J., 2003. Deep sea pockmark environments in the eastern Mediterranean. Marine Geology 195, 263–276.

Ding, F., 2008. Near-surface Sediment Structures at Cold Seeps and their Physical Control on Seepage: A Geophysical and Geological Study in the Southern Gulf of Mexico and at the frontal Makran Accretionary Prism/Pakistan. Ph.D. thesis, Department of Geosciences, Univ. of Bremen, Bremen.

Ding, F., Spiess, V., Brüning, M., Fekete, N., Keil, H., and Bohrmann, G., 2008. A conceptual model for hydrocarbon accumulation and seepage processes around Chapopote asphalt site, southern Gulf of Mexico: from high resolution seismic point of view. Journal of Geophysical Research, 113 (B8), B08404.

Ding, F., Spiess, V., MacDonald, I. R., Brüning, M., Fekete, N., and Bohrmann, G., 2010. Shallow sediment deformation styles in north-western Campeche Knolls, Gulf of Mexico and their controls on the occurrence of hydrocarbon seepage. Marine and Petroleum Geology, 27(4), 959-972.

Dyadin, Y.A., Aladko, E.Y., and Larionov, E.G., 1997. Decomposition of methane hydrates up to 15kbr. Mendeleev Commun., 34.

Etiope G and Milkov AV, 2004. A new estimate of global methane flux from onshore and shallow submarine mud volcanoes to the atmosphere. Environ Geol 46:997–1002.

Etiope, G., Lassey, K. R., Klusman, R. W., and Boschi, E., 2008. Reappraisal of the fossil methane budget and related emission from geologic sources. Geophys. Res. Lett. 35.

Etiope, G., and P. Ciccioli. 2009. Earth's degassing: a missing ethane and propane source. Science 323:478.

Fleischer, P., Orsi, T.H., Richardson, M.D. and Anderson, A.L., 2001. Distribution of free gas in marine sediments: a global overview. Geo-Marine Letters, 21, 103−122.

Floodgate, G. D. and Judd, A. G., 1992. The origin of shallow gas. Continental Shelf Res. 12, No. 10, 1145–1156.

Gay, A., Lopez, M., Cochonat, P., Séranne, M., Levaché, D., and Sermondadaz, G., 2006. Isolated seafloor pockmarks linked to BSRs, fluid chimneys, polygonal faults and stacked Oligocene-Miocene turbiditic paleochannels in the Lower Congo Basin. Marine Geology, 226, 25-40.

Gay, A., Lopez, M., Cochonat, P., Sultan, N., Cauquil, E., Brigaud, F., 2003. Sinuous pockmark belt as indicator of a shallow buried turbiditic channel on the lower slope of the Congo Basin, West African margin. Geological Society Special Publications, Subsurface Sediment Mobilization 216, 173–189.

Ge, S. and Garven, G., 1992. Hydromechanical modeling of tectonically driven groundwater flow with application to the Arkoma Foreland basin. Journal of Geophysical Research, 97, 9119–9144.

Geir Ersland, 2010. Natural Gas Hydrates, Natural Gas, PrimoÃ…Â¾ PotoÃ„Â nik (Ed.), ISBN: 978-953-307-112-1, InTech, Available from: http://www.intechopen.com/books/natural-gas/natural-gas-hydrates.

Gillet Herve, Lericolais Gilles, and Rehault Jean Pierre, 2007. Messinian event in the black sea: Evidence of a Messinian erosional surface. Marine Geology, 244(1-4), 142-165.

Ginsburg, G.D., and Soloviev, V.A., 1994. Mud volcanoes and gas hydrates in the Caspian Sea. Bull. Geol. Soc. Denmark, 41: 95-100.

Ginsburg, G.D., and Soloviev, V.A., 1997. Methane migration within the submarine gas-hydrate stability zone under deep-water conditions. Marine Geology, 137: 49-57.

Ginsburg, G.D., Kremlev, A.N., Grigor, M.N., Larkin, G.V., Pavlenkin, A.D. and Saltykova, N.A., 1990. Filtrogenic gas hydrates in the Black Sea (21st voyage of the research vessel Evpatoriya). Soviet Geol Geophys, 31: 101-152.

Gozhik P.F., Maslunr N.V., Ivanikl M.M., Plotnikoval L.F., Yakushinl, L.N., 2008. Stratigraphic model of the Mesozoic and Cenozoic of the Western Black Sea Basin. Геология и полезные ископаемые Мирового океана, (1), 55-69.

Grant, J.A., and Schreiber, R., 1990. Modern Swathe Sounding and Sub-Bottom Profiling Technology for Research Applications: The Atlas Hydrosweep and Parasound Systems. Marine Geophys Researches, 12: 9-19.

Greinert, J., Artemov, Y, Egorov, V., De Batist, M., and McGinnis, D, 2006. 1300-m-high rising bubbles from mud volcanoes at 2080m in the Black Sea: Hydroacoustic characteristics and temporal variability. EPSL, 244: 1-15.

Haacke, RR, Westbrook, GK and Hyndman, RD, 2007. Gas hydrate, fluid flow and free-gas: formation of the bottom-simulating reflector. Earth and Planetary Science Letters, 261 . pp. 407-420.

Henry, P., Le Pichon, X., Lallemant, S., Foucher, J.P., Westbrook, G.K., and Hobart, M.A., 1990. Mud volcano field seaward of the Barbados accretionary complex; a deep-towed scan sonar. Journal of Geophysical Research 95, 8917–8929.

Holbrook, W.S., Gorman, A.R., Hornbach, M., Hackwith, K.L., Nealon, D., Lizarralde, D., and Pecher, I.A., 2002. Seismic detection of marine methane hydrate. The Leading Edge, 21(7): 686-689.

Hovland, M. and Judd, A.G., 1988. Seabed Pockmarks and Seepages. Impact on Geology, Biology and the Marine Environment. Graham and Trotman, London. 293 pp.

Hovland, M., Gardner, J.V. and Judd, A.G., 2002. The significance of pockmarks to understanding fluid flow processes and geohazards. Geofluids, 2, 127-136.

Hovland, M., Talbot, M., Olaussen, S., and Aasberg, L., 1985. Recently formed methane-derived carbonates from the North Sea floor. In: Thomas, B.M. (Ed.), Petroleum Geochemistry in Exploration of the Norwegian Shelf. Norwegian Petroleum Soc., Graham and Trotman, pp. 263–266.

http://folk.uio.no/karenel/research.html

http://jan.ucc.nau.edu/~rcb7/paleogeographic_alps.html

http://www.awi.de

http://www.ngi.no

http://www.pet.hw.ac.uk/

http://www.vanco-energy.com/

Ivanov, M.K., Limonov, A.M. and van Weering, T.C.E., 1996. Comparative characteristics of the Black Sea and Mediterranean Ridge mud volcanoes. Marine Geology, 132: 253-271.

Jakubov, A.A., Alizade, A.A., and Zeinalov, M.M., 1971. Mud volcanoes of Azerbaijan. SSR: Atlas. Elm-Azerbaijan Acad. of Sci. Pub. House, Baku (in Russian).

Jouzel, J., N.I. Barkov, J.M. Barnola, M. Bender, J. Chappellaz, C. Genthon, V.M. Kotlyakov, V. Lipenkov, C. Lorius, J.R. Petit, D. Raynaud, G. Raisbeck, C. Ritz, T. Sowers, M. Stievenard, F. Yiou, and P. Yiou. 1993. Extending the Vostok ice-core record of palaeoclimate to the penultimate glacial period. Nature 364:407-12.

Judd, A. and Hovland, M., 2007. Seabed Fluid Flow. Impact on Geology, Biology, and the Marine Environment. Cambridge University Press. Cambridge, UK, pp 1-5, 165-178, 293.

Judd, A. G., Hovland, M., Dimitrov, L. I., Garc´ıa-Gil, S., and Jukes, V., 2002a. The geological methane budget at continental margins and its influence on climate change. Geofluids, 2, 109–26.

Judd, A., 2003. The global importance and context of methane escape from the seabed. Geo-Marine Letters, 23: 147-154.

Judd, A., G. Davies, J. Wilson, R. Holmes, G. Baron, and I. Bryden. 1997. Contributions to atmospheric methane by natural seepages on the UK continental shelf (vol 137, pg 165, 1997). Marine Geology 140(3-4): 427-455.

Kennett, J. P., K. G. Cannariato, I. L. Hendy, and R. J. Behl, 2003. Methane Hydrates in Quaternary Climate Change: The Clathrate Gun Hypothesis, Spec. Publ. 54, 216 pp., AGU, Washington, D. C.

King, L.H. and MacLean, B., 1970. Pockmarks on the Scotian Shelf. Geological Society of America Bulletin 81, 3141–3148.

Klaucke, I., Sahling, H., Weinrebe,W., Blinova, V., Burk, D., Lursmanashvili, N., and Bohrmann, G., 2006. Acoustic investigation of cold seeps offshore Georgia, eastern Black Sea. Marine Geology 231, 51–67.

Kohl, B., and Roberts, H.H., 1994. Fossil foraminifera from four active mud volcanoes in the Gulf of Mexico. Geo-Marine Letters, 14: 126-134.

Kopf, A. J., 2002. Significance of mud volcanism. Reviews of Geophysics, 40: 1-52.

Kopf, A. J., 2003. Global methane emission through mud volcanoes and its past and present impact on the Earth's climate. International Journal of Earth Sciences, 92, 806 – 816.

Kutas R.I., Paliy S.I. and Rusakov O.M., 2004. Deep faults, heat flow and gas leakage in the northern Black Sea. Geo-Mar Letter; 24:163-168.

Kvenvolden KA, 1998. Methane hydrates and global climate. Global Biochemical Cycles, 2:221–229.

Kvenvolden, K. A. and B. W. Rogers, 2005. Gaia's Breath—Global methane exhalations, Mar. Pet. Geol., 22(4), 579– 590.

Kvenvolden, K.A., 1993. Gas Hydrates - Geological Perspective and Global Change. Reviews of Geophysics, 31: 173-187.

Kvenvolden, K.A., and Barnard, L.A., 1983. Gas hydrates of the Blake Outer Ridge, Site 533, Deep Sea Drilling Project Leg 76. Initial Reports of the Deep Sea Drilling Project, 76: 353-365.

Kvenvolden, K.A., and Lorenson, T.D., 2001. The Global Occurrence of Natural Gas Hydrate. Geophysical Monograph, 124: 3-16.

Kvenvolden, K.A., and McDonald, T.J., 1985. Gas hydrates of the Middle America Trench. Deep Sea Drilling Project Leg 84. Initial Reports of the Deep Sea Drilling Project, 84: 667-682.

Lawrence, S.R. and Corn ford, C., 1995. Basin geofluids. Basin Research, 7, 1-7.

Le Pichon, X., Foucher, J.P., Boulegue, J., Henry, P., Lallemant, S., Benedetti, M., Avedik, F., and Mariotti, A., 1990. Mud volcano field seaward of the Barbados accretionary complex; a submersible survey. Journal of Geophysical Research 95, 8931–8943.

Lee, M.-K. and Bethke, C.M., 1994. Groundwater flow, late cementation, and petroleum accumulation in the Permian Lyons sandstone, Denver basin. AAPG Bulletin, 78, 217–237.

Lee, M.-K. and Williams, D.D., 2000. Paleohydrology of the Delaware basin, western Texas: Overpressure development, hydrocarbon migration, and ore genesis. AAPG Bulletin, 84, 961–974.

Lee, Y. and Deming, D., 2002. Overpressures in the Anadarko Basin, southwestern Oklahoma; static or dynamic? AAPG Bulletin, 186, 145–160.

Leifer, I., and A. G. Judd, 2002. Oceanic methane layers: A bubble deposition mechanism from marine hydrocarbon seepage, Terra Nova, 16, 471.

Leifer, I., B.P. Luyendyk, J. Boles, and J.F. Clark., 2006. Natural marine seepage blowout: Contribution to atmospheric methane. Global Biogeochemical Cycles 20 (3).

Leifer, I., J.R. Boles, B.P. Luyendyk, and J.F. Clark., 2004. Transient discharges from marine hydrocarbon seeps: spatial and temporal variability. Environmental Geology 46 (8): 1038-1052.

Limonov, A.F., van Weering, Tj.C.E., Kenyon, N.H., Ivanov, M.K., and Meisner, L.B., 1997. Seabed morphology and gas venting in the Black Sea mud volcano area: Observation with the MAK-1 deep tow side scan sonar and bottom profile. Marine Geology, 137: 121-136.

Liu, Bei; Yuan, Qing; Su, Ke-Hua; Yang, Xin; Wu, Ben-Cheng; Sun, Chang-Yu; Chen, and Guang-Jin. 2012. Experimental Simulation of the Exploitation of Natural Gas Hydrate. Energies 5, no. 2: 466-493.

Long D, Lammers S, and Linke P., 1998. Possible hydrate mounds within large sea-floor craters in the Barents Sea. In: Gas Hydrates: Relevance to World Margin Stability and Climate Change, Geological Society of London Special Publication No. 137 (Eds Henriet J-P, Mienert J), pp. 223–37. Geological Society, London.

Luo, X.R. and Vasseur, G., 1996. Geopressuring mechanism of organic matter cracking: Numerical modeling. AAPG Bulletin, 80, 856–874.

Luyendyk, Bruce P, Cann, Joe R, and Steiner, M., 2005. Paleomagnetic measurements on DSDP Hole 49-407.

MacLeod, M.K., 1982. Gas hydrates in ocean bottom sediments. American Association Petroleum Geologists Bulletin 66, 2649–2662.

Mau, S., H. Sahling, G. Rehder, E. Suess, P. Linke, and E. Soeding., 2006. Estimates of methane output from mud extrusions at the erosive convergent margin off Costa Rica. Marine Geology 225(1-4): 129-144.

Max, M.D., 2000. Natural gas hydrate in oceanic and permafrost environments: Kluwer Academic Publishers, London, England, 1-415.

McAdoo, B. G., Pratson, L. F., and Orange, D. L., 2000. Submarine landslide geomorphology, US Continental Slope. Marine Geology, 169, 103–36.

Michaelis, W., Seifert, R., Nauhaus, K., Treude, T., Thiel, V., Blumenberg, M., Knittel, K., Gieseke, A., Peterknecht, K., Pape, T., Boetius, A., Amann, R., Jörgensen, B.B., Widdel, F., Peckmann, J., Pimenov, N.V., and Guli, M.B., 2002. Microbial reefs in the Black Sea fuelled by anaerobic oxidation of methane. Science, 297: 1013-1015.

Milkov AV, Sassen R, Apanasovich TV, and Dadashev FG, 2003. Global gas flux from mud volcanoes: a significant source of fossil methane in the atmosphere and the ocean. Geoph. Res. Lett. 30(2):1037, doi:10.1029/2002GL016358

Milkov, A.V., 2000. Worldwide distribution of submarine mud volcanoes and associated gas hydrates. Marine Geology, 167: 29-42.

Minshull, T., and White, R.S., 1989. Sediment compaction and fluid migration in the Makran accretionary prism. J Geophys Res, 94: 7387-7402.

Naudts L, Greinert J, Artemov Y, Staelens P, Poort J, Van Rensbergen P, and De Batist M., 2006. Geological and morphological setting of 2778 methane seeps in the Dnepr paleo-delta, northwestern Black Sea. Marine Geology 227:177-199.

Nikishin, A.M., Korotaev, M.V., Ershov, A.V., and Brunet, M.-F., 2003. The Black Sea basin: tectonic history and Neogene–Quaternary rapid subsidence modelling. Sedimentary Geology 156, 149-168.

Nisbet, E. G., 2002. Have sudden large releases of methane from geological reservoirs occurred since the Last Glacial Maximum, and could such releases occur again?, Philos. Trans. R. Soc. London, Ser. A, 360, 581 – 607, doi:10.1098/rsta.2001.0958

Nunn, J., 1996. Buoyancy-driven propagation of isolated fluid-filled fractures: Implications for fluid transport in Gulf of Mexico geopressured sediments, J. Geophys. Res., 101, 2963– 2970.

Obzhirov, A., Shakirov, R., Salyuk, A., Suess, E., and Biebow, N.S.A., 2004. Relations between methane venting, geological structure and seismo-tectonics in the Okhotsk Sea. Geo-Marine Letters 24, 135–139.

Pape, T., Bahr, A., Klapp, S. A., Abegg, F., and Bohrmann, G., 2011. High-intensity gas seepage causes rafting of shallow gas hydrates in the southeastern Black Sea. Earth and Planetary Science Letters, 307(1), 35-46.

Paull, C. K., 1997. Drilling for gas hydrates: offshore drilling program Leg 164. Proceedings of the Offshore Technology Conference, Houston, TX, OTC Paper 8294.

Paull, C.K., Usller, W., and Borowski, E.S., 1994. Sources of biogenic methane to form marine gas hydrates. In: Sloan, E.D., Happel, J., and Hnatow, M.A. (eds.), International Conference on Natural Gas Hydrates. Ann. N.Y. Acad. Sci., 715: 392-409.

Pierce, B.S. and Collett, T.S., 2004. Energy Resource Potential of Natural Gas Hydrates. 5th Conference & Exposition on Petroleum Geophysics, Hyderabad, India PP 899-903.

Pilcher, R., and Argent, J., 2007. Mega-pockmarks and linear pockmark trains on the West African continental margin. Marine Geology 244, 15–32.

Plaza-Faverola, A., Bünz, S., and Mienert, J., 2012. The free gas zone beneath gas hydrate bearing sediments and its link to fluid flow: 3-D seismic imaging offshore mid-Norway. Marine Geology, 291, 211-226.

Prather, M., R. Derwent, D. Ehhalt, P. Fraser, E. Sanhueza, and X. Zhou, 1995. Other trace gases and atmospheric chemistry, in Climate Change 1994: Radiative Forcing of Climate Change and an Evaluation of the IPCC IS92 Emission Scenarios, edited by J. T. Houghton et al., pp. 73– 126, Cambridge Univ. Press, New York.

Querellou, J., 2003. Biotechnology of marine extremophiles. Book of Abstracts, International Conference on the sustainable development of the Mediterranean and Black Sea environment, Thessaloniki, Greece, 28May –1 June (extended abstract).

Race, D. D. and Claypool, G. E., 1981. Generation, accumulation, and resource potential of biogenic gas American Association of Petroleum Geologists ( Bulletin ), 65, 5-25

Revil, A., Cathles, L.M. III, Shosa, J.D., Pezard, P.A. and de Larouziere, F.D., 1998. Capillary sealing in sedimentary basins: A clear field example. Geophysical Research Letters, 25, 389–392.

Rice, D. D., and Claypool, G. E., 1981. Generation, accumulation, and resource potential of biogenic gas. Am. Assoc. Pet. Geol. Bull., 65:5-25.

Ripmeester, J. A., Tse, J. S, Ratcliffe, C. I., and Powell, B. M. (1987): "A New Clathrate Hydrate Structure", Nature, 325, 135.

Robinson, A.G., Rudat, J.H., Banks, C.J. and Wiles, R.L.F., 1996. Petroleum Geology of the Black Sea. Marine and Petroleum Geology, 13(No. 2): 195-223.

Römer M., Sahling H., Pape T., Bahr A., Fesker T., Wintersteller P., and Bohrmann G., 2012. Geological control and magnitude of methane ebullition from a high-flux seep area in the Black Sea - The Kerch seep area. Marine Geology 319-322, 57-74. doi: 10.1016/j.margeo.2012.07.005.

Rowland, F. S., 1985. Methane and chlorocarbons in the Earth's atmosphere, Origins Life Evol. Biosphere, 15, 279-298.

Ruppel, C. D., 2007. Tapping methane hydrates for unconventional natural gas, Elements, 3(3), 193-199.

Ruppel, C. D., 2011. Methane Hydrates and Contemporary Climate Change. Nature Education Knowledge 3(10):29.

Ryskin, G., 2003. Methane-driven oceanic eruptions and mass extinctions: Geology, v. 31, p. 741–744.

Sager, W.W., MacDonald, I.R., and Hou, R., 2003. Geophysical signatures of mud mounds at hydrocarbon seeps on the Louisiana continental slope, northern Gulf of Mexico. Marine Geology 198, 97-132.

Schroot, B.M., Klaver, G.T. and Schüttenhelm, R.T.E., 2005. Surface and subsurface expressions of gas seepage to the seabed-examples from the Southern North Sea. Marine Petroleum Geology, 22, 499-515.

Sharp, J.M., 1983. Permeability control on aquathermal pressure. AAPG Bulletin, 67, 2057–2061.

Shi, Y. and Wang, C. 1986. Pore pressure generation in sedimentary basins: overloading versus aquathermal. Journal of Geophysical Research, 91, 2153–2162.

Shipley, T., Houston, M., and Buffer, R., 1979. Seismic reflection evidence for the widespread occurrence of possible gas hydrate horizons on continental slopes and rises. AAPG Bulletin, 63: 2204-2213.

Shu Jiang, 2012. Clay Minerals from the Perspective of Oil and Gas Exploration, Clay Minerals in Nature - Their Characterization, Modification and Application, Dr. Marta Valaskova (Ed.), ISBN: 978-953-51-0738-5, InTech, DOI:10.5772/47790.

Sloan, E.D., 1990. Clathrate Hydrates of natural gas. Marcel Deker, New York: 641 pp.

Sloan, E.D. and Koh, C.A., 2008. Clathrate Hydrates of Natural Gases, 3rd Edition, 53, 553-608.

Sloan, E.D., 1998. Physical/chemical properties of gas hydrates and applications to world margin stability and climatic change. In: Henriet, J.-P. and Mienert, J. (eds) Gas Hydrates: Relevance to world margin stability and climate change. Geological Society, London, Special Publications, 137: 31-50.

Solomon, S., D. Qin, M. Manning, Z. Chen, M. Marquis, K.B. Averyt, M. Tignor, and H.L. Miller (eds.), 2007. Climate Change 2007: The Physical Science Basis. Contribution of Working Group I to the Fourth Assessment Report of the Intergovernmental Panel on Climate Change. Cambridge, UK, and New York, NY: Cambridge University Press.

Stackelberg, M. and Müller, H. R., 1954. Feste Gashydrate, Z. für Elektrochemie, 58, 25.

Starostenko, V.I., Rusakov, O.M., Shnyukov, E.F., Kobolev, V.P., and Kutas, R.I., 2010.Methane in the northern Black Sea: characterization of its geomorphological and geological environments. Geological Society, London, Special Publications 340 (1), 57–75.

Sturz, A.A., Kamps, R.L., and Earley, P.J., 1992. Temporal changes in mud volcanoes, Salton Sea geothermal area. In: Water-Rock Interactions, edited by Kharaka, Y.K., and Maest, A.S.. Balkema, Brookfield, Vt., 2: 1363-1366.

Suess, E., Carson, B., Ritger, S.D., Morre, J.C., Jones, M.L., Kulm, L.D., and Cochrane, G.R., 1985. Biological communities at vent sites along the subduction zone off Oregon. Biol. SOc. Wash. Bull., 6: 475-484.

Thakur, N. K. and Rajput, S., 2011. Exploration of Gas hydrates: Geophysical Techniques, 1st Edition, 75, 99-142.

Toth, J., 1962. A theory of groundwater motion in small basins in central Alberta, Canada. Journal of Geophysical Research, 67, 4375–4387.

Vassilev, A., Dimitrov, L., 2002. Spatial and quantity evaluation of the Black Sea gas hydrates. Russian Geology and Geophysics 43 (7), 637–649.

Wagner-Friedrichs, M., 2007. Seafloor seepage in the Black Sea: mud volcanoes, seeps and diapiric structures imaged by acoustic methods. Ph.D. thesis, Department of Geosciences, Univ. of Bremen, Bremen.

Wagner-Friedrichs, M., Krastel, S., Spiess, V., Ivanov, M., Bohrmann, G., and Meisner, L., 2008. Three- dimensional seismic investigations of the Sevastopol mud volcano in correlation to

gas/fluid migration pathways and indications for gas hydrate occurrences in the Sorokin Trough (Black Sea). Geochemistry, Geophysics, Geosystems, 9 (5).

Whelan, J., Eglinton, L., Cathles, L., Losh, S., and Roberts, H., 2005. Surface and subsurface manifestations of gas movement through a N–S transect of the Gulf of Mexico. Marine and Petroleum Geology, 22(4), 479-497.

Wolf, L.W., Lee, M.-K., Browning, S. and Tuttle, M.P., 2005. Numerical analysis of overpressure development in the New Madrid Seismic Zone. Bulletin of Seismological Society of America, 95, 135–144

Woodside, J.M., Ivanov, M.K., and Limonov, A.F., 1997. Neotectonics and fluid flow through seafloor sediments in the Eastern Mediterranean and Black Seas. Parts I and II. UNESCO IOC Tech Ser, no 48: 224 pp.

www.marum.de

Yamano, M., Uyeda, S., Aoki, Y., and Shipley, T.H., 1982. Estimates of heat flow derived from gas hydrates. Geology, 10: 339-343.

Zonenshain, L. P., and X. Le Pichon, 1986. Deep Basins of the Black-Sea and Caspian Sea as Remnants of Mesozoic Back-Arc Basins, Tectonophysics, 123(1-4), 181-211.

## Chapter 2. Shallow Gas Transport and Reservoirs in the Vicinity of Deeply Rooted Mud Volcanoes in the Central Black Sea
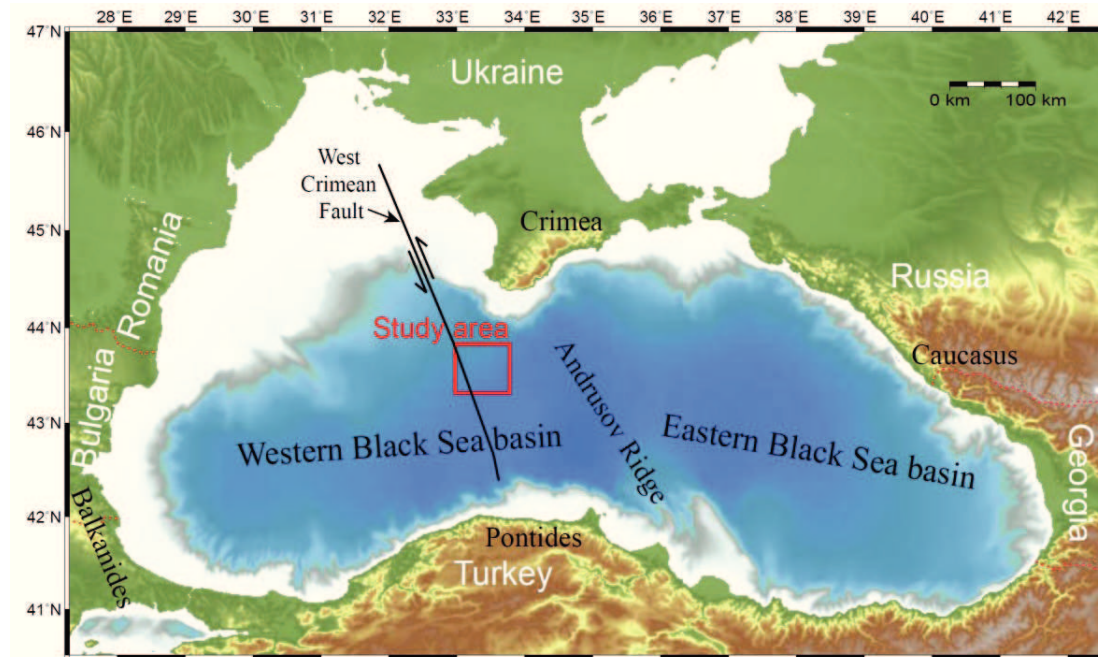
### 2.1. Introduction



**Figure 1** Bathymetric map of the Black Sea and the surroundings (Gebco 1-min grid). The Location of the study areas is marked as red rectangle. Location of West Crimean Fault is from Slack et al. (1998).

The Black Sea, containing thick sedimentary sequences with high organic matter concentrations, provides an excellent area to study mud volcanism. Among the Black Sea regions, large mud volcanoes occur in the central part of the Black Sea (Ivanov et al., 1996; Limonov et al., 1997) and in the Sorokin Trough (Ginsburg et al., 1990; Woodside et al., 1997; Krastel et al., 2003). The central Black Sea is located in the Western Black Sea basin south of the Crimean Peninsula (Fig. 1), in water depths > 2000 m. Generally, deep water mud volcanoes are often associated with gas hydrate occurrences (Woodside et al., 1997). And gas discharge in the central Black Sea is commonly associated with mud volcanism. Thus the central Black Sea is a very suitable area for researching the relationship between gas migration, gas hydrate occurrence and mud volcanism. High resolution multichannel seismic profiles were collected in the area by the University of Bremen during R/V Meteor Cruise M52/1 in January 2002, and 11 seismic Lines GeoB02-026 through GeoB02-036 have been shot to image main structures associated with six previously identified mud volcanoes (Ivanov et al., 1989): MSU, Yuzhmorgeologiya, Malyshev, Kornev, Goncharov and Vassoevitch (Fig. 2). Although

45

these mud volcanoes have been studied by seismic data of the TTR-1 Cruise in 1991, our new seismic data reveal a higher vertical and lateral resolution, which shall serve for a better understanding of gas/gas hydrate accumulations and gas/fluid migration pathways in their vicinity.

The main objectives of this study have been focused on following aims and questions:

- What are the main pathways for gas/fluid migration?
- What are the types of gas reservoirs?
- Which subsurface structures are associated with mud volcanoes?
- When did the mud volcanoes erupt and what is the possible reason causing the eruptions?
- Are there any evidences for gas hydrates existing in the vicinity of these mud volcanoes?

## 2.2. Geological setting

The Black Sea basin is surrounded by Late Cenozoic mountain belts (the Great Caucasus, Pontides, Southern Crimea and Balkanides), and represents the world's largest anoxic intercontinental basin (Finetti et al., 1988; Nikishin et al., 2003). It is widely accepted that the Black Sea was originated by a back-arc extension due to the subduction of the Tethyan Ocean in late Cretaceous time (Zonenshain and Le Pichon, 1986; Görür, 1988; Nikishin et al., 2003). The Black Sea basin is composed of two deep subbasins, the Western Black Sea basin and the Eastern Black Sea basin. The Western Black Sea basin is underlain by oceanic to suboceanic crust and contains a sedimentary cover of up to 19 km thickness, and the Eastern Black Sea basin is underlain by thinned continental crust approximately 10 km in thickness, containing up to 12 km thick sediments. The two basins are separated by the Andrusov Ridge (Finetti et al., 1988; Robinson, 1997; Nikishin et al., 2003). The margins of the Black Sea undergo compressive deformation due to the collision between Arabia and Eurasia since the Eocene (Robinson et al., 1995; Spadini et al., 1996).

The central Black Sea is located in the Western Black Sea basin south of the Crimean Peninsula (Fig. 1). Topography within this area is very flat (Gaynanov et al., 1998) with water depths >- 2000 m. The Western Black Sea contains an up to 15 km thick sedimentary basin-fill on top of the basement. These sediments include ~6 km of Paleocene-Eocene deposits, more than 5 km of the Maikopian (Oligocene-Lower Miocene) Formation and about 2.5 km of Plio-Quaternary sediments (Finetti et al., 1988). The sedimentary layers as shown on seismic profiles are almost horizontal. However, in the mud volcano area they are locally influenced by low amplitude folds (Ivanov et al., 1996), flexures and normal faults. These features are probably related to the West Crimean Fault (Fig. 1) which is the major regional strike-slip fault in the eastern part of the Western Black Sea basin and which was active from the Cretaceous through Miocene

times. Seismically imaged normal faults cut the Quaternary sediments, suggesting possible reactivation of the West Crimean fault (Limonov et al., 1997; Finetti et al., 1988; Slack et al., 1998).

The mud volcanoes in the central Black Sea are well expressed on the sea bottom as chamber-shaped features of 300-2000 m diameter and up to 120 m height. Some of them have craterlike depressions on the top with rims. The feeder channels of the mud volcanoes vary in diameter from several hundred meters to 3.5 km (Gaynanov et al., 1998). The roots of these mud volcanoes are not exactly known, but their origin is clearly related to the layers of plastic clay of the Maikopian Formation (Ivanov et al., 1996), which are highly enriched in organic matter (Dimitrov, 2002).

## 2.3. Previous acoustic studies

Mud volcanoes in the central Black Sea which were first discovered and sampled at the end of the 1980s by the Geological Faculty of Moscow State University (MSU) and Yuzhmorgeologiya, and were named as Kornev, Goncharov, Malyshev, MSU, Yuzhmorgeologiya and Vassoevitch (Ivanov et al., 1989).

Hydroacoustic studies of mud volcanoes in the central Black Sea were carried out during Cruises TTR-1, TTR-3, TTR-6 and TTR-11 in 1991, 1993, 1996 and 2001 as part of UNESCO "Training-through-Research" program (Ivanov et al., 1996; Limonov et al., 1997; Dimitrov, 2002). Mud volcanoes occur in the central part of the Black Sea in a great variety of sizes, up to 2.5 km in diameter, and they may rise more than 120 m above the seafloor. Morphologically, they can be subdivided into three types (Ivanov et al., 1996): the first type includes the largest mud volcanoes, Yuzhmorgeologiya and MSU, with a seabed diameter of ~4 km and a relative height of ~100 m. Both mud volcanoes are gentle structures with complex craters. Mud volcanoes Kornev, Malyshev and Goncharov represent the second type. They have a diameter between 1.7 and 3.8 km at the base and a height of 100 m above the seafloor, with relatively steep flanks. The third type includes the Vassoevitch mud volcano, with a very distinct, irregular shape and a collapse structure.

During RV Meteor Cruise M52/1, seismic lines were shot across these six mud volcanoes in WNW to ESE direction. Lines shot during the TTR-1 Cruise revealed a shallower penetration of ~0.9 s than the new GI Gun data with 2 s. Furthermore, compared to ~15 m vertical resolution of the TTR data, the new GI gun data provided a higher vertical resolution of ~7 m.

## 2.4. Materials and methods

A 2D high-resolution seismic data set was collected during R/V Meteor Cruise M52/1 in early 2002 (Krastel et al, 2003). A GI-gun (generator-injector gun, 2 x 1.7 L) towed in 1.4 m water depth was used as seismic source, generating main frequencies in the range

of 50 to 500 Hz. The multichannel seismic streamer (SYNTRON) includes a tow-lead, a stretch section of 50 m and six active sections of 100 m length each. GI Gun data were recorded by a 600 m long streamer using 48 channels at a group distance of 12.5 m. The streamer was kept in a water depth of 3 m (+/- 0.5 m) by the attachment of 9 cable levelers (4 MultiTrak Remote Units (MTC birds) and 5 DigiCOURSE Birds (DigiBirds)). Positioning was based on GPS recordings. 11 seismic profiles were acquired in the central Black Sea.
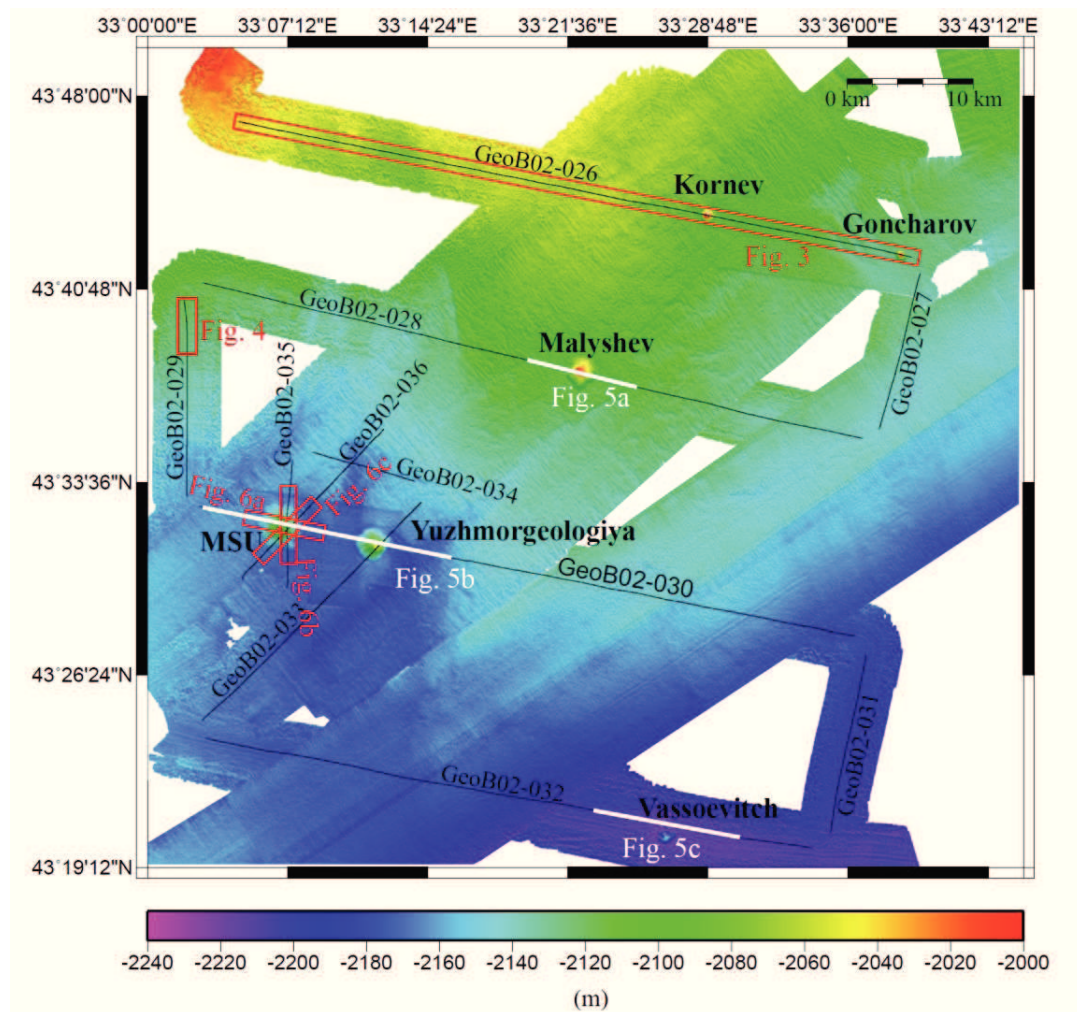


**Figure 2** Bathymetry of the area of investigation in the central Black Sea together with the seismic lines (bathymetric data from Cruises TTR6, M52-1, M72-3, MSM15-2 and M84-2). Six mud volcanoes were mapped.

The seismic data were processed, using the commercial software package Vista seismic processing. The custom-made WinGeoapp software was used for geometry calculation, CMP binning distance was chosen to be 10 m, leading to ~15-fold coverage. Dead and extremely noisy channels were removed from the data. Traces with random

spike noise were marked as dead traces and also removed. Velocity analysis was carried out on all profiles, and its results were used for the normal move-out (NMO) correction and CMP stacking. The stacked dataset was band-pass filtered (50/100-600/800 Hz) to preserve the high resolution, but optimize deeper penetration with 50 Hz coherent noise suppression. The stacked profiles were time migrated with the finite difference method. Both stacked and migrated profiles are exported from the Vista software as SEG-Y data and imported into the Kingdom Suite software for further interpretation work.

Bathymetric data used in this study were collected during the Cruises TTR-6, R/V Meteor Cruises M52/1, M72-3, and M84-2 as well as R/V MS Merian Cruise MSM15-2 (Fig. 2). The larger southwest - northeast trending block was mapped with the Simrad EM12-S multibeam system during the TTR-6 Cruise, whereas tracks parallel to the seismic lines were surveyed with the HYDROSWEEP DS2 multibeam system during Cruise M52/1. The other parts were collected with the swath echo sounders Kongsberg Simrad EM120 with a frequency of 12 kHz (during Cruises M72/3 and MSM15/2), and Kongsberg Simrad EM 122 also with a frequency of 12 kHz (during Cruise M84/2). All bathymetric data of the study area and the locations of seismic lines were plotted in Figure 2 using the Generic Mapping Tool (GMT, Wessel and Smith, 1991).

**Table 1**

Morphological characteristics of the mud volcanoes

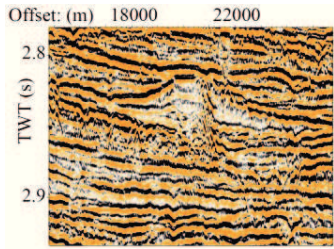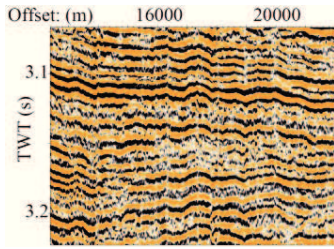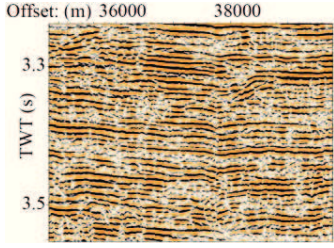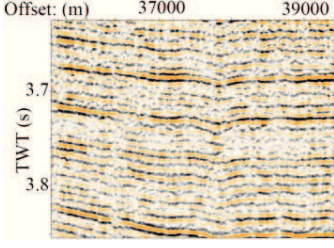| Mud volcano | Line GeoB02- | Chamber | | | Shape |
|---|---|---|---|---|---|
| | | Width (m) | Height (m) | Dipping angle (°) | |
| **Kornev** | 026 | 1450 | 116 | 9.1 | Cone-shaped |
| **Goncharov** | 026 | 1340 | 120 | 10.1 | Cone-shaped |
| **Malyshev** | 028 | 2160 | 120 | 6.3 | Cone-shaped |
| **MSU** | 030 | 3290 | 80 | 2.8 | Flat topped |
| **Yuzhmorgeologiya** | 030 | 2650 | 114 | 4-6.3 | Cone-shaped |
| **Vassoevitch** | 032 | —— | —— | —— | Depression structure |

## 2.5. Results

### 2.5.1. Morphological features of the study area

The study area is essentially flat with a southeasterly dip, its water depth varies from 2000 m in the NE to ~2200 m in the SW corner. Five cone-shaped and one depression-shaped feature were crossed by the seismic lines (Fig. 2). Table 1 presents specific morphological characteristics of the six mud volcanoes in the study area.

### 2.5.2. General seismic characteristics

**Table 2** Four seismic facies types identified in the central Black Sea

| Seismic facies | Reflection Characteristics | Example | Distribution in units |
|---|---|---|---|
| FA | Subparallel to convergent reflectors and partly transparent with medium to high amplitudes, disrupted by some chaotic reflection patches with low to medium amplitude |  | Middle to upper part of U1 |
| FB | Parallel, continuous and medium amplitude reflections |  | Lower part of U1 |
| FC | Subparallel and slightly irregular reflections with medium to high amplitudes |  | U2 |
| FD | Parallel and continuous reflections with low to medium amplitudes |  | U3 and U4 |

The 2D high resolution seismic data provide a penetration of approximately two seconds TWT bsf (two-way travel time below seafloor). Sedimentary sequences typical for the area are presented in Figure 3. The profile is divided into four seismic Units U1 to U4, which are defined according to a similar reflection configuration and regionally continuous reflectors, but excluding anomalous structures around the mud volcanoes (Fig. 3b). The middle to upper part of Unit U1 is characterized by subparallel to convergent reflectors with medium to high amplitudes. However, some parts are disrupted by some chaotic reflection patches with low to medium amplitude (seismic facies FA in Table 2). The lower part of Unit U1 shows parallel, continuous and medium amplitude reflections (seismic facies FB in Table 2). Unit U2 is characterized by subparallel and slightly irregular reflections with medium to high amplitudes (seismic facies FC in Table 2). Seismic Units U3 and U4 are characterized by parallel and continuous reflections with low to medium amplitudes (seismic facies FD in Table 2). Units U2 through U4 are disrupted by faults with vertical offsets on the order of ~5 ms TWT, and show columnar zones and wide acoustic curtains (details in Chapter 2.5.3).
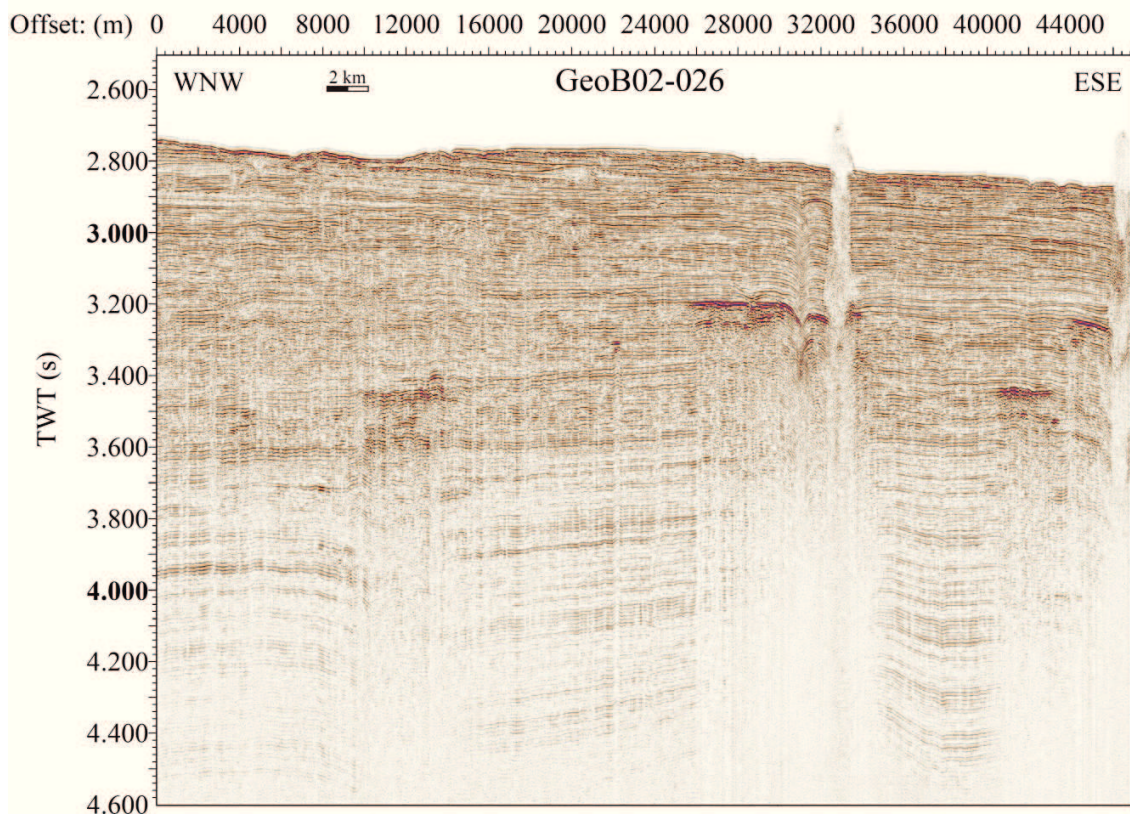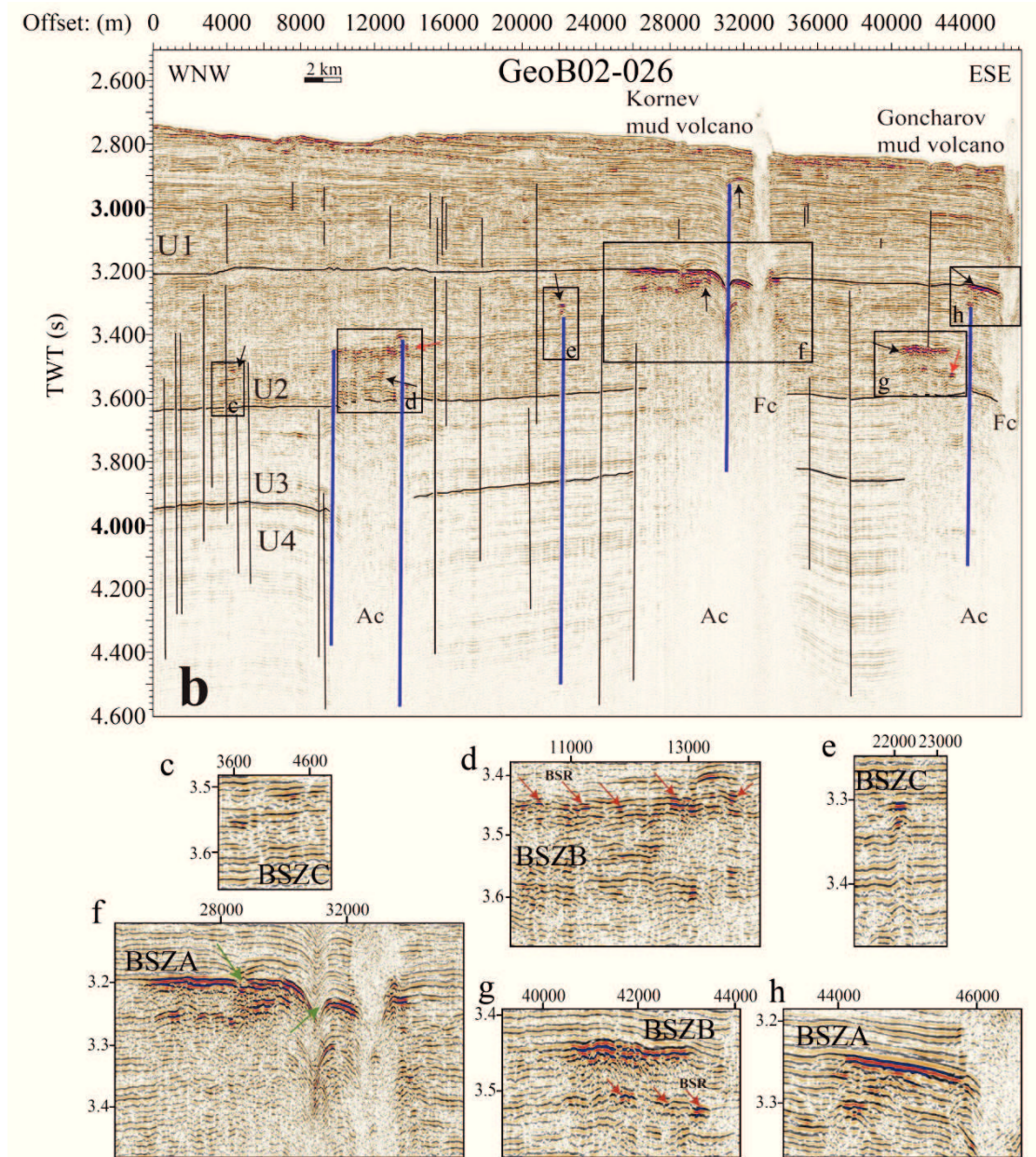
**Figure 3** Uninterpreted (a) and interpreted (b) migrated seismic Line GeoB02-026. Enlarged parts with anomalous seismic features are marked by black boxes and are shown in c-h below. Five seismic units are identified. The black arrows indicate the bright spots. The red arrows show the BSR. The black lines indicate the faults, and the blue lines mark columnar zones. The green arrows in the figure f indicate the possible paleo-pockmarks. Fc is the feeder channel, and Ac is the acoustic curtain. See the location of the profile in Figure 2.
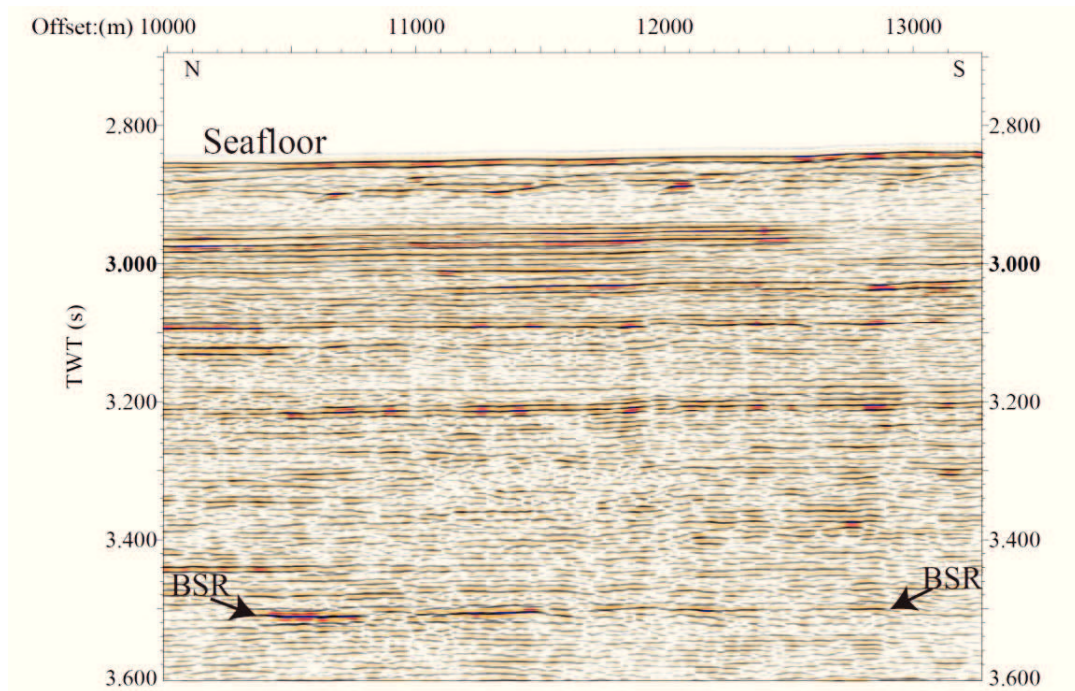
**Figure 4** A close-up of seismic line GeoB02-029. A BSR can be identified at a depth of ~650 ms TWT bsf. See the location of the profile in Figure 2.
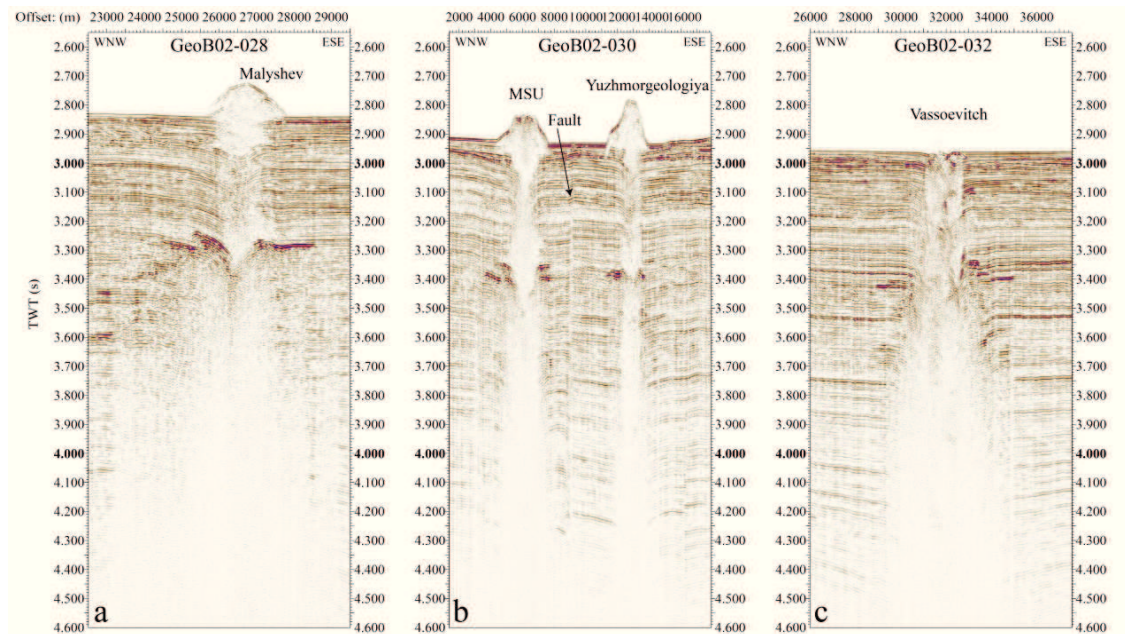


**Figure 5** Parts of Uninterpreted migration seismic profiles GeoB02-028 (a), GeoB02-030 (b), GeoB02-032 (c) crossed the MSU, Yuzhmorgeologiya, Malyshev, and Vassoevitch mud volcanoes. The fault in Figure b may indicate the location of the West Crimean Fault.
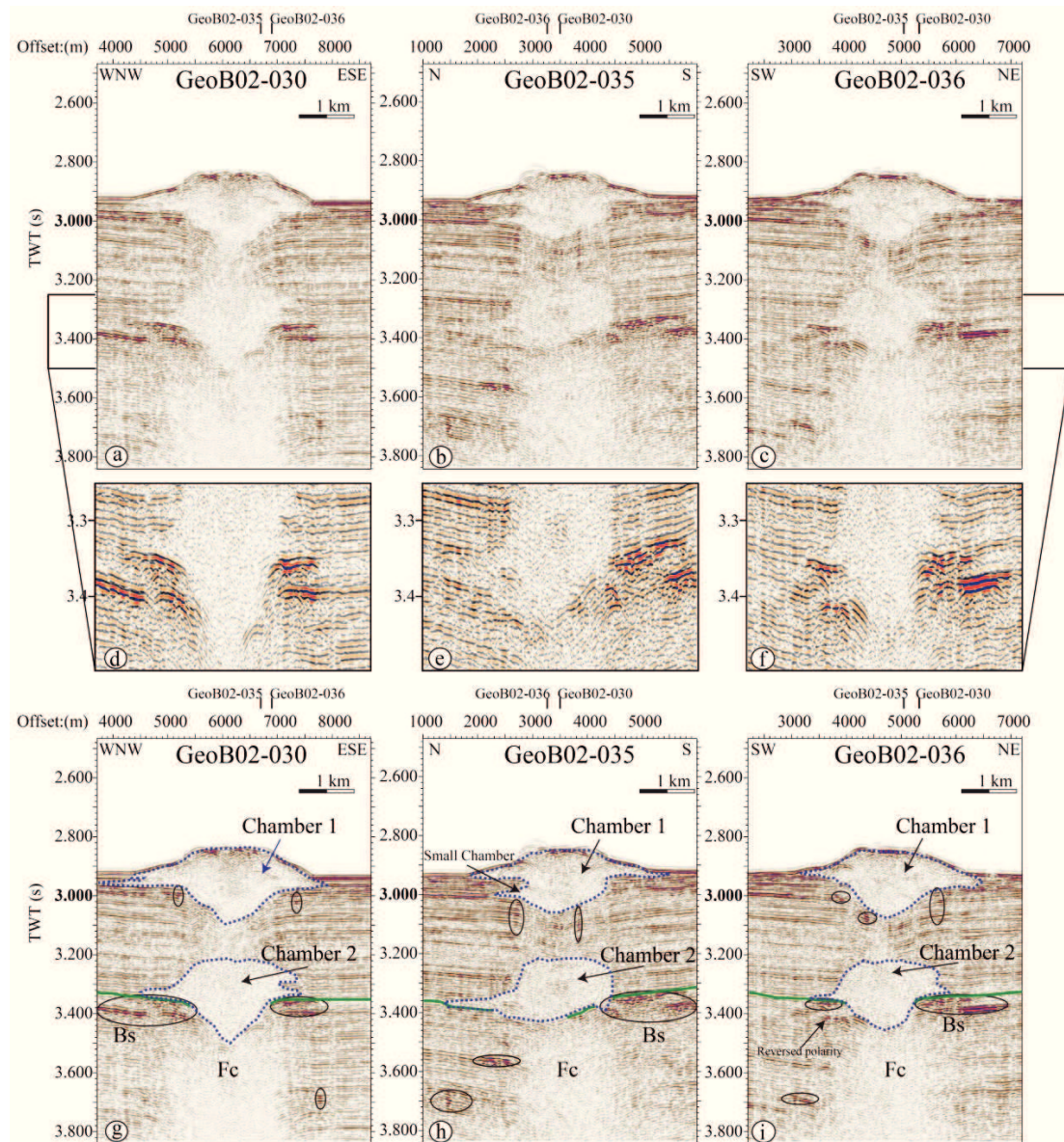
**Figure 6** Parts of uninterpreted (a-f) and interpreted (g-i) migrated seismic Lines GeoB02-030, GeoB02-035 and GeoB02-036 crossed MSU mud volcano. And closeups (d-f) for the depth interval 3250 to 3500 ms TWT. Black ellipses indicate bright spots. Mud chambers were marked by the blue dotted lines. A reversed polarity reflector was found in figure i. Fc is the feeder channel. Bs is the bright spots. Green lines present the boundary between Unit U1 and U2. See the location of the profiles in Figure 2.

### 2.5.3. Anomalous seismic features

In Figure 3a, a zone of reduced amplitudes can be observed beneath the mud volcano with a width similar to the diameter of the mud volcano. Such a vertical zone was called a feeder channel by Ivanov et al. (1996). Feeder channels of mud volcanoes are narrow

within the upper sedimentary unit and appear slightly wider with increasing depth. They are mostly transparent, and no coherent reflectors are visible, but some chaotic reflection patches occur within the feeder channels or can be traced into the surrounding sediments. The feeder channel width of Kornev, Goncharov, Malyshev, MSU, Yuzhmorgeologiya and Vassoevitch mud volcanoes are ~730-1070 m, ~800-1000 m, ~1280-2100 m, ~520-2800 m, ~950-1690 m and ~1330 m respectively (Fig.s 3 and 5). Further details are discussed in Chapter 2.5.4.

The columnar zones are characterized by vertical and narrow zones of reduced amplitudes with reflections bending upward or downward towards the center (Fig. 3) as e.g. in Figures 3e and 3f. Most of the tops of these columnar zones do not reach the seafloor, and mainly terminate in the depth range of ~3.2 - 3.6 s TWT. The vertical extent of the columnar zones cannot be determined due to general signal attenuation but the base appears to be deeper than 5200 ms TWT.

Acoustic curtains (a term used by Popescu et al., 2007) are the wide areas on the seismic sections, which are characterized by the chaotic and discontinuous reflections (Fig. 3). The marginal reflectors of the acoustic curtains are bent slightly downward. The base of acoustic curtains can't be observed, similar to columnar zones.

Many but small vertical reflector offsets (~5 ms TWT) are clearly seen in the seismic profile (Fig. 3b), which are interpreted as faults and which seem to extend to greater depth, like the columnar zones. Most of the deeper faults reach into seismic Units U2 and U3. Fewer faults were observed within seismic Unit U1.

In organic rich marine sediments, seismic profiles may also reveal amplitude anomalies mimicking the seafloor ("Bottom Simulating Reflector", BSR), which are linked to the presence of gas (methane) hydrates. They are generally caused by the impedance contrast between gas hydrate-bearing and free gas-bearing sediments (Shipley et al., 1979). In the study area, a BSR is mostly absent except for three locations indicated in Figures 3d, 3g and 4. There it is characterized by high amplitudes, reversed polarity and it is slightly crosscutting the strata. The BSR appears discontinuous in Figures 3d and 3g. The BSR is located at a depth of ~650 ms TWT bsf.

Bright spots, which are reflections of particularly high amplitude, were observed in several areas in Figure 3b, and they can be grouped into three types: (1) Bright Spot Zone A (BSZA) around the feeder channels, including the one in Figure 3f with a lateral extent of ~8330 m and a vertical extent of ~60 ms TWT bsf, and the one in Figure 3h with a lateral extent of ~168 m and a vertical extent ~60 ms TWT bsf. Their average sediment depth is ~400 ms TWT bsf. Similar bright spots can also be observed at the feeder channels of all other mud volcanoes in the study area (Fig. 5), and all the tops of these bright spot zones cluster around the same depth; (2) Bright Spot Zones B (BSZB), as in Figures 3d and 3g, are located above the acoustic curtains. Their lateral extent is found to

be ~3120 m and ~2670m, respectively, the vertical extent is ~152 and ~90 ms TWT bsf, respectively, and the average depth is ~650 ms TWT bsf. Parts of the BSZB are disrupted by chaotic reflection patches; (3) Bright Spot Zone C (BSZC) at the top or at the sides of faults and columnar zones (Fig.s 3c and 3e) with average depths of ~700 and ~550 ms TWT bsf, respectively. The width of BSZA and BSZB is nearly equal to the width of acoustic curtains beneath. The polarity of the bright spot reflections is uncertain, as we are facing superposition of several reflections due to dense layering. A clear reversed polarity of a bright spot was observed in Figure 6i on the side of the feeder channel of MSU mud volcano. Other bright spots, however, reveal positive polarity and follow the sediment strata. The amplitude within the bright spot zones is stronger than the sea floor reflection amplitude in the same region.

## 2.5.4. Mud volcanoes

**Table 3**
Depth of base reflectors of the mud chambers for six mud volcanoes traced at some distance, where the thickness of the upper sediments has little changed.

| Mud volcanoes | Base reflector depth in ms TWT (from deep to shallow) | | |
|---|---|---|---|
| | deep | intermediate | shallow |
| Kornev | 411 | 88 | 16 |
| Goncharov | 413 | 76 | 22 |
| Malyshev | 420 | 83 | 18 |
| MSU | 418 | 66 | 21 |
| Yuzhmorgeologiya | 419 | - | 20 |
| Vassoevitch | 393 | 164 | 20 |

Six mud volcanoes are located in the central Black Sea. While Kornev and Goncharov mud volcanoes are shown in Figure 3, MSU, Yuzhmorgeologiya, Malyshev, and Vassoevitch mud volcanoes are displayed in Figure 5. Within the feeder channel, wider transparent zones of rhombic shape are identified, residing near the feeder channel conformably on downward bent sedimentary layers, which we call 'mud chambers'. The base reflectors of these mud chambers were traced to some distance from the mud volcanoes and their depths were determined (Table 3), allowing to assign approximate ages based on the seismic stratigraphy introduced in Chapter 2.6.2. If these 'mud chambers' represent muddy deposits originating from the feeder channel, they may well reveal major eruption phases - at least two of them are found in the vicinity of all mud volcanoes at 390-420 ms TWT and at 16-22 ms TWT, and a third unit at four mud

volcanoes between 66 and 88 ms TWT and at 164 ms TWT at Vassoevitch mud volcano (Table 3).

We use the MSU mud volcano as an example to study the details of the subsurface structures of the mud volcanoes, as we can analyze three seismic Lines GeoB02-030, GeoB02-035 and GeoB02-036 across the top, which can reveal its internal structure in three different directions: WNW-ESE, N-S and SW-NE (Fig. 6). A close-up of the depth range 3250 to 3500 ms TWT is shown beneath each line. The MSU mud volcano has a flat top of ~1360 m width, while the other mud volcanoes have the cone-shaped tops. The feeder channel was clearly identified from reduced reflection amplitudes. Its diameter varies with depth. Two mud chamber structures Chamber 1 and Chamber 2 (Fig. 6) and a small chamber beneath the Chamber 1 (Fig. 6b) can be clearly seen at the seafloor and from 3200 to 3500 ms TWT. The mud chambers are distinguished by low reflection amplitudes next to parallel undisturbed seismic reflections. Also, transparent to chaotic reflectors can be observed in the inner parts. The transparent to discontinuous reflectors between Chamber 1 and Chamber 2 are bent downward, and can be traced to adjacent reflectors of sediment. A few small bright spot patches distribute at those reflectors and the edge of the feeder channel. Large bright spot zones BSZA are found beneath Chamber 2, with a maximum lateral extent of ~1700 m, and at the depth of ~400 ms TWT bsf around the feeder channel. Beneath Chamber 2, reflectors are also bent downward. The feeder channel connects to the wider acoustic curtain at greater depth. A high amplitude and reverse polarity reflector was clearly observed in Figure 6i with a depth of ~520 ms TWT bsf.

## 2.6. Interpretation and Discussion

### 2.6.1. Sedimentary processes

Based on its complex seismic facies (Table 2), the middle to upper part of U1 can be attributed to the Danube and Dniepr deep sea fan complexes, as interpreted by Winguth et al. (2000), representing e.g. channel-levee deposits and mass transport deposits. The lower part of U1 with parallel and continuous reflectors is predominantly constructed by fine-grained deposits, which are likely formed by the unchannelized distal fan deposition during earlier stages of fan development. U2 is interpreted as a more coarse-grained unit possibly representing sandy terminal lobes from surrounding rivers, e.g. the Paleo-Don River in the Northeast which entered the Black Sea during the middle Pliocene to late Pliocene (Popov et al., 2004; Barg, 2007; Tari, 2011). According to Wagner-Friedrichs (2007) who studied sediments in the Sorokin Trough to the Northeast of the study area, the Paleo-Don River fan was observed during the early Pleistocene in the Sorokin Trough, which was likely formed earlier than the Danube and Dniepr fan. Therefore, the Paleo-Don River might enter the Black Sea during the middle Pliocene to late Pliocene and form a large deep sea fan during the early Pleistocene. U2 probably indicated the sandy terminal lobes from Paleo-Don River. Unit U3 and U4 are characterized by parallel and

continuous reflections, which might be the distal finer grained turbidites or hemipelagic sediments, because the Black Sea basin remained a deep water basin during most of the Cenozoic (Hsü and Giovanoli, 1979; Popov et al., 2004). The other areas of the Black Sea during the Pliocene and early Quaternary was dominated by a shallow marine environment characterized by varved clays, micrites, and diatomaceous shales.

About 900 ka ago, the Danube River reached the Black Sea for the first time and has subsequently built up the Danube fan, and appx. 800 ka ago, the Dniepr fan started to form (Winguth et al., 2000). The two large fan systems deliver sediment with a high sand fraction, which most likely corresponds to Unit U1 in our seismic profiles. While the average sedimentation rates of Winguth et al., (2000) have been determined for the delta and slope region west of the study area, appearance of fan sediment may be delayed due to progradation, and typical fan structures therefore only appear in the middle to upper part of Unit U1, while unchannelized finer-grained deposits have formed during earlier stages of fan development. The sedimentation rate of the Unit U1 should have some changes, due to the Danube and Dnieper fan deposits causing a higher sedimentation rate in the middle to upper part, while a lower sedimentation rate was in the lower part of U1. But it's difficult to calculate the sedimentation rates at the different depths accurately. Therefore, an average sedimentation rate will be calculated and used for correcting the age of seismic units of the study area in the Chapter 2.6.2.

Quaternary sedimentation in the Black Sea is strongly influenced by glacial-interglacial cycles, which in turn affected its sea level beyond the rise and fall of global sea level (Paluska and Degens, 1979). Sea level change also controlled the progradation and builtup of Danube fan and Dniepr fan. Winguth et al., 2000 concluded that during highstand, the deep Black Sea basin was sediment-starved, receiving condensed hemipelagic sediments, while during lowstand, channelized transport and mass wasting provided coarse-grained sediments.

## 2.6.2. Seismic stratigraphy

Stratigraphic information from the central Black Sea is rare, as there is no detailed information on deep penetration drill sites published. Therefore, we attempt to derive age estimates from information provided by petroleum corporations for different areas of the Black Sea, namely the Western Black Sea (Bega and Ionescu, 2009), the Eastern Black Sea (Meisner et al., 2009) and the Turkish Black Sea (Menlikli et al., 2009), and some published seismic profiles are close to the vicinity of the study area. For example, in Figure 7, the interpreted seismic profile close to the central Black Sea provides a thickness of the Quaternary and Pliocene sections to be ~1.2 s TWT and ~0.5 s TWT, respectively. Accordingly, we assign a Quaternary age to Units U1 through U3 (Fig. 3b), which thickness of is nearly the same with 1.2 s TWT, and a Pliocene age to Unit U4.
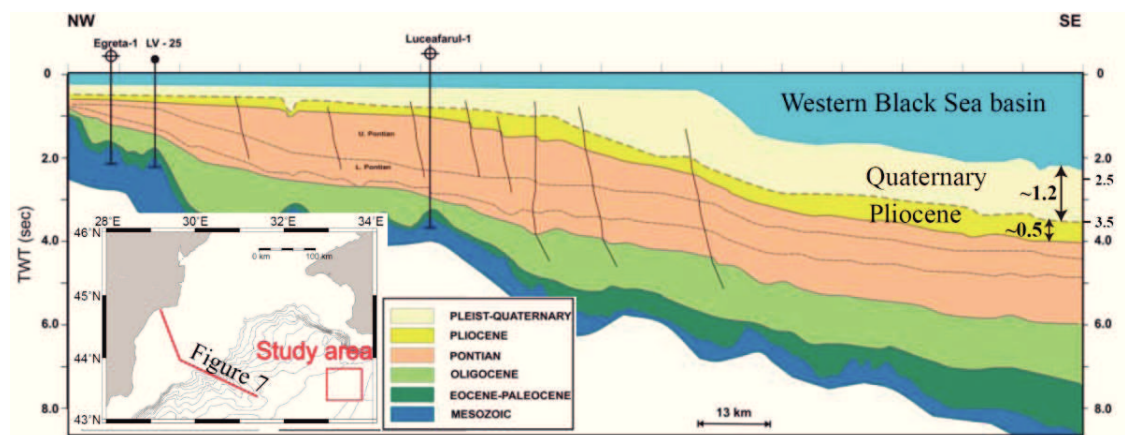
**Figure 7** Geo-seismic section through the Western Margin of the Black Sea modified from Bega and Ionescu, 2009. The thickness of the Quaternary section near the study area is ~1.2 s TWT, and thickness of the Pliocene section is ~0.5 s TWT, respectively.

For an age of ~2.6 Ma for the Pliocene-Pleistocene boundary (Cohen et al., 2013), an average sedimentation rate for the Quaternary can be estimated to 0.37 m/ka (v=1600 m/s), which is consistent with sedimentation rates of 0.3-0.4 m/ka derived for the Quaternary section from Deep Sea Drilling Project Leg 42B in the Black Sea (Ross et al., 1978). Ages for other reflectors are estimated by linear interpolation. Accordingly, the base of U1 has an approximate age of 900 ka BP, and the base of U2 is in the age of ~1.8 Ma.

Comparing with the seismic profiles, U3 and U4 are dominated by the seismic facies FD, which probably presents the distal finer grained turbidites, and indicates similar sedimentary processes between the very early Pleistocene (U3, ~1.8-2.6 Ma) and the late Pliocene (U4). During the early Pleistocene (~1.8-0.9 Ma), the seismic facies FC occurred in the seismic Unit U2 presents the coarse grain sediments, which are probably from the sandy terminal lobes from Paleo-Don River. During the middle to late Pleistocene (after ~900 ka), the seismic facies FB shows the fine grain sediments in the lower part of U1, which might be formed by the unchannelized distal fan deposition during earlier stages of Danube and Dnieper fan development. The seismic facies FA appears in the middle to upper parts of U1 and shows the Danube and Dniepr deep sea fan complexes reaching the study area.

Although the method of age assignments might be simplicity and naturally carry a certain error, the principal result of the age correlation should be valid.

### 2.6.3. Free gas and gas hydrate occurrences

Almost 91% of the deep-water basin of the Black Sea provides favourable conditions for gas hydrate formation (Vassilev and Dimitrov 2002). Gas hydrates were found to

occur in mud breccias of mud volcanoes in the central Black Sea (Ivanov et al. 1989, 1998; Konyukhov et al. 1990; Kruglyakova et al. 1993; Limonov et al. 1994). Gas hydrates in marine sediments can usually be inferred from the existence of a BSR in seismic reflection profiles (e.g. Kvenvolden and Barnard, 1983). Most BSRs are formed due to the high acoustic impedance contrast between gas hydrates and associated free gas underneath. They can cut across the stratigraphy of sediments, and run roughly parallel to the topography of the seafloor. They can generate a (strong) reflector with reversed polarity compared to the seafloor (Shipley et al. 1979). If sedimentary layers are generally parallel to the seafloor, as in this study area, the BSR may be difficult to identify. A BSR seems to be absent in most parts of the study area except for three locations (Fig.s 3d, 3g and 4) based on medium to high amplitude, reversed polarity, mimicking of the seafloor and slightly crosscutting the strata. The BSR was observed at a depth of ~650 ms TWT bsf. Assuming a bottom water temperature of 9 °C, a thermal gradient can be estimated from the BSR depth (Yamano et al., 1982). For a sediment velocity of 1600 m/s and the average depth of the BSR of 650 ms TWT bsf, a temperature gradient of 23 °C/km can be estimated, which is consistent with the average temperature gradient of 26±4 °C/km in this area derived from heat flow measurements (Kutas and Poort, 2008).
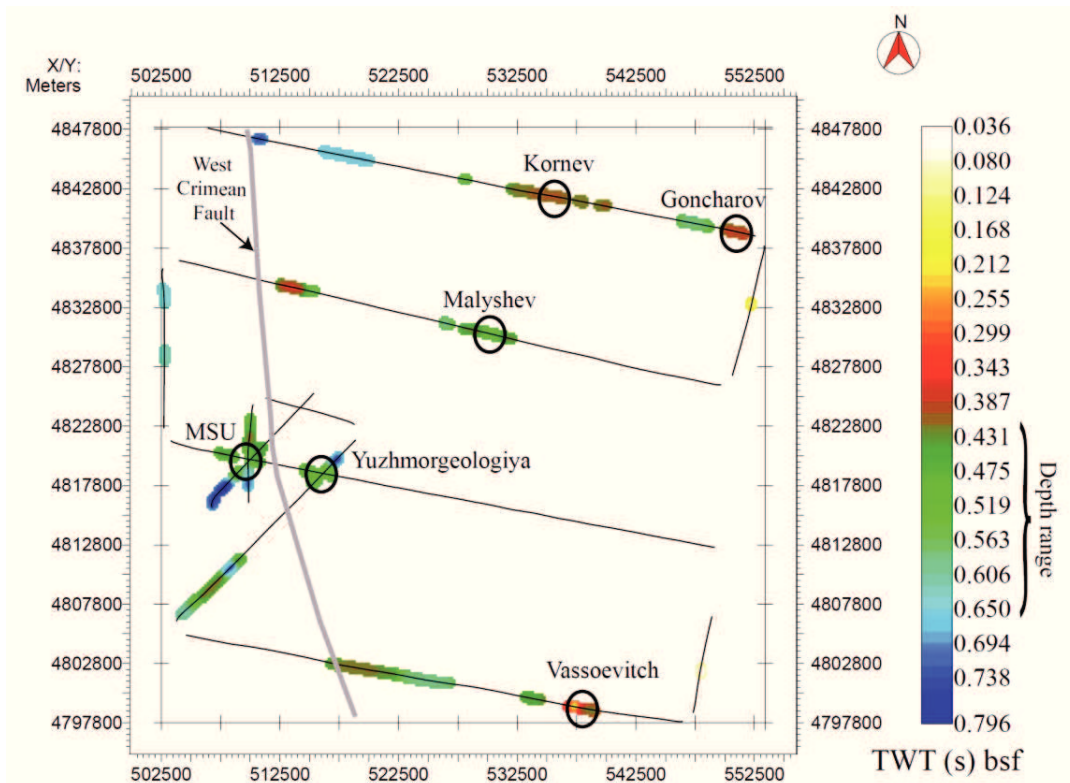


**Figure 8** Distribution and depth in s TWT bsf of the Bright Spots and the BSR, together with the locations of the mud volcanoes and the West Crimean Fault.

In the study area, many bright spots were also observed at different depths (Fig. 8), such as around the feeder channels of mud volcanoes (BSZA), above the acoustic curtains (BSZB), and on the tops and sides of the faults and columnar zones (BSZC). The bright spots relate to feeder channels, faults, columnar zones and acoustic curtains, which are typically associated with migration of gas/fluid. Further evidence for free gas would be a reversed polarity of seismic reflectors due to a decrease in velocity and impedance, which seemed to be, however, obscured by interference of multiple layers. Only in one case, polarity of bright spots could be clearly identified as reversed (Fig. 6i). But it is evident that all bright spot zones reveal significantly higher amplitudes than the sea floor. According to the identification of the BSR, the base of the gas hydrate stability zone (BGHSZ) is likely located at ~650 ms TWT bsf. Our seismic data show that the bright spots occur in a depth range between ~400 and ~650 ms TWT bsf, which is shallower than BGHSZ. The bright spots locate within the GHSZ, and therefore may indicate gas hydrate (transformed from free gas accumulations) and/or free gas.

As described above, three types of bright spots zones (BSZA, BSZB and BSZC) were observed in the seismic profiles. They are distributed in seismic Units U2, which are supposedly rich in sand (coarse-grained) and provided a suitable reservoir for gas. The top of U2 is marked by a transition to finer-grained turbidites from unchannelized distal fan deposition, providing a seal for gas migration due to lower (vertical) permeability, forming a reservoir-seal combination. All the BSZAs of relatively wide lateral extent appear at a depth of ~400 ms TWT bsf. We suggest that the onset of distal fan sedimentation with fine-grained turbidites provided a major control on vertical gas migration and trapping. The free gas in the Zones BSZB and BSZC, which occur in different depths within Units U2, are more probably trapped by gas hydrate layers

## 2.6.4. Gas and fluid migration pathways besides the feeder channels (columnar zones, acoustic curtains and faults)

Columnar zones and acoustic curtains have not been reported in the central Black Sea before, but similar seismic features were observed on the shelf and continental slope of the western Black Sea, named as acoustic columns and acoustic curtains by Popescu et al. (2007). The root of these features could not be imaged, but must be in the study area deeper than 1.9 s TWT within the sedimentary column. Feeder channels of mud volcanoes, most columnar zones and bright spots occur in association with acoustic curtains, which may hint to vertical pathways for methane migration. As rock fragments in mud breccia from the mud volcanoes are of Maikopian age or younger (Ivanov et al., 1996; Limonov et al., 1997, Dimitrov, 2002), the organic-rich Maikopian formation appears to be the most probable source sediment. The Maikopian is also the main regional hydrocarbon source around the Black Sea (Robinson et al., 1996).

Most of the columnar zones terminate at sediment layers within the GHSZ, and bright spots show up at their top. This combination hints to vertical gas migration and the presence of an efficient seal, which could be formed by impermeable (fine-grained) layers or gas hydrates. Due to the 2D nature of the seismic grid, the shape cannot be determined, but we suggest that the columnar zones represent gas blow-out pipes, as they are found e.g. in the Niger Delta in water depths between 1100 m and 1350 m (Løseth et al., 2010). The reasons for the upward bending of seismic reflections inside the columnar zones (Fig. 3e) are still debated (Hustoft et al., 2007). Løseth et al. (2010) suggested that the upward or downward bending of inner reflections may be a geophysical artefact. The features in Figure 3f (green arrows) might represent paleo-pockmarks, one ~970 m in diameter and ~35 m depth is similar in size to those large pockmarks reported from the western African margin by Gay et al., (2003), and they are too large to be artefacts.

Large mud volcanoes in the central Black Sea occur close to the trace of the southeastward continuation of the West Crimean fault, and some are apparently located at fault intersections (Slack et al., 1998). Both deep multichannel seismic profiles from Yuzhmorgeologiya (Limonov et al., 1997) and high resolution seismic profiles of this study imaged normal faults, extending upward into mid-Quaternary sediments. These fault systems may be caused by a possible reactivation of West Crimean fault in the Quaternary as proposed by Slack et al. (1998). But the West Crimean fault seems not to reach to the seafloor (the fault is likely located between MSU and Yuzhmorgeologiya mud volcanoes, see Fig.s 5b and 8), the reason may be that it was quickly covered by the Danube and Dniepr fan deposits. Such deep faults may have also served as main pathways for gas/fluid migration, probably appearing as columnar zones. Acoustic curtains in the vicinity may indicate that larger volumes of gas and strong bright spot reflections are present, where columnar zones are found.

### 2.6.5. Mud volcanoes

In Table 3, we estimated the depth of the reflectors at the base of the mud chambers in the all six mud volcanoes. Kornev, Goncharov Malyshev, MSU and Vassoevitch mud volcanoes have three eruption episodes, while Yuzhmorgeologiya mud volcano appears to have two major eruption episodes. The base reflectors of the chambers are bent downwards, making the rhombic shape of the mud chambers, which are the same reflectors that we implied by the dating of eruptions. These bending downwards reflectors may represent the collapsed and settled disturbed sediment layers (Hovland et al., 1997). By tracing the base reflectors of the chambers of all mud volcanoes, these base reflectors appear in a very narrow depth range, represented by very few reflectors. That suggests that the mud volcanoes started to erupt during almost the same time range, and then continued activity for quite some time to build up the mud chamber. According to the calculated average sedimentation rate of the Quaternary section 0.37 m/ka and a sediment velocity of 1600 m/s, approximate times for the initiation of intense mud

volcanism could be calculated (Fig. 9). Although the age assignments naturally carry a certain error, we hypothesize from a comparison to a sea level curve for the Black Sea (Winguth et al., 2000) that all eruption episodes may have started during times of distinct falls of sea level by more than 100 meters. A drop in sea level gradually reduces the overburden pressure away from neutral buoyancy conditions. In overpressured gas reservoirs, pressure may exceed lithostatic pressure and promote mobilization of gas, fluids and mud. Therefore, sea level falls related to glacial-interglacial cycles (Paluska and Degens, 1979) may have provided a trigger for mud volcano eruptions in the study area. Similar situations were also observed on the mud volcanoes in the western Alborán Sea (Somoza et al., 2012).
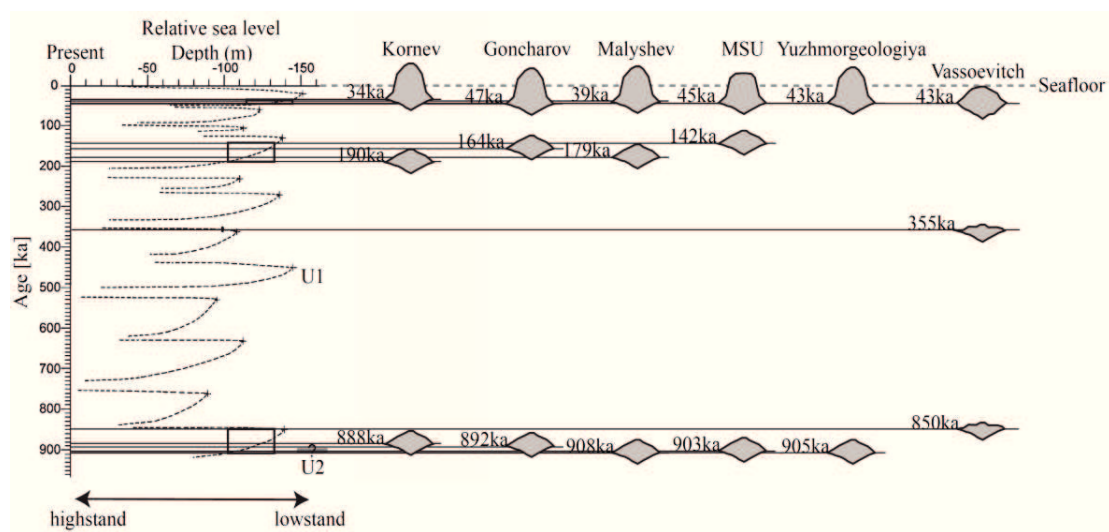


**Figure 9** The age of the boundary between seismic Units U1 and U2 is estimated to be ~900 ka. Eruption times of the six mud volcanoes are annotated on the left of the mud chamber. All mud volcanoes have three eruption times except for Yuzhmorgeologiya mud volcano. A regional sea level curve of the northwestern Black Sea is taken from Winguth et al. (2000). The dotted line indicates the seafloor. Black rectangles indicate the sea level range of mud volcanoes' eruption.

MSU mud volcano is covered by three seismic lines providing spatial information in contrast to the other surveyed mud volcanoes. Previous studies (Limonov et al., 1997; Dimitrov, 2002) showed that the MSU mud volcano was active over a longer time period and shows multiple eruptive phases, but seems to be in a quiescent stage nowadays. We use the MSU mud volcano to study the internal structures and the evolution of mud volcanoes in the central Black Sea during the Quaternary. To summarize structural information, we suggest the conceptual model for MSU shown in Figure 10.

The architecture of the MSU mud volcano comprises two mud chambers, a small chamber and a feeder channel (Fig. 10). Transparent seismic reflections on both sides of the mud chambers are interfingering with adjacent parallel undisturbed seismic

reflections. These transparent seismic reflections represent mud flows deposited during eruptive episodes. Therefore, three mud chambers represent three periods of intense eruptive activity.
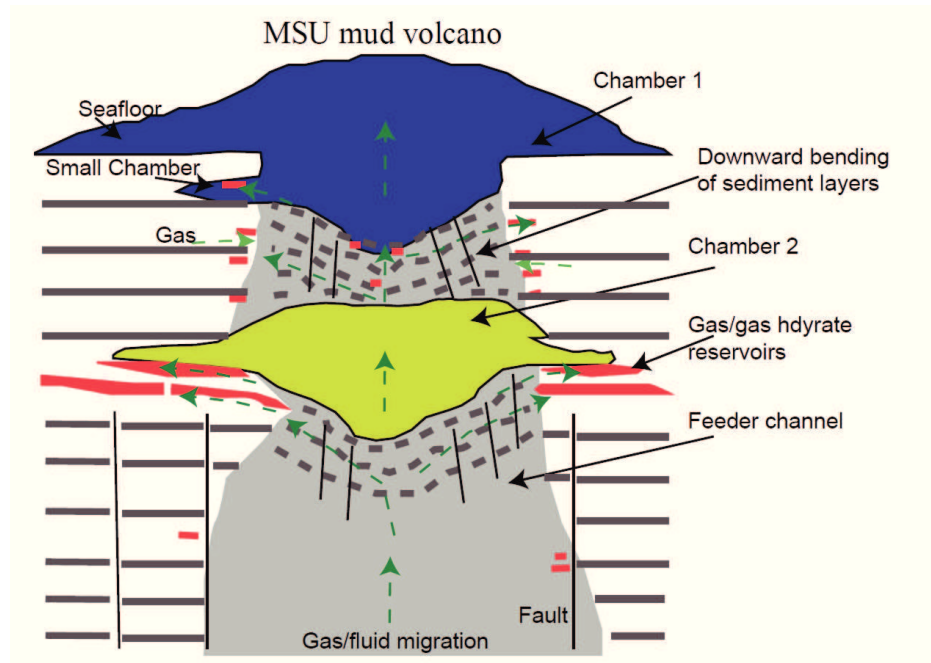


**Figure 10** Structural and evolutionary of the MSU mud volcano. Red patches indicate the gas/gas hydrate reservoirs. Dark green arrows show the gas/fluid migration pathways. Light green arrows show the gas may derive from the shallow subsurface. Dotted lines indicate the downward bending of sediment layers in the feeder channel, which can be traced towards the undisturbed sedimentary strata. Two mud chambers and a small chamber are included. Faults are indicated the vertical black lines.

Feeder channels of mud volcanoes are interpreted in six locations as the main pathways for gas and fluid upward migration. Main characteristics are a flat top, wide mud chambers and wide feeder channels, which indicate low mud viscosity, transport of large gas and mud volume and long lasting activity, similar to the evidence provided by Somoza et al. (2012). Downward bending of reflections at the base of mud chambers reveals a significant collapse due to a volume loss and depressurization associated with mud eruptions. On the flanks of the feeder channel, bright spots and blurred margins indicate the lateral transport of gas into the surrounding high permeable (sandy) sediment layers. This may originate from free gas transported with the mud, but also from gas hydrate decomposition in case that the mud eruption provides fast vertical heat transport. Isotopic analysis showed that the gas is of mixed biogenic and thermogenic origin (Ivanov et al., 1996; Limonov et al., 1997). The biogenic gas may derive from the shallow subsurface, which is rich in the terrigenous organic matter from the Danube and Dniepr rivers (Limonov et al., 1997). Particularly the thermogenic gas migrates upward

along the feeder channel from the deeper sources, e.g. the Maikopian Formation (Dimitrov, 2002). Biogenic gas is widely produced and concentrated above and beneath the BGHSZ.

## 2.7. Conclusions

- Four types of pathways for gas and fluid migration can be recognized: feeder channels of mud volcanoes, columnar zones, acoustic curtains and faults. Also three types of gas reservoirs in the central Black Sea are identified: a) Large gas/gas hydrate reservoirs around the feeder channels of mud volcanoes (BSZA); b) Large gas/gas hydrate reservoirs located above the acoustic curtains (BSZB); c) Small gas/gas hydrate reservoirs at the top or sides of the faults and columnar zones (BSZC).

- No regional BSR exists in the central Black Sea. A BSR is difficult to identify and absent in most parts of the study area, possibly due to the nearly parallel sedimentary layers to the seafloor and the local gas supply. Only a few local BSR segments can be recognized. The BGHSZ is found at a depth of ~650 ms TWT bsf, which suggests a geothermal gradient of 23°C/km.

- Bright spots occur in a depth range between ~400 and ~650 ms TWT bsf within the GHSZ. A few bright spots with reverse polarity indicate the free gas, while most of the bright spots with positive polarity may suggest an increase in impedance, which we interpret as charging with gas hydrates only.

- Our age model suggests that seismic Unit U1 has been deposited since ~900 ka, representing Danube and Dniepr fan sediments, with an upward increase in grain size/reflectivity due to fan progradation. Unit U2 is related to coarser material particularly from the Paleo-Don River, while the early Quaternary Unit U3 consists of uniformly layered sediment, probably made of distal finer grained turbidites. Unit U4 is of Pliocene age. Overall grain size variations distinctly influence porosity and potential for the presence of gas accumulations and gas trapping.

- All the BSZAs of relatively wide lateral extent appear at the boundary between Units U1 and U2, which is marked by a change from supposedly more sandy material to fine-grained turbidites, providing a seal for gas migration due to lower (vertical) permeability, forming a reservoir-seal combination. The bright spots Zones BSZB and BSZC are more probably formed by massive gas hydrate layers, converted originally from free gas, which are associated with normal polarity reflections.

- Mud volcanoes are composed of wide and deep feeder channels, showing several wide mud chambers, residing on collapsed sediment strata in the center. They show both gas and gas hydrate accumulations near the feeder channel, where gas may be of biogenic and thermogenic origin and from hydrate decomposition during eruptive phases. Kornev, Goncharov Malyshev, MSU and Vassoevitch mud volcanoes reveal three major eruption episodes, while at Yuzhmorgeologiya mud volcano only two major eruption episodes can be interpreted. All of the eruptive episodes of the mud volcano might be related to distinct sea level falls, which seem to be one of the main trigger factors of the mud volcano eruptions in the central Black Sea.

## Acknowledgements

## References

Barg, I., 2007. Age and origin of the Kerch Strait and the Sea of Azov. Doklady Earth Sciences 412 (1), 17–18.

Bega, Z., and Ionescu, G., 2009. Neogene structural styles of the NW Black Sea region, offshore Romania. The Leading Edge, September 2009, 1082-1089.

Cohen, K.M., Finney, S., and Gibbard, P.L., 2013. International Chronostratigraphic Chart, International Commission on Stratigraphy.

Damuth, J. E., and Kumar, N., 1975. Amazon Cone: morphology, sediments, age, and growth pattern. Geological Society of America Bulletin, v. 86, pp. 863-878.

Dimitrov, L.I., 2002. Mud volcanoes - the most important pathway for degassing deeply buried sediments. Earth-Science Reviews, 59: 49-76.

Finetti, I., Bricchi, G., Del Ben, A., Pipan, M., and Xuan, Z., 1988. Geophysical study of the Black Sea. Bolletino di Geofisica Teorica ed Applicata, 30: 197-324.

Gay, A., Lopez, M., Cochonat, P., Sultan, N., Cauquil, E., and Brigaud, F., 2003. Sinuous pockmark belt as indicator of a shallow buried turbiditic channel on the lower slope of the Congo Basin, West African Margin. Geological Society, London, Special Publications, 216 (1), 173-189.

Gaynanov VG, Bouriak SV, Ivanov MK, 1998. Seismic evidence for gas accumulation related to the area of mud volcanism in the deep Black Sea. Geo-Mar Lett 18:139–145.

Ginsburg, G.D., Kremlev, A.N., Grigor, M.N., Larkin, G.V., Pavlenkin, A.D. and Saltykova, N.A., 1990. Filtrogenic gas hydrates in the Black Sea (21st voyage of the research vessel

Evpatoriya). Soviet Geol Geophys, 31: 101-152.

Görür, N., 1988. Timing of opening of the Black Sea basin. Tectonophysics 147, 247-262.

Hovland, M., Hill, A., and Stokes, D., 1997. The structure and geomorphology of the Dashgil mud volcano, Azerbaijan. Geomorphology, 21: 1-15.

Hsü, K.J. and Giovanoli, F., 1979. Messinian event in the Black Sea. Palaeogeogr. Palaeoclimatol. Palaeoecol. 29, 75-93.

Hustoft, S., Mienert, J., Bünz, S., and Nouzé, H., 2007. High-resolution 3D-seismic data indicate focussed fluid migration pathways above polygonal fault systems of the mid-Norwegian margin. Marine Geology, 245 (1), 89-106.

Ivanov, M.K., Konyukhov, A.I., Kulnitskiy, L., and Musatov, A.A., 1989. Mud volcanoes in the deep part of the Black Sea. Vestnik oscovskogo Un-ta, Ser. Geal., 3: 21-31 (in Russian).

Ivanov MK, Limonov AF, and Weering TCE, 1996. Comparative characteristics of the Black Sea and Mediterranean Ridge mud volcanoes. Mar Geol 132:253-271.

Ivanov MK, Limonov AM, Woodside JM, 1998. Extensive deep fluid flux through the sea floor on the Crimean continental margin (Black Sea). In: Henriet JP, Mienert J (eds) Gas hydrates; relevance to world margin stability and climate change. Geol Soc Spec Publ, pp 195-214.

Krastel, S., Spiess, V., Ivanov, M., Weinrebe, W., Bohrmann, G., Shashkin, P., and Heidersdorf, F., 2003. Acoustic images of mud volcanoes in the Sorokin Trough, Black Sea, Geo-Marine Letters, 23, 230-238.

Kutas, R. I., and Poort, J., 2008. Regional and local geothermal conditions in the northern Black Sea. International Journal of Earth Sciences, 97 (2), 353-363.

Kvenvolden, K.A., and Barnard, L.A., 1983. Gas hydrates of the Blake Outer Ridge, Site 533, Deep Sea Drilling Project Leg 76. Initial Reports of the Deep Sea Drilling Project, 76: 353-365.

Limonov, A.F., van Weering, Tj.C.E., Kenyon, N.H., Ivanov, M.K., and Meisner, L.B., 1997. Seabed morphology and gas venting in the Black Sea mud volcano area: Observation with the MAK-1 deep-tow side scan sonar and bottom profiler. Marine Geology, 137: 121-136.

Løseth, H., Wensaas, L., Arntsen, B., Hanken, N.-M., Basire, C., and Graue, K., 2010, 1000 m Long Gas Blow-Out Pipes: Marine and Petroleum Geology.

Meisner, A., Krylov, O. and Nemcok, M., 2009. Development and structural architecture of the Eastern Black Sea. The Leading Edge, 28(9): 1046-1055.

Menlikli, C., A. Demirer, O. Sipahioglu, L. Korpe, and V. Aydemir, 2009, Exploration plays in the Turkish Black Sea: Leading Edge, v. 28/9, p. 1066-1075.

Nikishin, A.M., Korotaev, M.V., Ershov, A.V., Brunet,M.-F., 2003. The Black Sea basin: tectonic history and Neogene–Quaternary rapid subsidence modelling. Sediment. Geol. 156, 149-168.

Paluska A., Degens E. T, 1979. Climatic and tectonic events controlling the Quaternary in the Black Sea region. Geol. Rdsch 68:284–301.

Popescu, I., Lericolais, G., Panin, N., De Batist, M., and Gillet, H., 2007. Seismic expression of gas and gas hydrates across the western Black Sea. Geo-Marine Letters, 27 (2-4), 173-183.

Popov SV, Rögl F, Rozanov AY, Steiniger FF, Shcherba IG, Kovac M, 2004. Lithological-paleogeographic maps of Parathethys: 10 maps Late Eocene to Pliocene Courier Forschunginstitut Senckenberg.

Robinson, A.G., Banks, C.J., Rutherford, M.M., Hirst, J.P.P., 1995. Stratigraphic and structural development of the Eastern Pontides, Turkey. Journal of Geological Society, London 152, 861- 872.

Robinson, A.G., and Kerusov, E., 1997. Stratigraphic and structural development of the Gulf of Odessa, Ukrainian Black Sea: implications for petroleum explorations. In: Robinson, A.G. (Ed.), Regional and Petroleum Geology of the Black Sea and Surrounding Region. American Association of Petroleum Geologists, Memoir, vol. 68, pp. 369-380. Tulsa, OK.

Robinson, A.G., Rudat, J.H., Banks, C.J. and Wiles, R.L.F., 1996. Petroleum Geology of the Black Sea. Marine and Petroleum Geology, 13 (No. 2): 195-223.

Ross, D. A., Neprochnov, Y. P., and Supko, P. R., 1978. Introduction and explanatory notes, Leg 42B, Deep Sea Drilling Project. Init. Rep. Deep Sea Drilling Proj, 42, 3-15.

Shipley, T., Houston, M., and Buffer, R., 1979. Seismic reflection evidence for the widespread occurrence of possible gas hydrate horizons on continental slopes and rises. AAPG Bulletin, 63: 2204-2213.

Slack, J. F., Turner, R. J. W. and Ware, P. L. G., 1998. Boron-rich mud volcanoes of the Black Sea region: Modern analogues to ancient sea-floor tourmalinites associated with Sullivan-type Pb-Zn deposits? Geology, 26, 439-442.

Somoza, L., Medialdea, T., León, R., Ercilla, G., Tomás Vázquez, J., Farran, M. L., Hernández-Molina, J., González , J., Juan , G., and Fernández-Puga, M. C., 2012. Structure of mud volcano systems and pockmarks in the region of the Ceuta Contourite Depositional System (Western Alborán Sea). Marine Geology, Volumes 332–334, Pages 4-26.

Spadini, G., Robinson, A. and Cloetingh, S., 1996. Western versus Eastern Black Sea tectonic evolution: pre-rift lithospheric controls on basin formation. Tectonophysics, 266: 139-154.

Tari, G., 2011. Exploration Country Focus: Ukraine*. Search and Discovery Article #10359.

Vassilev, A., and Dimitrov, L., 2002. Spatial and qualitative evaluation of methane hydrates in the Black Sea. Russian Geology and Geophysics, 43, 7, 637-649 (in English and Russian)

Wessel, P. and Smith, W. H. F. 1991. Free software helps map and display data. EOS 72, 445-446.

Winguth, C., Wong, H. K., Panin, N., Dinu, C., Georgescu, P., Ungureanu, G., Krugliakov, V.V., and Podshuveit, V., 2000. Upper Quaternary water level history and sedimentation in the northwestern Black Sea. Marine Geology, 167 (1), 127-146.

Woodside, J.M., Ivanov, M.K., and Limonov, A.F., 1997. Neotectonics and fluid flow through seafloor sediments in the Eastern Mediterranean and Black Seas. Parts I and II. UNESCO IOC Tech Ser, no 48: 224 pp.

Yamano, M., Uyeda, S., Aoki, Y., and Shipley, T.H., 1982. Estimates of heat flow derived from gas hydrates. Geology, 10:339−343.

Zonenshain, L.P., Le Pichon, X., 1986. Deep basins of the Black Sea and Caspian Sea as zemnants of Mesozoic back-arc basins. Tectonophysics 123, 181-211.

## Chapter 3. Sedimentary Evolution of the Kerch Peninsula margin, Black Sea

### 3.1. Introduction

The study area is located on the continental slope of the Kerch Peninsula margin in the northern part of the Eastern Black Sea. Sediments of the continental margin can preserve significant information on sediment flux, on paleoclimate, and also on sea level fluctuations (Winguth et al., 2000). A number of key papers (such as Robinson et al. 1995 and 1996, Nikishin et al. 2003) have discussed the stratigraphy, tectonics and evolution of the Black Sea region. However, there is little to no detailed description of the sedimentary evolution of the Kerch Peninsula margin available with respect to seismic facies and high resolution seismic stratigraphy.

The purpose of this paper is to interpret seismic features and to document the sedimentary structures from late Miocene to Recent, and then to gain some insight into the sedimentary evolution of the Kerch Peninsula margin. We describe and interpret six seismic units in terms of their approximate geological ages, seismic facies character and distribution, depocenter locations, provenance, and tectonic movement of the Crimean Mountains and Black Sea basin. Examples of seismic profiles, isopach and seismic facies maps are presented to illustrate the seismic characteristics, areal distribution and thickness in temporal and spatial variation of each seismic unit.
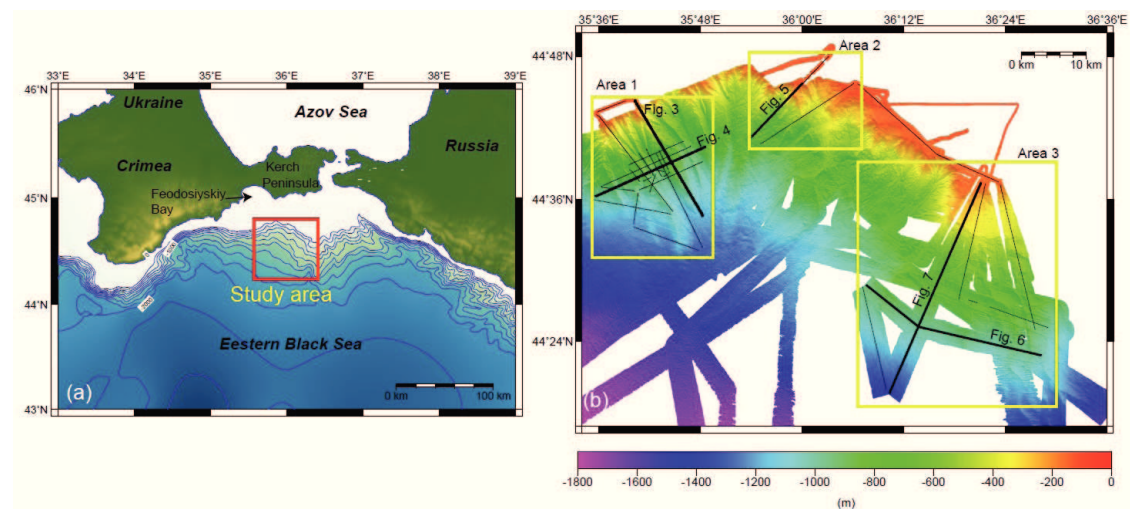


**Figure 1** (a) The northeastern area of the Black Sea and the surroundings (Gebco 1-min grid). The location of the study areas is marked as a red rectangle. (b) Bathymetric map of the study area with the locations of seismic profiles, and three sub-study-areas. The locations of figures are indicated by thick lines and marked with their respective figure numbers.

### 3.2. Geological setting

The Black Sea is a large anoxic and intracontinental basin surrounded by Alpine orogenic belts: the Crimean Mountains in the North, the Caucasus in the Northeast, and the Balkanides in the West and the Pontides in the South. The collision of Arabia with

Eurasia lead to a compressional tectonic regime since the Eocene (Nikishin et al., 2003; Robinson et al., 1995), and thus the margins of the Black Sea are characterized by deformation (Robinson et al., 1995). The Black Sea is separated by the Andrusov and the Archangelsky Ridge into two subbasins, the Western and the Eastern Black Sea Basin (Fig.s 1 and 2), both containing a 10-19 km thick sediment cover (Tugolesov et al., 1985). The Eastern Black Sea Basin contains some troughs and barriers developed in the Oligocene and Miocene, such as the Sorokin Trough, Kerch-Taman Trough and Indolo-Kuban Trough (Fig. 2) (Wagner-Friedrichs, 2007).

The rifting of the Eastern Black Sea basin most likely began in the Early Cretaceous. Inversion tectonics and compressional events affected the whole Crimean Black Sea region during the Middle Eocene, Late Eocene, Early Miocene and Middle Miocene. These compressional phases occurred along with the continuing post-rift basin subsidence. The geometry of probably EW–trending structures such as Sorokin Trough and Tetyaev–Shatsky ridge indicated that the southeastern Crimean Black Sea was influenced by the North-South directed compression, and numerous anticline structures have formed as a response to the shortening (Stovba et al., 2009).
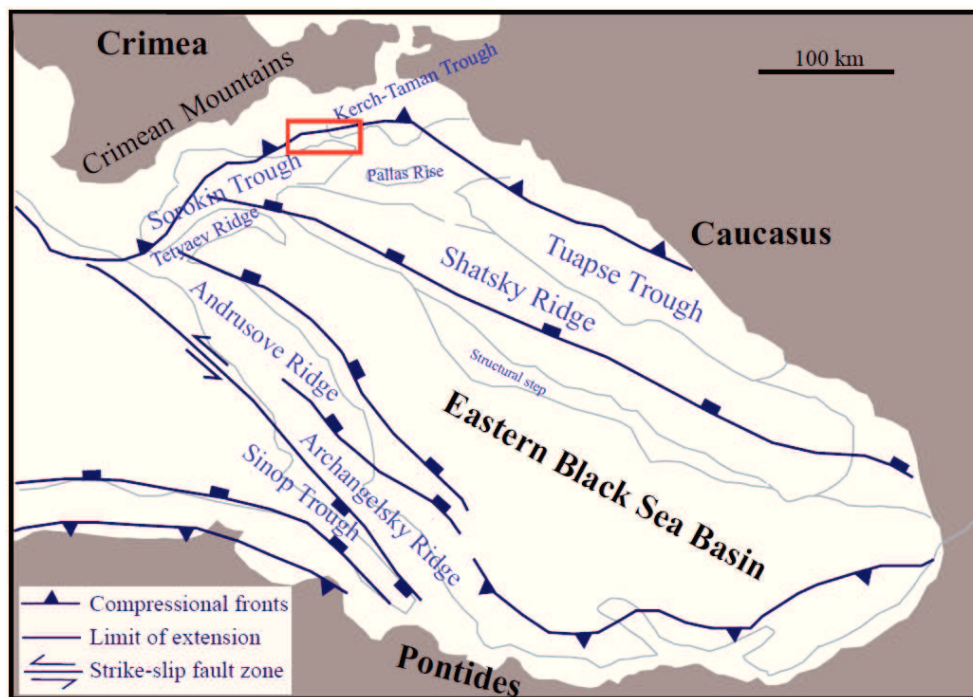


**Figure 2** Schematic map of the main tectonic zones within the Eastern Black Sea Basin (modified after Robinson et al., 1996). The red rectangle marks the location of the study area which was investigated during the M72/3b Cruise.

The Kerch Peninsula is a prominent geographic feature located in the eastern portion of Crimea. It is located between two neighboring seas: the Azov Sea and the Black Sea. The study area is located south of the Kerch Peninsula (Fig. 1) on the continental slope, bordered by the Crimean Mountains in the North and Northwest, the Sorokin Trough in the South-West, the Kerch-Taman Trough in the East and Tetyaev-Shatsky Ridge in the

South (Fig. 2). The water depth in this area ranges from ~100 m to ~1500 m. The sedimentary cover of our study area consists in ages of Jurassic to Paleogene, Upper Eocene to Lower Miocene, Middle Miocene and Upper Miocene to Quaternary sedimentary sequences, with a total thickness up to 15 km (Stovba et al., 2009).

## 3.3. Data sets and methods

Thirty two high resolution seismic lines were acquired in the study area during R/V Meteor Cruise M72/3b in March/April, 2007. The seismic source was a Sodera Generator – Injector (GI) airgun with extended chamber volume (4.1 L generator and 1.7 L injector, frequency range from 30 - 300 Hz) towed in 7 m water depth. The multichannel seismic streamer (SYNTRON) includes a tow-lead, a stretch section of 44 m and ten active sections of 50 m length each. A 30 m long meteor rope with a buoy at the end was connected to the tail swivel, and resulting in a total tow length of 574 m. Data were recorded by a 500 m long streamer section (SYNTRON) with 80 channels at a group distance of 6.25 m. The streamer was kept in a water depth of 3 m (+/- 0.5 m) by the attachment of 5 birds (cable levelers). Positioning was based on GPS recordings. 32 seismic profiles were recorded in this study area (Bohrmann et al. 2007).

The multichannel seismic data were processed with the Vista seismic processing software package. The custom-made WinGeoapp program (H. Keil, University of Bremen) has been used for geometry calculations. CMP binning distance was chosen to be 2 m. Dead and extremely noisy channels were removed. Traces with random spike noise were marked as dead traces. Velocity was picked for all profiles, and used for normal move-out (NMO) correction and CMP stacking. The datasets were filtered with a broad band-pass filter of 10/30 - 250/400 Hz. The stacked profiles were time migrated with the finite difference method. Both stacked and migrated profiles were exported from the Vista software as SEG-Y data and imported into the Kingdom Suite software for further interpretation work.

The bathymetric data of the study area were collected with the multibeam echo sounders Kongsberg Simrad EM120 with a frequency of 12 kHz (during M72/3 and MSM15/2), and Kongsberg Simrad EM 122 also with a frequency of 12 kHz (during M84/2). The bathymetric map and the locations of seismic line were plotted by the Generic Mapping Tool (GMT, Wessel and Smith, 1991).
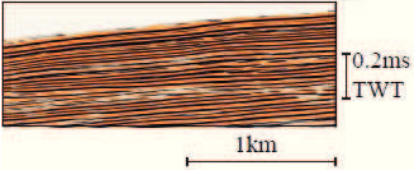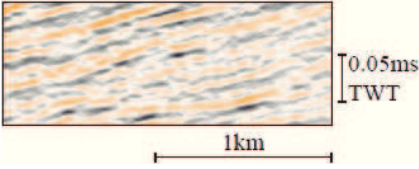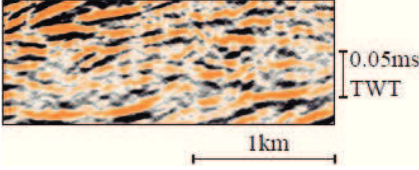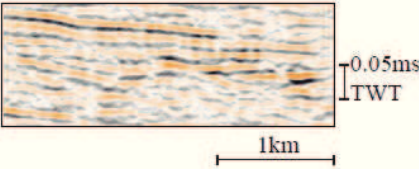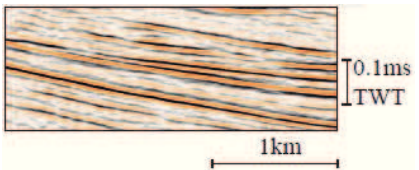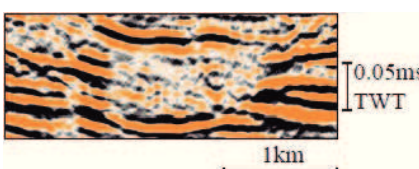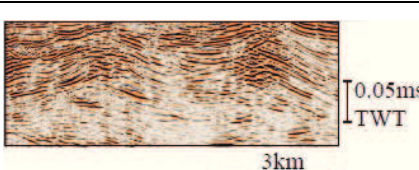
## 3.4. Results

The study area was discussed in three separate parts: Area 1, Area 2 and Area 3 (Fig. 1). First, the seismic facies and seismic units of the whole study are described in general. Then, more details about the seismic facies and seismic units of the three different areas, and the differences among them will be discussed. Isopach maps and the seismic facies distribution maps were created for Area 1 only, because for this task seismic line density is only sufficient in Area 1.

### 3.4.1. Seismic facies

**Table 1: Facies concept for the Kerch Peninsula continental margin**

Seven seismic facies types in the continental slope of the Kerch Peninsula margin, the northeastern Black Sea. The table includes seismic facies name, characteristics and examples. The characteristics of the seismic facies are described according to reflection configuration, continuity, amplitude, external geometry, etc.

| Seismic facies | Characteristics | Facies example |
|---|---|---|
| Seismic facies A | High amplitude, widespread, moderately to good continuous and parallel reflectors |  |
| Seismic facies B | Low to moderate amplitude, moderately to good continuous and parallel reflectors |  |
| Seismic facies C | Low to high amplitude, low continuous reflectors |  |
| Seismic facies D | Variable amplitude, chaotic to low continuous reflectors |  |
| Seismic facies E | Moderately to good continuous and parallel reflectors, interbedded high and low amplitude horizons |  |
| Seismic facies F | The chaotic semi-transparent reflection pattern disrupting the higher amplitude reflectors |  |
| Seismic facies G | Mound shapes with high amplitude and chaotic internal reflections, downlap |  |
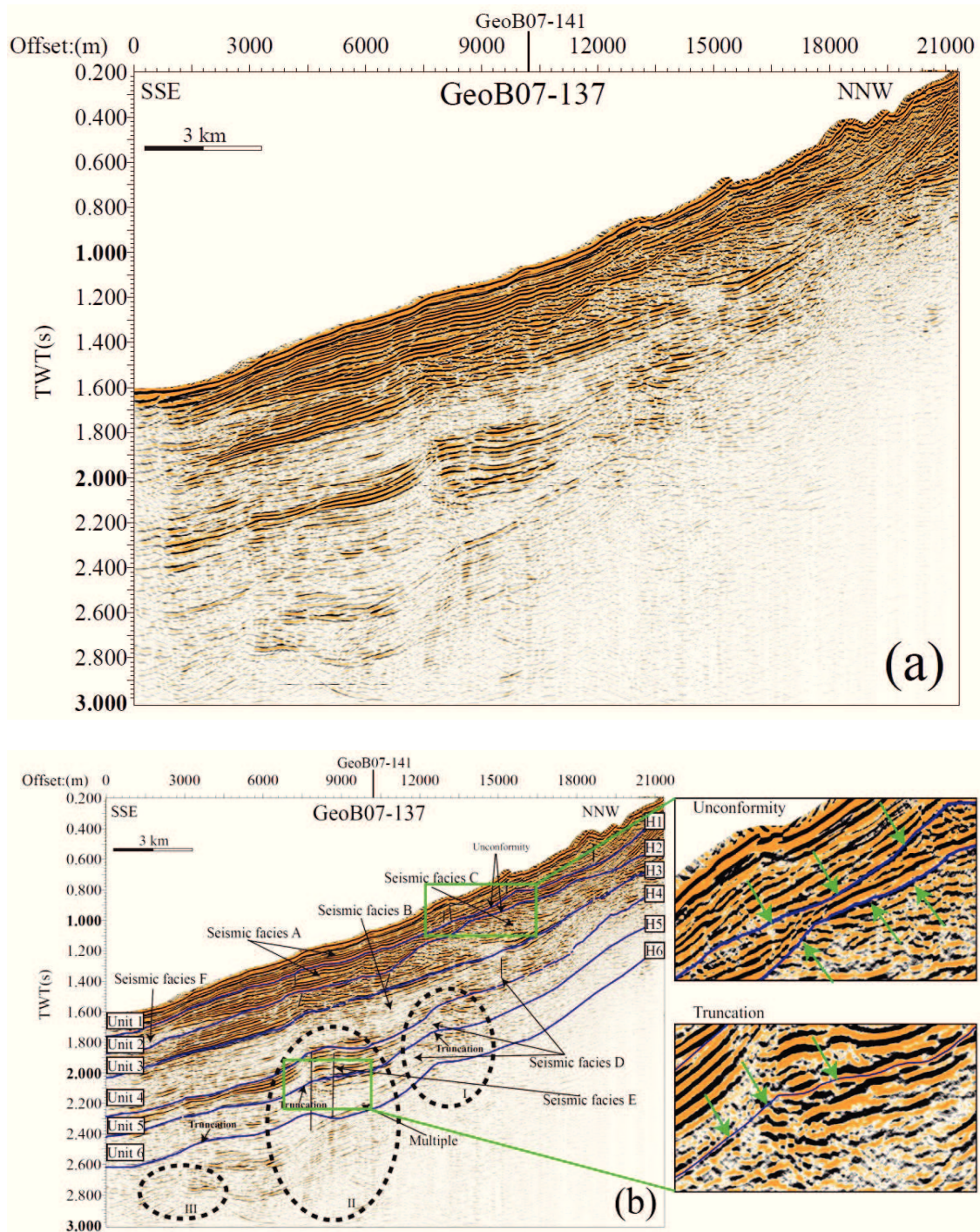
**Figure 3** (a) Uninterpreted migrated seismic Line GeoB07-137 in Area 1. (b) Six seismic units are indicated based on identified unconformities and boundaries between different domains of seismic amplitude. Six basal horizons for the six units are named H1 to H6. Different seismic facies can be identfied as marked. Three upbending reflection structures are marked by black dotted ellipses and named I, II, III. The truncation and unconformity surfaces are indicated by the green arrows in the enlarged figures. See the location of the profile in Figure 2.
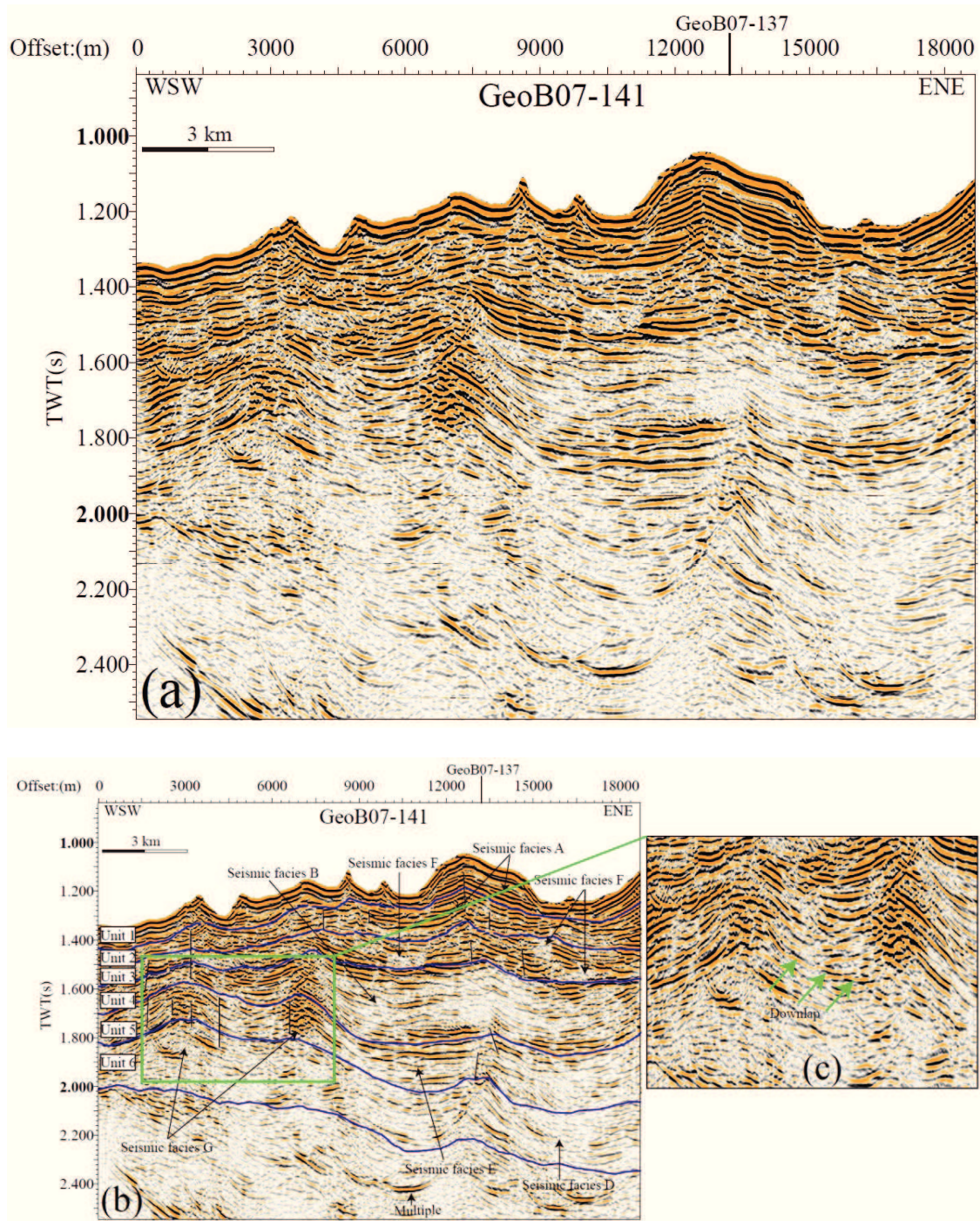
**Figure 4** (a) Uninterpreted migrated seismic Line GeoB07-141 in Area 1. (b) Interpreted seismic Line GeoB07-141, showing seismic facies A, B, D, E, F and G, and seismic units (1-6). (c) Seismic facies G, green arrows indicate the downlap. See Figure 2 for location.

Seven seismic facies types were distinguished on the basis of reflection character and geometry (Table 1), such as reflection configuration, continuity, amplitude and external geometry.

Seismic facies A is characterized by widespread, high amplitude, moderately to good continuous and parallel reflectors. Seismic facies B is composed of low to moderate amplitude, moderately to good continuous and parallel reflectors. Seismic facies C is composed of low to high amplitude, low continuous reflectors. Seismic facies D is characterized by variable amplitude, chaotic to low continuous reflectors. Seismic facies E is characterized by moderately to good continuous and parallel reflectors, interbedded high and low amplitude horizons. Seismic facies F is made of the chaotic semi-transparent reflection pattern disrupting the higher amplitude reflectors. Seismic facies G appears mound shapes, with high amplitude and chaotic internal reflections, and the right mound downlap on the left mound. The location and distribution of these seismic facies will be shown in the seismic facies maps.

### 3.4.2. Seismic units

Six horizons are mapped throughout the study area. These horizons are defined according to unconformities and marked boundaries between distinct seismic facies. Six seismic units are identified according to the six horizons. These seismic units are characterized by the seven seismic facies types. The six horizons and six seismic units are referred to as H1 to H6 and Unit1 to Unit 6, respectively (Fig. 3b).
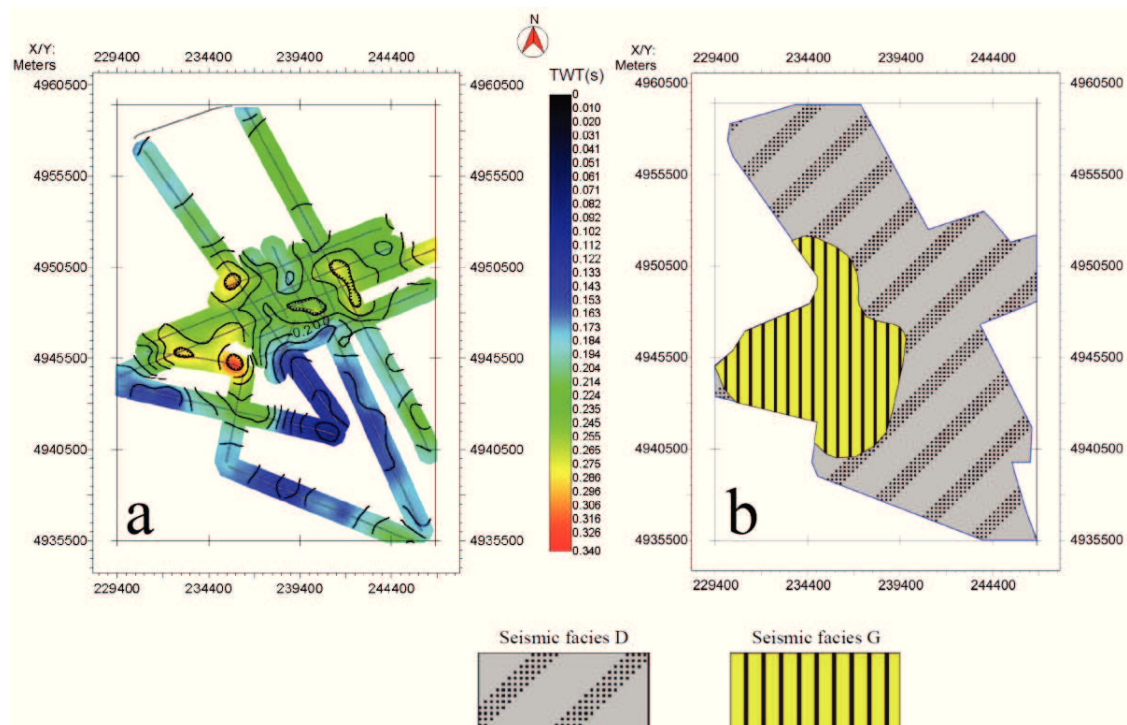


**Figure 5** (a) Isopach map of Unit 6. (b) Seismic facies map of Unit 6. The maximum thickness of Unit 6 is located in the WSW part of the study area, consists of seismic facies G. The rest of the study area consists of seismic facies D.

### 3.4.3. Observations on Area 1 profiles

The isopach maps for the seismic units in Area 1 were constructed using the two-way travel time (TWT). The seismic facies distribution maps for each seismic unit in Area 1 were created using the dominant seismic facies.

### 3.4.3.1. Seismic Unit 6

Seismic Unit 6 has an average thickness of ~200 ms TWT (Fig. 5a), with a maximum of ~350 ms TWT in its western part. It mainly consists of seismic facies G (Fig. 5b), which is mounded with moderate continuity and variable amplitude. However, the extent of seismic facies G narrows from seismic Unit 6 to seismic Unit 5 (Fig. 6b), and disappeared in seismic Unit 4 (Fig. 7b). The northern part of seismic Unit 6 is thicker than in the southern part, with an ENE-WSW oriented depocenter. The thickness minimum is located in the WSW part with ~100 ms TWT (Fig. 5a). Seismic Unit 6 consists mainly of seismic facies D besides seismic facies G. Seismic facies D reveals variable amplitude, chaotic to low continuous reflectors. The base of seismic Unit 6 (H6) is marked by a truncation surface.
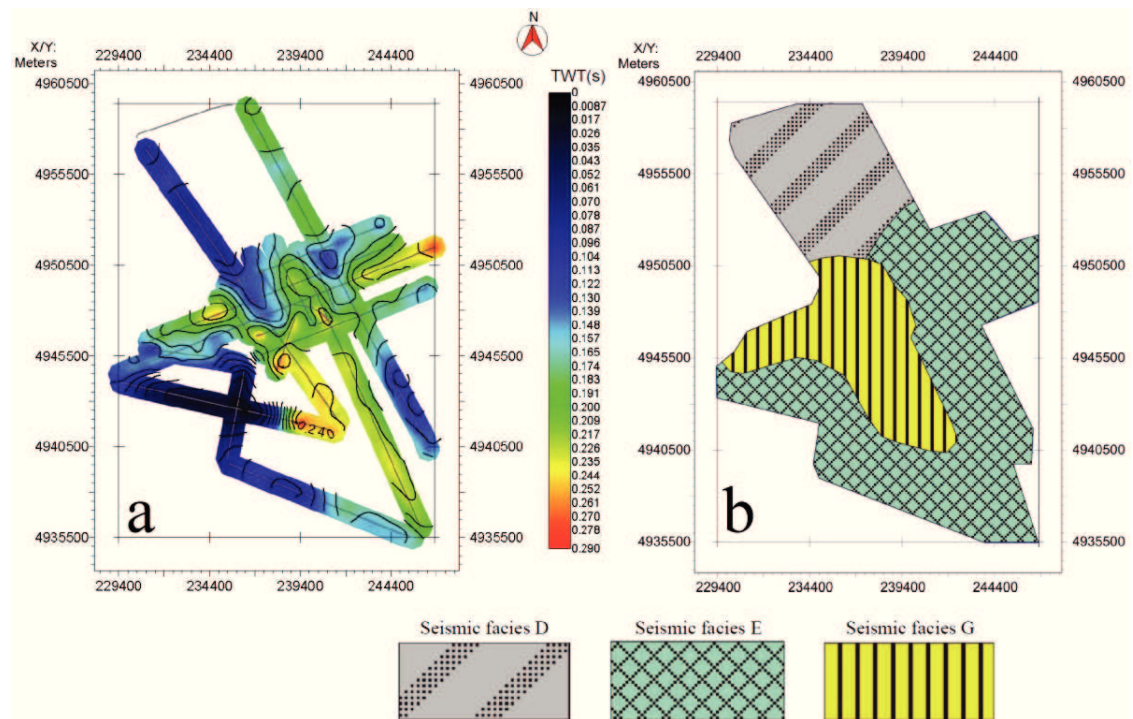


**Figure 6** (a) Isopach map of Unit 5. (b) Seismic facies map of Unit 5. The maximum thickness of Unit 5 is located in the SSE part of the study area, consists of seismic facies G and E. Seismic facies E occurred from the mid-slope to the downslope part of the study area. Seismic faceis D mainly occurred in the upper part.

### 3.4.3.2. Seismic Unit 5

Seismic Unit 5 ranges in thickness from <17 ms TWT to 280 ms TWT (Fig. 6a). The orientation of the elongated main sediment depocenter started to change from ENE-WSW in seismic Unit 6 into NNW-SSE. The maximum thickness of Unit 5 is located in the SSE part. Another depocenter is located in the ENE. The boundary between seismic Units 5 and 6 (H5) is also represented by an erosional truncation surface. Seismic facies D and E can be found in seismic Unit 5 (Fig. 6b). Seismic facies E occurred in the mid-slope to downslope part, with moderate to good continuous and parallel reflectors, interbedded high and low amplitude horizons. Seismic facies D mainly occurred in the upper part. The depocenter is characterized by seismic facies G and E.

### 3.4.3.3. Seismic Unit 4

The boundary (H4) between seismic Units 5 and 4 is clearly marked by a seismic amplitude change (Fig. 3). It also marks an obvious eastward shift in depocenter (Fig. 6a and 7a) with a maximum thickness ~330 ms TWT in the ENE part, and a minimum thickness of ~10 ms TWT in the WSW part (Fig. 7a). The depocenter of seismic Unit 4 is characterized by seismic facies B (Fig. 7b), which shows low to medium amplitude, moderately to good continuous and parallel reflectors. The seismic facies of seismic Unit 4 develops into higher amplitude, more continuous reflections from the center of the area to the WSW part, from seismic facies B to seismic facies E. Seismic facies D can be observed in the NNW corner.
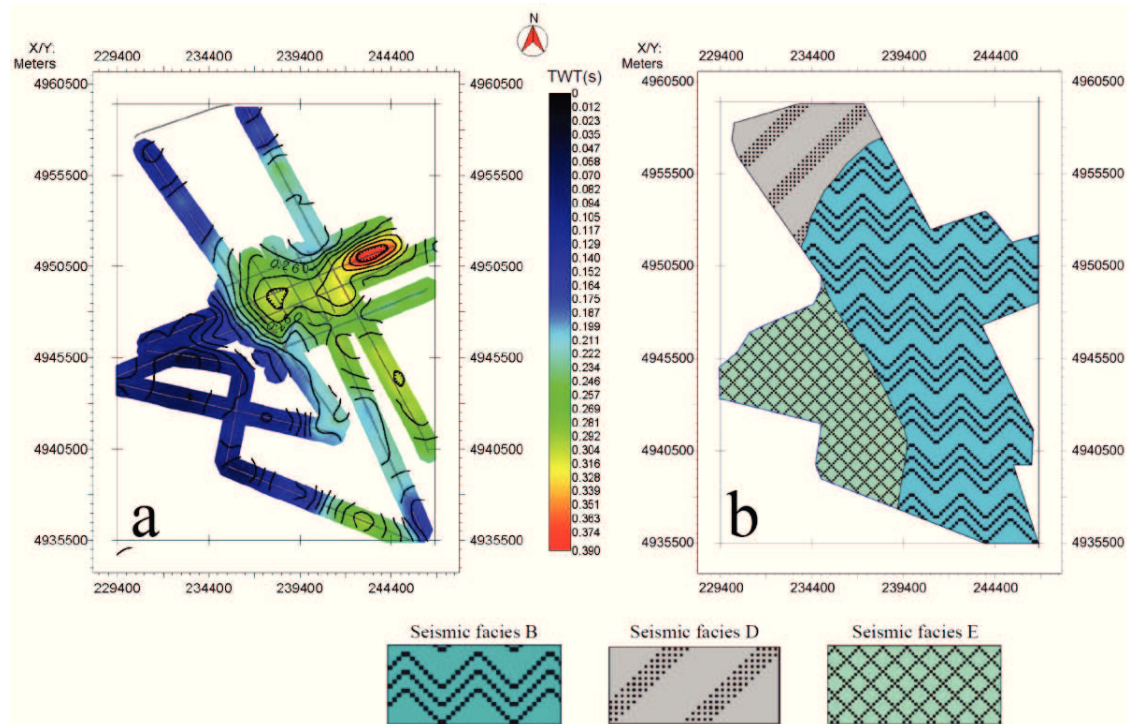


**Figure 7** (a) Isopach map of Unit 4. (b) Seismic facies map of Unit 4. The maximum thickness of Unit 4 is located in the NNE part of the study area, consists of seismic facies B. The seismic facies changed from Seismic facies B to seismic facies E, from the middle part to the WSW part. The NNW part consists of seismic facies D.

Beneath seismic Unit 4, three mounded reflection patches (I, II and III) can be clearly identified at different depths (Figure 3), which are marked by black ellipses. Similar reflection types also exist in parallel profiles. Therefore, a trend of the mounded reflection patches can be observed from ENE to WSW direction. The thickness on both sides (landward and basinward) of their crest is different. Vertical reflector offsets of up to ~6 ms TWT are clearly observed in several places in each unit of the seismic profiles (Fig.s 3b and 4b), which are interpreted as faults. The vertical extent of deep faults is larger than ~460 ms TWT around these mounded reflection patches.

### 3.4.3.4. Seismic Unit 3

Seismic Unit 3 is generally characterized by seismic facies A (Fig. 8a), with widespread, high amplitude, moderately to good continuous and parallel reflectors. The transition from seismic Unit 4 to Unit 3 (H3) is also clearly indicated by a seismic amplitude variation and a parallel reflection with good continuity. Two main depocenters are shown in the isopach map (Fig. 8a), one in the northeast corner with a sediment thickness of ~230 ms TWT, the other in the southwest part with a sediment thickness of ~210 ms TWT. Seismic facies C and seismic facies F were clearly identified in seismic Unit 3 (Fig. 8b). Seismic facies C represents low to high amplitude, low continuous reflectors. Seismic facies F shows the chaotic semi-transparent reflection pattern disrupting the higher amplitude reflectors. The trend of seismic facies C and F is oriented from NW to SE.
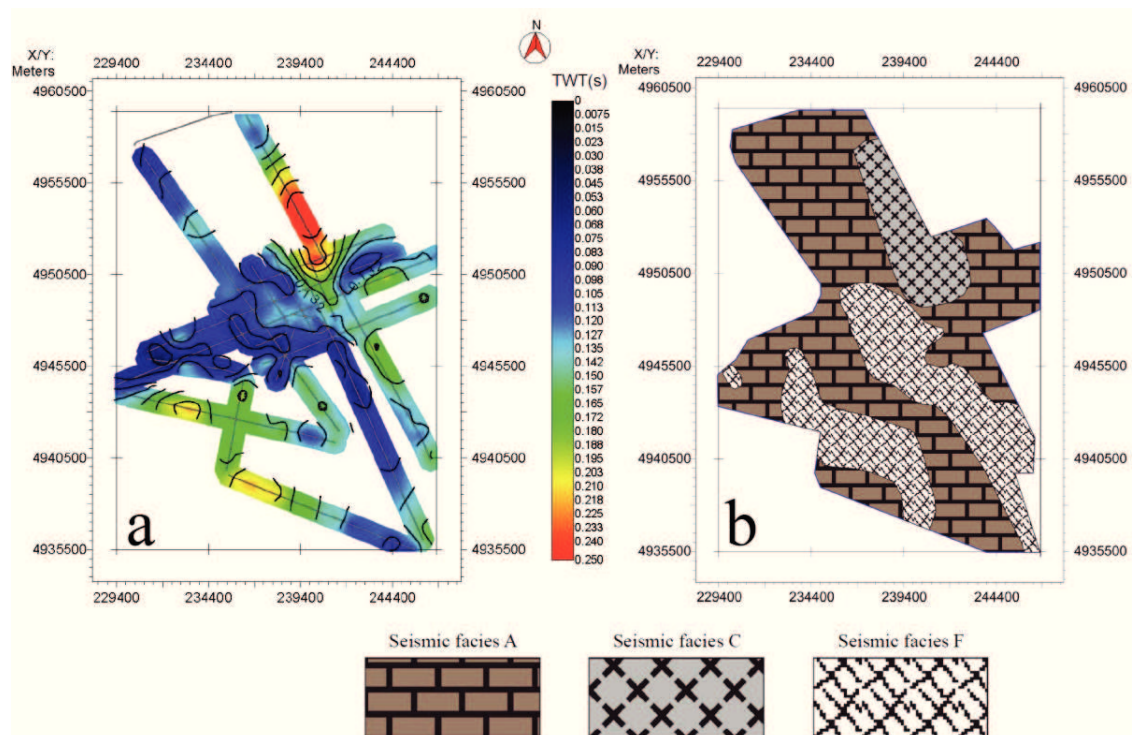


**Figure 8** (a) Isopach map of Unit 3. (b) Seismic facies map of Unit 3. Seismic Unit 3 is generally characterized by seismic facies A, C and F. Two main depocenters located in the northeast corner and in the southwest part of the study area.

### 3.4.3.5. Seismic Unit 2

An unconformity (H2) was recognized between seismic Units 2 and 3, which can be identified in Figure 3. The depocenter locates in the southeastern part, with a maximum thickness of ~200 ms TWT (Fig. 9a). Seismic Unit 2 is mainly composed of seismic facies A (Fig. 9b), generally with high amplitude and good continuous reflectors interbedded with low to middle amplitude and poor continuous reflectors. Seismic facies F occurred in the central and eastern parts of the study area with an average sediment thickness of ~150 ms TWT. The trend of seismic facies F is from NW to SE.
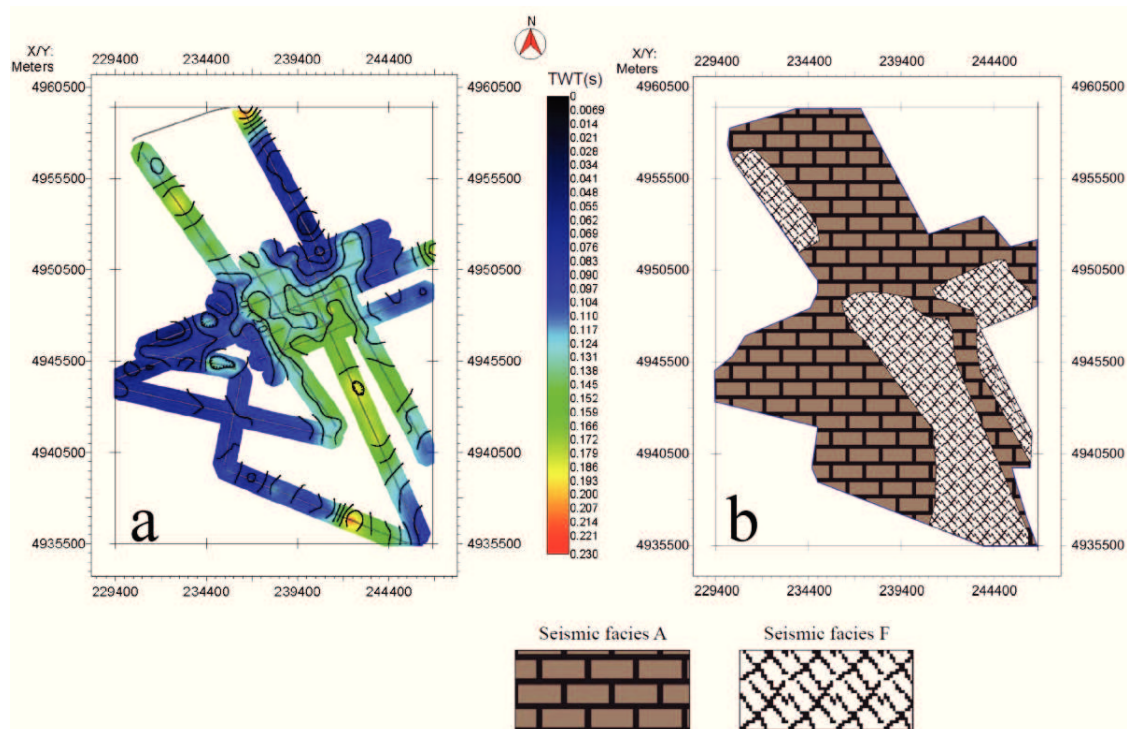


**Figure 9** (a) Isopach map of Unit 2; (b) Seismic facies map of Unit 2. Seismic Unit 2 is generally characterized by seismic facies A and F. A main depocenter is located in the southeast part of the study area.

### 3.4.3.6. Seismic Unit 1

The main depocenter of seismic Unit 1 occurs in the NNW corner of the study area, with a maximum sediment thickness of ~200 ms TWT (Fig. 10a). An unconformity (H1) between the seismic Units 1 and 2 is observed in the upper slope in Figure 3. The seismic facies types in seismic Unit 1 (Fig. 10b) are similar to seismic Unit 2, it also consists of seismic facies A and seismic facies F. However, seismic facies F is less present in seismic Unit 1 than in seismic Unit 2. Seismic facies F is only located in the northern and southeastern corners of the study area. Most parts of seismic Unit 1 consist of seismic facies A.
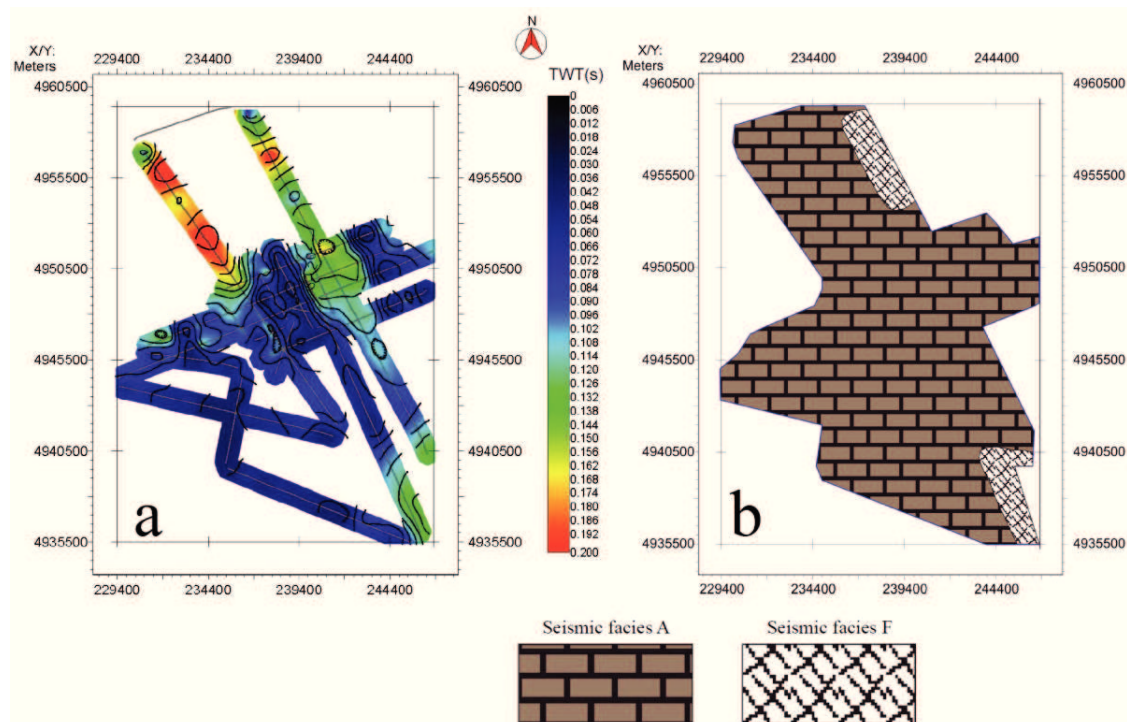
**Figure 10** (a) Isopach map of Unit 1. (b) Seismic facies map of Unit 1. Seismic Unit 1 is generally characterized by seismic facies A and F. A main depocenter is located in the northwest part of the study area.

### 3.4.4. Observations on Area 2 profiles

In Area 2, one seismic profile (Fig. 11) is shown to illustrate the situation of seismic units and seismic facies. Compared to Area 1, Area 2 has similar types of seismic facies and a similar association with seismic units, but seismic facies B seems to be absent in Area 2. More widespread seismic facies F occurs in seismic Units 4 and 3. The unconformities, which are the boundaries between these seismic units, can be even more clearly observed. The thickness of seismic Unit 4 in Area 2 is ~100 ms TWT thinner than that in the Area 1, while the other seismic units in Area 2 have nearly the same thickness as those in Area 1.

### 3.4.5. Observations on Area 3 profiles

For Area 3, two seismic profiles (Fig. 12 and 13) illustrate seismic units and seismic facies. Compared to Areas 1 and 2, seismic facies types A, B, D, E and F can be observed also in Area 3. Seismic facies B is located in seismic Units 3 and 2, while seismic facies F appears more widespread in seismic Units 3 and 4. The thickness of the seismic units increases gradually from SW to NE (Fig. 13) and from NW to SE (Fig. 12). In Figure 13, due to the strong seismic multiples, only the lower left part of the profile could be analyzed. The faults with offset of ~6 ms TWT can also be observed in each unit of the seismic profiles in Area 3. Especially in Units 1 and 2, some reflector offsets are much larger, and the maximum vertical extent of faults is up to ~280 ms TWT.
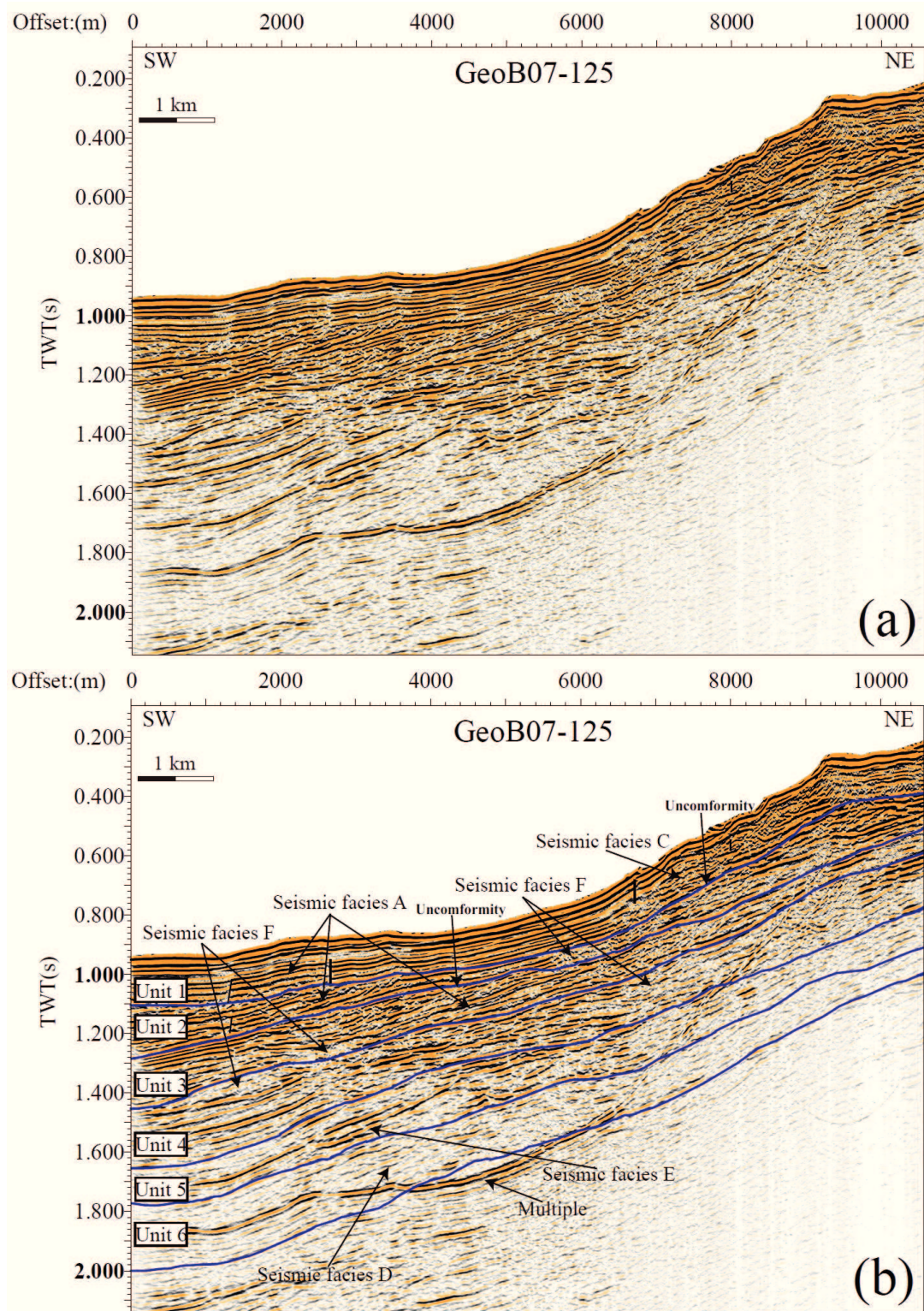
**Figure 11** (a) Uninterpreted migrated seismic profile GeoB07-125 in the Area 2, (b) Interpreted seismic profile GeoB07-125, showing seismic facies A, C, D, E and F, and seismic units (1-6). See Figure 2 for location.

**Figure 12** (a) Uninterpreted migrated seismic profile GeoB07-130 in the Area 3. (b) Migrated seismic profile GeoB07-130, showing seismic facies A, B, D, E and F, and seismic units (1-6). See Figure 2 for location.
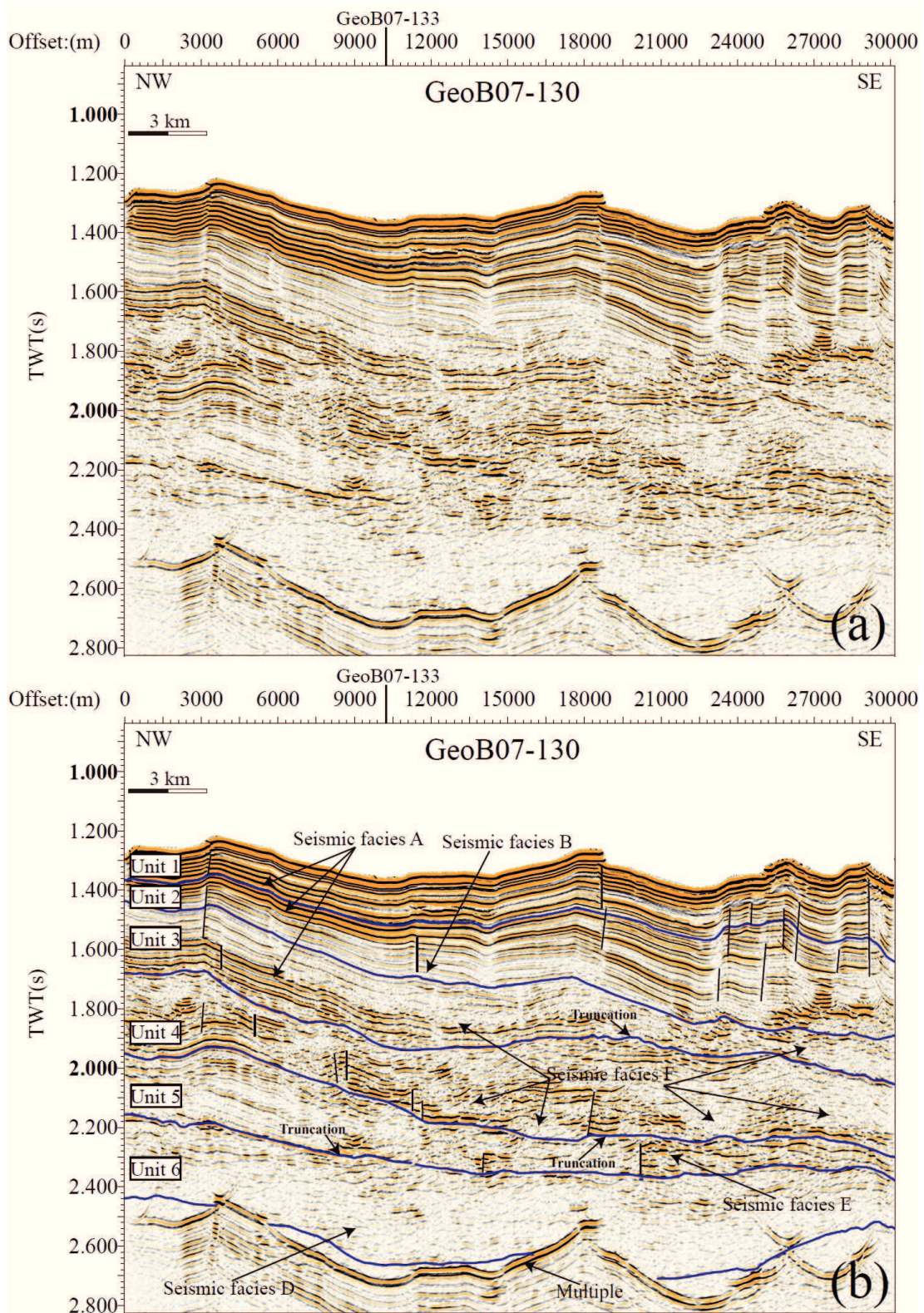
**Figure 13** (a) Uninterpreted migrated seismic profile GeoB07-133 in the Area 3. (b) Migrated seismic profile GeoB07-133, showing seismic facies A, B, D, E and F, and seismic units (1-6). See Figure 2 for location.
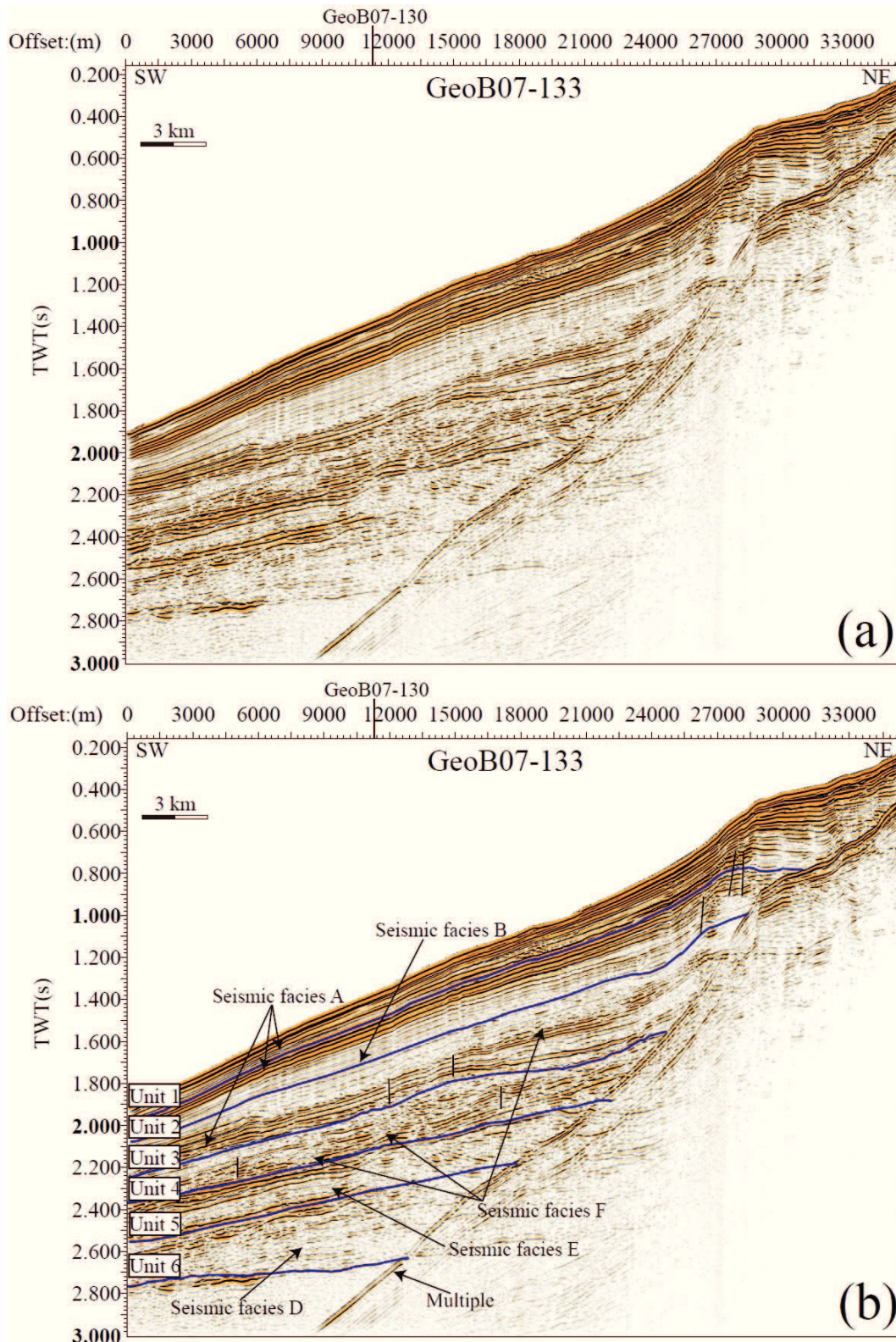
## 3.5. Interpretation and Discussion

### 3.5.1. Chronostratigraphy

Although for our study area published information on deep penetration drill sites is rare, age estimates for seismic units can be derived from some published seismic studies in adjacent areas. Tari (2011) showed an interpreted seismic line (Fig. 14) which clearly indicated an erosional unconformity between the Miocene and Pliocene sediments. The line is located in the Southwest of our study area. Meisner (2011) presented an interpreted seismic section through Tuapse Trough in the Eastern Black Sea basin, which showed the boundary between the Quaternary and Pliocene at 1.2 s TWT in the deep basin. Drill site Subbotina-403 from the mouth of the Kerch Strait, which is in the Northeast of our study area, and three seismic lines close to our study area are published by Stovba et al. (2009), providing a crude stratigraphic framework. All the above-mentioned seismic studies provide a reference to estimate the age of seismic units in the study area. The age correlation is simple and limited in accuracy, and main results are summarized in Table 2.
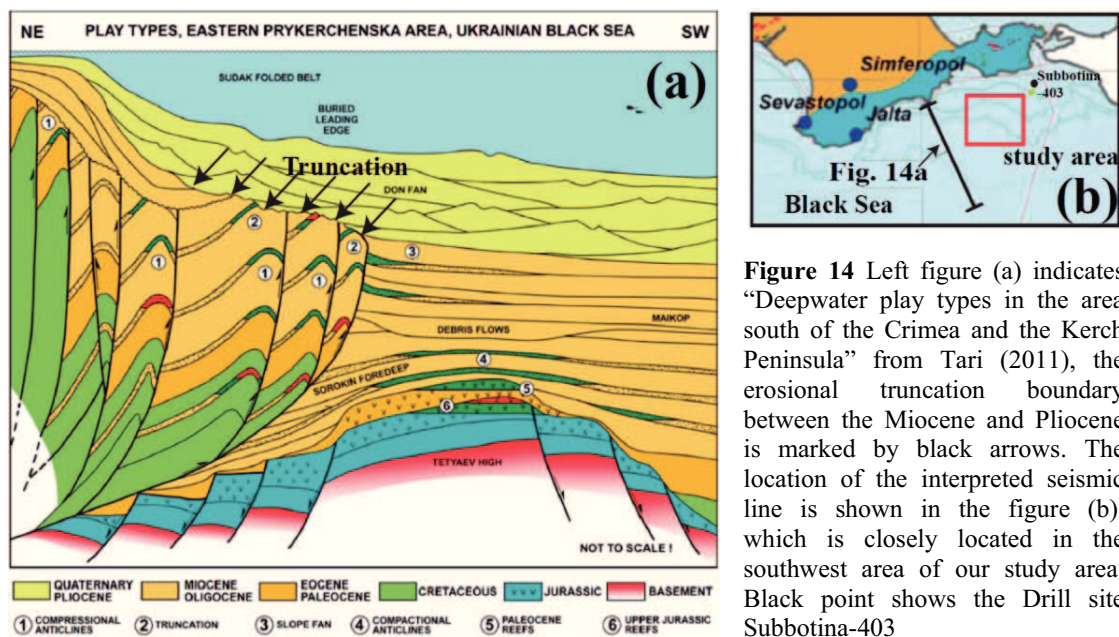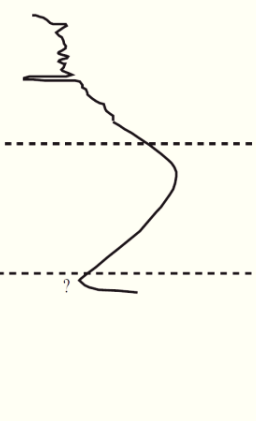


**Figure 14** Left figure (a) indicates "Deepwater play types in the area south of the Crimea and the Kerch Peninsula" from Tari (2011), the erosional truncation boundary between the Miocene and Pliocene is marked by black arrows. The location of the interpreted seismic line is shown in the figure (b), which is closely located in the southwest area of our study area. Black point shows the Drill site Subbotina-403

Based on these age assignments, we interpreted H5 as the boundary between the Miocene and Pliocene, which may coincide with the Messinian erosional truncation surface (5.3 Ma BP) (Tari, 2011; Stovba et al., 2009). The Messinian erosional truncation surface is a major unconformity between Miocene and Pliocene deposits, which is associated with a substantial drop of sea level during the Messinian Salinity Crisis (less than 6 Ma ago). It has been confirmed by several boreholes (Ryan and Cita, 1978; Hsü and Giovanoli, 1979; Gillet et al., 2007) and seismic data (Finetti et al., 1988; Robinson et al., 1996) from offshore areas in the Mediterranean Sea and the Black Sea. H3 is the

boundary between the Pliocene and Quaternary (Meisner et al., 2011), the age is 2.6 Ma BP according to the updated international chronostratigraphic chart (Cohen et al., 2013). The ages of horizons H1, H2 and H4 are interpolated using average sedimentation rates, which amount to 11.4 cm/kyr for the Quaternary and to 14.5 cm/kyr for the Pliocene. The sedimentation rate of the Black Sea basin is 5.5 cm/kyr during the Miocene according to Hsü and Giovanoli (1979). But as the study area is located at the margin of the Black Sea depression (Popov et al., 2004), estimates of sedimentation rate are relatively uncertain for Unit 6, which is probably of late Miocene age. Using the average values, the ages of horizons H1, H2 and H4 calculate approximately to 0.64, 1.47 and 3.9 Ma BP, respectively (Table 2).

**Table 2**

Age correlation of seismic units according to previous seismic studies in adjacent areas.

| International stratigraphic scale | | Age (Ma) | Tari (2011) & Stovba (2009) -the Kerch Peninsula margin | Meisner (2011) -Eastern Black sea basin | Our units | | Sea-level curve (m) -80 -40 0 40 80 120 160 |
|---|---|---|---|---|---|---|---|
| | | | | | Name | Age (Ma) | |
| Quaternary | | | | | Unit 1 | ~0.64 ? | |
| | | | | | Unit 2 | ~1.47 ? | |
| | | | | | Unit 3 | | |
| | | 2.6 | | | | | |
| Pliocene | | | | | Unit 4 | ~3.9 ? | |
| | | | | | Unit 5 | | |
| | | 5.3 | METS | | Unit 6 | | ? |
| Miocene | U | | | | | ? | |
| | | 10.4 | | | | | |
| | M | | | | | | |

*The ages of international stratigraphic scale in the Black Sea are taken from Harland et al. (1990). The age axis is not to scale. The sea - level curve is from Konerding et al. (2010), and it is relative to the present-day sea level (0 m). METS: Messinian erosional truncation surface.

### 3.5.2. Geologic interpretation of seismic data

### 3.5.2.1. Anticline structures

The northeastern Black Sea was affected by inversion tectonics and compressional events during the Middle Eocene, Late Eocene, Early Miocene, and Middle Miocene, accompanied by continuing post-rift basin subsidence. The study area was influenced by intense inversion tectonics (Nikishin et al., 2003; Stovba et al. 2009). Numerous anticline structures were formed by NS-directed compression, which also provides structural traps for oil and gas (Fig. 14). A similar example of anticline traps is found in the Subbotina Field on the Kerch Shelf (Stovba et al. 2009) which is located to the Northeast of the study area. In Area 1, the three black ellipses in Figure 3b mark three anticline structures I, II and III, which were formed before the late Miocene, likely representing the Oligocene-Miocene Maikopian clay formation. They likely contributed to a steepening of

slope angles within the Area 1 gradually. Sediments were therefore trapped on the landward side of the anticline crests, imaged by the depocenter distribution in the Unit 6. The Maikopian formation most probably serves as the source of the methane gas, feeding many seeps in the Black sea (Ivanov et al., 1996). Steep upthrust faults (Alexander and Irina, 2005) occurred on the basinward side of the anticline structures (Fig. 3) suggesting the tectonic movements. Many shallow faults exist in the upper three seismic Units U1 to U3 of the three areas (Fig.s 3, 4, 11, 12 and 13), which might be caused by the instability of large sediment input during the Quaternary. The Crimean and the Caucasus regions are characterized by recent seismic activity (Neprochnov and Ross, 1978; Barka and Reilinger, 1997), and stress field measurements (Rastsvetaev, 1977) and GPS data (Barka and Reilinger, 1997; Reilinger et al., 1997) indicate a compressional environment in the Eastern Black Sea region also in recent geologic times.

### 3.5.2.2. Seismic facies

Seismic facies types characterize the main sedimentary processes and environments. They are usually interpreted according to similar regional seismic stratigraphic studies in other regions, such as the Mississippi Fan (Weimer, 1989), the southern and southwestern Caspian Sea (Abdullayev, 2000) and the northwestern Black Sea (Winguth et al., 2000).

According to characteristics of the seismic facies in Table 1, seismic facies A through G are interpreted as follows. Seismic facies A is possibly caused by pronounced lithologic variations between distinct layers. It is interpreted to represent hemipelagic fine-grained sediments deposited during the high stand sea level, intebedded with the coarser grained sediments deposited during the low stand sea level, which was driven by a series of the glacial and interglacial events (Ross and Degens, 1974; Jones and Gagon, 1994; Winguth et al., 2000). Seismic facies B with low amplitude and moderately to good continuity is possibly caused by mostly fine-grained, relatively uniform deposits. It may be related to distal fan deposits (Limonov et al., 1997; Wagner-Friedrichs, 2007). Seismic facies C might derive from fan deposits with coarse grained sediments, due to the thick body with low to high amplitude and low continuous reflectors (Weimer, 1989; Winguth et al., 2000). Seismic facies D likely represents mass transport deposits with fine grained material partly mixed with coarse grained (Winguth et al., 2000), because the amplitude of facies D is variable, and the reflectors are chaotic to low continuity. Seismic facies E is similar to seismic facies A which is interbedded high and low amplitude horizons. Facies E probably originates from hemipelagic sediments intebedded with coarser grained sediments during the transgression (Nielsen and Van Weering, 1998). Seismic facies F may suggest slumps or channels, indicated by the chaotic semi-transparent reflection pattern disrupting the higher amplitude reflectors (Weimer, 1989; Abdullayev, 2000). The origin of seismic facies G may be slope fan deposits (Shanmugam et al., 1996), because of the mounded shape, high amplitude and chaotic internal reflections, and that the base reflectors of one mound are downlapping to another one (Fig. 4c).

### 3.5.2.3. Seismic units

Seismic Unit 6

Seismic Unit 6 belongs to the Upper Miocene section. In Area 1, based on the observation of thickness variations and seismic facies (Fig. 5), slope fan deposits (seismic facies G) are located in the depocenter of seismic Unit 6 in Area 1, which suggest that sediments were probably supplied mainly from NNW and northern direction, probably from Crimean Mountains and the Kerch Peninsula. However, we don't know the information about the river at that time, which formed the slope fan. Other parts of seismic Unit 6 in Area 1 are dominated by mass transport deposits (seismic facies D). Similar mass transport deposits also developed in Areas 2 and 3.

Seismic Unit 5

The surface between seismic Units 5 and 6 is marked by erosional truncation (Fig.s 3b and 12) spanning the transition from Miocene to Pliocene. Seismic Unit 5 dates to the lower Pliocene. In Area 1, slope fan deposits (seismic facies G) probably continued developing, forming an elongated sediment depocenter in the NNW-SSE direction (Fig. 6). Another depocenter in the ENE part may suggest that sediments filled the depression created by the anticline formation. Hemipelagic sediments interbedded with coarser grained sediments during the transgression (Seismic facies E) were observed in the mid-slope to downslope part, which may suggest an overall sea-level rise in the study area. Mass transport deposits (seismic faceis D) mainly occurred in the upper part of the Unit 5.

Seismic Unit 4

Seismic Unit 4 is of middle to late Pliocene age. In Area 1, a shift in depocenter (Fig. 7a) compared to seismic Units 5 and 6 suggest a large input of sediment from a northeasterly direction. The dominant seismic facies is facies B (Fig. 7b), which is interpreted as distal fan deposits. Seismic facies D and E still exist in Unit 4. Concurrently, slumps or channels (seismic facies F) occurred in Areas 2 and 3 without seismic facies B. Local truncation surfaces can be observed at the boundary between seismic Units 4 and 5 in Area 3 (Fig. 12).

Seismic Unit 3

Seismic Unit 3 belongs to the early Pleistocene. Seismic facies A (Fig. 8b) started to appear in seismic profiles since the formation of Unit 3. Seismic facies A was interpreted as hemipelagic sediments interbedded with coarse grained sediments. Changes in sea level may have lead to cyclic deposition of finer (highstand) and coarser (lowstand) grained material. Within this unit, the Paleo-Don River fan deposits (seismic facies C) were observed in Area 1 indicating a possible shift of the river mouth. Slumps or channels (seismic facies F) occurred in all the three areas, which probably suggests higher sediment input and/or more intense tectonic movement, e.g. uplift of the Great Caucasus and Crimean Mountains (Brunet, 2003) and the basin subsidence of the Black Sea (Nikishin et al., 2003). In Area 1, two depocenters (Fig. 8a) were formed by seismic facies C and F, respectively. And the trend of the river fan deposits (seismic facies C), slumps or channels (seismic facies F) lines up in NW to SE direction (Fig. 8b), which may be the evidence of the uplift of the Crimean Mountain in the northwest of the study

area or the subsidence of the Black Sea basin in the south, creating a sediment source and according downslope erosive sediment fluxes.

Seismic Unit 2

Seismic Unit 2 dates to the middle Pleistocene. It is also characterized by seismic facies A (Fig. 9), and accompanied by seismic facies F in Areas 1 and 2, and in Area 3 by seismic facies B (Fig.s 12 and 13). An unconformity can be observed on the upper slope of Areas 1 and 2, suggesting erosional processes. In Area 3, seismic facies F is less present and an unconformity cannot be observed. Uniform deposits in Area 3 (seismic facies B) were interpreted as hemipelagic sediments or distal fan deposits. In Area 1, the depocenter is also dominated by channel-fills or slumps extending in NW to SE direction.

Seismic Unit 1

Seismic Unit 1 covers middle Pleistocene to Holocene times, revealing a distinct similarity to Unit 2. In Areas 1 and 2, slumps or channels (Fig. 10), and river fan deposits (Fig. 11) occurred on the upper slopes, but less of them occurred inside Unit 1. In Area 3 (Fig.s 12 and 13), seismic Unit 1 consists of hemipelagic sediments interbedded with coarse grained sediments (seismic facies A).

### 3.5.3. Sedimentary evolution of the study area

According to the lithological-paleogeographic maps of Paratethys during the late Miocene (Popov et al., 2004), the Kerch Peninsula was covered by sea water, and the study area was likely in a relatively deep water marine environment. Seismic Unit 6 shows that mass transport deposits occurred in the study area, while slope fan deposits started developing in the Area 1. Subsequently, the Black Sea was influenced by the Messinian Salinity Crisis, which was associated with a dramatic fall in sea level with a maximum at the Miocene-Pliocene boundary, and with erosional surfaces on the shelves of the Black Sea (Gillet et al., 2007; Hsü and Giovanoli, 1979; Kojumdgieva, 1983; Popov et al., 2004). Deep water environments existed only in the deepest parts of the Black Sea basins. The Black Sea became an isolated basin, and did not connect to the Mediterranean Sea and the Caspian Sea at this time (Paluska and Degens, 1979). DSDP Leg 42B drill sites indicated a subtropical dry climate, and lithology was mainly composed by laminated carbonates indicating shallow marine or lake environments. Aragonite and gravel appeared at the unconformity between the Miocene and Pliocene near the Bosporus on the basin apron of the Black Sea (DSDP, Site 380, Hsü and Giovanoli 1979).

During the Pliocene to Quaternary, the intensity of tectonic movements increased. There was an acceleration of the basin subsidence of the Black Sea with a rate reaching 85 m/Ma (Nikishin et al., 2003), and the most rapid subsidence occurred from the late Pliocene to the Quaternary (Meisner et al., 2011). The reason for the rapid subsidence was illustrated by kinematic and dynamic modeling (Nikishin, 2003) attributing it to compression-induced downward bending of the lithosphere. The unusually rapid

subsidence was coincident with the uplift of the Great Caucasus and Crimean Mountains during the Pliocene and Quaternary (Brunet, 2003; Meisner et al., 2011). The slope gradient in the study area has increased gradually, and nowadays, the gradient varies between 5° and 6°. These tectonic movements should also have an influence on the water depth of the study area. However, a simple trend of the water depth variation may be estimated from the sea-level curve (Table 2) and basin subsidence rate (~85 m/Ma) of the Black Sea. Nowadays, the water depth of the middle part of the Area 1 is ~800 m, and we infer results ~500 m during the middle Pliocene and ~650 m during the early Quaternary. Therefore, the water depth was probably increasing gradually from the Pliocene to the Quaternary.

After the Messinian sea level fall, the transgression started in the early Pliocene (seismic Unit 5). The study area gradually came into a deep water environment again. The hemipelagic sediment interbedded with coarse grained sediments during the transgression (seismic facies E) appeared in the study area. In Area 1, slope fan deposits continued to develop when the deep water environment recovered again. The slope fan deposits might be formed by some small rivers from the uplifting Crimean Mountains, but little is known about rivers at this time. During the middle to late Pliocene (seismic Unit 4), the sea level gradually came into a high stand (Table 2, Konerding et al., 2010). Seismic facies B in Unit 4 indicates fine grained sediments, which likely represent distal Paleo-Don River fan deposits, while coarser grained sediments deposited in Unit 5 (Fig. 4b). The development of the present day paleogeographic features and large river systems were initiated by vertical movements (Popov et al., 2004). The Kerch Strait was separated by the branched the Paleo-Don River system from the Enikal Strait, which was a tectonic depression between the Crimean and Caucasus mountains (Barg, 2007). Then sediments could be transported directly into the Black Sea by the Paleo-Don River (Popov et al., 2004; Barg, 2007; Starostenko et al., 2010; Meisner et al., 2011). The Paleo-Don River fan deposits accumulated south of the Kerch Peninsula margin. Many channels and coarse grained sediments occurred in Areas 2 and 3, which are closer to the mouth of the Kerch Strait. The distal Paleo-Don fan deposits were observed in the east part of Area 1 being rich in the fine grained sediments.

During late Pliocene to Quaternary times, the Kerch-Taman region was affected by a major compressional event (Saintôt and Angelier, 2000). The uplift of the Crimean Mountains obtained their basic hypsographic features through the most intense tectonic movements around the Pliocene-Pleistocene boundary. During the Quaternary, the climate of Black Sea was influenced by a series of glacial and interglacial cycles (Gozhik et al., 2008). The sea level fell below the present-day sea level due to these climatic changes. Incoming sediment changed gradually from the fine grained Unit 4 into the coarse grained Units 3 through 1. In Unit 3 through 1, hemipelagic fine-grained sediments interbedded with coarse grained sediments (seismic facies A) developed along with slumps or channels (seismic facies F), and Paleo-Don and Kuban River fan deposits (seismic facies C). As sediment source we assume the Crimean Mountains and the fan of the Paleo-Don and Kuban River. Due to the sea level fall, the mouth of Paleo-Don River might have moved to Area 1, while fewer channels occurred in Areas 2 and 3. During the early Pleistocene (seismic Unit 3), the slumps documented in Area 1 may be related to

the intense tectonic activity in the Crimean Mountains in conjunction with rapid subsidence of the Black Sea basin, steepening of slopes and enhanced earthquake activity (Jan Hradecký et al., 2000; Nikishin, 2003). During the middle to late Pleistocene, less or smaller river fan deposits bodies accumulate in Units 2 and 1 than were present in Unit 3, which indicates the gradual decrease of sediment flux from the Paleo-Don River fan. The Paleo-Kuban River was most active during the late Pleistocene and flowed directly into the Black Sea (Stadnitskaia, 1997). The Paleo-Don and Kuban Rivers developed a large delta and fan at the mouth of the Kerch Strait. A large transgression during the Neoeuxinian phase exceeded the erosion base level of the two rivers (Barg, 2007). Therefore, the Don and Kuban Rivers enter the Sea of Azov and accordingly the delivery of sediments to the Black sea is reduced (Stadnitskaia, 1997).

## 3.6. Conclusions

From this study, we get the following conclusions.

1) For the first time, high resolution multichannel seismic data were interpreted from the Kerch Peninsula margin of the Black Sea. A seismostratigraphic framework was established for late Miocene to Recent times, and based on seismic facies distribution and isopach maps of Area 1, the sedimentary evolution was reconstructed.

2) Three anticline structures were observed in Area 1, which had formed before the late Miocene, likely originating from the Maikopian clay formation of Oligocene-Miocene age.

3) During the late Miocene and early Pliocene, the slope fan deposits occurred in Area 1 of the study area. At the Miocene-Pliocene boundary, the major erosional truncation caused by the Messinian event was observed.

4) During the Pliocene, the water level started a transgression after the Messinian sea-level fall. The Paleo-Don River flowed into the Black Sea during the middle Pliocene to late Pliocene. Distal fan deposits with finer grained fan sediments deposited in the eastern part of Area 1, while channels occurred in Areas 2 and 3, which are located closer to the Kerch Strait.

5) During the Quaternary, high terrigenous input sourced from the Crimean Mountain and the Paleo-Don and Kuban rivers. Hemipelagic fine-grained sediments interbedded with coarse grained sediments developed in the study area, along with slumps or channels and river fan deposits. The sea-level changes may influence the grain size variation of the sediments and the shift of the river mouth.

## Acknowledgements

## References

Abdullayev, N. R., 2000. Seismic stratigraphy of the Upper Pliocene and Quaternary deposits in the South Caspian Basin. Journal of Petroleum Science and Engineering, 28 (4), 207-226.

Alexander Kitcka, Irina Nedosekova, 2005. Exploring Offshore Ukraine Using Space-born Data: Submarine Seeps, Oil Slicks, and Promising Prospects. EAGE 67th Conference & Exhibition — Madrid, Spain, P341.

Barg, I., 2007. Age and origin of the Kerch Strait and the Sea of Azov. Doklady Earth Sciences 412 (1), 17–18.

Barka, A. and R. Reilinger, 1997. Active Tectonics of Eastern Mediterranean region: deduced from GPS, neotectonic and seismicity data, Annali Di Geofisica, X2 (3), 587–610.

Bohrmann G., T. Pape, and cruise participants, 2007. Report and preliminary results of R/V METEOR Cruise M72/3, Istanbul – Trabzon – Istanbul, 17 March – 23 April, 2007.Marine gas hydrates of the Eastern Black Sea. Berichte, Fachbereich Geowissenschaften, Universität Bremen, No. 261, 176 pages. Bremen, 2007.

Brunet, M. -F., M. V. Korotaev, et al., 2003. "The South Caspian Basin: a review of its evolution from subsidence modelling." Sedimentary Geology 156 (1–4): 119-148.

Cohen, K.M., Finney, S., and Gibbard, P.L., 2013. International Chronostratigraphic Chart, International Commission on Stratigraphy.

Finetti, I., Bricchi, G., Del Ben, A., Pipan, M. and Xuan, Z., 1988. Geophysical study of the Black Sea. Boll. Geofis. Teor. Appl., 30(117-118), 197-324.

Gillet Herve, Lericolais Gilles, Rehault Jean Pierre, 2007. Messinian event in the black sea: Evidence of a Messinian erosional surface. Marine Geology, 244 (1-4), 142-165.

Gozhik P.F., Maslunr N.V., Ivanikl M.M., Plotnikoval L.F., Yakushinl, L.N., 2008. Stratigraphic model of the Mesozoic and Cenozoic of the Western Black Sea Basin. Геология и полезные ископаемые Мирового океана, (1), 55-69.

Harland, W. B., Armstrong, R. L., Cox, A. V., Craig, L. E., Smith, A. G. & Smith, D. G., 1990. A Geologic Time Scale 1989. Cambridge University Press, Cambridge.

Hsü, K.J. and Giovanoli, F., 1979. Messinian event in the Black Sea. Palaeogeogr. Palaeoclimatol. Palaeoecol. 29, 75-93.

Ivanov MK, Limonov AF, van Weering TCE, 1996. Comparative characteristics of the Black Sea and Mediterranean Ridge mud volcanoes. Mar Geol 132:253-271.

Jan Hradecký, Ivan Kruhlovk, Tomáš Pánek, Jan Prášek, 2000. Geomorphic evolution and present-day geomorphic processes of the southern part of the Crimean Peninsula (Ukraine). Acta Universitatis Carolinae Geographica, XXXV, Supplementum, Pag. 111-131.

Jones G.A. and Gagnon A.R., 1994. Radiocarbon chronology of Black Sea sediments. Deep-sea Research, 41 (3) : 531-557.

Kojumdgieva, E., 1983. Paleogeographic environment during the desiccation of the Black Sea. Palaeogeogr. Palaeoclimatol. Palaeoecol. 43, 195-204.

Konerding, C., Dinu, C., and Wong, H. K., 2010. Seismic sequence stratigraphy, structure and subsidence history of the Romanian Black Sea shelf. Geological Society, London, Special Publications, 340 (1), 159-180.

Limonov, A.F., van Weering, Tj.C.E., Kenyon, N.H., Ivanov, M.K., and Meisner, L.B., 1997. Seabed morphology and gas venting in the Black Sea mud volcano area: Observation with the MAK-1 deeptow side scan sonar and bottom profiler. Marine Geology, 137: 121-136.

Meisner, A., Sheya, C., and Nemcok, M., 2011. Ancient Depositional Environments of the Eastern Black Sea. Search and Discovery Article #50388.

Neprochnov, Y. P. and D. A. Ross, 1978. Black Sea geophysical framework, in Initial Reports of the Deep Sea Drilling Project 42, Part 2, edited by J. L. Usher and P. Supko, pp. 1043–1055.

Nielsen, T., and Van Weering, T. C. E., 1998. Seismic stratigraphy and sedimentary processes at the Norwegian Sea margin northeast of the Faeroe Islands. Marine Geology, 152 (1), 141-157.

Nikishin, A.M., Korotaev, M.V., Ershov, A.V., Brunet, M.-F., 2003. The Black Sea basin: tectonic history and Neogene–Quaternary rapid subsidence modelling. Sedimentary Geology 156, 149-168.

Paluska A., Degens E. T, 1979. Climatic and tectonic events controlling the Quaternary in the Black Sea region. Geol. Rdsch 68:284–301.

Popov SV, Rögl F, Rozanov AY, Steiniger FF, Shcherba IG, Kovac M, 2004. Lithological-paleogeographic maps of Paratethys: 10 maps Late Eocene to Pliocene Courier Forschunginstitut Senckenberg.

Rastsvetaev, L. M. 1977. The Mountain Crimea and Northern Black Sea area. In: SUVOROV, A. I., PEYVE, A. V., BELIAEVSKY, N. A. & UNKSOV, V. A. (eds) Faults and Horizontal Movements of Mountain Chain in the USSR. Nauka, Moscow, 95-107 (in Russian).

Reilinger, R. E., S. C. McClusky, and B. J. Souter, 1997. Preliminary estimates of plate convergence in the Caucasus collision zone from GPS measurements, Geophys. Res. Lett., 24, 1815–1818.

Robinson, A., Spadini, G., Cloetingh, S., Rudat, J., 1995. Stratigraphic evolution of the Black Sea: inferences from basin modelling. Marine and Petroleum Geology 12, 821-835.

Robinson, A.G., Rudat, J.H., Banks, C.J. and Wiles, R.L.F., 1996. Petroleum Geology of the Black Sea. Marine and Petroleum Geology, 13 (No. 2): 195-223.

Ross D.A. and Degens E.T., 1974. Recent sediments of The Black Sea. In: Degens and Ross (eds.), The Black Sea – geology, chemistry, AAPG Memoir, Vol. 20, Tulsa, 183-199, Oklahoma, U.S.A..

Ryan W.B.F. and Cita M.B., 1978. The nature and distribution of Messinian erosion surfaces, indicators of a several-kilometer-deep Mediterranean in the Miocene. Marine Geology, 27, 193-230.

Saintôt A. and Angelier J., 2000. Plio-Quaternary paleostress regimes and relation to structural development in the Kertch-Taman Peninsulas (Ukraine and Russia). Jour. Structural Geology, no. 22, p. 1049-1064.

Shanmugam, G., Bloch, R. B., Mitchell, S. M., Damuth, J. E., Beamish, G. W. J., Hodgkinson, R. J., ... and Shields, K. E., 1996. Slump and debris-flow dominated basin-floor fans in the North Sea: an evaluation of conceptual sequence-stratigraphical models based on conventional core data. Geological Society, London, Special Publications, 103(1), 145-176.

Stadnitskaia A., 1997. Gas and Fluids in Marine Sediments: Gas Hydrates, Mud Volcanoes, Tectonics, Sedimentology and Geochemistry in Mediterranean and Black Seas, Distribution and composition of hydrocarbon gas in the seabed sediments of the Sorokin Trough (south-eastern part of the Crimea margin) IOC Workshop Report No 129.

Starostenko, V.I., Rusakov, O.M., Shnyukov, E.F., Kobolev, V.P. and Kutas, R.I., 2010. Methane in the northern Black Sea: characterization of its geomorphological and geological environments. Geological Society, London, Special Publications, 340 (1): 57-75.

Stovba, S., Khriachtchevskaia, O., Popadyuk, I., 2009. Hydrocarbon-bearing areas in the eastern part of the Ukrainian Black Sea. The Leading Edge 28, 1042-1045.

Tari, G., 2011. Exploration Country Focus: Ukraine*. Search and Discovery Article #10359.

Tugolesov, D.A., Gorshkov, A.S., Meisner, L.B., Soloviev, V. and Khakhalev, E.M., 1985. Tectonics of the Mesozoic-Cenozoic deposits of the Black Sea (in Russian). Nedra, Moscow.

Wagner-Friedrichs, M., 2007. Seafloor seepage in the Black Sea: mud volcanoes, seeps and diapiric structures imaged by acoustic methods. Ph.D. thesis, Department of Geosciences, Univ. of Bremen, Bremen.

Weimer, P.R., 1989. Sequence stratigraphy, facies geometries and depositional history of the Mississippi fan, Gulf of Mexico. AAPG Bull. 74, 182–272.

Wessel, P. and Smith, W. H. F. 1991. Free software helps map and display data. EOS 72, 445-446.

Winguth, C., Wong, H. K., Panin, N., Dinu, C., Georgescu, P., Ungureanu, G., Krugliakov, V.V., and Podshuveit, V., 2000. Upper Quaternary water level history and sedimentation in the northwestern Black Sea. Marine Geology, 167 (1), 127-146.

# Chapter 4. Distribution of shallow gas in the subsurface, gas flares and the role of gas hydrate near the Kerch Peninsula, Black Sea

## 4.1. Introduction

Gas seeps have been reported from every sea and ocean, and from a wide range of water depths. Their potential environmental impact is significant not only on the geosphere but also on the biosphere, the hydrosphere and the atmosphere (Judd, 2003). Recent studies focus on the question if and how gas seeps could affect the carbon cycle and global warming (Judd et al., 2002). Furthermore, gas seeps also became economically interesting as they indicate locations of shallow or deep hydrocarbon accumulations. And they may have a large influence on the stability of the seabed and the development of submarine landslides (Naudts et al., 2006).

The Black Sea is well known for the presence of gas seeps and seep-related structures, which have been reported from various areas, e.g. at the north-western margins (Peckmann et al., 2001; Michaelis et al., 2002; Mazzini et al., 2004; Naudts et al., 2006), in the central and north-eastern parts (Ivanov et al., 1989, 1998; Limonov et al., 1994; Woodside et al., 1997; Kenyon et al., 2002; Blinova et al., 2003; Bohrmann et al., 2003; Krastel et al., 2003; Aloisi et al., 2004; Mazzini et al., 2004; Greinert et al., 2006) as well as along the south-eastern slopes of the Black Sea (Cifci et al., 2002; Ergün et al., 2002; Klaucke et al., 2006). However, the study area, which is located at the continental slope in the eastern part of the Ukrainian Black Sea, south of Kerch Peninsula, was not investigated in detail before R/V Meteor Cruise M72/3b in 2007, where a 2D high resolution seismic dataset was acquired. During three later cruises (R/V MARIA S. MERIAN Cruise MSM15/2 in 2010, R/V Meteor Cruise M84/2 in 2011, FS POSEIDON Cruise POS427 in 2012) further acoustic data had been acquired in the vicinity of gas seeps.

Gas hydrates are commonly associated with gas seeps or mud volcanoes in the Black Sea below ~700 m water depth (Ginsburg et al., 1990). Stable gas hydrate deposits can prevent the upward migration of methane (dissolved in the pore water or as free gas forming gas bubbles) into the water column. In the western part of the Ukrainian Black Sea, for example, Naudts et al. (2006) showed that the seep distribution coincides with the phase boundary of methane hydrate. Nevertheless, gas bubble emissions can also occur in areas within the gas hydrate stability zone (GHSZ), for instance at mud volcanoes in the Sorokin Trough and in the central Black Sea (Limonov et al., 1994; Limonov et al., 1997; Woodside et al., 1997), or at the Batumi seep area offshore Georgia (Klaucke et al., 2005, 2006). The Kerch seep area (Römer et al., 2012) located in the

study area at ~900 m water depth is also placed well within the GHSZ. Therefore, seeps are found in the study area both above and below the pinchout depth of the GHSZ, and mechanisms of gas migration and emission can be studied with respect to sediment properties and deformation, lithologic variations, migration pathways and different mechanisms of gas trapping.

In this study, we imaged the active gas seeps in the water column detected directly with a parametric single beam echosounder in conjunction with the subseafloor structures using a high resolution multichannel seismic dataset. We integrate the exact locations of the seeps with the seismic dataset to explain gas supply, migration and the formation of observed seeps and their distribution with respect to the gas hydrate occurrence. The Kerch seep area is studied in detail, combining the tectonic and sedimentary evolution of the Kerch Peninsula margin (see Chapter 3) to unravel its occurrence within the GHSZ.

## 4.2. Geological setting



**Figure 1** Bathymetric map of the Eastern Black Sea and the surroundings (Gebco 1-min grid), with the insert showing the main tectonic zones around the study area. The location of the study area is marked as red rectangle.

The Black Sea, divided into the Western and Eastern basin, is the world's largest anoxic basin with anoxic conditions below 100-150 m water depth (e.g. Rangin et al., 2002). It is generally considered as a backarc basin formed in the Late Cretaceous (Nikishin et al., 2003). The study area is located at the continental slope in the eastern part of the Ukrainian Black Sea (Fig. 1), with water depths ranging from ~100 m to 1400 m. Abundant shallow gas seeps and the high intensity Kerch seep have been found in this area (Römer et al., 2012). Structurally, the study area is surrounded by the Sorokin Trough in the South-west, Crimean Mountains in the North and Northwest, the Kerch-Taman Trough in the East and the Tetyaev-Shatsky Ridge in the South (Robinson et al., 1996; Nikishin et al., 2003). The whole eastern Ukrainian Black Sea was affected by inversion tectonics and compressional events, acting during the Middle Eocene, Late Eocene, Early Miocene and Middle Miocene (Stovba et al., 2009). These compressional phases took place along with the continuing post-rift basin subsidence. Sorokin Trough and Tetyaev–Shatsky ridge are oriented from East to West, indicated the eastern Ukrainian Black Sea influenced by the North-South directed compression. Numerous anticline structures formed by these compressional events (Stovba et al., 2009), which may serve as structural traps for oil and gas accumulations. The sedimentary cover of the study area consists of Jurassic to Paleogene, Upper Eocene to Lower Miocene, Middle Miocene and Upper Miocene to Quaternary sequences, with a total thickness of up to 15 km (Stovba et al., 2009). The Oligocene-Miocene Maikopian formations are buried beneath younger sediments, and most probably represent the gas source of several seeps in the Black Sea (Ivanov et al., 1996) together with biogenic gas formed in shallower sediment. The steep upthrust faults (Alexander and Irina, 2005) occurring on the basinward side of the anticlines, might serve as the main pathway for gas migrating into the shallow sediments.

## 4.3. Data and methods

In March and April, 2007, a set of 2D high resolution seismic data was acquired near the Kerch Peninsula (Black Sea) during R/V Meteor Cruise M72/3b. A Sodera Generator – Injector (GI) airgun with extended chamber volume (4.1 L generator and 1.7 L injector volume, frequency range 30 - 300 Hz) was used as a seismic source and towed in 7 m water depth. The multichannel seismic streamer (SYNTRON) includes a tow-lead, a stretch section of 44 m and ten active sections of 50 m length each. A 30 m long meteor rope with a buoy at the end was connected to the tail swivel, and resulting in a total tow length of 574 m. Data were recorded by a 500 m long streamer section (SYNTRON) with 80 channels at a group distance of 6.25 m. The streamer was kept in a water depth of 3 m (+/- 0.5 m) by the attachment of 5 birds (cable levelers). Positioning was based on GPS. 21 seismic profiles were shot in this study area (Bohrmann et al. 2007).
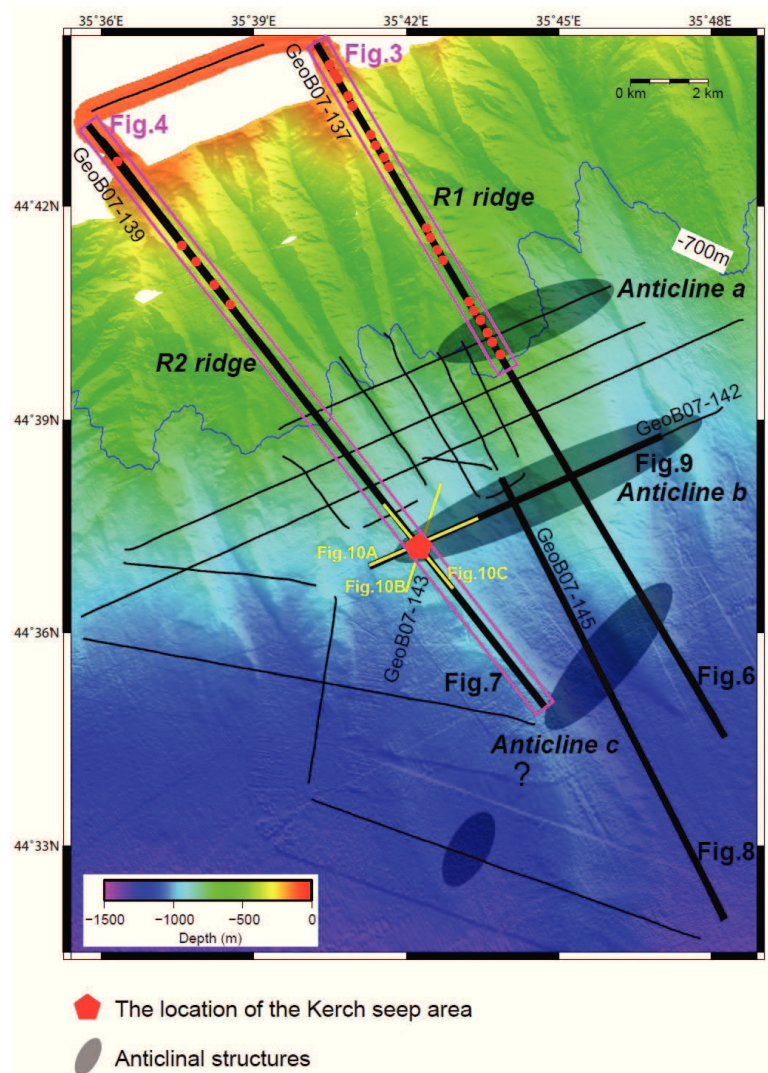
**Figure 2** Bathymetry of the study area with locations of seismic lines. The red pentagon indicates the location of the Kerch seep area. Anticline structures are mapped from the seismic data and shown as grey ellipses. Red points indicate the gas seeps. The bathymetric data of the study area were already published by Römer et al. (2012). The Generic Mapping Tool (GMT, Wessel and Smith, 1991) was chosen to plot the bathymetric map in combination with the locations of the seismic lines.

The multichannel seismic processing method and the Vista seismic processing software package were used to process the seismic dataset. The custom software WinGeoapp (H. Keil, University of Bremen) has been used for geometry calculation. Different CMP binning distances were tested, and finally 2 m was chosen for an optimum slope and detail imaging. Dead and extremely noisy channels were identified and removed. Traces with random spike noise were marked as dead traces. Velocity analysis was used for all seismic profiles, and the velocity files were used for the normal move-out (NMO) correction and CMP stacking. The dataset was filtered by a broad

band-pass filter in the range of 10/30 - 250/400 Hz. Time Migration is applied to the stacked seismic profiles using the finite difference method. Then the stacked and migrated profiles were exported from the Vista software as SEGY data, and imported into the Kingdom Suite software for next interpretation work.
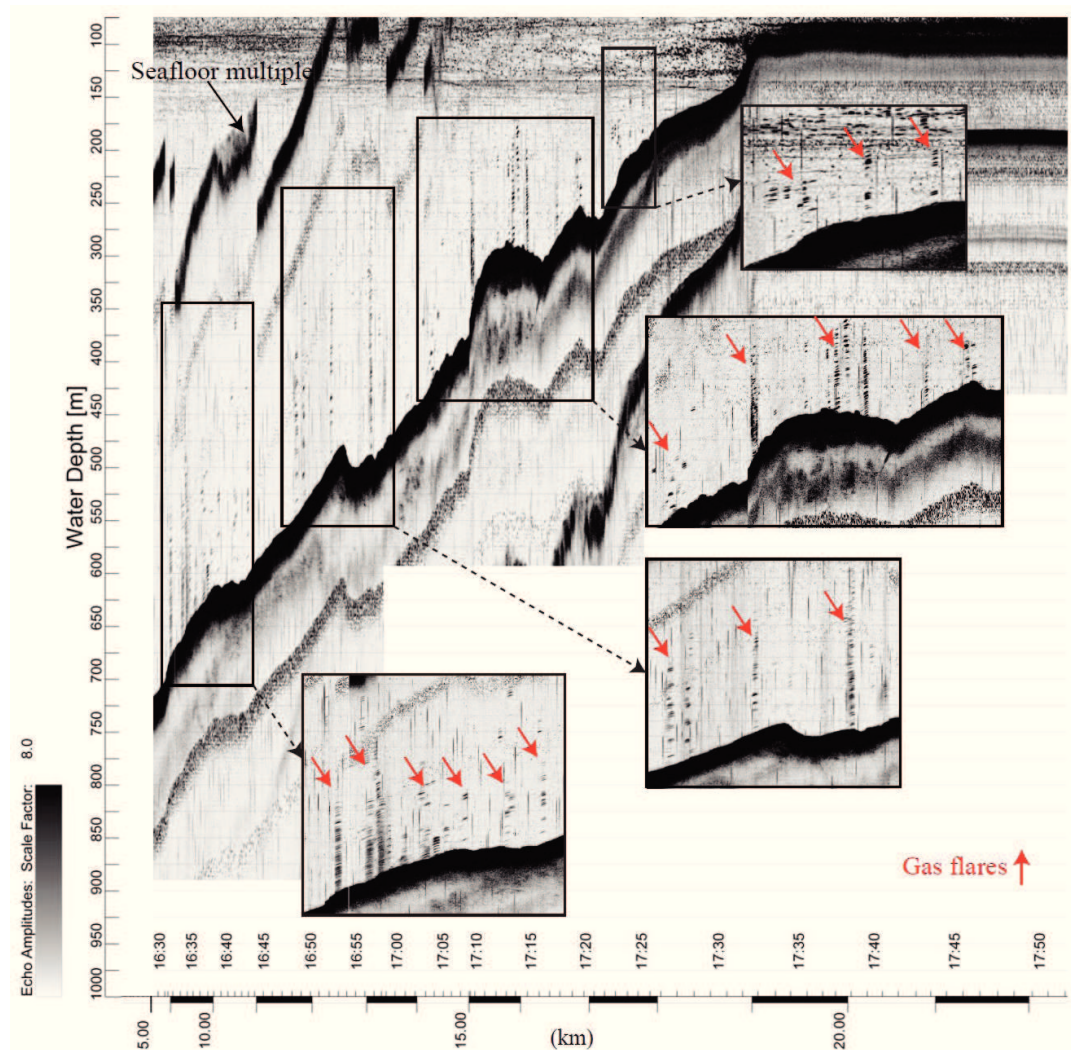


**Figure 3** Digital Parasound recording of the water column (PHF 18 kHz) along R1 ridge (Line GeoB07-137). Red rows indicate the numerous gas flares within the enlarged extractions.

A deep sea single beam echosounder Parasound (ATLAS Hydrographics) was us on R/V Meteor for water column and subsurface imaging. It is operated at a primary frequency (PHF) of 18 kHz and secondary low frequency (SLF) of 4 kHz. These signals were recorded simultaneously. The PHF data were used to detect the gas flares in the water column, while the SLF data image subbottom structures. The software ATLAS PARASTORE was used for online processing. Before the final images were generated, the resulting PS3 files were processed by the custom-made program SeNT (H. Keil,

University of Bremen). At the same time, the PS3 files were also transformed into SEG-Y files and loaded into 'The Kingdom Software' (SMT) for interpretation.
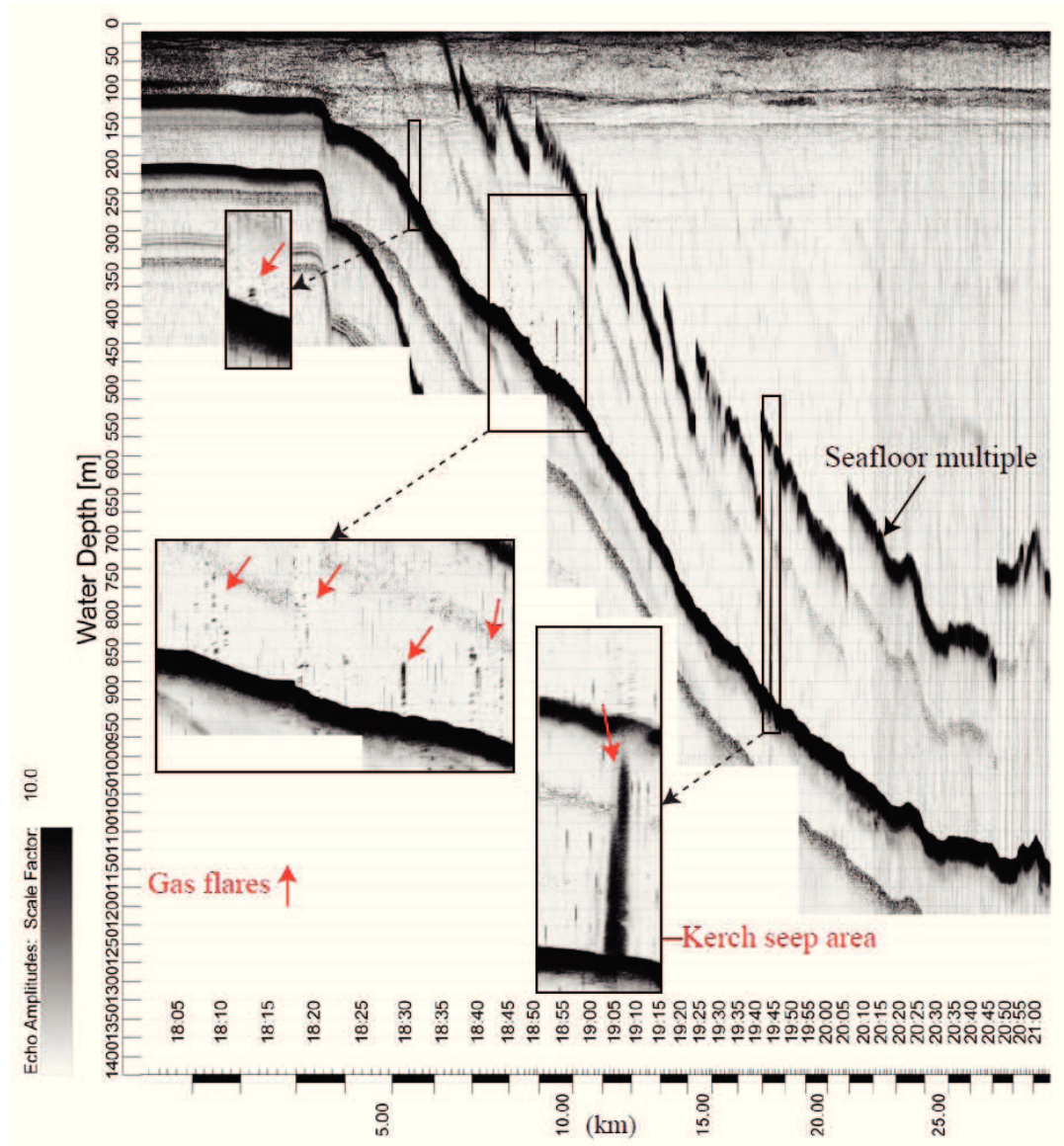


**Figure 4** Digital Parasound recording of the water column (PHF 18 kHz) along R2 ridge (Line GeoB07-139). Red arrows in the enlarged extractions indicate the gas flares. The Kerch seep area is located in a water depth of ~ 900 m, with the gas flare more than 400 m high above the sea floor.

## 4.4. Results

### 4.4.1. Bathymetric features

The bathymetric data show two large ridges and several small ridges extending southeastwards, which are separated by some incised valleys. The water depth ranges from ~100 m to ~1400 m. The two ridges with a gradient between 5° and 6° (named Ridges R1 and R2 in this study) were imaged by two seismic lines (GeoB07-137 and GeoB07-139, respectively; Fig. 2) running along their crest. The Kerch seep area is located on the crest of Ridge R2 in a water depth of ~900 m. It was ~60 m higher elevated than the adjacent seafloor.

### 4.4.2. Distribution of gas flares in the study area
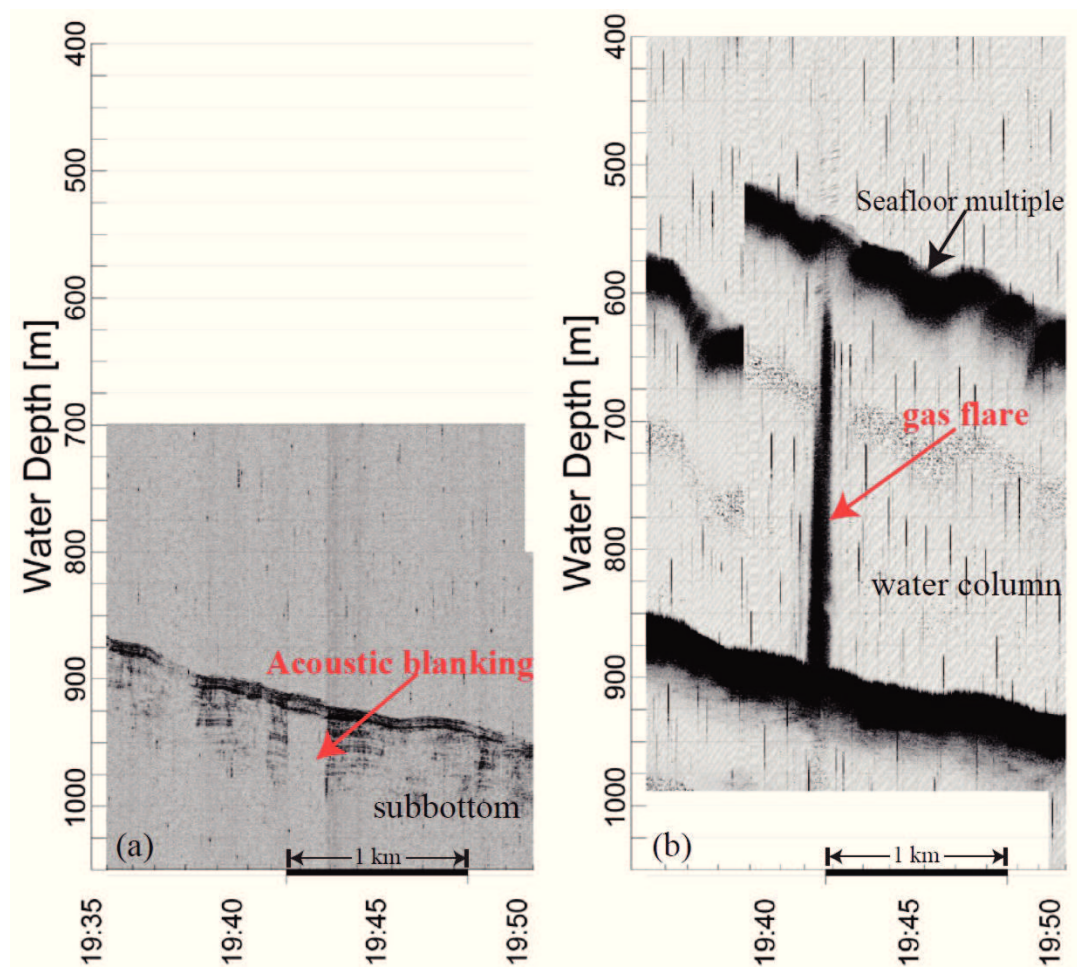


**Figure 5** Digital Parasound recordings of the sub-seafloor (a) and the water column (b) in the Kerch seep area. A pronounced zone of acoustic blanking (SLF 4 kHz) is locates beneath the gas flare visible in the water column data (PHF 18 kHz).

Parasound data were used to map the distribution and location of gas flares in the study area exactly on the seismic lines. The PHF profiles along Ridge R1 (GeoB07-137)

and Ridge R2 (GeoB07-139) show several gas flares released from the seafloor (red arrows in Fig.s 3 and Fig. 4). These gas flares mainly appear on local morphological highs. Amplitudes returned from gas flares are quite variable, which could be due to a variable amount of bubbles, the ratio of wavelength to bubble size, or location of the flare with respect to beam center. The gas flares cannot be traced to the sea surface, but all of them seem to terminate in the water column.

The SLF data were used to detect subbottom structures, for example, the subbottom profile underneath the Kerch seep area (Fig. 5). There is a clear indication of the acoustic blanking effect, which could be caused by high gas content in the very shallow sediment (Bohrmann et al. 2007).

### 4.4.3. Seismic structures and characteristics of the study area

### 4.4.3.1. Anticline structures

There are three anticline structures (Chapter 3) in the sub-surface within the study area, identified in the seismic profiles (Fig.s 6, 7 and 8). The crests of anticline structures (named Anticlines a, b and c) are located at a depth of approximately 500 ms TWT bsf (two travel time below seafloor). The locations and extent of the anticlines were mapped and displayed in Figure 2 together with the bathymetric data collected during Cruise M72/3b. The strike direction of Anticlines a and b is orientated ENE-WSW, whereas Anticline c is NE-SW directed.

The Kerch seep area is located above the buried Anticline b, and on top of Ridge R1. The topography of the seafloor shows the trend of the ridges is NW-SE, which are almost perpendicular to the anticline structures.

### 4.4.3.2. Ridges R1 and R2

Ridges R1 and R2 are the most pronounced features in the study area. Seeps (including the Kerch seep area) were observed above these two large ridges. The average elevation of the ridges reaches ~150 m and ~100 m, respectively, with respect to the neighbouring canyons. In the follow sections, we will define and describe the main seismic features of Ridges R1 and R2, and the difference between them.
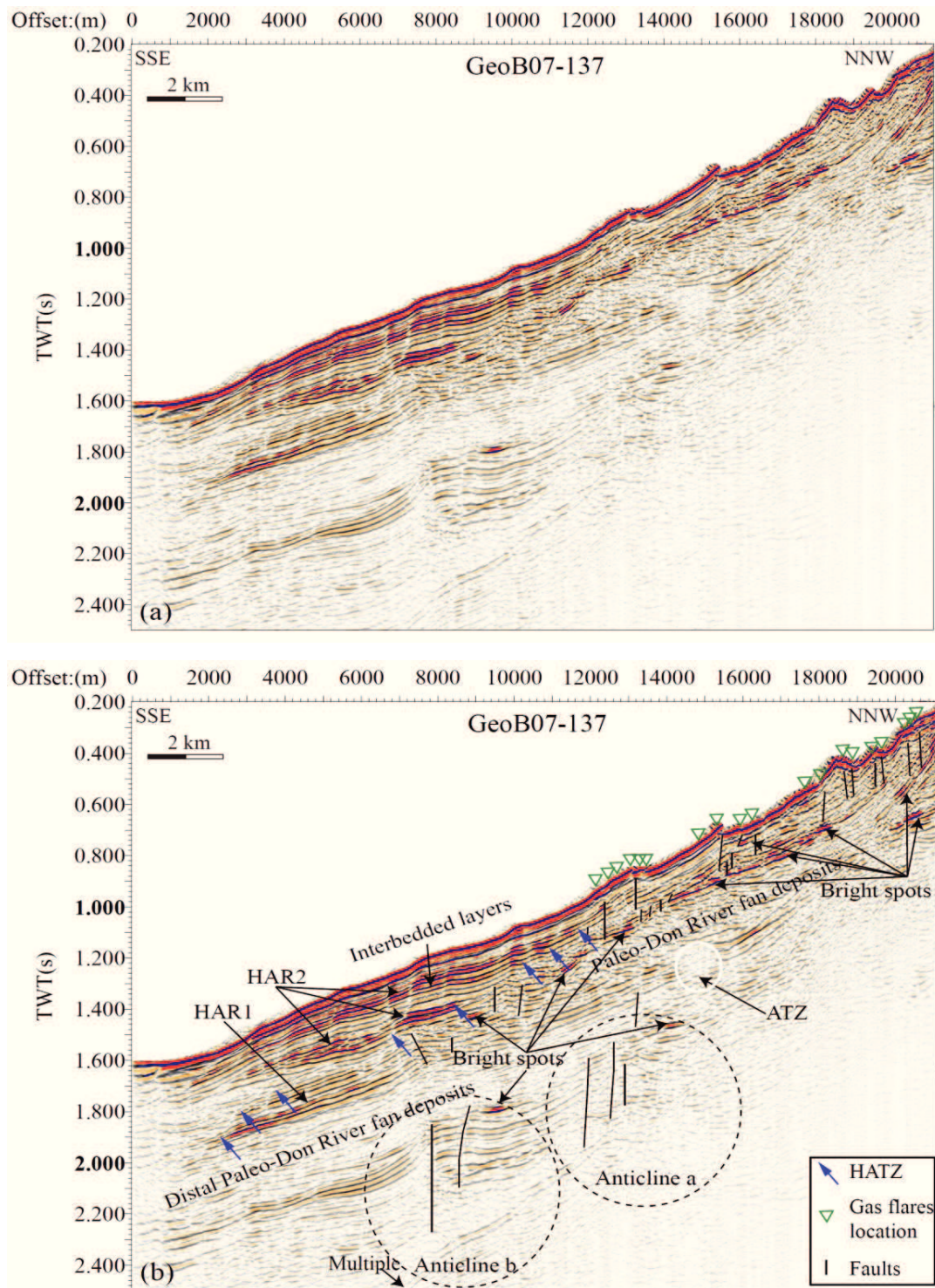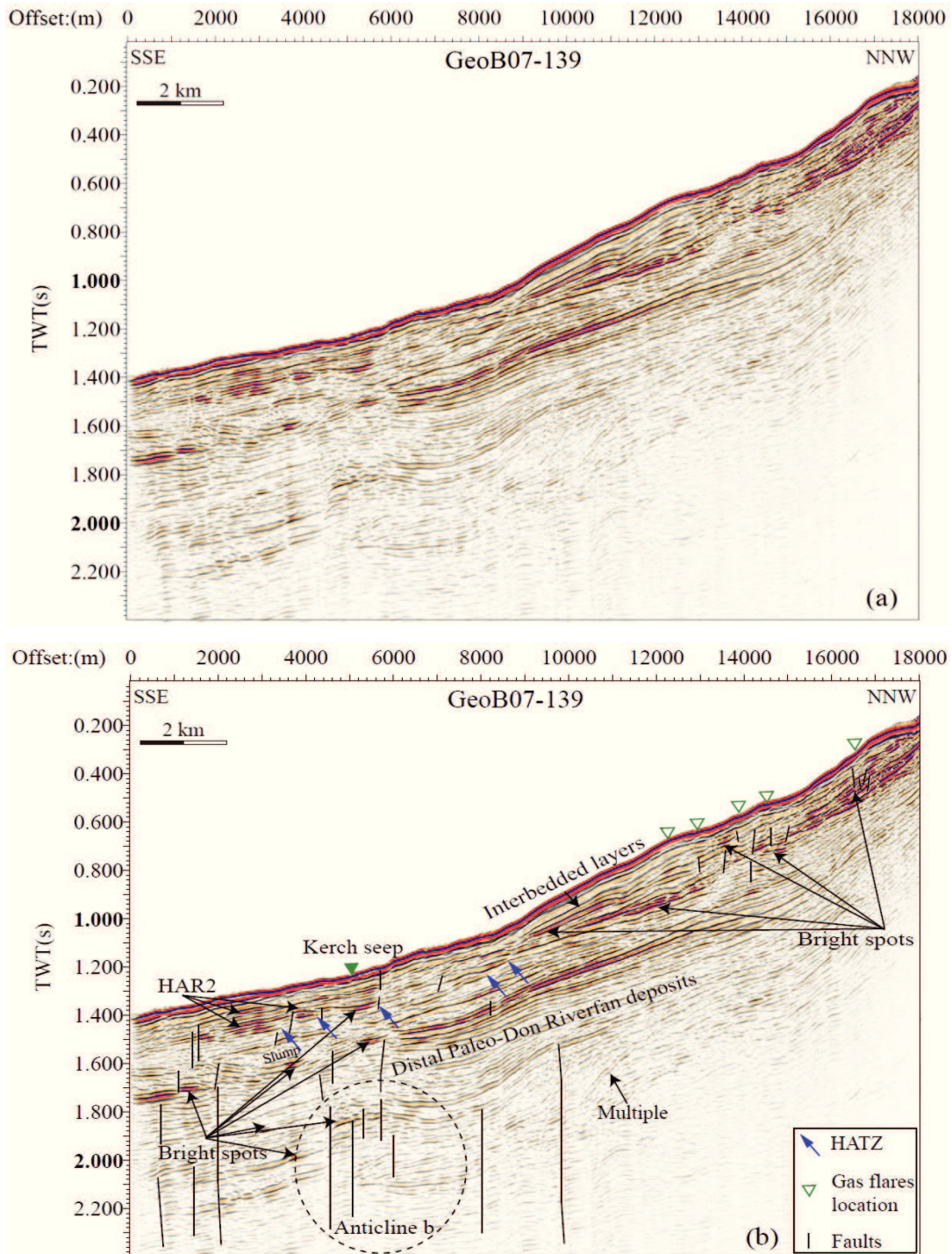
**Figure 6** (a) Uninterpreted migrated seismic profile GeoB07-137. (b) Interpreted migrated seismic profile GeoB07-137. Anomalous seismic reflections are indicated, such as bright spots, high amplitude reflections. Blue arrows indicate the high amplitude termination zone (HATZ). HAR1: high amplitude reflections below the HATZ. HAR2: high amplitude reflections above the HATZ. Green triangles indicate the gas

flares location. Anticline structures are presented by the circles. The white circle indicates the acoustically transparent zone (ATZ). See Figure 2 for location of the line.



**Figure 7** (a) Uninterpreted migrated seismic profile GeoB07-139. (b) Interpreted migrated seismic profile GeoB07-139. The Kerch seep area is shown by the green filled triangle. Blue arrows indicate the high

amplitude termination zone (HATZ). HAR2: high amplitude reflections above the HATZ Green triangles indicate the gas flares location. Anticline b is presented by the circle. See Figure 2 for location of the line.
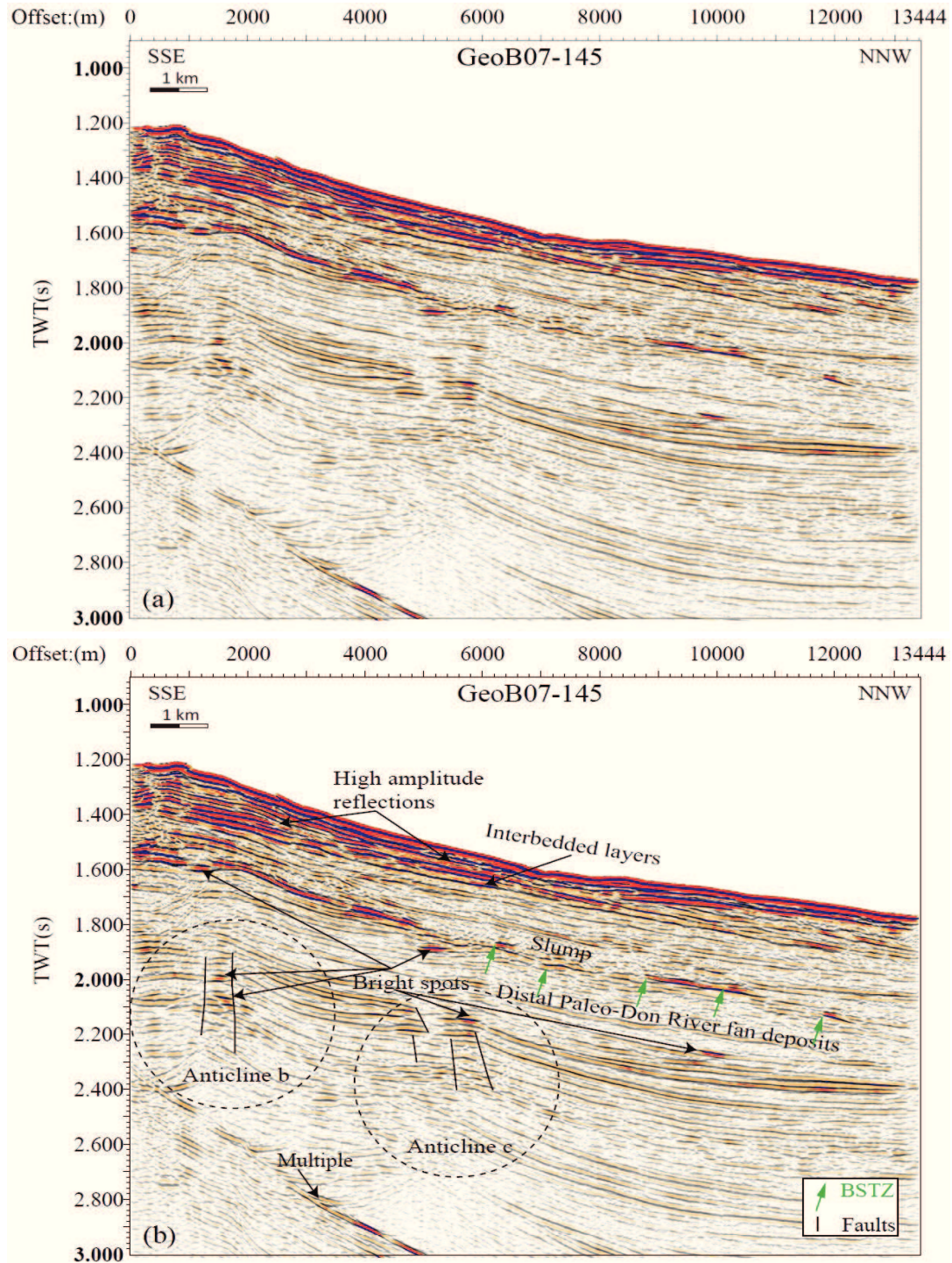


**Figure 8** (a) Uninterpreted migrated seismic profile GeoB07-145. (b) Interpreted migrated seismic profile

GeoB07-145. Green arrows indicate the location of the bright spots termination zone (BSTZ). Anticline b and c are presented by the circles. See Figure 2 for location of the line.

### 4.4.3.2.1. Bright Spots, BSR and high amplitude reflections

Bright spots, characterized by reverse polarity and local high amplitude anomalies, can be clearly identified beneath both ridges (Fig.s 6 and 7). Most shallow bright spots occur at a depth range of 50-230 ms TWT bsf in areas shallower than 700 m water depth. But in deeper water (>700 m), the depth of the bright spots varies between 300 and 800 ms TWT bsf, and they occur mainly around the crests of the anticline structures. The maximum lateral extent of the bright spots reaches ~870 m in WSW-ENE direction beneath the Kerch seep area (Fig. 9).

Bottom simulating reflectors (BSR) are characterized by amplitude anomalies mimicking the seafloor, and they are generally caused by the interface between gas hydrate and free gas-bearing sediments (Shipley et al., 1979). General characters of a BSR cannot be identified in the study area. However, some seismic features may indicate the possible base of the gas hydrate stability zone (BGHSZ). First, in Line GeoB07-145 (Fig. 8b), a bright spot termination zone (BSTZ) is visible, marked by the green arrows, at about 290-350 ms TWT bsf in water depths between 990 m and 1290 m. The BSTZ is characterized by a main frequency of 30-60 Hz, while the corresponding high resolution seismic data have a wider spectral band between 35 and 150 Hz. Second, in Lines GeoB07-137 (Fig. 6b) and GeoB07-139 (Fig. 7b), a high amplitude termination zone (HATZ) has been identified at both ridges in water depths between 760 and 960 m (see blue arrows).

Two types of high amplitude reflection occur in the area: high amplitude reflection 1 (HAR1) one beneath the HATZ; high amplitude reflection 2 (HAR2) above the HATZ and close to the seafloor (Fig. 6 and Fig. 7). HAR2 can be observed near the crests of Ridges R1 and R2 (Fig. 9) in water depth > 700 m.

### 4.4.3.2.2. Faults

Vertical reflector offsets of up to ~6 ms TWT are observed in several seismic profiles, which are interpreted as faults. The main faults are marked by black lines in the figures (e.g. Fig.s 6b and 7b). Several deep normal faults are shown around the anticline structures in the lower parts of the seismic profiles, while the shallow faults are imaged on the upper slope of the continental margin (Fig.s 6b and 7b).
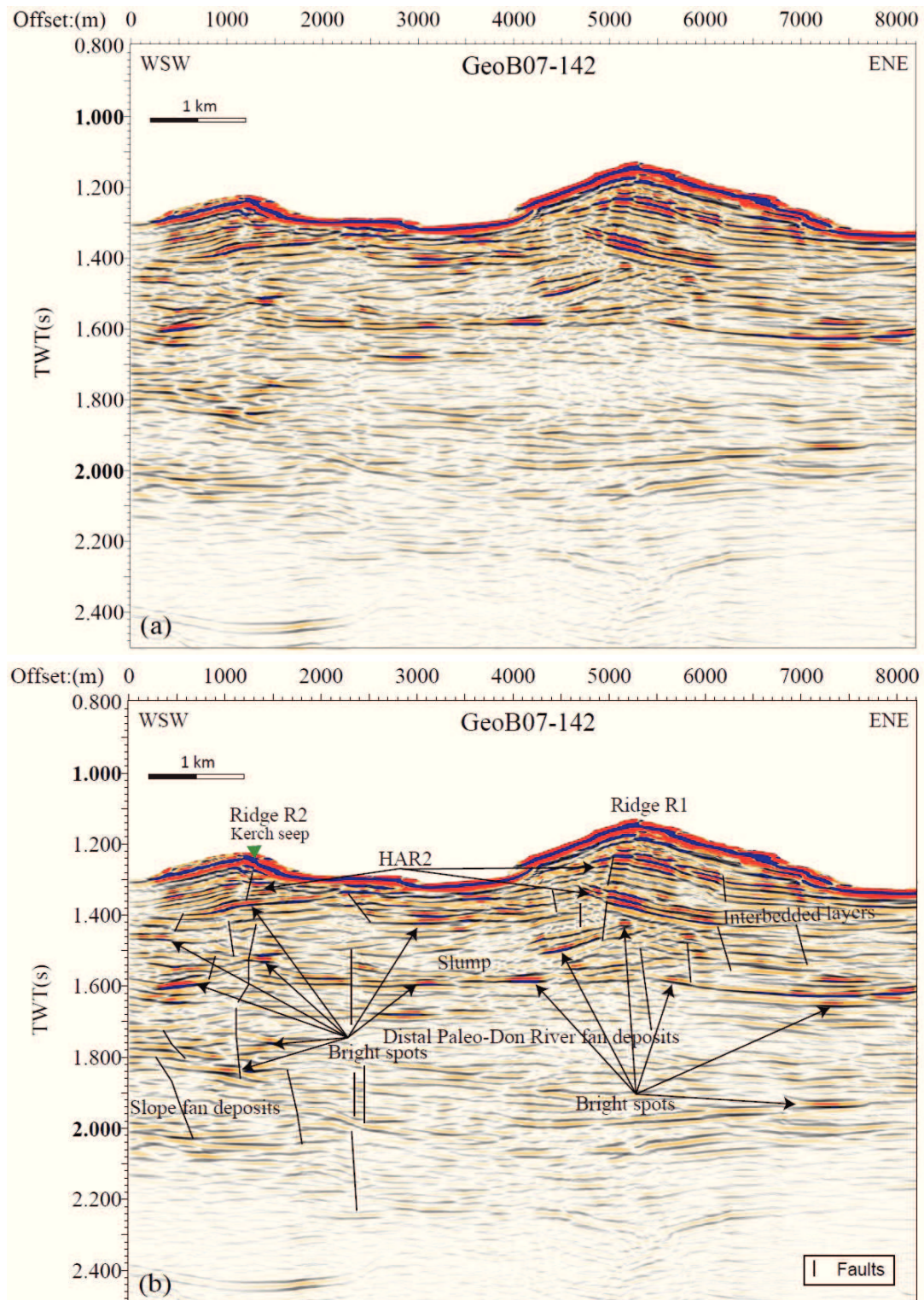
**Figure 9** (a) Uninterpreted migrated seismic profile GeoB07-142. (b) Interpreted migrated seismic profile GeoB07-142. Ridges R1 and R2 are shown on the profile. The Kerch seep area is located above some near vertical faults reaching down to the Bright Spots. See Figure 2 for location of the line.

### 4.4.3.2.3. Other anomalous seismic features

A large package characterized by low to high amplitude, low continuous reflectors can be identified in the upper slope in Figure 6. It has much lower reflection amplitude than the adjacent reflectors. Numerous shallow bright spots occur on the surface of the package. Additionally, there is a vertical acoustically transparent zone (ATZ) (Fig. 6b) beneath the package visible, reaching down to Anticline a.

In the study area, the crests of anticline structures are covered by a zone of low amplitude, moderate to good continuous and parallel reflections with a thickness of ~250-300 ms TWT (e.g. in Fig. 6). In the shallow part of the seismic profiles, the character of the reflectors reveals mainly high amplitudes, moderate to good continuity and parallel reflectors, and is locally disturbed by small chaotic reflections.
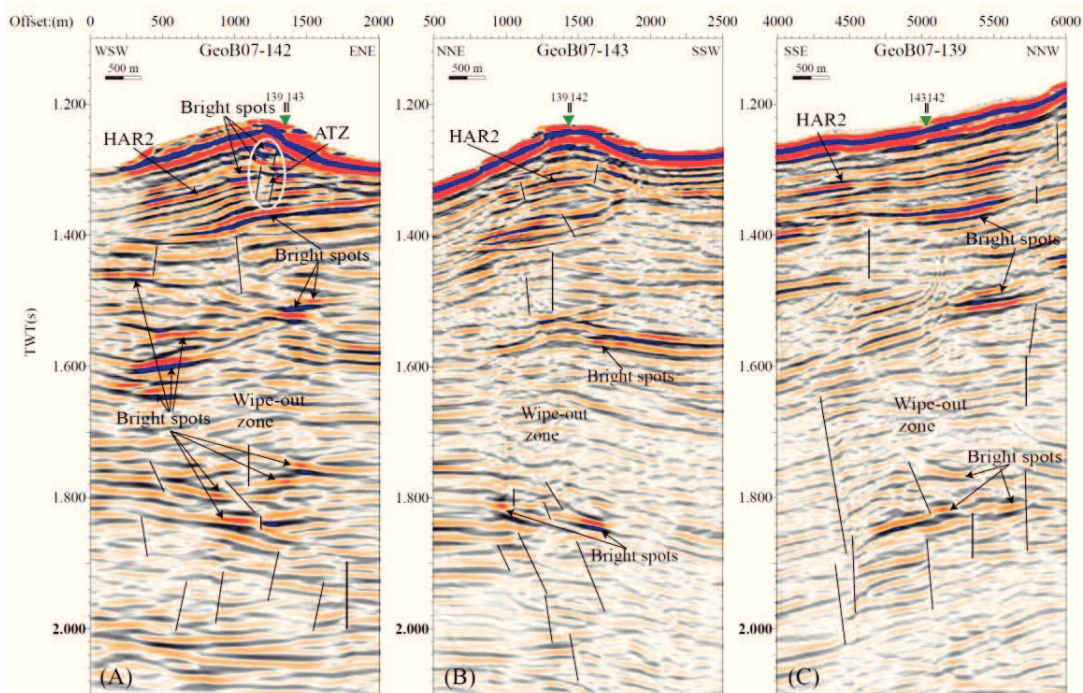
### 4.4.3.3. Kerch seep area



**Figure 10** Parts of migrated seismic Lines GeoB07-142 (A), GeoB07-143 (B) and GeoB07-139 (C), which are crossing the Kerch seep area. Bright Spots, wipe-out zone, near vertical faults and high amplitude reflections (HAR2) can be observed beneath the Kerch seep area. The white ellipse indicates the acoustically transparent zone (ATZ).

The Kerch seep area is imaged by three seismic profiles, shot in three different directions (Fig. 2). Three close-ups across the Kerch seep are shown in Figure 10. The

Kerch flares are located on the top of Ridge R2 marked by the green solid triangle. Beneath the Kerch seep, there are some high amplitude reflections and bright spots, which are evident in all the three seismic profiles, revealing a thickness of ~130 ms. An acoustically transparent zone and faults were observed in the vicinity of the high amplitude reflections and above the bright spots. The zone is marked by the white ellipse in the Figure 10A. Similar faults can also be observed in Figure 10B. Beneath the high amplitude reflections, an acoustic wipe-out zone in conjunction with many faults reaches down to Anticline b (Fig. 7b). Some bright spots are clustered within the acoustic wipe-out zone. No BSR can be recognized beneath the Kerch seep area.

## 4.5. Interpretation and Discussion

### 4.5.1. Sedimentary setting

Chapter 3 of the dissertation, dealing with the sedimentary evolution of the Kerch Peninsula margin, has provided information about the sedimentary setting of the study area, which will be used to understand the migration and accumulation of free methane gas. Six seismic units and seven seismic facies types were identified in Chapter 3, the isopach maps and the seismic facies distribution maps for the each seismic unit of the study area were created using the same seismic dataset. According to Chapter 3, the sedimentary setting of the study area will be summarized as follows.

During the Middle Eocene, Late Eocene, Early Miocene, and Middle Miocene, the northeast Black Sea was affected by inversion tectonics and compressional events accompanied with a continuing post-rift basin subsidence (Starostenko et al., 2011). Several anticline structures have formed as a result of NS directed compressional events, which in turn provide effective structural traps for oil and gas. About 20 local uplifts formed during the Paleogene and Neogene, and oil and gas-bearing sequences of the region were discovered by a multi-channel seismic survey east of the study area (Starostenko et al., 2011). A similar example of anticline traps is described from the Subbotina Field on the Kerch Shelf (Stovba et al. 2009), which is located northeast of the study area. Three anticline structures were imaged in the study area, formed probably before the late Miocene (See the location in Fig. 2 and 13). The organic-rich Oligocene-Miocene Maikopian clay formation (Chapter 3.5.2.1), may serve as the source of many gas seeps and mud volcanoes in the Black sea (Ivanov et al., 1996). Steep upthrust faults (Alexander and Irina, 2005) occur on the basinward side of the anticlines, which could act as the main pathways for gas migration to shallow sediments. During the Pliocene to Quaternary, the intensity of tectonic movements increased in conjunction with the uplift of the Great Caucasus and Crimean Mountains and the basin subsidence of the Black Sea, and the water depth was probably increasing gradually from the Pliocene to the Quaternary (Chapter 3.5.3).

Slope fan deposits with fine-grained sediments covered the location of Kerch seep area during late Miocene (Figure 5, Unit 6 in the Chapter 3.5.2.3), the possible mass transport deposits developed in the other part of the study area. The Messinian Salinity Crisis caused a dramatic fall in the sea level at the Miocene-Pliocene boundary. During the early Pliocene to middle Pliocene, the slope fan deposits continued developing at the location of Kerch seep area along with the recovery of water depth (Figure 6, Unit 5 in the Chapter 3.5.2.3), mass transport deposits became less frequent and appeared only on the upper slope, probably due to the increase of water depth. Hemipelagic sediments interbedded with coarser grained sediments during the transgression developed in the mid-slope to downslope part. The fine-grained distal Paleo-Don River fan covered the study area during the middle Pliocene to late Pliocene (Figure 7, Unit 4 in the Chapter 3.5.2.3), mainly in the middle and eastern part of the study area. During the Quaternary, high terrigenous input sourced from the Crimean Mountains and the Paleo-Don and Kuban rivers. The main deposits of the study area are hemipelagic fine-grained sediments interbedded with coarse grained sediments along with slumps or channels, and Paleo-Don and Kuban River fan deposits in the upper slope controlled by the sea level changes (Chapter 3.5.3). In Unit 3 (Figure 8, in the Chapter 3.5.2.3), possible slump deposits occurred at the location of Kerch seep area, while the Paleo-Don and Kuban River fan deposits with coarse grained sediments occurred at the location of Ridge R1. In Unit2 through Unit 1 (Figures 9 and 10, in the Chapter 3.5.2.3), the study area is mainly covered by hemipelagic fine-grained sediments interbedded with coarse grained sediments. Paleo-Don and Kuban River fan deposits decreased.

### 4.5.2. Gas and gas hydrate occurrences related to gas seeps

The Kerch seep area is located in a water depth of ~900 m, which is situated well within the GHSZ. Gas hydrates were discovered and sampled in the Kerch seep area, and samples from venting gas and hydrate-bound gas were contained 99.259% methane with a very small amount of ethane (Römer et al., 2012). A gas hydrate phase diagram (Fig. 11) of the Kerch seep area (modified after Römer et al., 2012) shows that the water depth of the upper boundary of the GHSZ is ~700 m. Almost all gas flares detected by Parasound data (Fig.s 3 and 4) are located above this water depth except for the Kerch seep area flares.

A BSR reflector, which is generally used to identify the BGHSZ, could not be found in the seismic data. However, two possible indicators (BSTZ and HATZ) for the BGHSZ have been identified in our seismic data instead. The calculated BGHSZ (using a sediment velocity of 1600 m/s, a bottom water temperature of 8.95°C and subsurface temperature gradient of 23°C/km) is there nearly coincident with the actual observed depth of the BSTZ (Fig. 12a) and HATZ (Fig. 12b) in the seismic records with only minor deviation between the calculated and observed depths, which may be attributed to

anomalies in subsurface temperatures/heat flow or erosive events. A classical BSR, which should mimic the seafloor and clearly cut across the sedimentary layers, is not evident in the data (Fig. 12). This might certainly be the case, if permeability is limited due to finer-grained sediments in the upper units (Ross and Degens, 1974; Jones and Gagon, 1994) or if the base of the GHSZ would run parallel to the sediment layering (Berndt et al., 2004). Another possible reason for the absence of a clear BSR may be the fact that sea level fluctuations influence the temperature and pressure conditions of the depth of the GHSZ. During the recent lowstand period, lasting from 11 to 8.5 kyr ^{14}C BP, the Black Sea water level was ~100 m lower than at present (Ryan et al., 2003; Popescu et al., 2004; Lericolais et al., 2009). The sea level fluctuations in conjunction with tectonic uplift/subsidence and high sedimentation rate can cause hydrate recycling, which can control the appearance of the BSRs (Grevemeyer et al., 2000). The bright spots beneath and close to the BGHSZ may then indicate the locations of paleo-BSRs (Fig. 12), which was also proposed for the western Black Sea (Popescu et al., 2007).
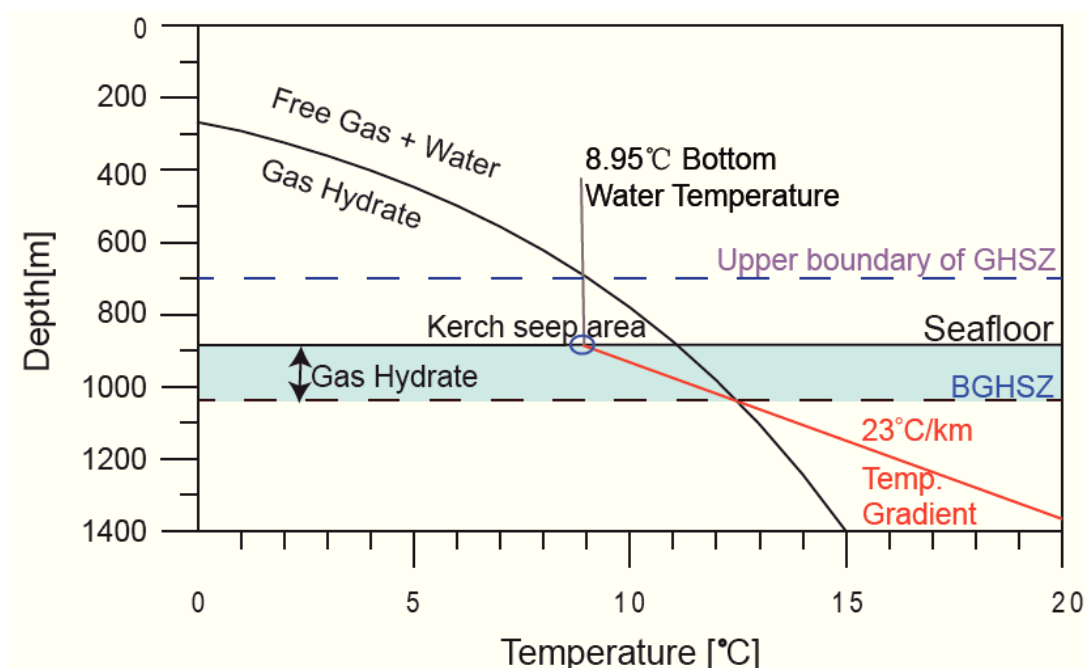


**Figure 11** Gas hydrate stability field at 890 m water depth in the Kerch seep area (modified after Römer et al., 2012). Stability curve for pure methane hydrates forming gas hydrate structure I was estimated after Dickens and Quinby-hunt (1997). Assuming a subsurface temperature gradient of 23 °C/km as measured during M84/2 (see Römer et al., 2012), the depth of the base of the GHSZ is located about 155m below the seafloor.
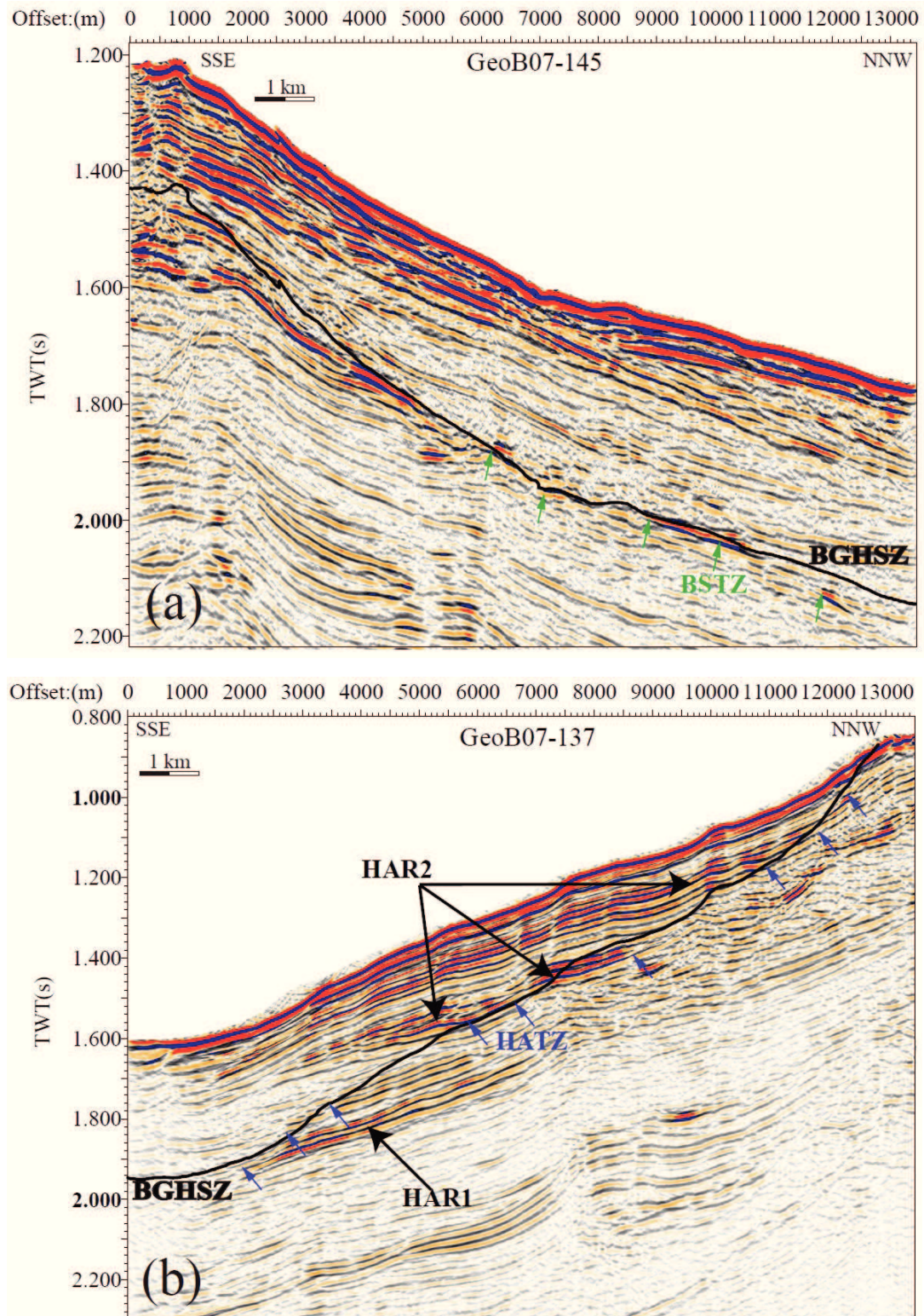
**Figure 12** Possible locations of BGHSZ. Two seismic indicators are identified. Figure a: BSTZ is shown

by the green arrows; Figure b: HATZ is shown by the blue arrows. HAR1: high amplitude reflections below the HATZ. HAR2: high amplitude reflections above the HATZ.

Two types of termination of high amplitude reflections are shown in Figure 12b. The first type is the termination of HAR1 found beneath the BGHSZ, which is usually used as one method to identify the location of a BSR-equivalent, such as at the mid-Norwegian margin (e.g. Berndt et al., 2004). The high amplitude reflections beneath the BGHSZ are caused by the accumulation of free gas in porous sediments underneath the sediments impregnated with gas hydrate, which can inhibit the upward migration of free gas and fluids. The second type is the termination of HAR2 detected above the BGHSZ (Fig. 12b), which is nearly coincident with the calculated BGHSZ, is barely observed by the seismic research in other areas.
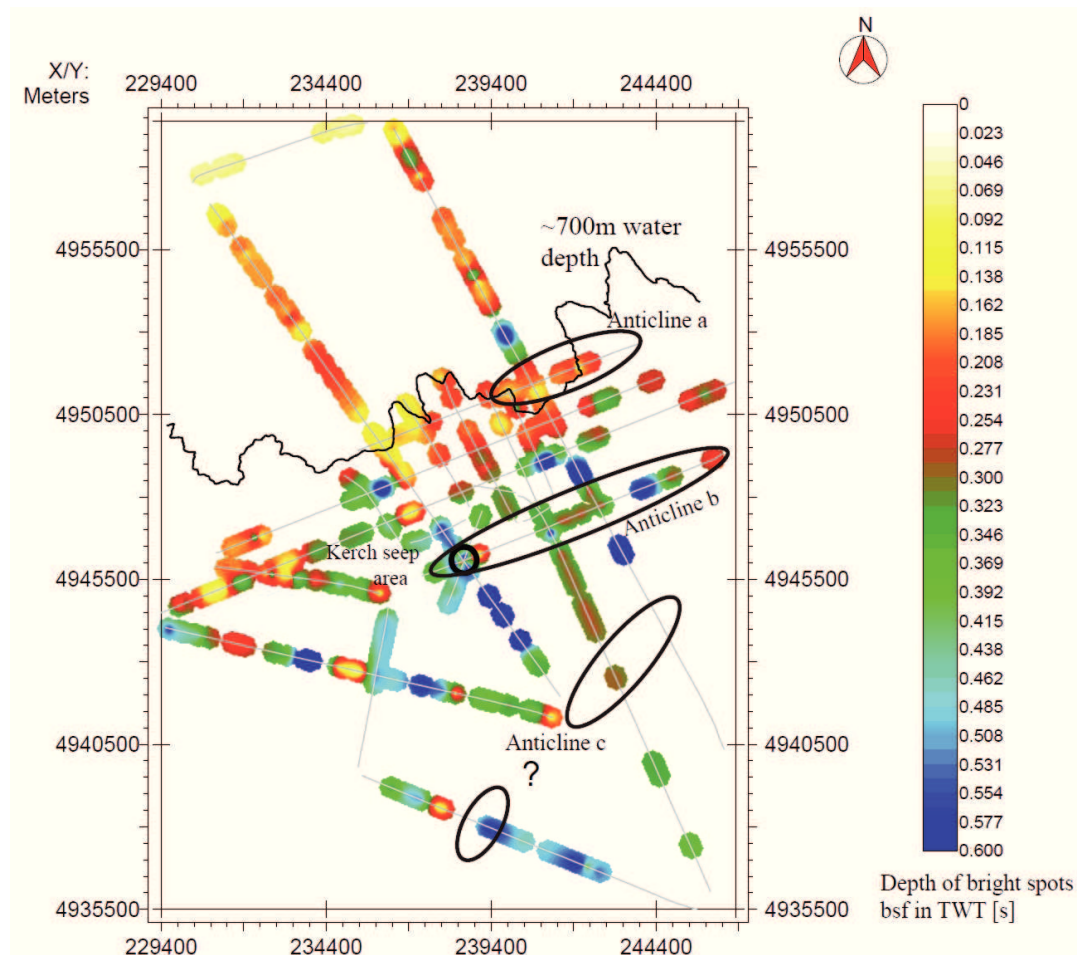


**Figure 13** Distribution and depth of the Bright Spots in s TWT bsf. The black circle indicates the Kerch seep area. The black ellipses indicate the anticline structures.

The high amplitude reflections within the GHSZ (HAR2) could also represent the presence of gas hydrates, if the hydrate concentrations in the sediments are above 30-42%

bulk hydrate or even higher, which would result in an increased sediment velocity and enhanced reflectance (Hornbach et. al., 2003). On the other hand, an amplitude blanking zone above the BSR can be used to detect limited gas hydrate content with 13-23% bulk hydrate in sediments of the same lithology (Holbrook et. al., 2002; Hornbach et. al., 2003). Another possible explanation for high amplitude reflections are authigenic carbonate precipitates, which commonly form at gas seeps close to the seafloor derived from the anaerobic oxidation of methane (AOM) (Wagner-Friedrichs, 2007; Crémière et. al., 2011). Römer et al. (2012) described the lithology of five gravity cores retrieved during M84/2 in the Kerch seep area. Massive layered gas hydrates were observed at the base of the core, and gas hydrates in form of small platy chips distributed in several thin horizontal layers. Carbonates were not observed throughout the entire cores (Römer et al., 2012). Therefore, HAR2 probably reflects the presence of the gas hydrate accumulations, and the termination of HAR2 might indicate the BSR's location, but more studies and evidences are required from this study area or other areas.

Many bright spots were detected on the seismic profiles (Fig.s 6, 7, 8, 9 and 10), which reveal high amplitude, reverse polarity and low frequency. High amplitude of bright spots results from high acoustic impedance contrasts when sediment layers are gas charged. Reverse polarity of bright spots is caused by the negative reflection coefficient at the interface of sediment to gas-charged sediment (e.g. Kou-Yuan Huang and King-Sun Fu, 1984; Max, 1990). The polarity change of the seismic signal would be a useful tool to identify free gas. Bright spots detected in the study area are distributed at various depths (Fig. 13). Furthermore, almost all deeper bright spots are distributed around the anticline structures. We suggest that the free gas accumulations are related to gas migration from greater depths associated with the anticline structures. The approximate depth of the bright spots in water depth >700 m does not match the depth of the calculated BGHSZ. We can distinguish two depth ranges, one is at about 270-300 ms TWT bsf, the other at about 500-640 ms TWT bsf. The shallower zone of bright spots might indicate free gas being trapped by impermeable hydrated-charged layers beneath the BGHSZ or might represent a paleo-BSR location. The deeper zone of the bright spots clusters near the summits of the anticline structures which act as structural traps, indicating the presence of free gas accumulated by focused fluid flow in the vicinity of the anticlines. In addition, many shallow bright spots are detected on the upper slope less than 700 m water depth, where gas hydrates are not present in the sediments (Fig. 13). Lateral dimensions of these shallow bright spots are larger than those of the deeper bright spots. Shallow faults occur above those shallow bright spots connecting them to gas flares detected at the seafloor.

### 4.5.3. Role of gas hydrates and gas trap-leakage processes

Two geological models for the gas hydrate occurrence and gas trap-leakage processes for the Kerch seep area and for the upper slope are presented in Figures 14 and 15. They are based on three seismic lines crossing the Kerch seep area (Lines GeoB07-137, 142 and 143) and the seismic Line GeoB07-137 along Ridge R1.

### 4.5.3.1. Model of Kerch seep area

The Kerch seep area is located in a water depth of ~900 m, which is positioned within GHSZ. Flares of more than 400 m height above the sea floor were observed in Parasound data. The Parasound profile at the Kerch seep area indicates a zone of acoustic blanking, which could be caused by free gas bubbles and/or a gas hydrate layer within the sediment (Bohrmann et al. 2007).

Since gas flares within the GHSZ are a rare phenomenon, geologic boundary conditions need to be studied to explain migration of free methane gas across the GHSZ and its seepage. As major elements sedimentary processes and lithologies and the tectonic history need to be considered (see Chapter 3). Based on our seismic observations, a conceptual geological model (Fig. 14) of the gas trap-leakage system beneath the Kerch seep area is presented.

At Anticline b, located beneath the Kerch seep area, gas accumulations are visible near the crest of the anticline. This gas likely originated from deeper sources and migrated along steep upthrust faults (Alexander and Irina, 2005) on the basinward side of the anticline towards the crest. Slope fan deposits are characterized by fine grained sediments, which covered Anticline b beneath the Kerch seep area providing a lithologic seal. As the anticline both provides a structural trap at the lithologic boundary from coarse to fine-grained, gas may accumulate and build up overpressure. Distal finer-grained Paleo-Don River fan deposits (Chapter 3.5.2.3) covered the whole Anticline b, which might have lead free gas to migrate laterally towards the morphological heights built by the slope fan deposits beneath the Kerch seep area. That may contribute to the gas accumulations. An acoustic wipe-out zone (Fig. 10) in conjunction with many faults above Anticline b indicates the possible migration zone for free gas and fluids towards the Kerch seep.

In shallow sediments at the Kerch seep area, temperature measurements, conducted at seven stations with an ROV-operated T-stick, provided anomalous temperature gradients locally up to 620 °C/km (Römer et al. 2012), which can shift the BGHSZ as shallow as 5 meters below the seafloor. However, in the vicinity of a strongly advective seep system, such a local measurement may overestimate the shoaling of the BSR, and the value may be used as an upper limit for the regional temperature field. The uplifted BGHSZ due to higher heat flow would certainly further enhance the trapping, and decomposing hydrates

may add to gas accumulations. These gas reservoirs therefore likely represent the main gas source feeding the Kerch seep.
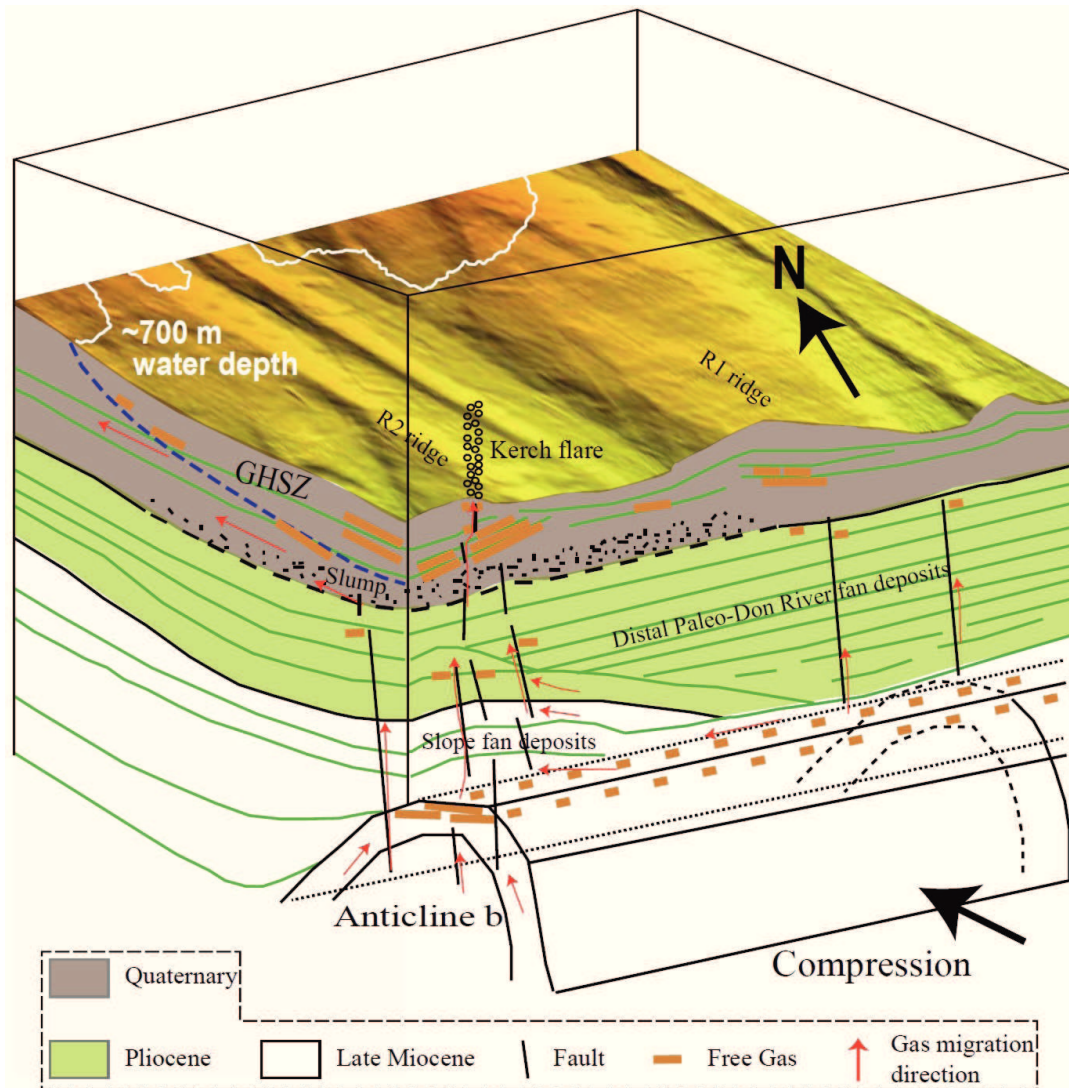


**Figure 14** A 3D model for mechanisms of gas migration in the Kerch seep area influenced by sedimentary processes and gas hydrates.

Around the calculated BGHSZ below the Kerch seep area, a BSR could not be detected. Only some high amplitude reflection patches and bright spots occurred shallower than the calculated BGHSZ. An acoustically transparent zone and faults are found in the Kerch seismic profiles, which may indicate fluid flow along a fault zone (Satyavani et al., 2008). For such a local heat flow anomaly, free gas can migrate much further up in the sediment column. Very shallow gas reservoirs exist on the top of this acoustically transparent zone. Hence, we suggest that free gas could migrate upwards

along the faults almost to the seafloor. Some geochemical and geophysical surveys elsewhere could show that free gas even could move through the GHSZ (Milkov et al., 2004; Pecher et al., 2007, Zühlsdorff et al., 1999).

Generally, the origin of the gas in the Kerch seep area might be related to: (1) in biogenic in situ methane generation, (2) dissociation of gas hydrates and (3) gas/fluid migration from deeper sediments. The seismic observations support a deep source, as some gas reservoirs occur at significant depth beneath the BGHSZ (Fig.s 6 and 7). However, biogenic gas could be generated also in relatively deep subsurface sediments (Kotelnikova, 2002; Popescu et al., 2007). Geochemical analyses of the gas samples taken at the Kerch seep area show that the methane predominantly originates from microbial (biogenic) methanogenesis without thermogenic input (Römer et al. 2012).
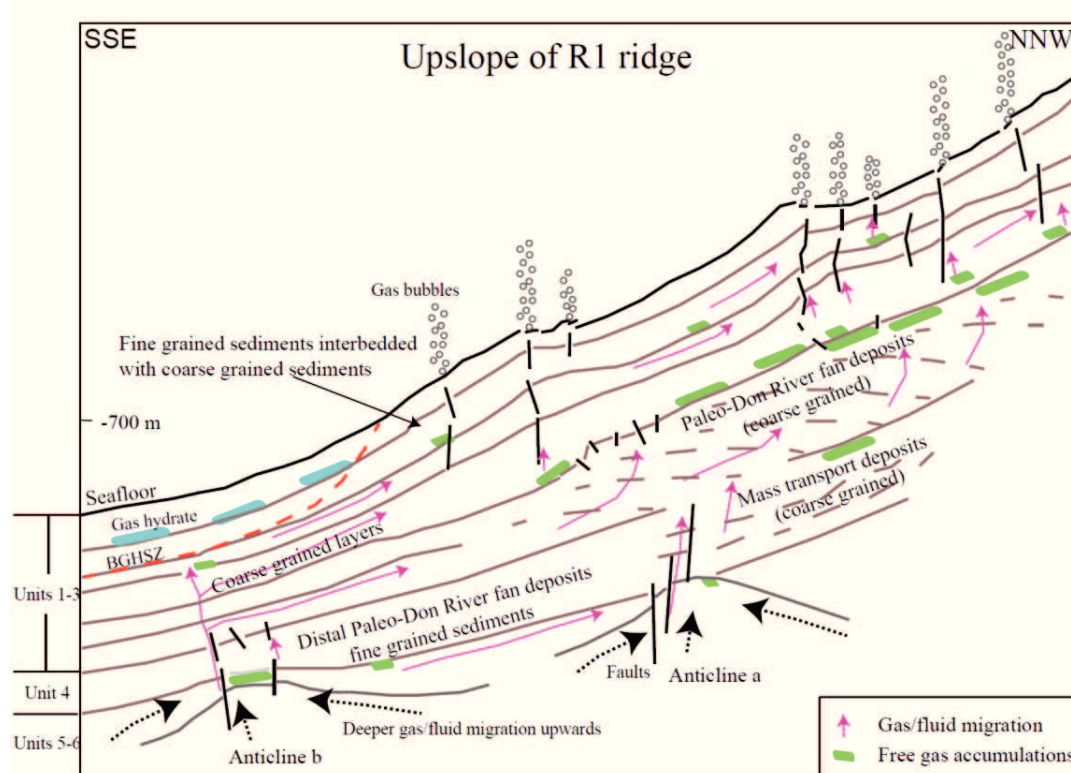
### 4.5.3.2. Gas migration at Ridges R1 and R2



**Figure 15** A geological model of the upper slope area of the Ridge R1 illustrating the gas hydrate and free gas systems based on the seismic line GeoB07-137. The pink arrows mark potential gas/fluid migration pathways. The green patches indicate the free gas accumulations. The black arrows indicate the migration directions of gas and fluids. The blue patches suggest the gas hydrates. The black lines present the faults. Units 1-6 are according to Chapter 3.

The narrow-beam Parasound data (4° opening angle) (Fig.s 3 and 4) show numerous gas seeps located exactly on the seismic lines in less than 700 m water depth, which complement the overall ~600 gas seeps reported by Römer et al. (2012) from water column imaging with a multibeam system. Except for the Kerch seep, however, no other gas emissions had been detected deeper than 700 m water depth in the area, which is the presumed boundary of the GHSZ. This observation confirms that the distribution of gas seeps is primarily controlled by the presence or absence of gas hydrates, which act as an effective seal. A similar gas seep distribution was reported from the continental margin of the northwestern Black Sea, west of the Crimea Peninsula (Naudts et al., 2006).

In general, on the Kerch margin gas/fluids are likely to migrate upwards along fault planes, fractures as well as more permeable horizons in upslope direction, as e.g. towards the top of anticline structures where in turn gas accumulations can form in reservoirs. Faults must have developed in Pliocene and Quaternary times at the top and the flanks of the anticlines due to the intense tectonic movements in conjunction with the Crimean Mountain uplift and Black Sea basin subsidence (Chapter 3), and further fracturing may have been supported through earthquake-triggered slope destabilization.

For the second scenario, the seepage on the upper slope, a geological model of the upper slope area of the Ridge R1 is presented in Figure 15. In this geological model, two potential major pathways for gas/fluid upward migration to the upper slope are shown (Fig. 15). The first migration path follows the deep faults from Anticline b across Unit 4, reaching the sediments of Units 1 to 3. Here, gas hydrates may serve as an effective seal to prevent further upward migration. Units 1-3 (Chapter 3.5.2.3) are characterized by hemipelagic fine-grained sediments interbedded with coarse grained sediments. The high permeability in coarser layers may support gas migration which diverts the gas flux in upslope direction, while interbedded finer layers inhibit further vertical migration. The second path is guided by fine-grained distal Paleo-Don River fan deposits of Unit 4, diverting gas/fluid fluxes layer-parallel within Unit 5 from Anticline b laterally towards Anticline a, complementing the gas accumulations from deeper sources at Anticline a. Subsequently, the gas/fluid can migrate vertically along faults or fractured and/or coarser sediment, which are the mass transport deposits and Paleo-Don River fan deposits (Units 4 and 3, Chapter 3.5.2.3). Also there the gas is likely trapped by the hemipelagic fine-grained sediment layers on the top of the Paleo-Don River fan deposits. This way shallow gas reservoirs can form on the upper slope. Shallow faults are observed above these gas reservoirs, which have formed within the uppermost units, probably due to slope instability and/or earthquakes, finally serving as vertical migration pathways to the seafloor and through the observed gas flares into the water column.

## 4.6. Conclusions

1) On the Kerch Peninsula continental margin, strong evidence was found in seismoacoustic water column and subsurface data for free gas, distributed in numerous bright spots within, beneath and above the GHSZ. The presence of gas hydrates in conjunction with the deformation history of the sedimentary units appears as the main factor for gas distribution, migration and seepage.

2) A BSR cannot be clearly identified in the study area, which may be attributed to limited permeability due to finer-grained sediments in the sedimentary units near the seafloor and at the base of the GHSZ. Instead, other seismic features like the boundary of zones, where high amplitude reflectors (HATZ) or bright spots terminate (BSTZ), may indicate the location of BGHSZ, inhibiting lateral migration of free gas by gas hydrate impregnation. Both types of terminations zones closely coincide with the calculated BGHSZ.

3) At the Kerch seep area, our model proposes that free gas is likely originating from deeper sources and migrating along steep upthrust faults on the basinward side of Anticline b towards their crest. Trapped gas is observed at the top of Anticline b. Furthermore, upward gas migration may be inhibited by distal Paleo-Don River fan deposits, leading to lateral migration to morphological highs or alternatively further upslope. Near the anticlines this may contribute to the builtup of gas accumulations. An acoustic wipe-out zone and an acoustically transparent zone in conjunction with many faults above Anticline b indicates the possible migration zone for free gas and fluids towards the Kerch seep. As a result of a local heat flow anomaly, the BGHSZ is further elevated, and free gas can migrate much further up along faults in the sediment column. Very shallow gas reservoirs were observed beneath the Kerch seep area, which could provide the continuous gas release found at the Kerch seep.

4) A second scenario for gas migration is presented for the area further upslope and at Ridges R1 and R2, and two possible migration pathways for gas/fluid are identified. The first migration path follows the deep faults beneath Anticline b and reaches shallower hemipelagic fine-grained sediments interbedded with coarse grained material. Here, gas hydrates may serve as an effective seal to prevent further upward migration. The high permeability in coarser layers may in turn divert gas migration upslope, while interbedded finer layers inhibit any further vertical migration. The second path basically follows coarser grained Unit 5, guided by fine-grained distal Paleo-Don River fan deposits, diverting gas/fluid fluxes layer-parallel from Anticline b laterally towards Anticline a. There, it connects to gas accumulations from deeper sources at Anticline a. Subsequently, the gas/fluid can migrate vertically along faults or fractured and/or coarser sediment, which are the mass transport deposits and more proximal Paleo-Don

River fan deposits. Being trapped by the hemipelagic fine-grained sediment layers on the top of the Paleo-Don River fan deposits, numerous shallow gas reservoirs have formed. Finally, shallow faults, probably formed within the uppermost units due to slope instability and/or earthquakes, can serve as vertical migration pathways above these gas reservoirs for free gas to the seafloor and through the observed gas flares into the water column.

## Acknowledgements

## References

Alexander Kitcka, Irina Nedosekova, 2005. Exploring Offshore Ukraine Using Space-born Data: Submarine Seeps, Oil Slicks, and Promising Prospects. EAGE 67th Conference & Exhibition — Madrid, Spain, P341.

Aloisi, G., Drews, M., Wallmann, K., and Bohrmann, G., 2004. Fluid expulsion from the Dvurechenskii mud volcano (Black Sea) Part I. Fluid sources and relevance to Li, B, Sr, I and dissolved inorganic nitrogen cycles. EPSL, 225: 347-363.

Berndt, C., Bunz, S., Clayton, T., Mienert, J. and Saunders, M., 2004. Seismic character of bottom simulating reflectors: examples from the mid-Norwegian margin. Marine and Petroleum Geology, 21, (6), 723-733.

Blinova, V.N., Ivanov, M.K., and Bohrmann, G., 2003. Hydrocarbon gases in deposits from mud volcanoes in the Sorokin Trough, north-eastern Black Sea. Geo-Marine Letters, 23: 250-257.

Bohrmann, G., Ivanov, M., Foucher, J.-P., Spiess, V., Bialas, J., Greinert, J., Weinrebe, W., Abegg, F., Aloisi, G., Artemov, Y., Blinova, V., Drews, M., Heidersdorf, F., Krabbenhöft, A., Klaucke, I., Krastel, S., Leder, T., Polikarpov, I., Saburova, M., Schmale, O., Seifert, R., Volkonskaya, A. and Zillmer, M., 2003. Mud volcanoes and gas hydrates in the Black Sea: new data from Dvurechenskii and Odessa mud volcanoes. Geo-Marine Letters, 23: 239-249.

Bohrmann, Gerhard; Pape, Thomas; cruise participants, 2007. Report and preliminary results of R/V METEOR Cruise M72/3, Istanbul - Trabzon - Istanbul, 17 March - 23 April, 2007. Marine gas hydrates of the Eastern Black Sea. Berichte aus dem Fachbereich Geowissenschaften der Universität Bremen, 261, 176 pp, urn : nbn : de : gbv : 46-ep000106850.

Cifci, G., Dondurur, D., Ergün, M., 2002. Sonar and high resolution seismic studies in the Eastern Black Sea. Turkish Journal of Earth Sciences, 11 (1): 61-81.

Crémière, A., Pierre, C., and Aloisi, G., 2011. Authigenic carbonates related to thermogenic gas hydrates in the sea of Marmara (Turkey). Proceedings of the 7th International Conference on Gas Hydrates (ICGH 2011), Edinburgh, Scotland, United Kingdom, July 17-21, 2011.

Dickens, G. R. and M. S. Quinby-Hunt, 1997. Methane hydrate stability in pore water: A simple theoretical approach for geophysical applications, J. Geophys. Res., 102 (B1), 773–783

Ergün, M., Dondurur, D., and Cifci, G., 2002. Acoustic evidence for shallow gas accumulations in the sediments of the eastern Black Sea. Terra Nova, 14: 313-320.

Ginsburg, G.D., Kremlev, A.N., Grigor, M.N., Larkin, G.V., Pavlenkin, A.D. and Saltykova, N.A., 1990. Filtrogenic gas hydrates in the Black Sea (21st voyage of the research vessel Evpatoriya). Soviet Geol Geophys, 31: 101-152.

Greinert, J., Artemov, Y, Egorov, V., De Batist, M., and McGinnis, D, 2006. 1300-m-high rising bubbles from mud volcanoes at 2080m in the Black Sea: Hydroacoustic characteristics and temporal variability. EPSL, 244: 1-15.

Grevemeyer, I., Rosenberger, A., and Villinger, H., 2000, Natural gas hydrates on the continental slope off Pakistan: Constraints from seismic techniques. Geophysical Journal International, 140, 295-310.

Holbrook, W.S., Gorman, A.R., Hornbach, M., Hackwith, K.L., Nealon, D., Lizarralde, D., and Pecher, I.A., 2002. Seismic detection of marine methane hydrate. The Leading Edge, 21 (7): 686-689.

Hornbach, M. J., W. S. Holbrook, A. R. Gorman, K. L. Hackwith, D. Lizarralde, and I. Pecher, 2003. Direct seismic detection of methane hydrate on the Blake Ridge, Geophysics, 68 (1), 92– 100.

Ivanov MK, Limonov AF, van Weering TCE, 1996. Comparative characteristics of the Black Sea and Mediterranean Ridge mud volcanoes. Mar Geol 132:253-271.

Ivanov MK, Limonov AM, Woodside JM, 1998. Extensive deep fluid flux through the sea floor on the Crimean continental margin (Black Sea). In: Henriet JP, Mienert J (eds) Gas hydrates; relevance to world margin stability and climate change. Geol Soc Spec Publ, pp 195-214.

Ivanov, M.K., Konyukhov, A.U., Kulnitskii, L.M., and Musatov, A.A., 1989. Mud volcanoes in deep part of the Black Sea. Vestnik MGU Serie de Geologia, 3: 21-31 (in Russian).

Jones G.A. and Gagnon A.R., 1994. Radiocarbon chronology of Black Sea sediments. Deep-sea Research, 41 (3): 531-557.

Judd, A., 2003. The global importance and context of methane escape from the seabed. Geo-Marine Letters, 23: 147-154.

Judd, A., Hovland, M., Dimitrov, L.I., Garcia-Gil, S., and Jukes, V., 2002. The geological budget at Continental Margins and its influence on climate change. Geofluids, 2: 109-126.

Kenyon, N.H., Ivanov, M.K., Akhmetzhanov, A.M., Akhmanov, G.G., 2002. Geological Processes in the Mediterranean and Black Seas and North East Atlantic. Preliminary results of investigations during the TTR-11 cruise of RV Professor Logachev. Intergovernmental Oceanographic Commission technical series, 62: 89pp.

Klaucke, I., Sahling, H., Bürk, D., Weinrebe, W., and Bohrmann, G., 2005. Mapping Deep-Water Gas Emissions With Sidescan Sonar. EOS, 86 (38): 341-343.

Klaucke, I., Sahling, H., Weinrebe, W., Blinova, V., Bürk, D., Lursmanashvili, N., and Bohrmann, G, 2006. Acoustic investigation of cold seeps offshore Georgia, eastern Black Sea. Marine Geology, 231: 51-67.

Kotelnikova S, 2002. Microbial production and oxidation of methane in deep subsurface. Earth-Sci Rev 58: 367-395

Kou-Yuan Huang and King-Sun Fu, 1984. Detection of bright spots in seismic signal using tree classifiers. Geoexploration 23, 121-145.

Krastel, S., Spiess, V., Ivanov, M.K., Weinrebe, W., Bohrmann, G. and Shashkin, P., 2003. Acoustic images of mud volcanoes in the Sorokin Trough, Black Sea. Geo-Marine Letters, 23: 230-238.

Lericolais, G., Bulois, C., Gillet, H., and Guichard, F., 2009, High frequency sea level fluctuations recorded in the Black Sea since the LGM: Global and Planetary Change, Volume 66, Issues 1–2, 65-75

Limonov, A.F., van Weering, Tj.C.E., Kenyon, N.H., Ivanov, M.K., and Meisner, L.B., 1997. Seabed morphology and gas venting in the Black Sea mud volcano area: Observation with the MAK-1 deeptow side scan sonar and bottom profiler. Marine Geology, 137: 121-136.

Limonov, A.F., Woodside, J.M., and Ivanov, M.K. (Eds.), 1994. Mud volcanism in the Mediterranean and Black Seas and shallow structure of the Eratostenes Seamount. Initial results of the geological and geophysical investigations during the third UNESCO-ESF 'Training Through Research' Cruise of RV Gelendzhik, June-July 1993. UNESCO Rep. Mar. Sci., 64. 173 pp.

Max, M.D., 1990. Gas hydrate and acoustically laminated sediments: probable environmental cause of anomalously low acoustic-interaction bottom loss in deep ocean sediments. Naval Research Laboratory report, 9235: 68pp.

Mazzini, A., Ivanov, M.K., Parnell, J., Stadnitskaya, A., Cronin, B.T., Poludetkina, E., Mazurenko, L., and van Weering, T.C.E., 2004. Methane-related authigenic carbonates from the Black Sea: geochemical characterisation and relation to seeping fluids. Marine Geology, 212: 153-181.

Michaelis, W., Seifert, R., Nauhaus, K., Treude, T., Thiel, V., Blumenberg, M., Knittel, K., Gieseke, A., Peterknecht, K., Pape, T., Boetius, A., Amann, R., Jörgensen, B.B., Widdel, F., Peckmann, J., Pimenov, N.V., and Guli, M.B., 2002. Microbial reefs in the Black Sea fuelled by anaerobic oxidation of methane. Science, 297: 1013-1015.

Milkov, A.V., Dickens, G.R., Claypool, G.E., Lee, Y.-J., Borowski, W.S., Torres, M.E., Xu, W., Tomaru, H., Tréhu, A.M., and Schultheiss, P., 2004. Co-existence of gas hydrate, free gas, and brine within the regional gas hydrate stability zone at Hydrate Ridge (Oregon margin): evidence from prolonged degassing of a pressurized core. EPSL, 222: 829-843.

Naudts, L., Greinert, Jens, Artemov, Yu., Staelens, P., Poort, J., Vans Regenbergen, P. and De Batist, M., 2006. Geological and morphological setting of 2778 methane seeps in the Dnepr paleo-delta, northwestern Black Sea Marine Geology, 227 (3/4). pp. 177-199.

Nikishin, A.M., Korotaev, M.V., Ershov, A.V., Brunet, M.-F., 2003. The Black Sea basin: tectonic history and Neogene–Quaternary rapid subsidence modelling. Sedimentary Geology 156,

149-168.

Pecher, I., S. Henrys, G. Crutchley, A. Gorman, W. Wood, R. Coffin, N. Kukowski and CHARMNZ Working Group, 2007. Seismic evidence for free gas in the regional gas hydrate stability zone beneath an antlicline on the Hikurangi margin, New Zealand, Geophysical Research Abstracts, v9, 02103

Peckmann, J., Reimer, A., Luth, U., Luth, C., Hansen, B.T., Heinicke, C., Hoefs, J., and Reitner, J., 2001. Methane-derived carbonates and authigenic pyrite from the northwestern Black Sea. Marine Geology, 177: 129-150.

Popescu I, Lericolais G, Panin N, Normand A, Dinu C, Le Drezen E, 2004. The Danube submarine canyon (Black Sea): morphology and sedimentary processes. Mar Geol 206: 249-265

Popescu Irina, Lericolais Gilles, Panin Nicolae, De Batist Marc De, Gillet Herve, 2007. Seismic expression of gas and gas hydrates across the western Black Sea. Geo-Marine Letters, 27 (2-4), 173-183.

Rangin, C., Bader, A.G., Pascal, G., Ecevitoglu, B., and Görür, N., 2002. Deep structure of the Mid Black Sea High (offshore Turkey) imaged by multi-channel seismic survey (BLACKSIS cruise). Marine Geology, 182: 265-278.

Robinson, A.G., Rudat, J.H., Banks, C.J. and Wiles, R.L.F., 1996. Petroleum Geology of the Black Sea. Marine and Petroleum Geology, 13 (No. 2): 195-223.

Römer M., Sahling H., Pape T., Bahr A., Fesker T., Wintersteller P., Bohrmann G., 2012. Geological control and magnitude of methane ebullition from a high-flux seep area in the Black Sea - The Kerch seep area. Marine Geology 319-322, 57-74. doi: 10.1016/j.margeo.2012.07.005.

Ross D.A. and Degens E.T., 1974. Recent sediments of The Black Sea. In: Degens and Ross (eds.), The Black Sea – geology, chemistry, AAPG Memoir, Vol. 20, Tulsa, 183-199, Oklahoma, U.S.A..

Ryan WBF, Major CO, Lericolais G, Goldstein SL., 2003. Catastrophic Flooding of the Black Sea. Annu Rev Earth Planet Sci 31/1: 525-554

Satyavani, N., Sain, K., Lall, M., Kumar, B.J.P., 2008, Seismic attribute study for gas hydrates in the Andaman Offshore India. Marine and Geophysical Research 29,167-175.

Shipley, T., Houston, M., and Buffer, R., 1979. Seismic reflection evidence for the widespread occurrence of possible gas hydrate horizons on continental slopes and rises. AAPG Bulletin, 63: 2204-2213.

Starostenko V.I., Krupskyi B.L., Pashkevich I.K., Rusakov O.M., Makarenko I.B., Kutas R.I., Gladun V.V, Legostaeva O.V., Lebed T.V., and Maksymchuk P.Ya., 2011. Fault Tectonics of the NE Black Sea Shelf and Its Relevance to Hydrocarbon Potential. Search and Discovery Article #30155.

Stovba, S., Khriachtchevskaia, O., Popadyuk, I., 2009. Hydrocarbon-bearing areas in the eastern part of the Ukrainian Black Sea. The Leading Edge 28, 1042-1045.

Wagner-Friedrichs, M., 2007. Seafloor seepage in the Black Sea: mud volcanoes, seeps and diapiric structures imaged by acoustic methods. Ph.D. thesis, Department of Geosciences, Univ. of Bremen, Bremen.

Wessel, P. and W. H. F. Smith, 1991. Free software helps map and display data. EOS, 72, 445-446

Woodside, J.M., Ivanov, M.K., and Limonov, A.F., 1997. Neotectonics and fluid flow through seafloor sediments in the Eastern Mediterranean and Black Seas. Parts I and II. UNESCO IOC Tech Ser, no 48: 224 pp.

Zühlsdorff, L., Spiess, V., Huebscher, C. and Breitzke, M., 1999. Seismic reflectivity anomalies in sediments at the eastern flank of the Juan de Fuca Ridge: Evidence for fluid migration? , Journal of Geophysical Research, 104 , pp. 15351-15364

# Chapter 5. Summary, conclusion and outlook

## 5.1 Summary and conclusion

This thesis investigates in detail the subsurface structures of mud volcanoes and gas seeps, and presents the gas/fluid migration mechanisms and intermediate gas reservoirs related to the mud volcanoes and gas seeps, influenced by sedimentary processes, tectonic movements, sea level changes and gas hydrate formation. In this case study, the PhD work focused on the central Black Sea and the continental slope of the Kerch Peninsula margin (particularly the Kerch seep area), where two different vent areas exist. The research objectives have been accomplished by processing the high resolution 2D seismic datasets, Parasound datasets and plotting the bathymetry map, and by interpreting and analysing anomalous seismic features, seismic facies, seismic stratigraphy and geological time scales. Main achievements are summarized below.

### 5.1.1 Sediment composition, tectonic and sedimentary evolution.

The age of sediments of the two study areas are not easy to constrain accurately because of the lack of boreholes in or around the study areas. The few existing DSDP drilling sites are also relatively far away from the study area. In this case, the age estimates of the seismic units can be derived from the comparison of our seismic data with interpreted seismic profiles acquired by petroleum corporations or research cruises in different areas of the Black Sea. Two age models were established for the central Black Sea and the Kerch Peninsula margin, respectively.

In the central Black Sea, four seismic units (U1 - U4) were recognized in Chapter 2, which are nearly horizontal and parallel units. U1-U3 belongs to the Quaternary, and U4 to the Pliocene according to the age correction. The central Black Sea is the deep basin which was in a deep water environment throughout the Cenozoic. However, the Black Sea was gradually evolving from a shallow water environment into a deep water environment from the Miocene to the early Quaternary. Sediments in U2 might be the coarse grain sediments, which were probably delivered by the Don River from the Northeast. The Don River likely entered the Black Sea during the middle Pliocene to late Pliocene and formed a large deep sea fan in the early Pleistocene, which has also reached the central Black Sea. About 900 ka ago (the base of U1), the Danube River reached the Black Sea for the first time and has built up the Danube fan subsequently. And ~800 ka ago, the Dniepr River flowed into the Black Sea and started to form the Dniepr fan. The two large fan systems deliver sediment with an increasingly higher sand fraction, which most likely corresponds to Unit U1 in the seismic profiles. Appearance of fan sediment may depend on progradation, and typical fan structures therefore only appear in the upper part of Unit U1, while unchannelized (finer grained) deposits formed during earlier stages of fan development. The climate of Black Sea underwent a series of glacial and interglacial events accompanied by intensive tectonic movement in the Quaternary (U3-U1), which could influence the Black Sea and cause the sea level to rise and fall. The sea level change controlled the development of Danube and Dniepr fans during highstands, the deep sea basin was sediment-starved so that condensed hemipelagic sections

deposited; during lowstands, the deep sea basin was covered by coarse grained sediment fed by channels and mass transport processes.

Six seismic units (Unit 1 - Unit 6) were distinguished at the Kerch Peninsula margin, which is located on the Northeast of the Black Sea. Our age model suggests Unit 6 to be of late Miocene age, Units 5 and 4 to be of Pliocene age, and Units 3 to 1 to be of Quaternary age. Based on the data analysis and previous studies, the working area underwent major sea level changes from a shallow water environment (during the Upper Miocene to early Quaternary) to a deep water environment (the Quaternary). During the late Miocene (Unit 6), the Messinian Salinity Crisis influenced the Black Sea, which caused the dramatic fall in sea level and formed erosion surfaces on the shelves. Fluvial delta deposition occurred in the study area. A slow transgression (Unit 5 and Unit 4) started after a major sea-level fall in the Upper Miocene and early Pliocene. During the middle Pliocene to late Pliocene (Unit 4), the Don River supplied for the first time sediment to the Black Sea as a response to vertical tectonics. The river provided abundant sediment to the Kerch Peninsula margin. Many channels formed and debris flows occurred near the mouth of the Kerch Strait, and finer grained sediment was transported to the western part of the study area. A large Don River fan formed gradually. Rapid subsidence occurred during the late Pliocene to Quaternary along with the uplift of the Great Caucasus and Crimean Mountains. The early Quaternary section is dominated by a shallow marine environment, and changed gradually into a deep water environment. According to the seismic facies in the seismic Units 3 - 1 (lower Pleistocene to Recent), the Kerch Peninsula margin was mainly covered by turbidity currents (coarse grained) interbedded with hemipelagic sediments (fine grained). In the meantime, mass transport deposits, debris flows and lots of sediment slump occurred, which may have been caused by intense neotectonic movements and sea level change. High terrigenous input was delivered from the Crimean Mountain and by the Paleo-Don and Kuban Rivers. The fan of the two rivers deposited at the mouth of the Kerch Strait with fewer channels (Unit 3 and Unit 2), and nowadays these rivers only enter the Sea of Azov, catching coarse grained material there.

### 5.1.2 Gas and fluid migration mechanisms and gas reservoirs, formation mechanisms of seabed fluid seepage

In the central Black Sea, sedimentary layers as shown on seismic profiles are almost horizontal. Six large deeply rooted mud volcanoes MSU, Yuzhmorgeologiya, Malyshev, Kornev, Goncharov and Vassoevitch are observed on these seismic profiles. The data cannot image the root of mud volcanoes. Previous acoustic studies suggested that the origin is clearly related to layers of plastic clay of the Maikopian Formation, which are highly enriched in organic matter. It is possible that earthquakes or active faults in conjunction with density contrast manifesting as a force of buoyancy, could be the triggers or contributing factors to mobilize high-pressured fluid and gas. This in turn could have initiated doming and fracturing of the overlying sediments, supporting fluid and gas mixed with mud to migrate upwards, and feeder channels may have formed. The fluid should derive from dehydration of Maikopian clay minerals and gas may have been generated from organic matter degradation.

In addition to the feeder channels, three other types of pathways for gas and fluid migration could be recognized: columnar zones, acoustic curtains and faults. And three types of gas reservoirs in the central Black Sea are identified: a) Large gas/gas hydrate reservoirs around the feeder channels of mud volcanoes (BSZA); b) Large gas/gas hydrate reservoirs located above the acoustic curtains (BSZB); c) Small gas/gas hydrate reservoirs at the top or sides of the faults and columnar zones (BSZC). The BSR is absent in most parts of the central Black Sea, probably due to sedimentary layers being almost parallel to the seafloor and due to a local gas supply. However, a local BSR segment was observed at a depth of ~650 ms TWT bsf. Although the accuracy is not very high, the thermal gradient and heat flow can be approximately estimated from the BSR. Assuming a sediment velocity of 1600 m/s and the average BSR depth, a temperature gradient of 23°C/km is suggested. All the BSZAs of relatively wide lateral extent appear at the boundary between Units U1 and U2, which is marked by a change from supposedly more sandy material to fine-grained turbidites, providing a seal for gas migration due to lower (vertical) permeability, forming a reservoir-seal combination. The bright spot Zones BSZB and BSZC are more probably formed by massive gas hydrate layers, converted originally from free gas, which are now associated with normal polarity reflections.

Mud volcanoes are composed of wide and deep feeder channels, showing several wide mud chambers, residing on collapsed sediment strata in the center. They show both gas and gas hydrate accumulations near the feeder channel, where gas may be of biogenic and thermogenic origin, and partially also from hydrate decomposition during eruptive phases. Kornev, Goncharov Malyshev, MSU and Vassoevitch mud volcanoes reveal three major eruption episodes, while at Yuzhmorgeologiya mud volcano only two major eruption episodes can be identified. All of the eruptive episodes of the mud volcano might be related to distinct sea level falls, which seem to be one of the main trigger factors of the mud volcano eruptions in the central Black Sea.

In Chapter 4, we studied the gas seeps in the western part (area 1 in Chapter 3) of the Kerch Peninsula margin, Black Sea. Strong evidence was observed in seismoacoustic water column and subsurface data for free gas, distributed in numerous bright spots within, beneath and above the GHSZ. The presence of gas hydrates in conjunction with the deformation history of the sedimentary units appears as the main factor for gas distribution, migration and seepage. No BSR can be clearly identified, which may be attributed to limited permeability due to finer-grained sediments in the sedimentary units near the seafloor and at the base of the GHSZ. Instead, other seismic features like the boundary of zones, where high amplitude reflectors (HATZ) or bright spots terminate (BSTZ), may indicate the location of BGHSZ, inhibiting lateral migration of free gas by gas hydrate impregnation. Both types of terminations zones closely coincide with the calculated BGHSZ. Three anticlinal structures were recognized in the study area (Chapter 3), which probably provide effective structural traps for oil and gas in the study area. For the special situation at the Kerch seep area, our model suggests that free gas is likely originating from deeper sources and migrating along steep upthrust faults on the basinward side of the Anticline b towards their crest. Gas reservoirs are found at the top of Anticline b. Furthermore, the distal Paleo-Don River fan may inhibit the upward gas migration, which is leading to lateral migration towards morphological highs or, alternatively, further upslope. Near the anticlines this may contribute to the builtup of gas

accumulations. An acoustic wipe-out zone and an acoustically transparent zone in conjunction with many faults above Anticline b indicate the possible migration zone for free gas and fluids towards the Kerch seep. A local heat flow anomaly was also found in the Kerch seep area. Therefore, the BGHSZ may be further elevated, and free gas can migrate much further up along faults in the sediment column. Very shallow gas reservoirs were observed beneath the Kerch seep area, which could provide the continuous gas release found at the Kerch seep. The mechanism of gas migration for the area further upslope and at Ridges R1 and R2 was studied. Two possible migration pathways for gas/fluid are identified. The first migration path follows the deep faults beneath Anticline b and reaches shallower hemipelagic fine-grained sediments interbedded with coarse grained material. Here, gas hydrates may serve as an effective seal to prevent further upward migration. The high permeability in coarser layers may in turn divert gas migration upslope, while interbedded finer layers inhibit any further vertical migration. The second path basically follows the coarser grained Unit 5, guided by fine-grained distal Paleo-Don River fan deposits, diverting gas/fluid fluxes layer-parallel from Anticline b laterally towards Anticline a. There, it connects to gas accumulations from deeper sources at Anticline a. Subsequently, the gas/fluid can migrate vertically along faults or fractures and/or coarser sediment, which are the mass transport deposits and more proximal Paleo-Don River fan deposits. Being trapped by the hemipelagic fine-grained sediment layers on the top of the Paleo-Don River fan deposits, numerous shallow gas reservoirs have formed. Finally, shallow faults, probably formed within the uppermost units due to slope instability and/or earthquakes, can serve as vertical migration pathways above these gas reservoirs for free gas to the seafloor and through the observed gas flares into the water column.

In all, this study shows that fluid seepage within the GHSZ, e.g. mud volcanoes in the central Black Sea and Kerch seep area in the Kerch Peninsula margin, are all probably related to the deeper sources and long migration pathways, such as feeder channels and steep upthrust faults. Free gas reservoirs could be observed beneath the fluid seepage in the near-surface sediments. The free gas is trapped by the fine-grained sediments or gas hydrate layers, and high overpressure is generated. Available pathways (feeder channels, column zones, shallow faults or coarse grained sediments) along with the heat flow anomaly would support the leakage of the free gas into the water column. For the gas seeps above the GHSZ, shallow faults were observed between the shallow gas reservoirs and the gas seeps. The shallow faults probably formed due to slope instability and/or earthquakes. The sedimentary processes and tectonic movements, and the presence of gas hydrates might play an important role in the formation of seabed fluid seepage.

## 5.2 Outlook

This thesis provides new insights into the controls of seabed fluid seepage, distribution and types of related gas reservoirs, and migration pathways for gas and fluid by sedimentary processes, structural characteristics and tectonic processes for two different vent areas in the Black Sea. The study revealed that both mud volcanoes and gas seeps must be fed from deep sources. However, 2D high resolution seismic data used here could only image the shallow subsurface structures. For a full understanding of such seabed fluid seepage systems, it would be desirable to incorporate deeper imaging of the

area, e.g. by using currently confidential industry seismic information. For the two study areas, published information on deep penetration drill sites is rare, and the accuracy of the age models is therefore limited. Improvements can be expected from more detailed age information derived from deep penetration industry drill sites, either existing or to be drilled in the future. For the most interesting research targets - MSU mud volcano and Kerch seep area - only three seismic profiles were available to image their subsurface structures. The data coverage is too low to learn about the threedimensional geometry and the subsurface structures of the seepage systems. Future 3D investigations are needed to understand more clearly the factors influencing the gas and hydrate distribution and evolution of mud volcanism, as well as the geometry and role fluid migration pathways and their relationship to the subsurface sediment tectonics and deformation.

For gas hydrate, imaging and quantification of gas hydrates could be improved in the study area by more carefully mapping secondary indicators based on somewhat denser survey grids, ultimately leading to quantification. Another important task for future research could be to map, summarize and compare all types of seabed fluid seepage in the Black Sea including aspects as, for examples, distribution and types of gas reservoirs, migration pathways of gas and fluid, structural characteristics, formation mechanisms and gas hydrate formation. It will be very helpful to understand the formation and evolution processes of seabed fluid seepage systems in the Black Sea.

# Acknowledgements

孟子曰："舜发于畎亩之中，傅说举于版筑之间，胶鬲举于鱼盐之中，管夷吾举于士，孙叔敖举于海，百里奚举于市。故天将降大任于是人也，必先苦其心志，劳其筋骨，饿其体肤，空乏其身，行拂乱其所为，所以动心忍性，曾益其所不能。人恒过，然后能改；困于心，衡于虑，而后作；征于色，发于声，而后喻。入则无法家拂士，出则无敌国外患者，国恒亡。然后知生于忧患而死于安乐也。"

------《孟子·告子下》